The Influence of Stern Vortices on Ship Manoeuvring

Jonathan Roger Horn

A Thesis Submitted for the Degree of Doctor of Philosophy

Department of Marine Technology
The University of Newcastle upon Tyne

September 2000

Abstract

This thesis is concerned with the steering and manoeuvring of surface ships. Recent developments in hull design have seen the introduction of the pram stern. This hullform has proved less directionally stable than more conventional stern shapes.

Recent theoretical developments include the effect of stern vortices in a slender-body treatment of the ships hull. The inclusion of these vortex effects explains the discrepancy between the distribution of force and moment coefficients along a hull obtained experimentally compared to those determined using slender body theory alone. As yet this approach requires the position and strength of the shed vortices to be determined by other means. The theory also offers a means of explaining the relative instability of the pram stern.

An experiment has been designed to directly test some of the predictions of this theory. The experiment entailed oblique towing of a set of 7 hullforms with segmented stern sections. The first group of five models are based on the British Bombardier with a variety of conventional and pram stern configurations. The remaining models were based on a simple elliptic hullform.

The experiments provide detailed data of the longitudinal distribution of force and moment sway derivatives of the stern regions of these models. The experimental evidence provided support for the theoretical predictions, although some results were inconclusive because of the effect of additional flow phenomena.

The physical insight provided by the generalised slender body theory has generated the impetus to use a semi-empirical approach to predict the manoeuvring derivatives from basic hull geometry. The equations developed for the linear velocity derivatives use predictors based on the physical phenomena and are formulated to recognise the interdependency of these derivatives. The new equations are statistically more satisfactory than previous analyses of this type.

Acknowledgements

This work was initiated with the encouragement of my supervisor Professor Grant E. Hearn. His guidance, continual supervision and expertise in research are greatly appreciated. My time was kindly funded by an EPSRC grant and the MOSES programme.

Many friends have helped significantly with encouragement, advice and assistance. I would particularly like to thank Dave Thomas, Christos Atalianis, Dave Lamb, Adam Osorio and Anita Arya. In general, I would also like to thank the technical, Administrative and teaching staff of the Marine Technology Department of Newcastle University.

Finally, I would like to thank Dave Clarke with whom it has been a very great pleasure to work.

Table of Contents

Abstract i

Acknowledgements. ii

Table of Contents. iii

List of Figures. vii

List of Tables. xi

Nomenclature. xv

1. INTRODUCTION. 1

1.1 Literature Review. 1

1.2 Start Point and Aims of this Thesis. 7

1.3 Chapter Layout. 9

2. THEORETICAL DETERMINATION OF HYDRODYNAMIC DERIVATIVES USING SLENDER-BODY THEORY. 11

2.1 Introduction. 11

2.2 Co-ordinate System. 12

2.3 Slender-Body Theory. 12

2.3.1 Development of the Slender-Body Strip Method. 14

2.3.2 Inertial Coefficients. 16

2.3.3 Added Mass Coefficients for Ship-Like Sections. 18

2.4 Experimental Examination of Slender-Body Theory. 19

2.4.1 Development of Segmented Model Experiments. 19

2.4.2 Results of British Bombardier Segmented Model Tests. 19

2.5 Vortex Influence Theory. 22

2.5.2 Determination of the Vortex Influence Coefficient. 24

2.5.3 Determination of the Impulse Position Derivative. 24

2.5.4 Determination of the Position Sway Derivative. 25

2.5.5 Evaluation of Impulse Position Derivatives by Numerical Mapping Methods. 26

2.6 Experimental Examination of the Vortex Influence Theory. 27

2.6.1 Analysis of Experimental Measurements. 28

2.7 Concluding Remarks. 29

3. DESIGN OF AN EXPERIMENT TO TEST THE VORTEX INFLUENCE THEORY. 31
3.1 INTRODUCTION. 31
3.2 VORTEX SHEDDING FROM SHIPS. 31
3.3 WHAT CONSEQUENCES OF THE VORTEX INFLUENCE THEORY CAN BE TESTED EXPERIMENTALLY? 33
3.4 SEGMENTED MODELS. 36
3.4.1 British Bombardier and Variations. 36
3.4.2 Elliptic Hull Form. 41
3.5 SOME EXPERIMENTAL CONSIDERATIONS. 42
3.6 CONSTRUCTION OF SEGMENTED MODELS. 43
3.7 DESIGN AND CONSTRUCTION OF FORCE MEASURING SYSTEM. 45
3.7.1 Development of Collar System. 45
3.7.2 Development of Modular Force Cell System. 46
3.7.3 Gauging and Calibration of Gauge Boxes. 48
3.8 EXPERIMENTAL PROCEDURES. 50
3.9 INITIAL TESTING OF THE MEASURING SYSTEM. 52
3.10 CORRECTION OF MEASURED FORCES AND MOMENTS. 53
3.13 CONCLUDING REMARKS. 55

4. RESULTS OF SEGMENTED MODEL EXPERIMENTS. 56
4.1 INTRODUCTION. 56
4.2 ADJUSTMENT OF EXPERIMENTAL DATA. 56
4.3 COMPARISON OF FORCES AND MOMENT ESTIMATES. 59
4.4 COMPARISON FOR FITTED DERIVATIVE VALUES. 60
4.5 SEGMENTAL FORCE AND MOMENT DERIVATIVES. 67
4.5.1 British Bombardier Conventional Stern. 68
4.5.2 British Bombardier Conventional Stern (no skeg) 69
4.5.3 British Bombardier Conventional Stern (no skeg with plate) 70
4.5.4 British Bombardier Pram Stern (with skeg) 71
4.5.5 British Bombardier Pram Stern (no skeg) 72
4.5.6 Elliptic Hull Form (with skeg) 73
4.5.7 Elliptic Hull Form (no skeg) 74

4.5.8 Appropriate Linear Fitting. 75
4.6 EFFECT OF VORTICES ON GOODNESS OF FIT. 76
4.7 CONCLUDING REMARKS. 78

5. DISCUSSION OF SEGMENTED MODEL EXPERIMENTS. 79
5.1 INTRODUCTION. 79
5.2 COMPARISON OF EXPERIMENTAL RESULTS WITH SLENDER-BODY THEORY. .. .79
5.3 COMPARISON OF EXPERIMENTAL RESULTS WITH GENERALISED SLENDER-BODY THEORY. 81
5.4 CONCLUSIONS. 85

6. SEMI-EMPIRICAL ESTIMATION OF LINEAR HYDRODYNAMIC MANOEUVRING DERIVATIVES. 87
6.1 INTRODUCTION. 87
6.2 DEVELOPMENT OF SEMI-EMPIRICAL METHODS. 88
6.3 REGRESSION THEORY. 93
6.4 DATA. 96
6.5 NON-DIMENSIONALISATION OF DERIVATIVES. 97
6.6 RE-ANALYSIS OF PREVIOUS EQUATIONS. 98
6.7 VORTEX INFLUENCE THEORY. 100
6.7.1 An Appropriate Form for I_H. 100
6.7.2 Regression for Velocity Derivatives. 105
6.8 T-SPACE. 108
7.2 CONCLUSIONS. 110

7. CONCLUSIONS. 112
7.1 CONCLUDING DISCUSSION. 112
7.2 CONCLUSIONS. 110
7.3 FURTHER WORK. 119

APPENDIX A1 – CORRECTION OF MEASURED FORCES AND MOMENTS

References

List of Figures

2.1 Co-ordinate System.

2.2 Double Body Mirrored in the Waterplane.

2.3 Comparison of Experimental and Slender-Body Theory Predictions of Linear Velocity Derivatives for the British Bombardier.

2.4 Position of Vortices Around an Arbitrary Section With and Without Sway Velocity.

2.5 Displacement of Vortices due to Pure Sway.

2.6 Displacement of Vortices due to Pure Yaw.

2.7 Comparison of Experimental and Generalised Slender-Body Theory Predictions of Y'_v for the British Bombardier.

2.8 Comparison of Experimental and Generalised Slender-Body Theory Predictions of N'_v Linear Velocity Derivatives for the British Bombardier.

3.1 Simplified Representation of Vortex Generation from U-Stern, Extreme V-Form and Pram Stern Hulls as Measured by Kuiper [32].

3.2 Rotation of Conventional Stern Geometry to Create Pram Stern Geometry.

3.3 Body Plan of British Bombardier with Conventional Stern.

3.4 GRP Model of British Bombardier with Conventional Stern.

3.5 Body Plan of British Bombardier with Modified Conventional Stern.

3.6 Centreline Profile of British Bombardier with Modified Conventional Stern.

3.7 GRP Model of British Bombardier with Modified Conventional Stern.

3.8 Body Plan of British Bombardier with Pram Stern.

3.9 Centreline Profile of British Bombardier with Pram Stern.

3.10 GRP Model of British Bombardier with Pram Stern.

3.11 Body Plan of Elliptic Hull Form.

3.12 Centreline Profile of Elliptic Hull Form.

3.13 GRP Model of Elliptic Hull Form.

3.14 Internal Structure of GRP Models at the Bow.

3.15 Internal Structure of GRP Models at the Stern.

3.16 Foam Strip at the Interface of Model Sections.

3.17 Assembled Rail Measured System.

3.18 Force Gauge Boxes and Rail Attachment.

3.19 Force Gauge Box with Details of Strain Gauges.

3.20 Deformations of Force Gauges.

4.1 Plot of Non-Dimensionalised Side Force, Y', Measured for Segments 1 to 1 of the Elliptic (With Plate) Model.

4.2 Plot of Non-Dimensionalised Side Force, Y', Measured for Segments 1 to 5 of the Elliptic (With Plate) Model.

4.3 Comparison of Non-Dimensionalised Side Force, Y', Measured for the British Bombardier Complete Model.

4.4 Comparison of Non-Dimensionalised Yaw Moment, N', Measured for the British Bombardier Complete Model.

4.5 Comparison of Non-Dimensionalised Side Force, Y', Measured for the British Bombardier Model up to Station 4.0.

4.6 Comparison of Non-Dimensionalised Yaw Moment, N', Measured for the British Bombardier Model up to Station 4.0.

5.1 British Bombardier Conventional Stern. Longitudinal Variation of Y_{vT}' and C_H. Second Order Fit.

5.2 British Bombardier Conventional Stern. Longitudinal Variation of N_{vT}' and C_H. Second Order Fit.

5.3 British Bombardier Conventional Stern (no skeg). Longitudinal Variation of Y_{vT}' and C_H. Second Order Fit.

5.4 British Bombardier Conventional Stern (no skeg). Longitudinal Variation of N_{vT}' and C_H. Second Order Fit.

5.5 British Bombardier Conventional Stern (no skeg with plate). Longitudinal Variation of Y_{vT}' and C_H. Second Order Fit.

5.6 British Bombardier Conventional Stern (no skeg with plate). Longitudinal Variation of N_{vT}' and C_H. Second Order Fit.

5.7 British Bombardier Pram Stern (with skeg). Longitudinal Variation of Y_{vT}' and C_H. Second Order Fit.

5.8 British Bombardier Pram Stern (with skeg). Longitudinal Variation of N_{vT}' and C_H. Second Order Fit.

5.9 British Bombardier Pram Stern (no skeg). Longitudinal Variation of Y_{vT}' and C_H. Second Order Fit.

5.10 British Bombardier Pram Stern (no skeg). Longitudinal Variation of N_{vT}' and C_H. Second Order Fit.

5.11 Elliptic Hull Form (with skeg). Longitudinal Variation of Y_{vT}' and C_H. Second Order Fit.

5.12 Elliptic Hull Form (no skeg). Longitudinal Variation of N_{vT}' and C_H. Second Order Fit.

5.13 Elliptic Hull Form (no skeg). Longitudinal Variation of Y_{vT}' and C_H. Second Order Fit.

5.14 Elliptic Hull Form (no skeg). Longitudinal Variation of N_{vT}' and C_H. Second Order Fit.

5.15 Differenced Experimental Measurements with Second and Third Order Fit for the British Bombardier Conventional Stern with and without Skeg.

5.16 Calculated Added Mass and Experimental Measurements for the British Bombardier Conventional Stern with and without Skeg.

5.17 Calculated Added Mass and Experimental Measurements for the British Bombardier Conventional Stern and Skeg Replaced with a Plate.

5.18 Calculated Added Mass and Experimental Measurements for the British Bombardier Conventional Stern with Skeg Replaced with a Plate and No Skeg.

5.19 Calculated Added Mass and Experimental Measurements for the British Bombardier Conventional Stern and Pram Stern.

5.20 Calculated Added Mass and Experimental Measurements for the British Bombardier Pram Stern with and without Skeg.

5.21 Calculated Added Mass and Experimental Measurements for the Elliptic Hull Form with and without Skeg.

5.22 Absolute Comparison of Experimental and Theoretical Sway Force Derivatives for 7 Model Variations. Bombardier Conventional (conv), Without Skeg (cons), With Plate (consp), Bombardier Pram (ps), Without Skeg (pns), Ellipse (ell), Without Skeg (ellns).

5.23 Percentage Comparison of Experimental and Theoretical Sway Force Derivatives for 7 Model Variations. Bombardier Conventional (conv), Without Skeg (cons), With Plate (consp), Bombardier Pram (ps), Without Skeg (pns), Ellipse (ell), Without Skeg (ellns).

6.1 Simplified Stern Shape.

6.2 Scatter Plot of Y_{vT}' Using New Predictors.

6.3 Scatter Plot of Y_{rT}' Using New Predictors.

6.4 Scatter Plot of N_{vT}' Using New Predictors.

6.5 Scatter Plot of N_{rT}' Using New Predictors.

6.6 Scatter Plot of Y_{vT}' Using T-Space Predictors.

6.7 Scatter Plot of Y_{rT}' Using T-Space Predictors.

6.8 Scatter Plot of N_{vT}' Using T-Space Predictors.

6.9 Scatter Plot of N_{rT}' Using T-Space Predictors.

A1.1 Applied Loads on Idealised Measurement System.

A1.2 Force Gauge Box Idealised to a Pair of Parallel Thin Flexures.

A1.3 Strain Gauge Bridge Considered as an Element of a Thin Walled Tube.

A1.4 Experimental Set-up for Testing Three Strain Gauge Box.

A1.5 Postulated Effect of Shear and Torsional Loads on the Gauge Box.

A1.6 Four Quadrant Test Space.

List of Tables

3.1 Principal Particulars of the British Bombardier with Conventional Stern.

3.2 Principal Particulars of the British Bombardier with Modified Conventional Stern.

3.3 Principal Particulars of the British Bombardier with Pram Stern.

3.4 Principal Particulars of the Elliptic Hull Form.

3.5 Summary of Experimental Programme.

3.6 Comparison of Measured and Applied Load on the Rail Apparatus.

4.1 Experimental Results for Elliptic Form (With Plate), Segments 1 to 1.

4.2 Experimental Results for Elliptic Form (With Plate), Segments 1 to 2.

4.3 Experimental Results for Elliptic Form (With Plate), Segments 1 to 3.

4.4 Experimental Results for Elliptic Form (With Plate), Segments 1 to 4.

4.5 Experimental Results for Elliptic Form (With Plate), Segments 1 to 5.

4.6 Experimental Results for Elliptic Form (No Skeg), Segments 1 to 1.

4.7 Experimental Results for Elliptic Form (No Skeg), Segments 1 to 2.

4.8 Experimental Results for Elliptic Form (No Skeg), Segments 1 to 3.

4.9 Experimental Results for Elliptic Form (No Skeg), Segments 1 to 4.

4.10 Experimental Results for Elliptic Form (No Skeg), Segments 1 to 5.

4.11 Experimental Results for British Bombardier Conventional Stern, Segments 1 to 1

4.12 Experimental Results for British Bombardier Conventional Stern, Segments 1 to 2

4.13 Experimental Results for British Bombardier Conventional Stern, Segments 1 to 3

4.14 Experimental Results for British Bombardier Conventional Stern, Segments 1 to 4

4.15 Experimental Results for British Bombardier Conventional Stern, Segments 1 to 5

4.16 Experimental Results for British Bombardier Conventional Stern, Segments 1 to 6

4.17 Experimental Results for British Bombardier Conventional Stern (No Skeg), Segments 1 to 3.

4.18 Experimental Results for British Bombardier Conventional Stern (No Skeg), Segments 1 to 4.

4.19 Experimental Results for British Bombardier Conventional Stern (No Skeg), Segments 1 to 5.

4.20 Experimental Results for British Bombardier Conventional Stern (No Skeg), Segments 1 to 6.

4.21 Experimental Results for British Bombardier Conventional Stern (No Skeg With Plate), Segments 1 to 3.

4.22 Experimental Results for British Bombardier Conventional Stern (No Skeg With Plate), Segments 1 to 4.

4.23 Experimental Results for British Bombardier Conventional Stern (No Skeg With Plate), Segments 1 to 5.

4.24 Experimental Results for British Bombardier Conventional Stern (No Skeg With Plate), Segments 1 to 6.

4.25 Experimental Results for British Bombardier Pram Stern (With Plate), Segments 1 to 1.

4.26 Experimental Results for British Bombardier Pram Stern (With Plate), Segments 1 to 2.

4.27 Experimental Results for British Bombardier Pram Stern (With Plate), Segments 1 to 3.

4.28 Experimental Results for British Bombardier Pram Stern (With Plate), Segments 1 to 4.

4.29 Experimental Results for British Bombardier Pram Stern (With Plate), Segments 1 to 5.

4.30 Experimental Results for British Bombardier Pram Stern (With Plate), Segments 1 to 6.

4.31 Experimental Results for British Bombardier Pram Stern (No Skeg), Segments 1 to 1.

4.32 Experimental Results for British Bombardier Pram Stern (No Skeg), Segments 1 to 2.

4.33 Experimental Results for British Bombardier Pram Stern (No Skeg), Segments 1 to 3.

4.34 Experimental Results for British Bombardier Pram Stern (No Skeg), Segments 1 to 4.

4.35 Experimental Results for British Bombardier Pram Stern (No Skeg), Segments 1 to 5.

4.36 Experimental Results for British Bombardier Pram Stern (No Skeg), Segments 1 to 6.

4.37 Newcastle. Sway Force Derivatives for British Bombardier with Conventional Stern Using a Second Order Fit.

4.38 Clarke and Hearn [204]. Sway Force Derivatives for British Bombardier with Conventional Stern Using a Second Order Fit.

4.39 Newcastle. Sway Force Derivatives for British Bombardier with Conventional Stern Using a Third Order Fit.

4.40 Clarke and Hearn [204]. Sway Force Derivatives for British Bombardier with Conventional Stern Using a Third Order Fit.

4.41 Newcastle. Yaw Moment Derivatives for British Bombardier with Conventional Stern Using a Second Order Fit.

4.42 Clarke and Hearn [204]. Yaw Moment Derivatives for British Bombardier with Conventional Stern Using a Second Order Fit.

4.43 Linear Force and Moment Sway Derivatives for British Bombardier with Conventional Stern Using a Second Order Fit.

4.44 Linear Force and Moment Sway Derivatives for British Bombardier with Conventional Stern Using a Third Order Fit.

4.45 Linear Force and Moment Sway Derivatives for British Bombardier with Conventional Stern (no skeg) Using a Second Order Fit.

4.46 Linear Force and Moment Sway Derivatives for British Bombardier with Conventional Stern (no skeg) Using a Third Order Fit.

4.47 Linear Force and Moment Sway Derivatives for British Bombardier with Conventional Stern (no skeg with plate) Using a Second Order Fit.

4.48 Linear Force and Moment Sway Derivatives for British Bombardier with Conventional Stern (no skeg with plate) Using a Third Order Fit.

4.49 Linear Force and Moment Sway Derivatives for British Bombardier with Pram Stern (with skeg) Using a Second Order Fit.

4.50 Linear Force and Moment Sway Derivatives for British Bombardier with Pram Stern (with skeg) Using a Third Order Fit.

4.51 Linear Force and Moment Sway Derivatives for British Bombardier with Pram Stern (no skeg) Using a Second Order Fit.

4.52 Linear Force and Moment Sway Derivatives for British Bombardier with Pram Stern (no skeg) Using a Third Order Fit.

4.53 Linear Force and Moment Sway Derivatives for Elliptic Hull Form (with skeg) Using a Second Order Fit.

4.54 Linear Force and Moment Sway Derivatives for Elliptic Hull Form (with skeg) Using a Third Order Fit.

4.55 Linear Force and Moment Sway Derivatives for Elliptic Hull Form (no skeg) Using a Second Order Fit.

4.56 Linear Force and Moment Sway Derivatives for Elliptic Hull Form (no skeg) Using a Third Order Fit.

4.57 Linear Force and Moment Sway Derivatives for British Bombardier Conventional Using a First Order Fit.

4.58 Linear Force and Moment Sway Derivatives for British Bombardier Pram (with skeg) Using a First Order Fit.

4.59 Clarke and Hearn [204]. Standard Error, s, on Fitting of Sway Force Experimental Data for British Bombardier with Conventional Stern.

4.60 Newcastle. Standard Error, s, on Fitting of Sway Force Experimental Data for British Bombardier with Conventional Stern.

6.1 Summary Statistics for the Hull Only Data Subset.

6.2 Comparison of Statistical Measures of Merit for Re-Appraised Regressions Equations.

6.3 Comparison of Statistical Measures of Merit for Regressions Equations With New Predictors.

6.4 Comparison of Statistical Measures of Merit for Regressions Equations With T-Space Predictors.

Nomenclature

The following list of symbols adheres as closely as possible to the recommendations of the Twelfth International Towing Tank Conference, Rome, 1969.

A	Coefficient having different values in the following equations.
A_n	Coefficient having different values and dimensions.
A_{-n}	Coefficient in Laurent series.
A_η	Inertia coefficient.
AR	Hull apparent aspect ratio.
a	Constant in equation, or Ellipse semi-major axis, or Parameter in z-plane.
B	Ship beam, or Coefficient having different values, or Limit of integration at bow.
b	Parameter in z-plane.
C	Origin of axes, or Periphery of section in contour integration.
C_B	Hull block coefficient.
C_H	Horizontal added mass coefficient at zero frequency.
C_L	Lift coefficient.
c	Parameter in hypergeometric series, or Parameter in transformation.
f	Mathematical function.
G	Centre of gravity.
g	Acceleration due to gravity.
I	Integral having different values in equations, or Finite impulse.
I_H	Vortex influence coefficient.
I_X, I_Y, I_Z	Moment of inertia about x, y or z axes.
I_{XY}, I_{YZ}, I_{ZX}	Product of inertia about xy, yz or zx axes.

I'_Z	Dimensionless moment of inertia about x axes, equation.
i	Imaginary number $\sqrt{-1}$, or integer, equation.
J	Real part of finite impulse.
j	Integer in equation
K	Imaginary part of finite impulse.
KE	Kinetic energy
k	Dimensionless location of turning pivot point, or Radius of gyration, or General integer, or Parameter in equation.
k'	Dimensionless radius of gyration.
L	Ship length between perpendiculars.
m	Mass of ship, or Integer.
m'	Dimensionless mass of ship.
N	Hydrodynamic yawing moment (inferred to be about z axis).
N'	Dimensionless hydrodynamic yawing moment, normalised using initial velocity U_0.
n	Outward normal from hull, or General integer.
O	Position of the origin of the frame of reference
p	Roll angular velocity about x axis.
q	Pitch angular velocity about y axis.
R	Radius of circle in ζ-plane, or Coefficient in equation.
r	Yaw angular velocity about z axis, or Radius of circle in ζ-plane, or General integer, or Bilge radius.
$\dot{r}$	Yaw angular acceleration about z axis.
r'	Dimensionless yaw angular velocity about z axis, normalised using initial velocity U_0.

$\dot{r}'$	Dimensionless yaw angular acceleration about z axis, normalised using initial velocity U_0.
S	Area of cross section, or Surface area of hull, or Limit of integration at stern.
s	Laplace operator, or Propeller slip, or Dimensionless time, or Distance around periphery of hull cross-section, or Length of line in complex z-plane.
T	Ship draught, or Fluid kinetic energy.
T_B	Ship draught at bow.
T_M	Ship mean draught.
T_S	Ship draught at stern.
t	Time, or Complex variable.
U	Absolute velocity of ship.
U_0	Initial steady state absolute velocity of ship.
u	Surge linear velocity along x axis, or Intermediate variable used in integration.
$\dot{u}$	Surge linear acceleration along x axis.
u'	Dimensionless surge velocity along x axis, normalised using initial velocity U_0.
$\dot{u}'$	Dimensionless surge acceleration along x axis, normalised using initial velocity U_0.
v	Sway linear velocity along y axis.
$\dot{v}$	Sway linear acceleration along y axis.
v'	Dimensionless sway linear velocity along y axis, normalised by initial velocity U_0.
w	Heave linear velocity along z axis, or Complex variable.

$\dot{w}$	Heave linear acceleration along z axis.
X	Longitudinal hydrodynamic force along x axis, or Distance of hull section from midship position.
X'	Dimensionless hydrodynamic longitudinal force, normalised using the initial velocity U_0, or Dimensionless distance of hull section from midship position.
X'_0	Dimensionless centre of action of side force.
X'_B	Dimensionless bow co-ordinate.
X'_P	Dimensionless co-ordinate of centre of lateral area of hull.
X'_S	Dimensionless stern co-ordinate.
x	Longitudinal axis pointing forward in ship.
x_G	Longitudinal distance of centre of gravity from midship position.
x'_G	Dimensionless longitudinal distance of centre of gravity from midship position.
x_p	Distance of pivot point in turn ahead of midship position.
Y	Lateral hydrodynamic force along y axis.
Y'	Dimensionless hydrodynamic lateral force, normalised using the initial velocity U_0.
y	Lateral axis pointing to starboard in ship.
y_G	Lateral distance of centre of gravity from midship position.
Z	Vertical hydrodynamic force acting along z axis, or Coefficient in equation.
z	Vertical axis pointing downwards in ship, or Complex number.
z_G	Vertical distance of centre of gravity from midship position.
α	Parameter having different values in equations.
β	Parameter in equation, or Ship drift angle, or Dimension of rectangle in complex t – plane, equation
Γ	Circulation
γ	Parameter in equation
Δ	Displacement weight of ship, or

	Incremental change of a variable.
∇	Displacement volume of ship.
δ	Angular deflection of rudder.
ξ	Complex number, or
	Vertical co-ordinate in cross-flow plane.
η	Horizontal co-ordinate in cross-flow plane.
ϑ	Angle of pitch about y axis, or
	Angular parameter in transformation.
λ	Constant parameter having different values in equations.
ρ	Mass density of fluid.
σ	Parameter having different values in equations.
Φ	Potential function.
Φ_1, Φ_2, Φ_3	Components of potential function in x, y and z directions, equation.
ϕ	Angle of roll about x axis, or
	Fluid velocity potential.
ϕ_v	Potential due to unit sway velocity in the cross-flow plane.
ψ	Angle of yaw, or heading change about z axis, or
	Fluid stream function.

Use of Superscripts and subscripts

The foregoing list of symbols can be used in conjunction with a superscript, which indicates that the variable has been non-dimensionalised.

$$' \left(X' = \frac{X}{\frac{1}{2}\rho U_0{}^2 L^2} \right)$$

Use is made in this thesis of operational subscripts following force and moment symbols, indicating a partial derivative of that force or moment with respect to the subscript. These subscripts usually denote the linear and angular velocities and accelerations, or rudder deflection. Higher order combinations of subscripts refer to higher order partial derivatives.

The subscripts used are,

$$u,\ \dot{u},\ v,\ \dot{v},\ r,\ \dot{r},\ \delta.$$

It is possible to introduce a dimensionless form for these partial derivatives. Some typical examples follow for the purpose of indicating the dimensionless form. Firstly, the linear terms,

N_r $N_r' = \frac{N_r}{\frac{1}{2}\rho U_0 L^4}$, partial derivative $\frac{\partial N}{\partial r}$

$N_{\dot{r}}$ $N_{\dot{r}}' = \frac{N_{\dot{r}}}{\frac{1}{2}\rho L^5}$, partial derivative $\frac{\partial N}{\partial \dot{r}}$

N_v $N_v' = \frac{N_v}{\frac{1}{2}\rho U_0 L^3}$, partial derivative $\frac{\partial N}{\partial v}$

$N_{\dot{v}}$ $N_{\dot{v}}' = \frac{N_{\dot{v}}}{\frac{1}{2}\rho L^4}$, partial derivative $\frac{\partial N}{\partial \dot{v}}$

Y_r $Y_r' = \frac{Y_r}{\frac{1}{2}\rho U_0 L^3}$, partial derivative $\frac{\partial Y}{\partial r}$

$Y_{\dot{r}}$ $Y_{\dot{r}}' = \frac{Y_{\dot{r}}}{\frac{1}{2}\rho L^4}$, partial derivative $\frac{\partial Y}{\partial \dot{r}}$

Y_v $Y_v' = \frac{Y_v}{\frac{1}{2}\rho U_0 L^2}$, partial derivative $\frac{\partial Y}{\partial v}$

$Y_{\dot{v}}$ $Y_{\dot{v}}' = \frac{Y_{\dot{v}}}{\frac{1}{2}\rho L^3}$, partial derivative $\frac{\partial Y}{\partial \dot{v}}$

N_δ $N_\delta' = \frac{N_\delta}{\frac{1}{2}\rho U_0{}^2 L^3}$, partial derivative $\frac{\partial N}{\partial \delta}$

Y_δ $Y_\delta' = \frac{Y_\delta}{\frac{1}{2}\rho U_0{}^2 L^2}$, partial derivative $\frac{\partial Y}{\partial \delta}$.

Several of the non-linear terms are,

$Y_{v|v|}$ $Y_{v|v|}' = \frac{Y_{v|v|}}{\frac{1}{2}\rho L^2}$, partial derivative $\frac{\partial^2 Y}{\partial v \partial |v|}$

$Y_{r|v|}$ $Y_{r|v|}' = \frac{Y_{r|v|}}{\frac{1}{2}\rho L^2}$, partial derivative $\frac{\partial^2 Y}{\partial r \partial |v|}$

$Y_{r|r|}$ $Y_{r|r|}' = \frac{Y_{r|r|}}{\frac{1}{2}\rho L^2}$, partial derivative $\frac{\partial^2 Y}{\partial r \partial |r|}$

Y_{vvv} $Y_{vvv}' = \frac{Y_{vvv} U_0}{\frac{1}{2}\rho L^2}$, partial derivative $\frac{\partial^3 Y}{\partial v^3}$

Y_{vvr}	$Y_{vvr}' = \frac{Y_{vvr}U_0}{\frac{1}{2}\rho L^3}$,	partial derivative $\frac{\partial^3 Y}{\partial v^2 \partial r}$
Y_{vrr}	$Y_{vrr}' = \frac{Y_{vrr}U_0}{\frac{1}{2}\rho L^4}$,	partial derivative $\frac{\partial^3 Y}{\partial v \partial r^2}$
Y_{rrr}	$Y_{rrr}' = \frac{Y_{rrr}U_0}{\frac{1}{2}\rho L^5}$,	partial derivative $\frac{\partial^3 Y}{\partial r^3}$
$Y_{\delta\delta\delta}$	$Y_{\delta\delta\delta}' = \frac{Y_{\delta\delta\delta}}{\frac{1}{2}\rho U_0{}^2 L^2}$,	partial derivative $\frac{\partial^3 Y}{\partial \delta^3}$

All the other partial derivative subscript variations are easily found by analogy with the above definitions.

In the slender-body formulation, the appearance of the factor $-\pi(T/L)^2$ is essentially an artifice. The presentation of equations involving the hydrodynamic derivatives may be simplified considerably by non-dimensionalising the ITTC derivatives by $-\pi(T/L)^2$.

Thus we can define a set of linear velocity derivatives as follows,

$$Y_{vT}' = Y_v' \Big/ -\pi(T/L)^2$$

$$Y_{rT}' = Y_r' \Big/ -\pi(T/L)^2$$

$$N_{vT}' = N_v' \Big/ -\pi(T/L)^2$$

$$N_{rT}' = N_r' \Big/ -\pi(T/L)^2$$

1. INTRODUCTION

This thesis is concerned with the manoeuvring of surface ships. The study of the motions of a surface ship has historically been divided into seakeeping and manoeuvring. Seakeeping is concerned with the behaviour of a ship under the action of waves with rudder fixed. Manoeuvring is concerned with the motions of a ship arising from the action of the rudder in calm water. This distinction is now somewhat more blurred as the effects of rough seas on manoeuvring have been considered.

1.1 LITERATURE REVIEW

The requirement to define the manoeuvring characteristics of a ship lead to the development of a set of standard manoeuvres referred to as the turning circle, the zigzag manoeuvre and the spiral. These manoeuvres can be carried out in full-scale sea trials or in free running model tests.

The turning circle manoeuvre is a means of studying the response of the ship to the deflection of the rudder to establish a steady turn. The manoeuvre is started at a steady speed on a straight course. The turn is initiated by applying a rudder deflection to a given angle.

The advance, the transfer and the tactical diameter of the resulting turn define the turning performance of the ship. The advance is defined as the distance travelled in the initial direction by the time the ship's heading has changed by 90 degrees. The transfer is the lateral distance travelled at the 90 degree heading point. The tactical diameter is the lateral distance travelled by the time the ship has changed heading by 180 degrees. The turning circle provides information about the ship's turning in equilibrium conditions.

The zigzag manoeuvre is a means of examining the transient response of a ship and provides information on the ship's yaw checking and directional stability characteristics. Proposed by Kempf [1], this manoeuvre is started in the straight-ahead

condition. The rudder is deflected at the maximum rate to a preselected angle, of say 20 degrees to port. The rudder angle is held until the heading of the ship changes by a preselected angle, usually the same as the rudder angle. Once this heading has been achieved, the rudder angle is reversed to 20 degrees to starboard. At this point the heading of the ship typically continues to increase to port, before gradually reversing to the new rudder angle. The maximum heading attained is known as the first overshoot. The cycle of rudder changes is usually repeated to obtain second and third overshoot angles.

Other important measures of manoeuvrability arising from the zig-zag are the time for the ship's heading to reach the first rudder angle and the time for the first heading to be checked, this latter measure is known as the reach.

The spiral manoeuvre was originally devised by Dieudonne [2], and is a means of testing the directional stability of ships. The manoeuvre is initiated in the steady condition by applying a rudder of say 15 degrees to port. This rudder angle is held until the ship's rate of change of yaw becomes steady. At this point the rudder is reduced by say 5 degrees and again the steady yaw rate is established. This procedure is repeated until the rudder angle of 20 degrees to starboard is achieved and then reversed until the original rudder angle is returned. For a stable ship, plots of yaw rate against rudder angle produces a curve that passes through the origin. For an unstable ship the plot results in a hysteresis loop about the origin.

A means of removing this area of hysteresis for an unstable ship was devised by Bech [3]. This modification to the spiral manoeuvre involves actively steering the vessel to maintain a selected rate of yaw. In this way the plots of yaw rate against rudder angle can be uniquely defined near the origin for directionally unstable ships.

Davidson and Schiff gave the first theoretical description of ship manoeuvring in 1946 [4]. In this treatment the ship was assumed to move with three degrees of freedom. First order derivatives and perturbation velocities represented the forces and moments of the resulting equations of motion. This approach followed existing aeronautical theory and is thought to have been originated by Bryan in 1911 [5].

The ship is initially assumed to be continuing on a straight course at a steady speed. This state is then disturbed or perturbed and the ship is subject to additional perturbation forces and moments. It is assumed that the perturbation velocities and accelerations at some instant uniquely determine the forces and moments at that instant. This quasi-steady assumption neglects any fluid memory effect. Bishop et al [6] considered the validity of this approach, given that the generally ponderous progress of a ship generates vortices at the bow, at some instant, that may affect the stern region at some later time. It has been determined by Burcher [7], that for gentle motions (i.e. where the ship is subject to forces and moments induced by its own rudder) the quasi-steady assumption is satisfactory.

It was found that, while the linear representation of hydrodynamic forces and moments, used by Davidson and Schiff [4], are adequate for analysing the turning ability of directionally stable ships, linear theory fails to predict accurately the characteristics of tight manoeuvres.

A non-linear description of the hydrodynamic forces and moments was offered by Abkowitz [8]. This approach again considered the forces and moments to be perturbations occurring due to the ship's motion being disturbed. The forces and moments were represented by a Taylor Series expansion about the steady state. Using experimental evidence and considerations of symmetry, the number of terms in the expansion can be reduced to include first and third order terms for the lateral force and moment and first and second order terms for the longitudinal force.

An alternative representation for the third order terms for the non-linear components is the use of a second order absolute-square term in the lateral force and moment equations. This representation was proposed by Gertler [9] and Goodman [10] and has its origins in submarine simulation.

The choice of third order or absolute-square terms can be made on the basis of 'goodness of fit' to the experimental force and moment data. Proponents of the absolute-square representation also suggest that the second order term is more

meaningful hydrodynamically as it is of the form of a cross flow drag. It is interesting that the most appropriate mathematical formulation for the non-linear hydrodynamic forces and moments is still an ongoing debate. Some consideration of this problem has been given in the analysis of experimental data in Chapter 5 of this thesis.

Today a number of mathematical models, based on Newton's laws of motion, have been put forward to describe the manoeuvring motion of ships. As well as the effects of hull, propulsion and steering mechanism, these models variously incorporate the effects of shallow water, confined channels, wind and waves. Hagen has given a catalogue of mathematical models used in ship manoeuvring [11].

For a given ship, synthesising the track of a manoeuvre, by simulation, is reduced to the problem of determining the constant terms or hydrodynamic derivatives in the forces and moment equations. There are three methods of determining these values: experimentally, theoretically or by using semi-empirical methods, which are based on analysis of experimental data.

Sway force and moment derivatives were first determined by towing models down existing towing tanks [12] at various drift angles. Yaw force and moment derivatives being measured by Rotating Arm Mechanism (RAM) test basins, in which models can be constrained to move in a circular path [13]. RAM test facilities were costly and Gertler [14] and Goodman [15] developed an alternative approach. The Planar Motion Mechanism (PMM) apparatus use conventional towing facilities and can be used to determine both sway and yaw forces and moments by oscillating the model during the passage down the tank. Actuators attached at the bow and the stern of the model can be oscillated in phase, out of phase or with same specific phase difference. This allows the model to be given a pure sway motion, pure yaw motion or a combination of both to yield both the sway and yaw moment derivatives. These techniques are now very well developed and can be used to accurately determine the hydrodynamic derivatives.

Whilst experimental methods are successful, they are costly and time consuming and this has made it desirable to develop theoretical means to determine the hydrodynamic derivatives from consideration of hull geometry. The requirement to assess the

manoeuvrability of a ship during the early design stages, in order to satisfy the criteria given in the recently adapted IMO Resolution A. 751(18), has given new impetus to these theoretical developments.

Several attempts have been made to develop theoretical means of estimating the hydrodynamic force and moment derivatives. These attempts are largely based on making the analogy of a ship to a low aspect ratio wing turned on its side. In this treatment it is usual for the free surface to be assumed to be a solid boundary, an assumption that has been shown by Tsakonas [16] to be satisfactory for low Froude Numbers. The solid boundary assumption effectively doubles the aspect ratio of the wing; two times the draught in the case of a ship. Inoue [17] and Brard [18] derived expressions for the linear derivatives of ships hull by considering the circulation shed by a low aspect ratio wing. Other methods have been based on the low aspect ratio wing theory of Jones [19].

Fedyaevsky and Sobolev [20], [21] used the Jones theory to develop a two-dimensional strip method. This method treated the hull sections as having an added mass coefficient, $C_H = 1.0$, which likens the hull to a thin flat plate or a ship with elliptic sections. In these methods the hydrodynamic derivatives can be obtained by integrating along the hull. For an ellipsoid, the side force contributions of the fore and aft sections, when integrating from bow to stern, cancel each other out. This leaves a resulting moment without any side forces, which is the Munk moment [22].

In order to obtain a non-zero side force, the integration along the hull must be terminated at some point ahead of the stern. Fedyaevsky and Soblev followed Jones and chose the section of maximum added mass. While this approach is satisfactory for wings, it has been shown by Clarke [23] that the hull sections beyond the section of maximum added mass do make a contribution.

Jacobs [24], [25] also used Jones theory as a start point, but, in addition to obtaining derivatives for the bare hull, Jacobs also argued that the skeg could be treated as an additional component and added the derivatives for the skeg to those obtained for the

bare hull. Jacobs also made use of a number of semi-empirical factors in deriving equations for the hydrodynamic derivatives.

In an attempt to improve upon these methods, Clarke [23], went back to the Jones low aspect ratio wing theory, but instead of idealising the hull to a thin flat plate, used results from missile aerodynamics [26, 27] to include the section shapes of ships in a slender body approach. This method was tested experimentally using a segmented model to estimate the hydrodynamic derivatives along the length of the ship [23]. The theoretical predictions show good agreement at the bow and in the mid-body of the ship, but were discrepant towards the stern.

More recently Clarke and Hearn [28] postulated that this discrepancy in the experimental and slender-body theoretical results was due to the neglect of the effects of stern vortices on the hydrodynamic derivatives. Clarke and Hearn [28] were able to account for the effects of these vortices by including a vortex influence within the framework of the slender body representation. Comparison of the predictions of this generalised slender-body theory with vortex measuring experiments on the British Bombardier and Mariner hullforms [29, 30] showed excellent agreement for these conventional hullforms.

Recent developments in hull geometry have lead to the pram stern design, which has improved resistance and propulsion efficiency over conventional stern shapes. However, it has been found that these pram sterns can exhibit poor course keeping qualities.

This lack of directional stability has been explained in part by Clarke [31], who used the original slender-body theory to show that a skeg was less effective in generating a stabilising side force when mounted under a square section stern (simplified from a pram stern) compared with being mounted under a triangular section (simplified from a conventional stern).

One of the reasons for the increased propulsive efficiency of the pram stern is due to the reduced vortices generated by the hull in the region of propeller. Kuiper [32] compared

conventional, triangular and pram sterns and showed that, the strength of the vortices generated by the pram stern were not only less than a conventional, but may in fact rotate in the opposite direction to those generated by the conventional stern.

1.2 START POINT AND AIMS OF THIS THESIS

The start point and impetus for the work presented in this thesis are three separate developments.

- Clarke and Hearn [28] generalised slender-body theory accurately predicts the distributed force and moment derivatives along conventional hullforms by including the effects of stern vortices.

- Pram stern hullforms have been found to be less directionally stable than conventional forms, an observation that can only in part be explained by examining the effectiveness of fins attached to different body section shapes.

- Experimental work by Kuiper [32] has shown that the pram stern hullforms generate vortices that rotate in the opposite sense to those generated by conventional stern hullforms.

The Kuiper work is very interesting and significant because the generalised slender-body theory [28] predicts not only that the influence of vortices on the hydrodynamic derivatives is related to the strength of the vortices, but also that the additive effect in conventional hulls would be reversed if the vortices rotated in the opposite direction. The effect of the vortices in the pram stern would therefore be to further reduce the stabilising side force derivative.

If the generalised slender-body theory is correct, then it should be possible to devise an experiment that demonstrates that the above observations by measuring the manoeuvring derivatives on a series of different hullforms. These hullforms represent the transition from conventional hullform to pram stern hullform.

Initially, two options were considered. Carry out experiments on a 'blank canvas' hullform, e.g. a V-form from Kuiper [32] and generate vortices of different strength and sense of direction. Alternatively, create a series of hullforms. The later choice was taken so that the results could be more easily validated against existing results.

A series of 7 hullforms were created based on the British Bombardier conventional stern, an elliptic form (which replaces the V-form of Kuiper) and a British Bombardier with a pram stern. In each case, the sterns were made in sections so that the distributed force and moment measurements could be obtained. The experimental design was such that results of hullforms could be differenced to determine the effects of the stern vortices.

As will be shown later, the results of the experiments support the hypothesis that the inclusion of stern vortices in the slender-body theory accurately predicts the manoeuvring derivatives for conventional and pram stern hullforms and explains the poor directional stability of the latter. However, it has been found that, for severely up-swept stern hullforms, the generalised slender-body theory is not a compete description. In these cases boundary layer phenomena need also to be considered.

The generalised slender-body theory approach requires a knowledge of the start point, strength and path of stern vortices for estimating the hydrodynamic derivatives. As yet, there is no theoretical means of determining these inputs.

Previously, the need to estimate hydrodynamic derivatives by means other than experimentally has lead to development of a variety of semi-empirical approaches. In general, these methods have used existing theoretical representations to guide the formulation of predictors, which are then used in regression analysis to derive equations for the hydrodynamic derivatives. These predictors are combinations of the primary ship geometric parameters of length, beam, draft and block coefficient.

Wagner Smitt [33] and Norribin [34] used Jones low aspect ratio wing theory and a set of experimental data to obtain regression equations for the linear velocity derivatives. Inoue [35] used the results of a coherent set of experimental data from a variety of

model types and derived regression equations for the hydrodynamic derivatives. These results were used as part of a modular manoeuvring prediction method. Clarke [36] and later Ankudinov [37] used the form of the original slender-body theory [23], to obtain regression equations for velocity and acceleration derivatives.

In each of these studies, the resulting equations were unable to completely explain all the variability in the data.

A second aim of the thesis was to determine whether the new physical insight provided by the generalised slender body theory could be used to enhance semi-empirical estimates of the manoeuvring derivatives.

1.3 Chapter Layout

The first part of this thesis (Chapters 2 – 5) is concerned with an experimental examination of the generalised slender body theory, with particular interest in the effect of stern vortices in the pram stern hull. The aim was to test the predictions of the generalised slender-body theory by examining a variety of hull forms with different stern shapes, graduating from the conventional stern to an elliptic form to the pram stern.

In Chapter 2, the theoretical treatment of a surface ship using slender body theory and originated by Clarke [23] is overviewed. An outline description of how Clarke and Hearn [28] then generalised this theory to include the effects of stern vortices is given. The supporting experimental evidence provided by Clarke [23] and Glasgow [29], [30] is then reviewed.

In Chapter 3, a review is given of some of the predictions of the generalised slender body theory and additional work on the influence of stern shape and hull form on the manoeuvring characteristics of a vessel is also considered. An experimental design to directly test some of these theoretical predictions is describe in detail. Particular attention is paid to the measures taken to ensure control over the experimental results.

In Chapter 4, the results of the experiment are presented with a description of the treatment of the force and moment data to determine the manoeuvring derivatives. A number of comparisons are made with published experimental data to estimate the accuracy of the results. In Chapter 5, the experimental results are compared with the theoretical prediction and conclusions are drawn about the generalised slender body theory and other aspects of the experimental findings.

In Chapter 6, development of semi-empirical methods is reviewed and a re-analysis of an approach by Clarke [36] is carried out using data available in the open literature. The results of this re-analysis are then used as a baseline for evaluating two further semi-empirical approaches presented here. The first is a simple polynomial regression that uses a different non-dimensionalising factor to form predictor variables. The second is a set of equations that encapsulate the physical insight provided by the generalised slender body theory and recognise the interdependency of the linear velocity derivatives.

Finally, in Chapter 7, the work is summarised and the main findings and limitations of the analysis are highlighted in the context of current developments. Some ideas for furthering the work presented here are set out.

2. THEORETICAL DETERMINATION OF HYDRODYNAMIC DERIVATIVES USING SLENDER-BODY THEORY

2.1 INTRODUCTION

The manoeuvring characteristic of a ship may be determined by the solution of a set of equations of motion. The forces and moments applied to the hull during the manoeuvre are expanded in a perturbation series about a steady state and the coefficients that arise are known as the hydrodynamic manoeuvring derivatives. The simulation of ship manoeuvres is therefore dependant on being able to determine values for these derivatives for a given hull form.

The derivatives have previously been obtained through experimental methods, but this is expensive and time consuming and can only be done at a late design stage when many aspects of the design are fixed. Alternatively, the derivatives may be estimated from regression equations, which are themselves based on a body of experimentally derived derivatives values. Typically these regression equations are functions of length, beam, draught and block coefficient and therefore are insensitive to relatively large changes in local geometry. This point is illustrated by the very great difference in the manoeuvring characteristics of modern pram sterns when compared with older forms such as the British Bombardier, despite the similarity of the global geometric parameters.

It has always been desirable to be able to calculate the manoeuvring derivatives theoretically, but with recent developments in IMO regulation regarding determination of manoeuvring characteristics at an early design stage, this need has become some what more pressing. No satisfactory theoretical method for calculating the manoeuvring derivatives has yet been found.

The slender-body theory approach developed by Clarke [23], was adapted from missile aerodynamics [26, 27] and relies on obtaining the horizontal added mass of ship sections and integrating along the length of the ship to obtain expressions for the

derivatives. This method was tested by comparing theoretical and experimentally derived the force and moment distributions along a segmented model [23] and showed good agreement for the fore-body of the hull: although discrepancy between theory and experiment was apparent towards the stern of the hulls.

More recently, a large scale experimental and theoretical programme has continued this work. Clarke and Hearn [28] postulated that the discrepancy in the experimental and theoretical results was due to the neglect of the effects of stern vortices on the manoeuvring derivatives. Experimental investigations [29], [30] have shown that the proposed vortices are indeed generated on the bilges and pass near the stern skeg area of the British Bombardier and Mariner hull forms. The strength and position of these vortices was measured at two stations in the stern region. The original slender-body theory was extended to include the effects of stern vortices on the linear force and moment derivatives. The inclusion of the vortex effects was accomplished using the conformal mapping techniques used in the slender-body theory and was therefore consistent with the earlier approach. It was now possible to calculate the linear manoeuvring derivatives for a given hull form including the effects of stern vortices, although the position and strength of these vortices had to be determined experimentally.

The vortex measurements obtained for the British Bombardier and Mariner models were used in conjunction with the earlier segmented model results which have been completely re-analysed to test the vortex influence addition to the slender-body theory. It was demonstrated that the discrepancy between slender-body theory and experimental results at the aft end of the hull forms was due to the influence of stern vortices.

The next three chapters of this thesis are concerned with the experimental examination of the vortex influence theory. In the following chapter, the theoretical arguments of Clarke in developing first the slender-body theory and later including the addition of the vortex influence are overviewed. The basic assumptions of the theory have been highlighted and a review of the existing experimental evidence has been given.

2.2 CO-ORDINATE SYSTEM

In general, the motion of a ship can be described in six degrees of freedom, surge, sway, heave, roll, pitch and yaw. The study of manoeuvring is usually confined to the determination of planar components of surge, sway and yaw.

A fixed Cartesian co-ordinate system that moves relative to some global frame can be used in the complete description of a ship's motion. A body fixed frame is most convenient when describing hydrodynamic forces and moments and advantage is taken of P-S symmetry. The position of the frame origin $O(0,0,0)$ is equidistant between perpendiculars and on a line defined by the intersection of the centreline plane and the waterline plane. The frame is right-handed, with x being forward along the longitudinal plane of symmetry, and parallel to the water surface, the y axis is to starboard and the z axis is vertically downward in the plane of symmetry. The centre of gravity is a point $G(x_G, y_G, z_G)$.

Figure 2.1 shows the coordinate reference frame with corresponding translational and rotational velocities u, v, w and p, q, r about the x, y, z axes respectively.

2.3 SLENDER-BODY THEORY

The following section describes the background to and the earlier application of slender-body theory to ship manoeuvring problems.

No complete theory exists that can satisfactorily predict the forces and moments acting on an arbitrary shaped body in a real fluid. Lamb [38] solved the problem for an arbitrary shaped body in an ideal inviscid fluid, and showed with one exception, that the forces and moments act on the body exist only in accelerated flow. The exception to this condition was the moment due to sway velocity, which later became known as the Munk moment after his work in the field of airship aerodynamics [22].

The prediction of forces and moments acting in steady, unaccelerated flow has met with considerable success in two areas. In aerodynamics, the geometry of the bodies of

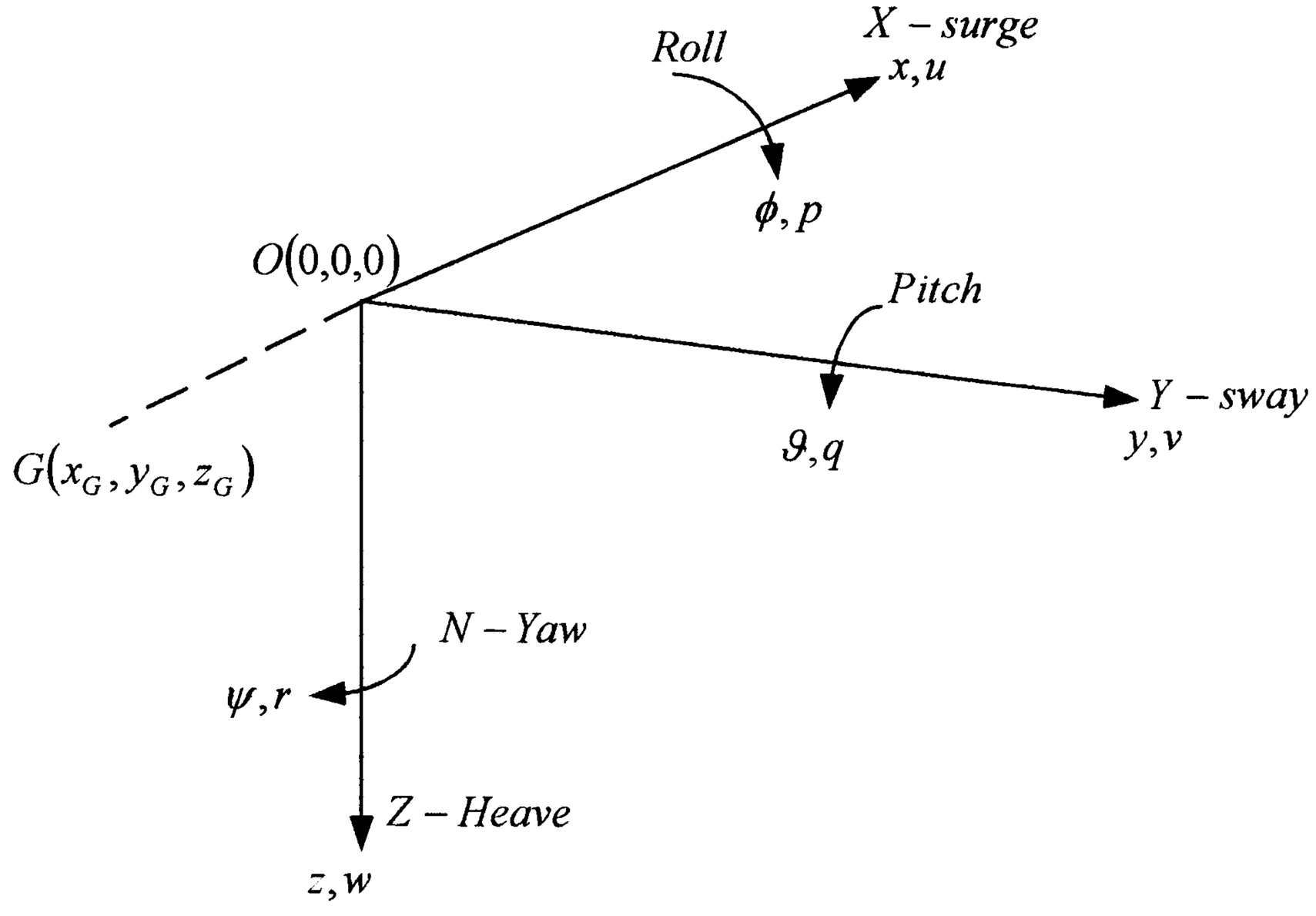

Figure 2.1 Co-ordinate System

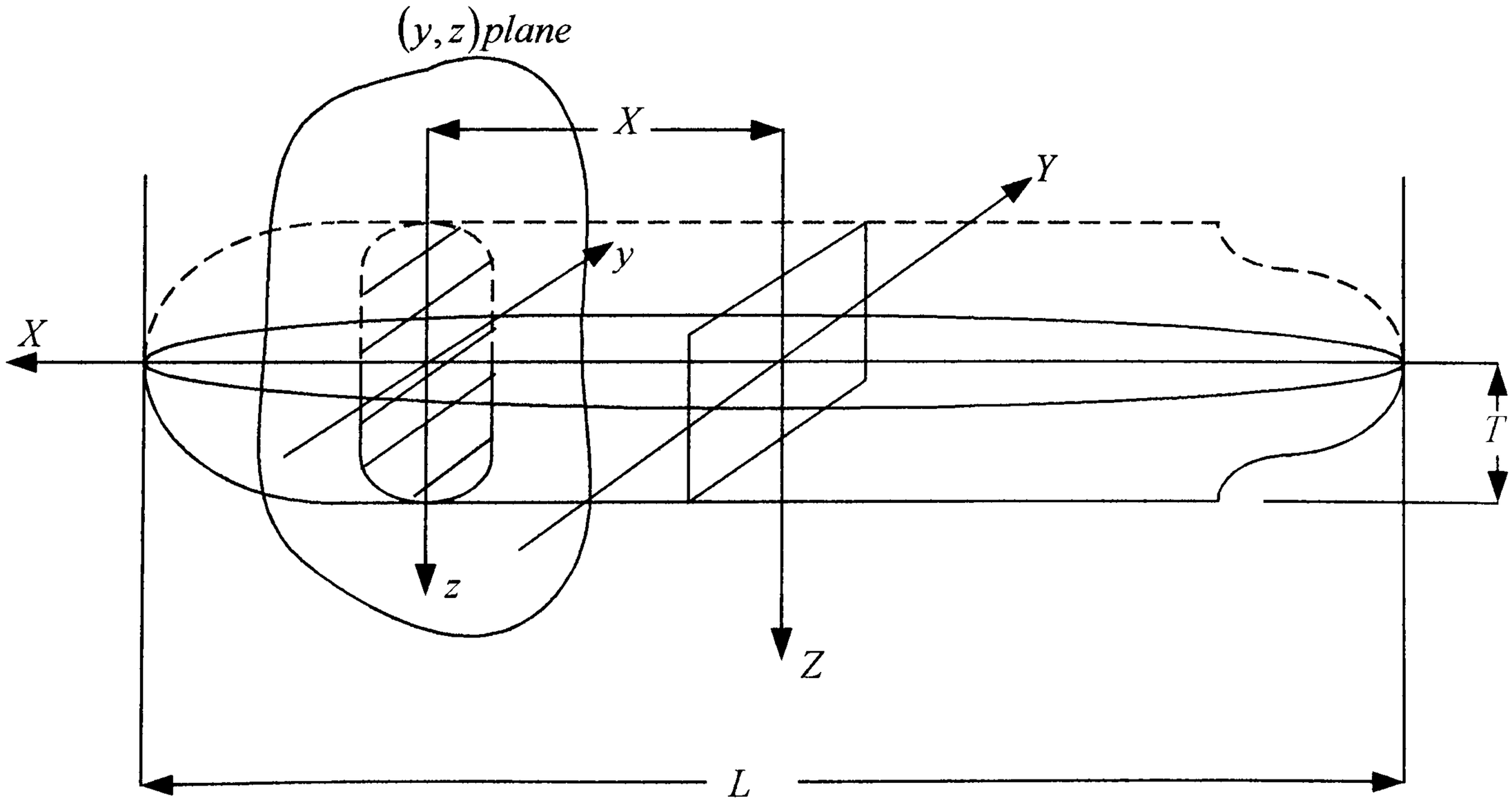

Figure 2.2 Double Body Mirrored in the Waterplane

interest are fitted with wings and fins. Forces and moments acting on these surfaces can be calculated in steady unaccelerated flow because the solution is dominated by the circulation potentials introduced to satisfy the Kutta [39] condition at the trailing edge of such surfaces.

The other area that may be analysed successfully is the calculation of forces and moments on slender bodies. These are elongated in the direction of motion and terminate at a blunt base from which the flow separates and forms a stream surface behind the body of the same cross section as the base. The flow around such a body is approximated by considering the geometry to be divided into a series of cross-flow planes, thus simplifying the three dimensional problem into the solution of a number of two dimensional problems. This approach was first used by Munk [22] to calculate the forces and moments acting on a turning airship. He found that the transverse forces on each two-dimensional section were directly related to the added mass of that section in its transverse plane.

The slender-body theory was developed and extended in application to the consideration of long slender wings of triangular plan form by Jones [19] in 1946 and included results for supersonic and subsonic flight. Ward [40], included the effects of winged bodies and further developments came from various workers such as Bryson [26] to deal with unsteady effects, allowing the direct calculation of stability derivatives.

The wide ranging application of slender-body theory which can be used in modelling both subsonic and supersonic flow regimes was made possible by the work of Tsien [41] in 1938. He discovered that the approach adopted by Munk could be used unchanged, to analyse flow around inclined pointed projectiles at supersonic speeds. This remarkable result means that the great wealth of data available from the development of missile theory by Bryson [26] and others can be applied to ship hydrodynamics.

The application of slender-body theory to calculation of forces and moments on ship hulls was first described by Fedyaevsky and Sobolev [20]. In this work the added mass

of each cross-flow plane was taken as unity and, in line with Jones [19], the body was terminated at the point of greatest cross section for the purposes of force and moment calculation.

The early development of a slender-body approach to the manoeuvring of ship hulls by Clarke [23] overcame these restrictions by using the concept of mirror imaging the submerged part of the hull in the waterplane to convert the problem from one in a semi-infinite domain to an infinite domain. In so doing, the full range of results by Bryson [42] could be brought to bear without modification, on the ship manoeuvring problem. Experimental justification for the use of the mirror image method in ship manoeuvring problems is given by Tsakonas [16], and shows that the approach is valid for low Froude numbers.

2.3.1 Development of the Slender-Body Strip Method

The ship hull and it's mirror image about the water plane form a single body which exists in an infinite fluid which is stationary at infinity, Figure 2.2. The body is constrained to move in that horizontal (x,y) plane and therefore only sway and yawing motions are considered.

Consider the flow in an arbitrary shaped two-dimensional (y,z) plane, which passes down the body from bow to stern at a translational velocity U along the X axis. It is assumed that the potential in this (y,z) plane depends only on the lateral velocity of that shaded cross-section in the Y direction, at the instant under consideration.

The body is constrained to sway and yaw motion, so the total lateral velocity of a given (y,z) plane can be expressed in terms of yaw velocity and sway velocity,

$$V = v + rX . \tag{2.1}$$

Following Kirchoff [43], the potential in the (y,z) plane can be expressed in terms of the total lateral velocity and the potential due to unit velocity,

$$\Phi = V\phi_v . \tag{2.2}$$

Lamb [38] gives an expression for the hydrodynamic side force in terms of the kinetic energy. In turn, the kinetic energy in the cross flow plane can be expressed in terms of a contour integral around the shaded section of the body. Clarke [23] used these results to derive expressions for the non-dimensionalised hydrodynamic side force and moment derivatives, Equations (2.3) and (2.4).

$$\frac{\partial Y'}{\partial \dot{v}'} = Y_{\dot{v}}{}' = -\int_S^B A_\eta dX'$$

$$\frac{\partial Y'}{\partial \dot{r}'} = Y_{\dot{r}}{}' = -\int_S^B X' A_\eta dX'$$

$$\frac{\partial Y'}{\partial v'} = Y_v{}' = \int_S^B \frac{\partial A_\eta}{\partial X'} dX'$$

$$\frac{\partial Y'}{\partial r'} = Y_r{}' = \int_S^B \left(A_\eta + X' \frac{\partial A_\eta}{\partial X'} \right) dX' \tag{2.3}$$

$$\frac{\partial N'}{\partial \dot{v}'} = N_{\dot{v}}{}' = -\int_S^B X' A_\eta dX'$$

$$\frac{\partial N'}{\partial \dot{r}'} = N_{\dot{r}}{}' = -\int_S^B X'^2 A_\eta dX'$$

$$\frac{\partial N'}{\partial v'} = N_v{}' = \int_S^B X' \frac{\partial A_\eta}{\partial X'} dX'$$

$$\frac{\partial N'}{\partial r'} = N_r{}' = \int_S^B \left(X' A_\eta + X'^2 \frac{\partial A_\eta}{\partial X'} \right) dX' \tag{2.4}$$

Equations (2.3) and (2.4) give the sway and yaw linear hydrodynamic derivatives in terms of inertia coefficient A_η, which is a function solely of section shape. By assuming that the ship hull could be mirrored in the waterplane it was possible to use the work of Bryson [42] which in turn depends on the work of Lamb [38] to express the sway and yaw linear hydrodynamic derivatives in terms of hull shape.

2.3.2 Inertial Coefficients

To obtain values for the required hydrodynamic derivatives it is necessary to evaluate the inertia coefficients. An expression for the inertia coefficient was found by Summers [44] and Bryson [42] using residue calculus,

$$A_\eta = \frac{\pi}{L^2}\left(2\left(r^2 - A_{-1}\right) - \frac{S}{\pi}\right). \tag{2.5}$$

Where r is the radius of the circle in the σ-plane, S is the area of the original shape in the x-plane and A_{-1} is the coefficient of σ^{-1} in the Laurent series. If the transformation from the x-plane to the σ-plane can be found, then the inertia coefficient could be determined.

Using Equation (2.5), the inertia coefficient for a circle of draught T and an elliptical section of semi-minor axis T is,

$$A_\eta = \frac{\pi T^2}{L^2}. \tag{2.6}$$

The horizontal added mass coefficient, C_H can now be defined as the ratio of the inertia coefficient for any general section to that of an elliptical section of the same draught.

$$C_H = \frac{1}{T^2}\left(2\left(r^2 - A_{-1}\right) - \frac{S}{\pi}\right) \tag{2.7}$$

The final adjustment necessary to the inertia coefficient is to calibrate the value at a given section to the local draught: this adjustment takes account of ship hulls that are, for example, trim by the stern. Thus,

$$A_\eta = \pi\left(\frac{T_m}{L}\right)^2\left(\frac{T}{T_m}\right)^2 C_H, \tag{2.8}$$

Where T_m is the mean draught.

In Equations (2.3) and (2.4) the velocity and acceleration force and moment derivatives were given in terms of the section inertia coefficient. It is now possible to restate these expressions in terms of the horizontal added mass coefficient by substituting Equation (2.8). The derivatives are grouped into acceleration derivatives,

$$Y'_{\dot{v}} = -\pi\left(\frac{T_m}{L}\right)^2 \int_S^B \left(\frac{T}{T_m}\right)^2 C_H dX' .$$

$$Y'_{\dot{r}} = -\pi\left(\frac{T_m}{L}\right)^2 \int_S^B \left(\frac{T}{T_m}\right)^2 C_H X' dX'$$

$$N'_{\dot{v}} = \pi\left(\frac{T_m}{L}\right)^2 \int_S^B \left(\frac{T}{T_m}\right)^2 C_H X' dX'$$

$$N'_{\dot{r}} = \pi\left(\frac{T_m}{L}\right)^2 \int_S^B \left(\frac{T}{T_m}\right)^2 C_H X'^2 dX' \tag{2.9}$$

and velocity derivatives, which after integration reduce to,

$$Y'_v = -\pi\left(\frac{T_m}{L}\right)^2 \left[\left(\frac{T}{T_m}\right)^2 C_H\right]_S^B .$$

$$Y_r' = -\pi\left(\frac{T_m}{L}\right)^2\left[\left(\frac{T}{T_m}\right)^2 C_H X'\right]_S^B$$

$$N_v' = \pi\left(\frac{T_m}{L}\right)^2\left\{\left[\left(\frac{T}{T_m}\right)^2 C_H X'\right]_S^B - \int_S^B \left(\frac{T}{T_m}\right)^2 C_H dX'\right\}$$

$$N_r' = \pi\left(\frac{T_m}{L}\right)^2\left\{\left[\left(\frac{T}{T_m}\right)^2 C_H X'^2\right]_S^B - \int_S^B \left(\frac{T}{T_m}\right)^2 C_H X' dX'\right\}. \tag{2.10}$$

The horizontal added mass coefficient was used because it has been calculated for many ship-like sections, in connection with ship vibration work. Some of these results will be discussed in the next section.

2.3.3 Added Mass Coefficients for Ship-Like Sections

The horizontal added mass coefficient can be determined for any arbitrary section by mapping that section onto a circle in another complex plane. The first term of that mapping function being used to obtain the required value of C_H. Any section, for which a mapping function can be found, the horizontal added mass can be determined.

A number of results presented in the earlier work could be used to find estimates for sectional added mass of most ship-like sections. Latterly, these methods have been largely overtaken by a numerical close fitting method.

One approach adopted by early aeronautics researchers to the mapping problem was to take a few terms in the Laurent series and map from the circle plane to the x-plane and see what shapes could be produced. Application of this approach to ship hull sections was first done by Lewis [45]. By manipulating a series containing only the coefficients A_{-1} and A_{-3} Lewis was able to generate a family of ship-like sections. The strength of this approach is that the hull sections are characterised by two parameters, the beam to draught ratio and the sectional area coefficient. Any hull section, which shares these

parameters with a given Lewis section, is assumed to have the same added mass coefficient.

2.4 EXPERIMENTAL EXAMINATION OF SLENDER-BODY THEORY

2.4.1 Development of Segmented Model Experiments

To test the validity of the predictions from the slender-body theory a joint experimental programme between BSRA and Admiralty Experiment Works (AEW), Haslar, Gosport was carried out at AEW. The results of the experiment and comparison with slender-body theory are reported by Clarke [23] and a full description of the experimental apparatus and facilities is given in a review of manoeuvring by Burcher [52].

The experiment used the rotating arm and oblique towing facilities to obtain the linear sway and yaw velocity derivatives for a 5.08 metre model of the British Bombardier. The model was tested without rudder or propeller fitted as the hydrodynamic forces on the hull only was sought. This hull form was chosen as it was thought no flow separation occurs at the stern end even for the bare hull.

The model was not simply tested in the normal way, but instead a method was devised that allowed the distribution of force and moment along the hull to be established. The model was divided longitudinally into 9 separate watertight segments. These segments were attached to a double rail system to form the complete hull shape, with the gaps in between the segments being filled with a foam strip. The double rail system consisted of two pairs of longitudinal rails running the full length of the model, the rails being joined by means of a pair of modular force gauges. The whole assembly was attached to the towing carriage via the outer rails.

2.4.2 Results of British Bombardier Segmented Model Tests

The data from the segmented model tests were adjusted and analysed in a similar way to that normally employed in model tests. The forces and moment data were plotted for the various sway and yaw velocities and drift angles to form carpet plots. There is a pair of these plots for each segment.

Before comparison of the experimentally determined force and moment distribution for the British Bombardier with slender-body predictions were made, the upper limit of integration on the derivative expressions must be relaxed. The integration of forces and moments was carried out from the bow to the longitudinal position corresponding to the end of each segment. The experimental and theoretically derived derivative values have been normalised with the universal multiplying factor, $\pi(T_m/L)^2$, arising from the slender-body theory. The resulting expressions for the acceleration and velocity sway and yaw derivatives become,

$$-\frac{Y'_{\dot{v}}}{\pi(T_m/L)^2} = \int_{X'_B}^{X'} \left(\frac{T}{T_m}\right)^2 C_H dX' .$$

$$-\frac{Y'_{\dot{r}}}{\pi(T_m/L)^2} = \frac{N'_{\dot{v}}}{\pi(T_m/L)^2} = \int_{X'_B}^{X'} \left(\frac{T}{T_m}\right)^2 C_H X' dX'$$

$$-\frac{N'_{\dot{r}}}{\pi(T_m/L)^2} = \int_{X'_B}^{X'} \left(\frac{T}{T_m}\right)^2 C_H X'^2 dX'$$

$$-\frac{Y'_{v}}{\pi(T_m/L)^2} = \left[\left(\frac{T}{T_m}\right)^2 C_H\right]_{X'} .$$

$$-\frac{Y'_{r}}{\pi(T_m/L)^2} = \left[\left(\frac{T}{T_m}\right)^2 C_H X'\right]_{X'}$$

$$-\frac{N'_{v}}{\pi(T_m/L)^2} = \left[\left(\frac{T}{T_m}\right)^2 C_H X'\right]_{X'} - \int_{X'_B}^{X'} \left(\frac{T}{T_m}\right)^2 C_H dX'$$

$$-\frac{N'_{r}}{\pi(T_m/L)^2} = \left[\left(\frac{T}{T_m}\right)^2 C_H X'^2\right]_{X'} - \int_{X'_B}^{X'} \left(\frac{T}{T_m}\right)^2 C_H X' dX' . \qquad (2.11)$$

Theoretical analysis of the British Bombardier used both Lewis section and Schwarz-Christoffel mapping techniques to evaluate the force and moment derivative distributions. At the bow, the assumption made was that,

$$\left[\left(\frac{T}{T_m}\right)^2 C_H\right]_{BOW} = 0. \tag{2.12}$$

It was argued that setting the added mass of the bow section to zero plausibly reflected the physical reality at a point in which the flow around the body must be three dimensional and therefore violate the basic assumptions of the slender-body theory.

Comparison of the sway and yaw velocity derivatives from segmented model tests and the slender-body predictions given by Clarke [51] are reproduced in Figures 2.3. It can be observed that there is agreement between theory and experiment for the bow to some point around Station 2. However, from there to the stern of the vessel the results diverge.

In a previous attempt to apply slender-body theory to the problem, Fedyaevsky and Sobolev [20] followed the work of Jones [19] and assumed the existence of a separation sheet which is generated at the point on the body with the greatest sectional area coefficient. Examining the results of the model tests it can be seen that the derivative values continue to vary along the length of the hull past the mid-body section. This means that the flow does not separate at the mid-body section.

One explanation of the divergence of the theoretical and experimental results is that the slender-body theory takes no account of the growth of the boundary layer along the length of the hull. The effect of the boundary layer is to increase the apparent draught of the section with a corresponding increase in local added mass. However, this effect is not large enough to explain the magnitude of the discrepancy observed in the Y_v' value at the stern end.

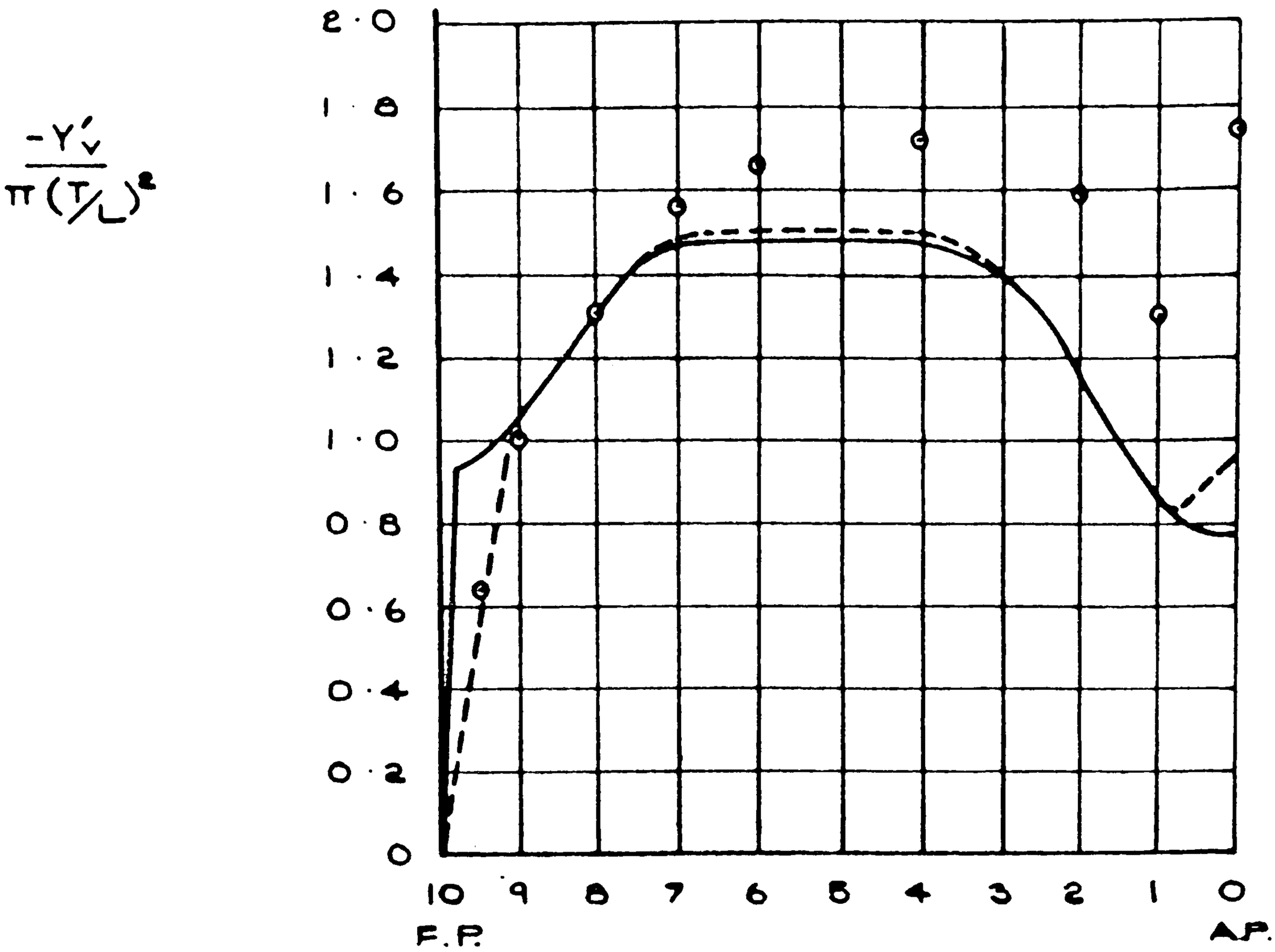

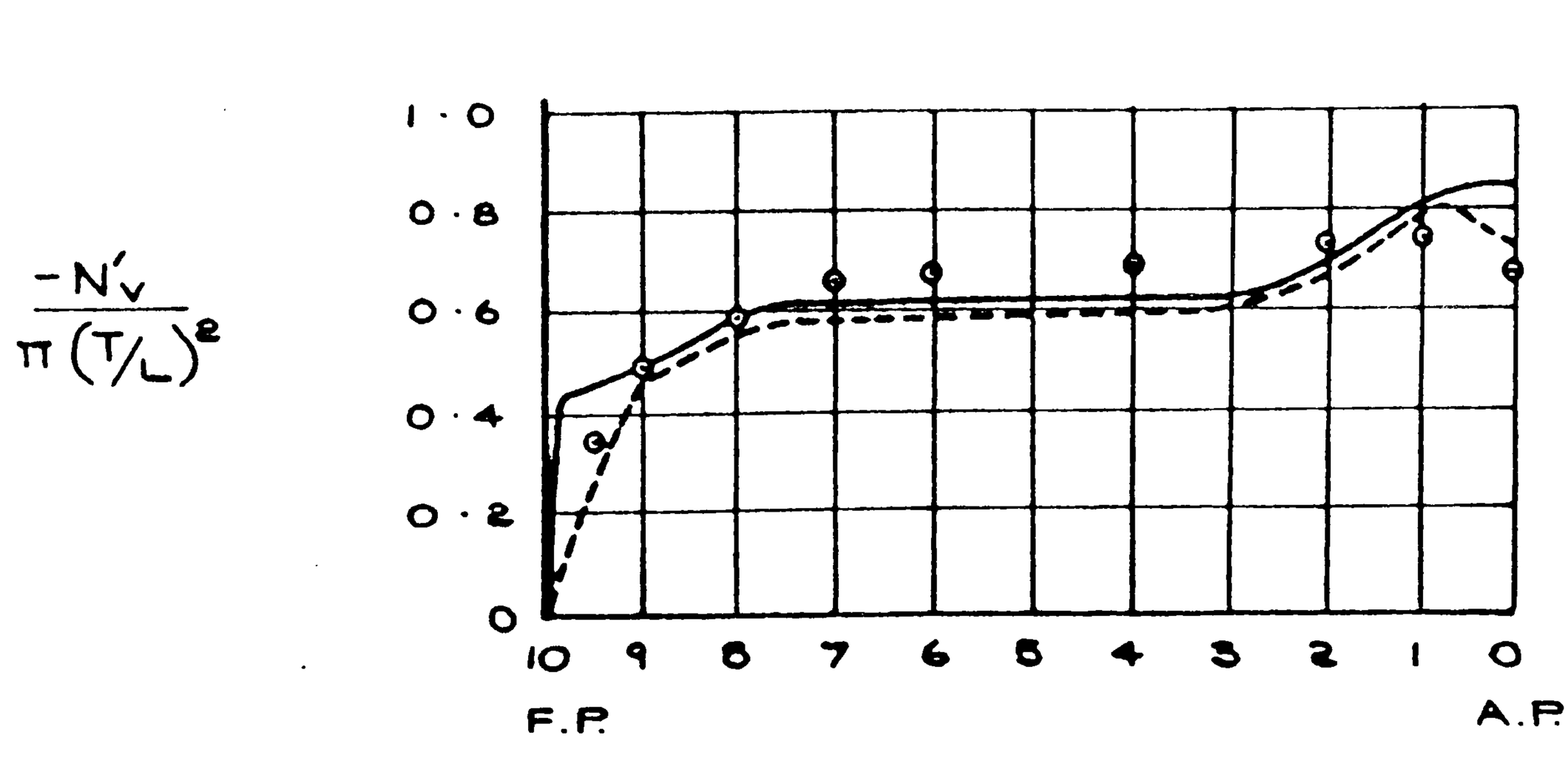

⊙ EXPERIMENTAL VALUES

—— THEORETICAL VARIATION USING LEWIS FORMS

--- THEORETICAL VARIATION USING SCHWARZ-CHRISTOFFEL METHODS

Figure 2.3 Comparison of Experimental and Slender-Body Theory Predictions of Linear Velocity Derivatives for the British Bombardier

2.5 VORTEX INFLUENCE THEORY

More recently [28], it was postulated that the short comings of the theoretical method were due to the neglect of stern vortices which are generated at the bilges and are transported up past the skeg. An extensive experimental and theoretical investigation of ship manoeuvring has been conducted to examine this proposition [28].

The slender-body theory has now been extended to include the effect of stern vortices. The remainder of this chapter rehearses the arguments put forward by Clarke and Hearn [28] to develop a method of evaluating the effect of stern vortices on ship manoeuvring and considers the experimental evidence to support this hypothesis.

The ship hull is mirrored in the water plane to convert the semi-infinite fluid domain to an infinite fluid domain problem, this double body being constrained to move in the (x,y) plane, illustrated in Figure 2.2.

It has been postulated that the presence of stern vortices affects the hydrodynamic derivatives and so these must be included in the derivative expressions. Consider a (y,z) plane passing down the body at a speed U. Any vortices generated on the body must pass through the translating (y,z) plane and are external to the two-dimensional body section. For an arbitrary section, the position of the vortices is given in Figure 2.4. If the body is moving ahead at a constant speed, the port and starboard vortices give rise to an impulse, I in the cross-flow plane, which is identical to zero. If the vessel has a yaw or sway velocity, then there will be a finite cross-flow velocity which will vary along the length of the body. This cross-flow will displace the vortices to some new asymmetric distribution about the section, Figure 2.4. The new position of the vortices gives rise to a finite impulse in the cross-flow plane.

The arguments to obtain expressions for the effect of these vortices on the linear derivatives is similar to that set out in Section 2.3.1 to obtain the slender-body results. The total lateral velocity in the (y,z) plane is

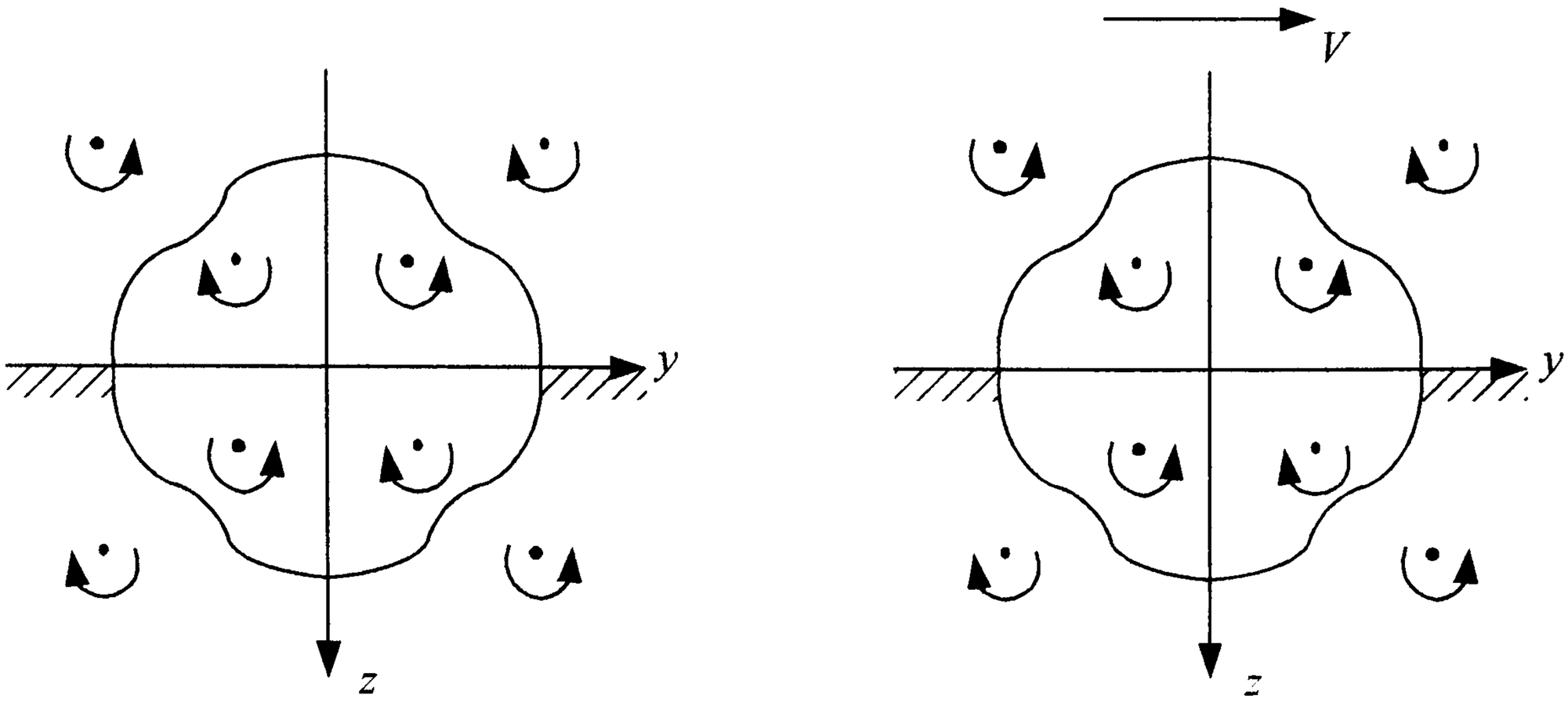

Figure 2.4 Position of Vortices Around an Arbitrary Section With and Without Sway Velocity

$$V = v + rX \,. \tag{2.13}$$

From Figure 2.4, the vortices are displaced from the original positions by the cross-flow velocity and this gives rise to a finite impulse, I. The impulse is taken to be proportional to V and dependent on the longitudinal position X,

$$I = \frac{\partial I(X)}{\partial V}.V \,. \tag{2.14}$$

The impulse results in a side force on the body. Using arguments similar to those used previously, a more general expression for force and moment derivatives, that includes the influence of vortices, can be derived.

$$\frac{Y'_{\dot{v}}}{-\pi\left(\frac{T}{L}\right)^2} = \int_S^B \left(C_H + I_H\right) dX'$$

$$\frac{Y'_{\dot{r}}}{-\pi\left(\frac{T}{L}\right)^2} = \frac{N'_{\dot{v}}}{-\pi\left(\frac{T}{L}\right)^2} = \int_S^B \left(C_H + I_H\right) X' dX'$$

$$\frac{N'_{\dot{r}}}{-\pi\left(\frac{T}{L}\right)^2} = \int_S^B \left(C_H + I_H\right) X'^2 dX' \tag{2.15}$$

$$\frac{Y'_{v}}{-\pi\left(\frac{T}{L}\right)^2} = -\left[C_H + I_H\right]_S^B$$

$$\frac{Y'_{r}}{-\pi\left(\frac{T}{L}\right)^2} = -\left[\left(C_H + I_H\right) X'\right]_S^B$$

$$\frac{N'_{v}}{-\pi\left(\frac{T}{L}\right)^2} = -\left[\left(C_H + I_H\right) X'\right]_S^B + \int_S^B \left(C_H + I_H\right) dX'$$

$$\frac{N'_{v}}{-\pi\left(\frac{T}{L}\right)^2} = -\left[\left(C_H + I_H\right) X'^2\right]_S^B + \int_S^B \left(C_H + I_H\right) X' dX' \tag{2.16}$$

2.5.1 Determination of the Vortex Influence Coefficient

In the slender-body theory it is normal to take the inertia coefficient A_η as,

$$A_\eta = \frac{\pi T^2}{L^2} C_H \tag{2.17}$$

where C_H is the zero frequency horizontal added mass coefficient. By analogy, Clarke and Hearn [28] define the vortex influence coefficient I_H as,

$$I_H = -\frac{1}{\pi\left(\frac{T}{L}\right)^2} \frac{\partial I'}{\partial V'} \tag{2.18}$$

If the vortices are assumed to be distributed symmetrically about the vertical axis, then $I_H = 0$. If there exists a finite fluid velocity in the cross-flow plane, then $I_H \neq 0$ because the displacement of the vortices gives rise to an impulse in the horizontal direction.

Writing $$I_H = -\frac{1}{\pi\left(\frac{T}{L}\right)^2} \frac{\partial I'}{\partial y'} \cdot \frac{\partial y'}{\partial V'}, \tag{2.19}$$

the vortex influence coefficient is defined as the product of the impulse position derivative $\partial I'/\partial y'$ and the position sway derivative, $\partial y'/\partial V'$, where y' is the non-dimensional lateral displacement of the vortices with respect to the body section. The problem is thus further decomposed into the determination of these two derivative coefficients.

2.5.2 Determination of the Impulse Position Derivative

The impulse position derivatives may be determined using conformal mapping techniques. The impulse exerted on a circular section by a system of vortices has been given by Milne-Thompson [49]. If we consider an arbitrary section in the x-plane with a pair of external vortices, these sections may be transform onto a circle of radius r in

some other complex σ plane. It is then a straightforward problem to construct a system of internal and external vortices to the circular section, which satisfy the various boundary conditions. From this start point the impulse due to lateral displacement of the external vortices can be derived in the circle plane. An expression for the impulse position derivative in the original x-plane can then be derived by numerical mapping methods.

2.5.3 Determination of the Position Sway Derivative

The position sway derivative $\partial y'/\partial V'$ relates the amount of lateral displacement y' of the vortices, with respect to the two dimensional body section, induced by the cross-flow velocity V' of the section. The vortices are generated at some longitudinal position on the body and are transported downstream. The total sway velocity within a particular cross-flow section is given by,

$$V = v + rX .$$

The motion of the vortices and consequently their position in subsequent cross-flow plane is dependent on the motion of the body. In pure sway, the flow in the cross-flow plane is constant in direction along the length of the hull, Figure 2.5. In pure yaw motion sections forward on the body have a flow into the body and those aft have flow away from the body, Figure 2.6. The position sway derivative is therefore dependent on the mode of motion and is determined differently for the sway and yaw derivatives.

Considering the position sway derivative for pure sway motion, yields the expression,

$$\left(\frac{dy'}{dV'}\right)_{r=0} = \frac{L'}{T'} X' \left(1 - \frac{X'_0}{X'}\right) \qquad (2.20)$$

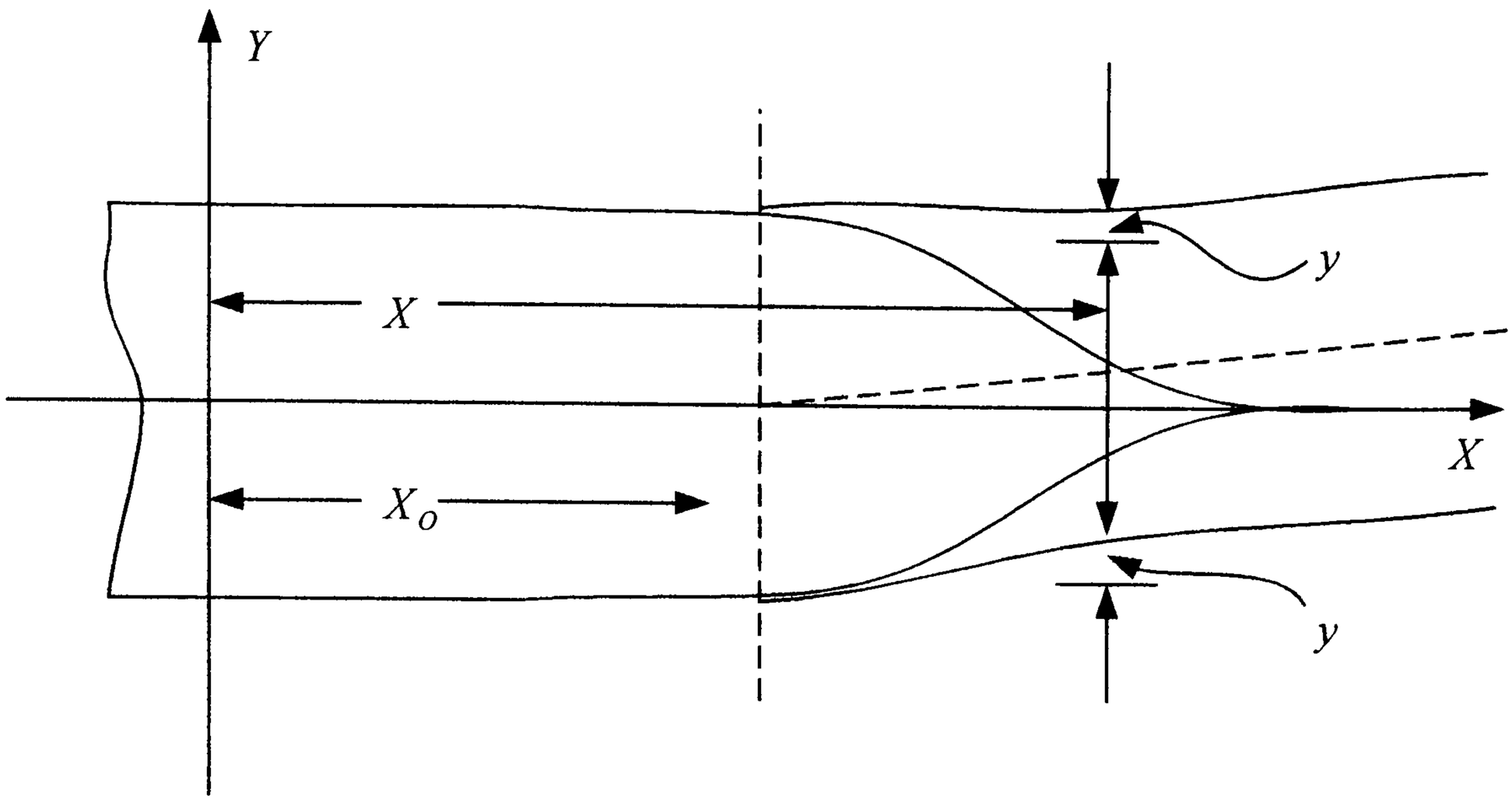

Figure 2.5 Displacement of Vortices due to Pure Sway

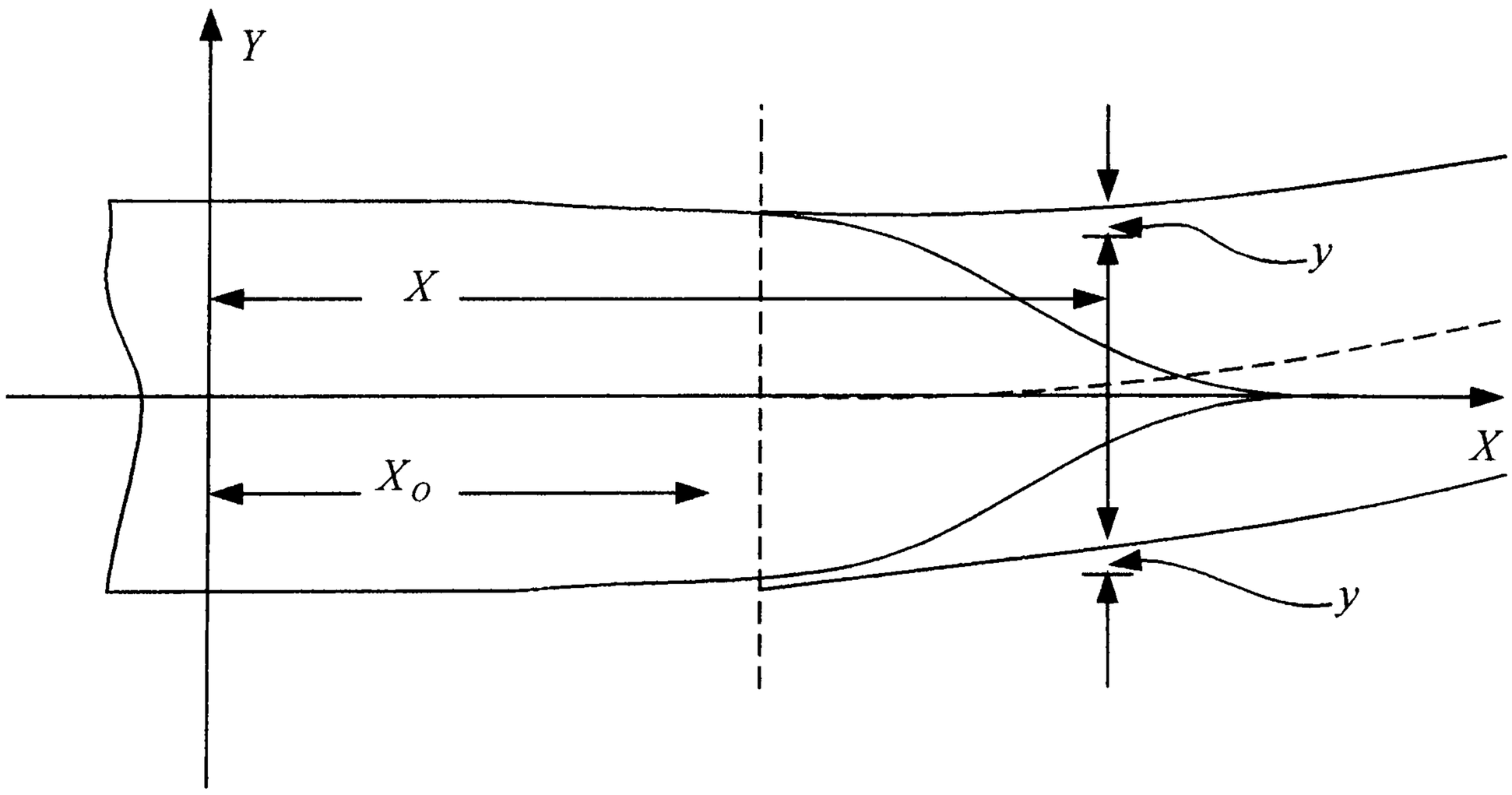

Figure 2.6 Displacement of Vortices due to Pure Yaw

Considering pure yaw motion, yields

$$\left(\frac{dy'}{dV'}\right)_{v=0} = \frac{dy'}{d(r'X')} = \frac{L'}{T'} X' \left[\frac{1-\left(\frac{X'_0}{X'}\right)^2}{3-\left(\frac{X'_0}{X'}\right)^2}\right]. \tag{2.21}$$

2.5.4 Evaluation of Impulse Position Derivatives by Numerical Mapping Methods

In the original slender-body theory, only horizontal added masses of the hull sections were required in determining the hydrodynamic derivatives. Lewis sections could be used, but these sections did not generally look like the required section, but had the same beam to draught ratio and sectional area coefficient. The result was a simple three parameter mapping with only the first coefficient of the series being used to obtain the added mass. If the vortex locations are to be mapped from one complex plane to another then, for an arbitrary section, this requires the use of and infinite Laurent series. In practise the transformation can be made to a tolerance with a truncated series.

The approach derived by Clarke to determine the impulse position derivative comes under the umbrella of 'close fitting' methods which were used extensively in sea keeping before the move towards solution of this type of problem with source distribution methods. Clarke and Hearn use a function minimisation method to map from a unit circle onto a section by progressively adjusting the values of the coefficients in the transformation series, such that the sum of squares of errors between the actual body co-ordinates and those derives from the transformation are minimised.

2.6 Experimental Examination of the Vortex Influence Theory

The generalised slender-body theory which includes the effects of stern vortices in the calculation of manoeuvring derivatives requires experimentally determined values for the strength and position of these stern vortices. In the original experimental testing of the slender-body theory [23], a series of segmented model tests were undertaken on the British Bombardier hull form in order to establish the distribution of the derivatives along the hull. A similar set of experiments were also carried out on the Mariner hull form [53].

To test the extended slender-body theory a number of steps were taken. The original experimental data for both the British Bombardier and the Mariner was re-analysed to remove any inconsistencies, and to estimate errors on the data points, with the final results being presented in non-dimensional form. Models of the British Bombardier and Mariner hull forms were constructed at Glasgow University [29] and oblique towing experiments undertaken to measure the strength and position of trailing vortices together with their start point.

The start point of the vortex is required to evaluate the position sway derivative. This point was determined for the British Bombardier and Mariner by injecting dye into the water at a convenient point on the hull and observing the subsequent vortex formation with a miniature underwater video camera. These tests had to be carried out at very slow speeds and the rate of the dye injection control in order to make the observations possible.

The strength and position of the stern vortices was measured at Stations 0.25 and 0.75 for the British Bombardier and Stations 19.5 and 18.5 in the case of the Mariner. Each station was divided into a matrix of measurement locations and the circulation at each of these positions was obtained using a probe with an unpitched propeller attached to the end. The speed of rotation of this propeller being recorded for a number of drift angles to port and starboard of the hull.

2.6.1 Comparison of Theory and Experimental for British Bombardier and Mariner Hull Forms

The vortex influence was calculated for the British Bombardier and Mariner models at the two stern stations measured. The added mass coefficient was calculated using the close fitting method. These theoretical calculations were then be compared with the re-analysed segmented model data. Note that in the Glasgow measurements of vorticity [30], only oblique towing tests could be carried and consequently only the sway force and moment derivatives can be considered.

The comparison of side force derivatives for the British Bombardier is illustrated in Figure 2.7. The distribution of sway force derivative with longitudinal position determined from the added mass only is shown as a solid line. Recalling that,

$$-\frac{Y_v'}{\pi(T/L)^2} = \left[C_H + I_H\right]_{STATION}.$$

The vortex addition to the sway force derivative is shown, at the two stern stations measured, by stars. Further it was argued by Clarke and Hearn [28] that the variation of the vortex influence coefficient I_H with longitudinal distance X can be assumed to follow a square law. On this basis, values for I_H at stations intermediate to those measured were obtained by interpolation and for the aft most station by extrapolation. These points are denoted by triangles in Figures 2.7 and 2.8. The agreement between experiment and theory is quite satisfactory [28].

The yaw moment can be calculated by,

$$-\frac{N_v'}{\pi(T/L)^2} = -\left[(C_H + I_H)X'\right]_S^B + \int_S^B (C_H + I_H)dX'$$

Figure 2.8 shows the comparison between experiment and theory and it can be seen that agreement is not as good as that seen in the force derivatives, the vortex correction for the moment derivative appearing too large. No complete explanation as to why the

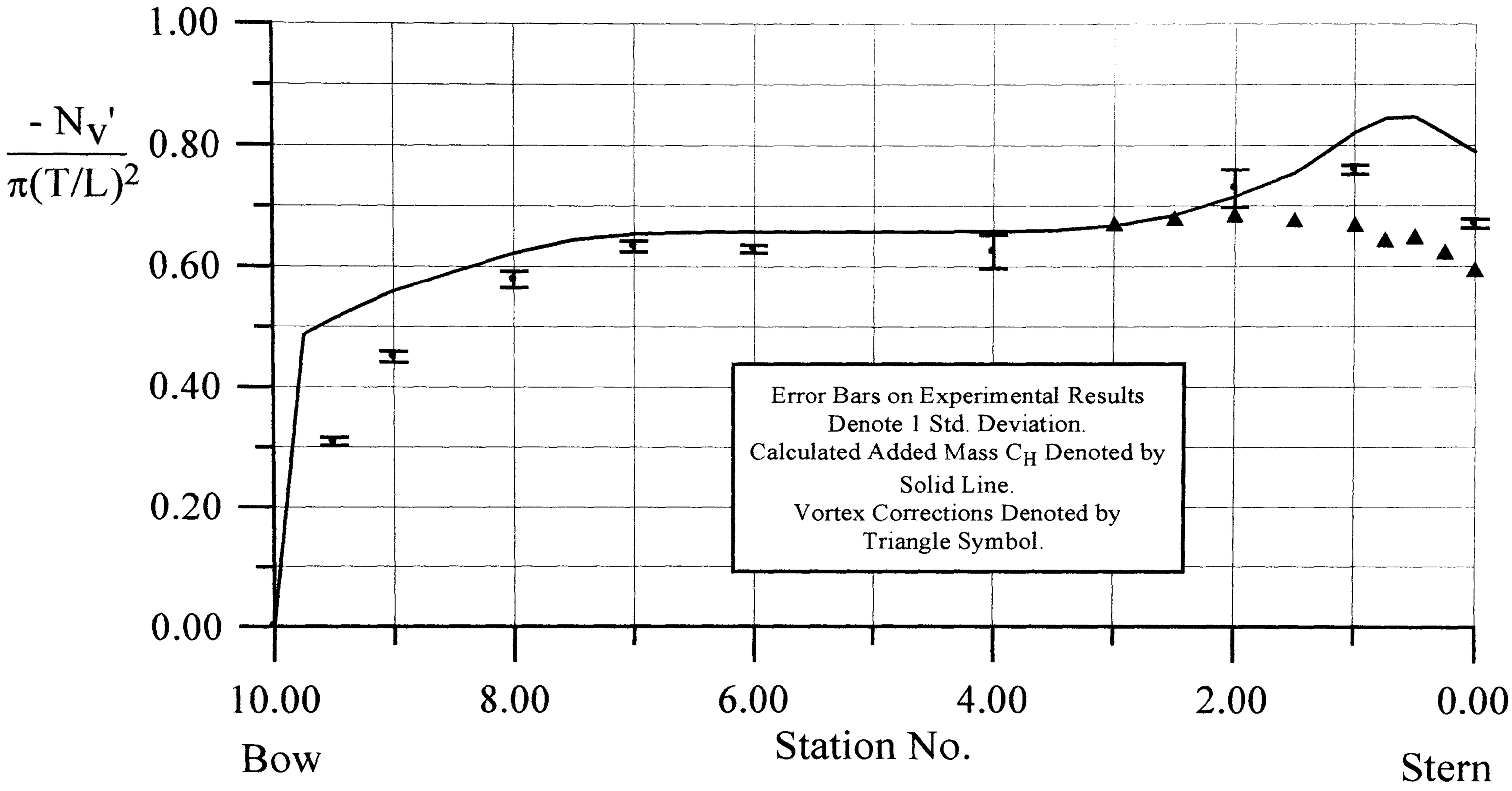

Figure 2.8 Comparison of Experimental and Generalised Slender-Body Theory Predictions of N_v' for the British Bombardier.

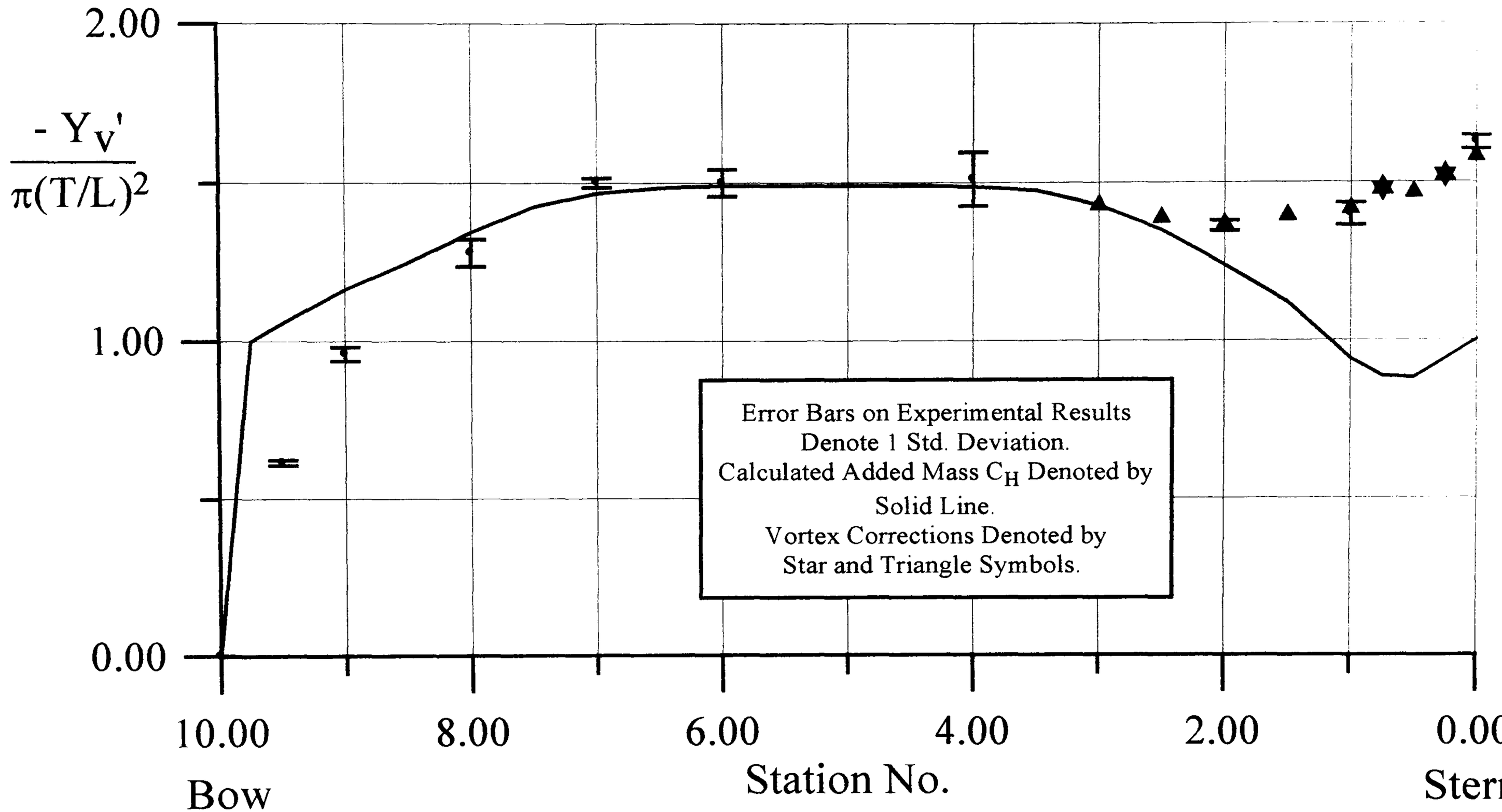

Figure 2.7 Comparison of Experimental and Generalised Slender-Body Theory Predictions of Y_v' for the British Bombardier.

moment derivative showed less satisfactory agreement with the theoretical predictions has been given, although it was noted that calculating $-N'_v/\pi(T/L)^2$ involves integration of the distributed added mass coefficient and vortex influence coefficient. It is therefore dependent on the values of vortex influence coefficient I_H at the measured stations as well as the assumed square law distribution.

2.7 CONCLUDING REMARKS

In this chapter a overview of the theoretical procedure to take account of the effect of trailing stern vortices was developed as developed by Clarke and Hearn [28] has been given. The experimental programme undertaken to test the theoretical development of the generalised slender-body theory has also been described. Experimental measurements were carried out at Glasgow [29], [30] of the vortex strength and position at two stern stations together with the vortex start point for the British Bombardier and Mariner hull forms. Re-analysis of segmented model data for these same two hull forms [23], [53] was used in conjunction with these vortex measurements to test the vortex influence extension to slender-body theory.

The agreement between theory and experiment indicates that the discrepancy previously noted between the slender-body theory and segmented model derivative distribution was due to the neglect of the effect of trailing stern vortices. The extension to the slender-body theory satisfactorily predicts the influence of these vortices for the British Bombardier and Mariner, but is not as yet complete since it still requires the experimental determination of the vortex strength and position and initial generation point.

The next chapter of this thesis will examine some of the implications of the vortex influence theory and an experiment is suggested that will be used to further test the validity of the theory.

3. DESIGN OF AN EXPERIMENT TO TEST THE VORTEX INFLUENCE THEORY

3.1 INTRODUCTION

In Chapter 2 a review was given of the generalised slender-body theory. It was shown that vortices influence the manoeuvring derivatives of the British Bombardier and Mariner hull forms in a way that can be predicted by the addition of vortex influence coefficient, I_H to the previous formulation of the slender-body theory [28]. This coefficient can be evaluated using conformal mapping techniques, although it is still necessary at this stage for the position and strength of vortices to be obtained experimentally, as well as the vortex start point. Experimental testing at Glasgow [29], [30] determined the required data for two sterns stations on the British Bombardier and Mariner models.

The aim of this chapter is to describe the design of an experiment that will further examine some of the implications of the vortex influence addition to the slender-body theory. This testing will be carried out by means of oblique towing of a variety of model shapes with segmented stern sections.

In the following sections flow separation and vortex formation around ship hulls is discussed further. Some of the basic assumptions of the vortex influence are highlighted. It is reasoned that certain hull form designs can be devised which allow direct testing of these assumptions. The chosen hull forms are described in detail together with the model making process.

3.2 VORTEX SHEDDING FROM SHIPS

Considerable research has been done to examine the phenomenon of vortex shedding from ship hulls with principal interest in application to resistance and propulsion.

The full pattern of vortex shedding and subsequent transport downstream from conventional ship hull forms has been determined by Tanaka et al [54]. The primary interest in propulsion studies as well as in manoeuvring studies are those vortices generated at the stern bilges and passing near the skeg area and into the propeller disc. For conventional hull forms stern shed vortices are generated by upward flow from the flat bottom area; this can be considered as analogous to a delta wing with the flow reversed. In the case of delta wing aircraft it is known that sheet flow separation along the leading edge of the wing rolls up to form a pair of counter rotating vortices [55]. A similar phenomenon has been produced for the stern of ships [56].

Attempts to quantify the strength of these shed vortices include empirical relationships between vortex strength and flat bottom area of the ship [54]. Oh et al [57] extended this work to develop a numerical method to predict the strength and path of vortices shed from the stern of tanker and wall sided models.

Experimental work carried out by Kuiper [32], considered the velocity distribution in the wake behind various stern geometries. The sense of rotation of the vortices shed from a conventional, U-form stern are in agreement with those measured by Tanaka [54], as illustrated in simplified form in Figure 3.1. Shedding from a pram form shows vortices of the opposite sense of rotation and what is called an optimised form shows no wake circulation. The work was concerned with the resistance and propulsion of ships and therefore an optimum was considered to be a minimum of circulation in the wake, resulting in low resistance and high propulsion efficiency.

The explanation given for the differences between these simple stern shapes reasons that, for the U-form, the fluid velocity at the sides of the hull is greater that at the keel. This results in pressure differences across the bilge, which causes an upward flow across the bilge radius leading to separation and vortex formation. In the case of the pram stern the lowest pressure exists at the keel with the result that the flow moves across the bilge in the opposite direction to the U-form and consequently the vortices generated rotate in the opposite sense.

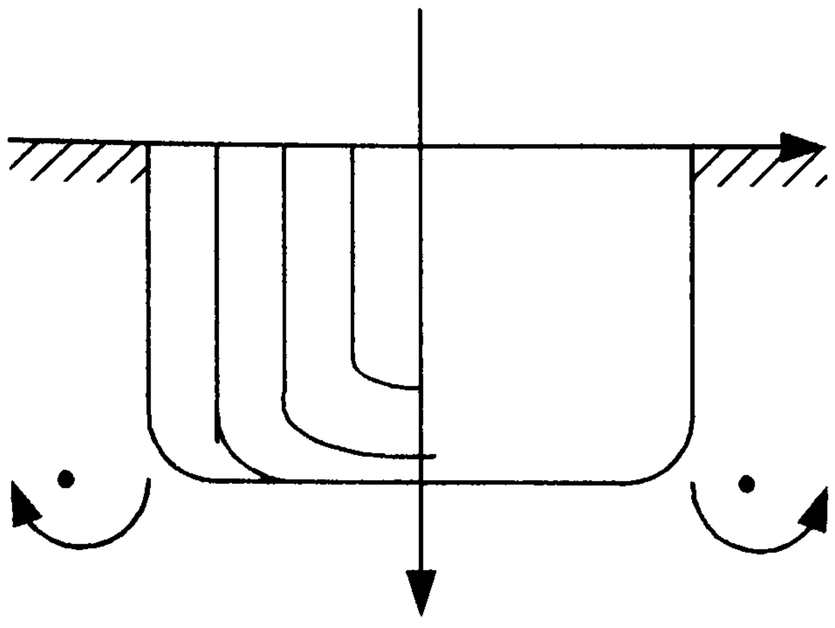

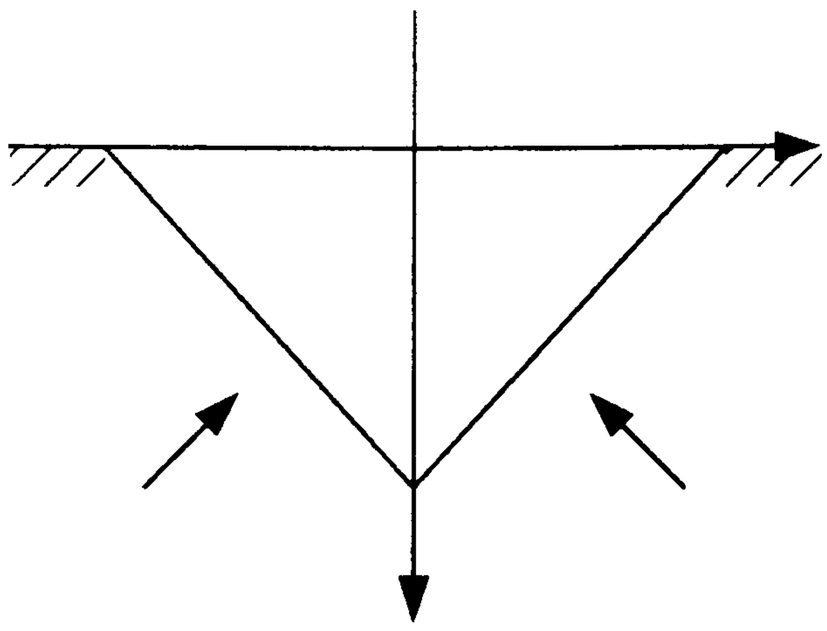

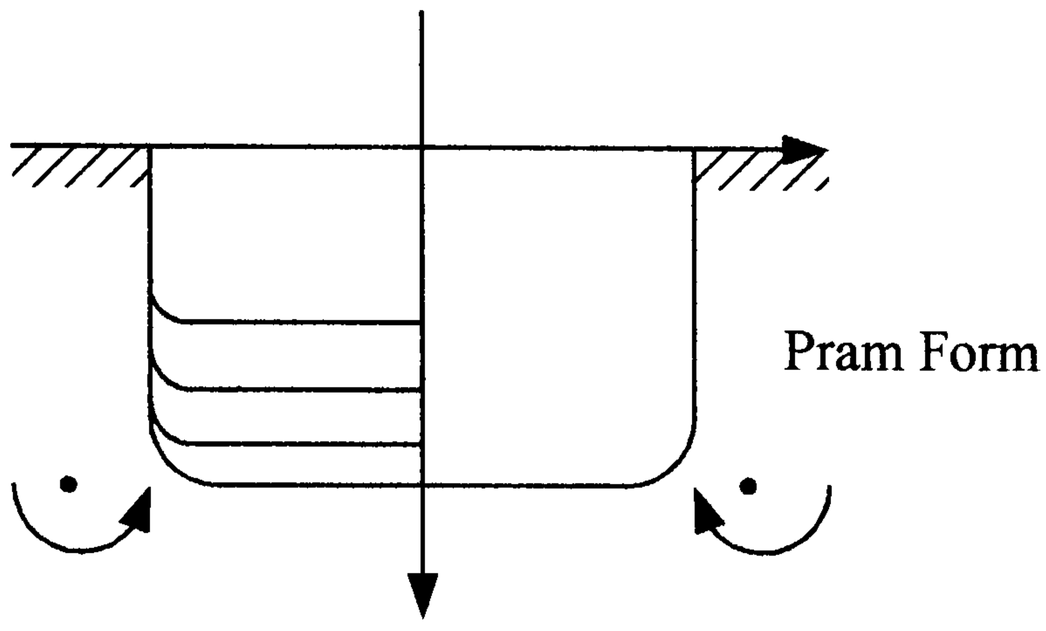

Figure 3.1 Simplified Representation of Vortex Generation from U-Stern, Extreme V-Form and Pram Stern Hulls as Measured by Kuiper [32].

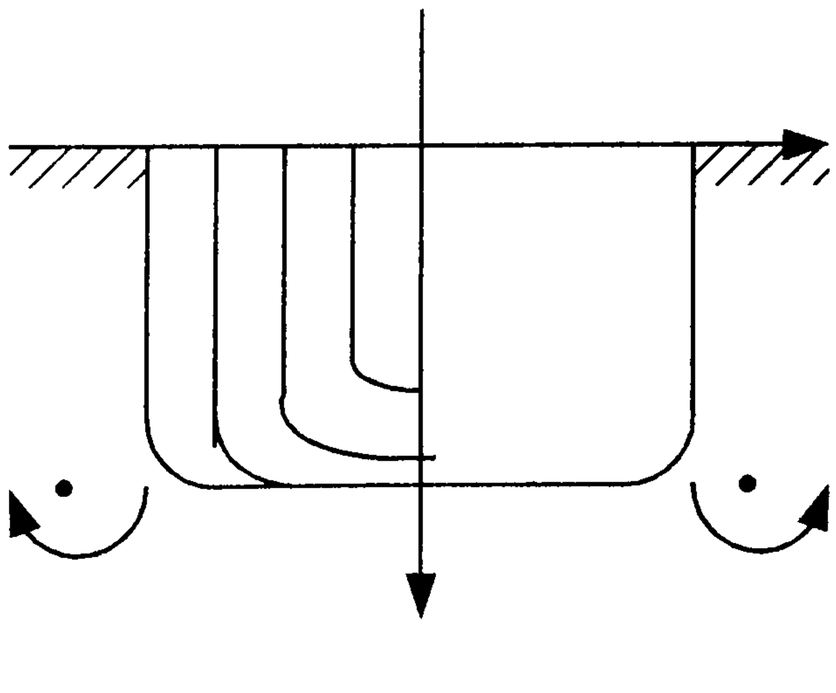

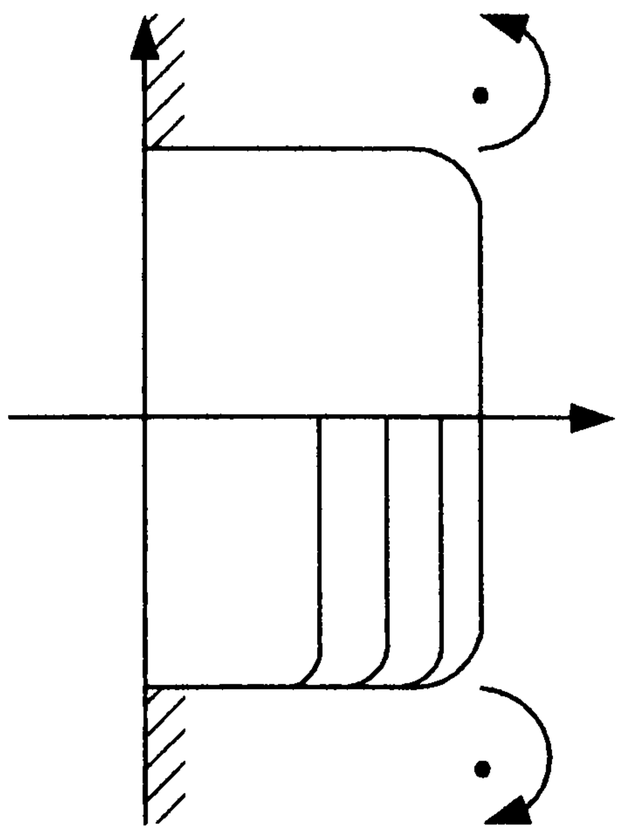

Figure 3.2 Rotation of Conventional Stern Geometry to Create Pram Stern Geometry

Varyani et al [29] have carried out experiments to obtain the strength and position of vortices shed from a pram stern British Bombardier. Unlike the Kuiper experiments, the sense of rotation of the vortices is shown as the same as that of a conventional hull. Although the experimental evidence may be unclear, it is interesting to note that we can consider the pram stern to be a 90 degree rotation of the conventional U-form as illustrated in Figure 3.2. It can be seen that the sense of the vortices suggested by such a transformation are consistent with the results of Kuiper [32].

Nonaka et al [58] have carried out experiments on three hull forms with the aim of obtaining data to be used in a numerical manoeuvring model which includes the effect of vortices. The fore-body of the models was the same in each case, but with the provision of different shaped stern ends. The velocity distribution in the wake was measured and a trend was found with the vortex strength reducing from the U-form to the V-form. In this work interest was centred on the cross-flow shedding of vortices at higher angles of attack and so the effect on the manoeuvring derivatives of perturbations about the straight ahead condition were not considered.

3.3 What Consequences of the Vortex Influence Theory can be Tested Experimentally?

The brief review of the literature above shows that there is experimental evidence to suggest that variations in stern geometry have a considerable effect on the strength and sense of rotation of shed vortices. The aim of this study is to design an experiment that directly tests some of the assumptions and implications of the vortex addition to the slender-body theory. It has already been established that, for conventional stern shapes at least, the discrepancy between slender-body theory and experimental results is greatest on the aft-body of the hull. This discrepancy is due to the presence of stern vortices for the British Bombardier and Mariner hull forms [28]. The full pattern of vortices shed from the hull of a ship includes vortices emanating from the bow, and it may be that these have some effect on the moment derivatives [54]. However, in this study interest is concentrated on those vortices that are formed from the flow separation at the stern end since this can be considered the dominant effect [28].

In the generalised slender-body theory, the sway force derivative is given by

$$-\frac{Y_v'}{\pi(T/L)^2} = \left[C_H + I_H\right]_{STATION}.$$

For the British Bombardier model [28] the value of the zero frequency horizontal added mass, C_H at Station 0.25 is 0.9403. The value of the vortex influence coefficient, I_H at Station 0.25 is 0.581. This gives a total value for the normalised derivative, $-Y_v'/\pi(T/L)^2$ of 1.521. In this case, the effect of the stern vortices is to augment the effectiveness of the stern section in generating side force. For both Mariner and British Bombardier hull forms, which can both be considered as instances of conventional U-form stern geometry, the vortex influence coefficient augments the added mass. This effect could be treated as the addition of an imaginary fin to the stern end of these vessels.

The vortex influence coefficient, I_H can be expressed as a function of the impulse position derivative and the position sway derivative,

$$I_H = -\frac{1}{\pi\left(\frac{T}{L}\right)^2}\frac{\partial I'}{\partial y'}\frac{\partial y'}{\partial V'}.$$

The impulse position derivative can be expressed as follows,

$$\frac{\partial I'}{\partial y'} = \pi\left(\frac{T}{L}\right)^2\left[\frac{8\Gamma' r'^2 \xi' \eta'}{\pi\left(\xi'^2 + \eta'^2\right)^2}\right]\Re\left(f'(x)\right).$$

It can be seen that the impulse position derivative is proportional to the strength of the vortex circulation, Γ'. In addition, all things being equal, the sense of rotation of the stern vortices dictates the sign of the vortex influence coefficient, I_H. Vortices that rotate in the opposite sense to those shed from a conventional U-form stern would diminish the effectiveness of that stern in generating side force.

New types of stern shapes, referred to as pram sterns, reduce the directional stability of ships and are consequently of particular interest to manoeuvring in general. Using conformal mapping techniques, it has been established previously [31] that the side force generated by a skeg attached to a rectangular body section, as is the case with pram sterns, is less than a skeg attached to a triangular section typically associated with conventional sterns. However, this result was obtained without consideration of the effects of trailing vortices. If it is the case that the vortices from these pram sterns rotate in the opposite sense to those from a U-form stern, then the effectiveness of the pram sterns in generating side force would be further diminished by the presence of these vortices. This effect could be treated as the removal of an imaginary fin from the stern end of this type of hull form.

The vortex influence coefficient is proportional to the strength of shed vortices, that is,

$$I_H \propto \Gamma' .$$

If the conventional U-stern and pram stern hull forms are considered to be at the two extremes with shed vortices rotating in opposite directions, then some intermediate geometry could be found which had little or no wake circulation. It has been suggested [32] that this could be a wall sided form which tapered towards the stern. However, in these experiments a fine form has been selected comprising only of elliptic sections: it is postulated that this type of body will not shed stern vortices. As the vortex strength goes to zero, the vortex influence coefficient also tends to zero. This implies that the results of the generalised slender-body theory will revert to those expressions, which neglect the presence of shed vortices. Since in this case all the sections are elliptic, the horizontal added mass coefficient is unity, for all sections.

The above considerations were made in the design of a series of segmented models, which are now described in detail.

3.4 SEGMENTED MODELS

This thesis is concerned with the effect of trailing stern vortices on the hull forces on a variety of ship shapes, and this is investigated by testing models with the same fore body, but with variously shaped segmented stern regions. In all, a total of 7 models where tested and these can be split into two groups. There is a set of five models based on the British Bombardier, the conventional version of which was tested by Clarke at A.E.W., Haslar [23]. The other group is a set of two models, which are based on a fine form, similar to that tested by Tsakonas in the Davidson Laboratory [16]. These two sets of models shall be described separately, and the reasons for this choice of hull shapes made explicit.

3.4.1 British Bombardier and Variations

The segmented model tests carried out by Clarke [23] used a 9-segment hull of the British Bombardier tanker form to evaluate the slender-body theory calculation of manoeuvring derivatives. This model was chosen because it was thought that no separation took place at the stern end when tested as a bare hull, that is, without rudder or propeller.

Before any comparisons can be made between the experimental results of the present study and theoretical predictions of the generalised slender-body theory, the experiment must be validated. Therefore, the models to be tested must include the British Bombardier conventional stern. The measured force and moment distributions can then be benchmark with the re-analysed data from the original A.E.W. experiment [23].

One of the most important findings of the original segmented experiments was that the slender-body theory reasonably predicted the distribution of forces along the forward part of the hull, but failed to do so at the stern. It has been shown by Clarke and Hearn [28] that could be explained if the presence of trailing vortices in the proximity of the stern were taken into account when calculating manoeuvring derivatives. Since the stern region is of primary interest in the present investigation, the rest of the models tested in this group are variations of the British Bombardier with the segmentation

being confined to the stern region. Thus, the models are made up of a solid segment 1, which extends from forward perpendicular to station 4 ($X' = -0.1$) and then 5 segments evenly dividing the reminder of the hull. The principal particulars of the British Bombardier with the conventional stern are given in Table 3.1 and a body plan of the hull form is shown in Figure 3.3. The completed GRP model British Bombardier conventional stern is shown in Figure 3.4.

Table 3.1 Principal Particulars of the British Bombardier with Conventional Stern

Model	**British Bombardier Cruiser Stern**
Length between perpendiculars (m)	221.0
Breadth (m)	29.6
Draught, Forward (m)	12.5
Draught, Aft (m)	12.5
Draught, Mean (m)	12.5
Trim (by stern) (m)	0.0
Displacement (tonnes)	67805
LCG (+ Forward) (m)	3.1
Model Designation	bbconv
Model Scale	1/88.39
Number of Segments	6
Rudder Fitted	No
Screw Fitted	No
Ship Speed (knots)	15.6
Model Speed (m/sec)	0.857

The vortex influence theory is concerned only with the horizontal component of the impulse created by vortices coming off the stern region of the vessel. If the skeg of the British Bombardier conventional stern was removed then the effect of the vortices

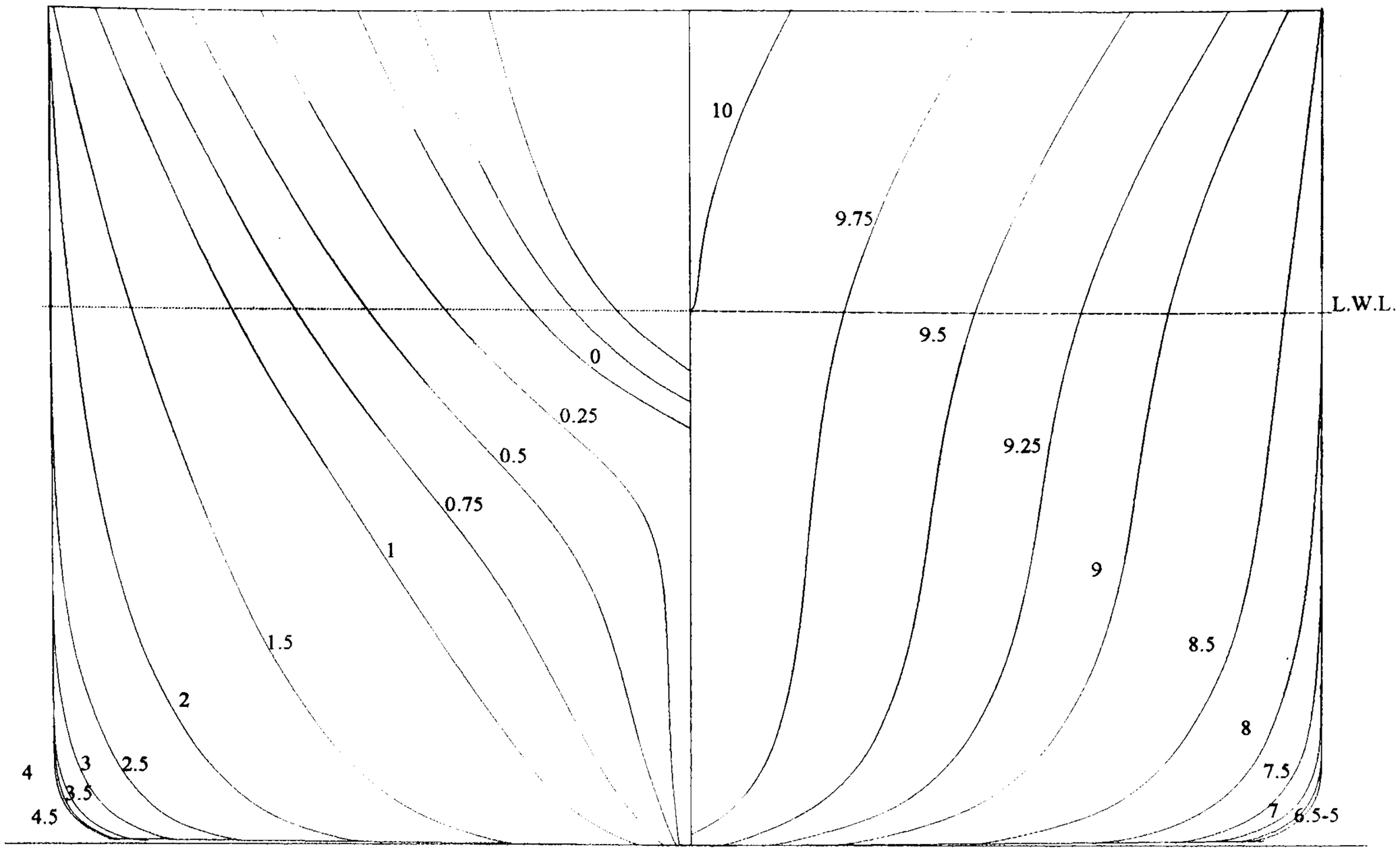

Figure 3.3 Body Plan of British Bombardier with Conventional Stern

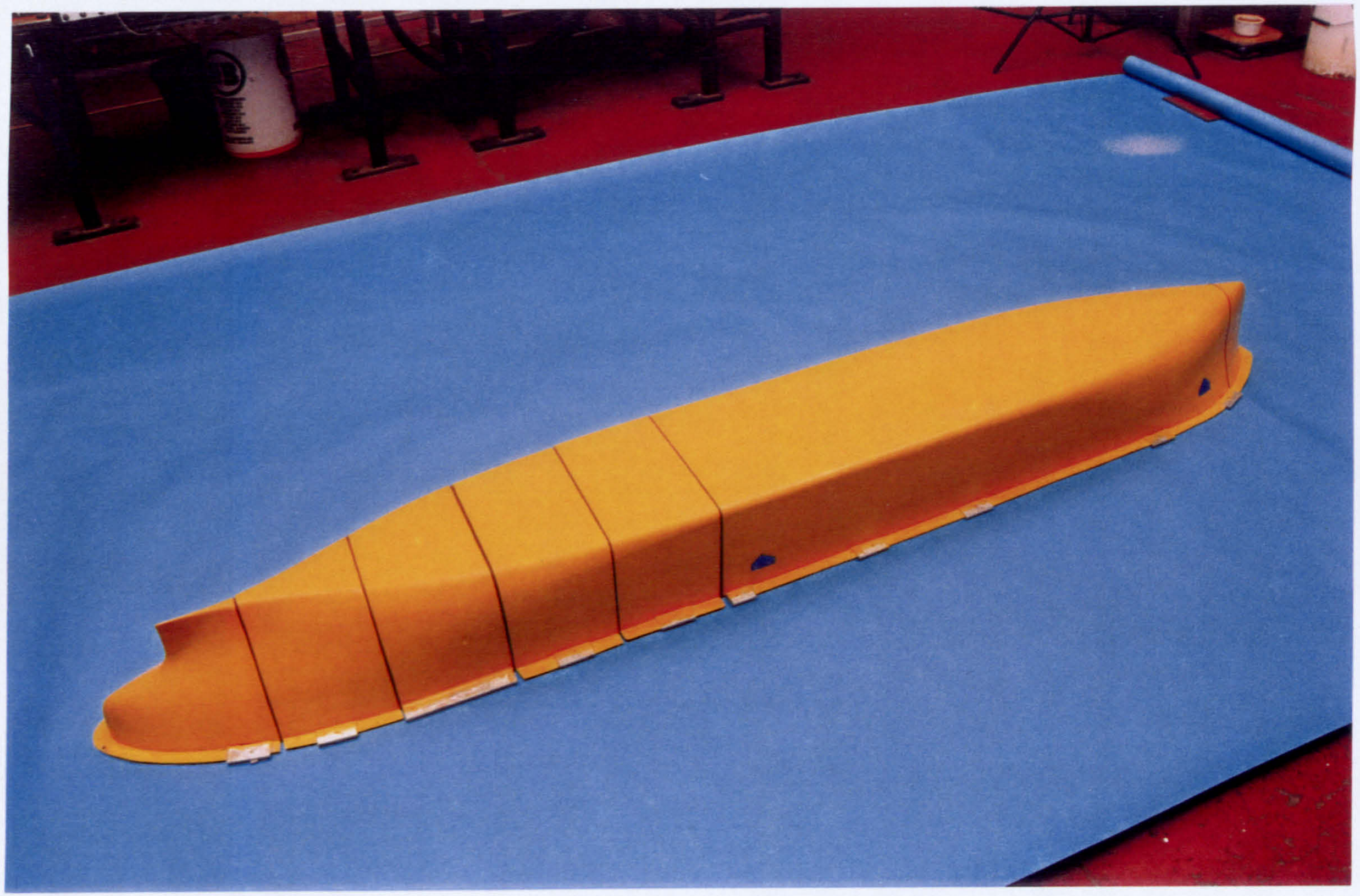

Figure 3.4 GRP Model of British Bombardier with Conventional Stern.

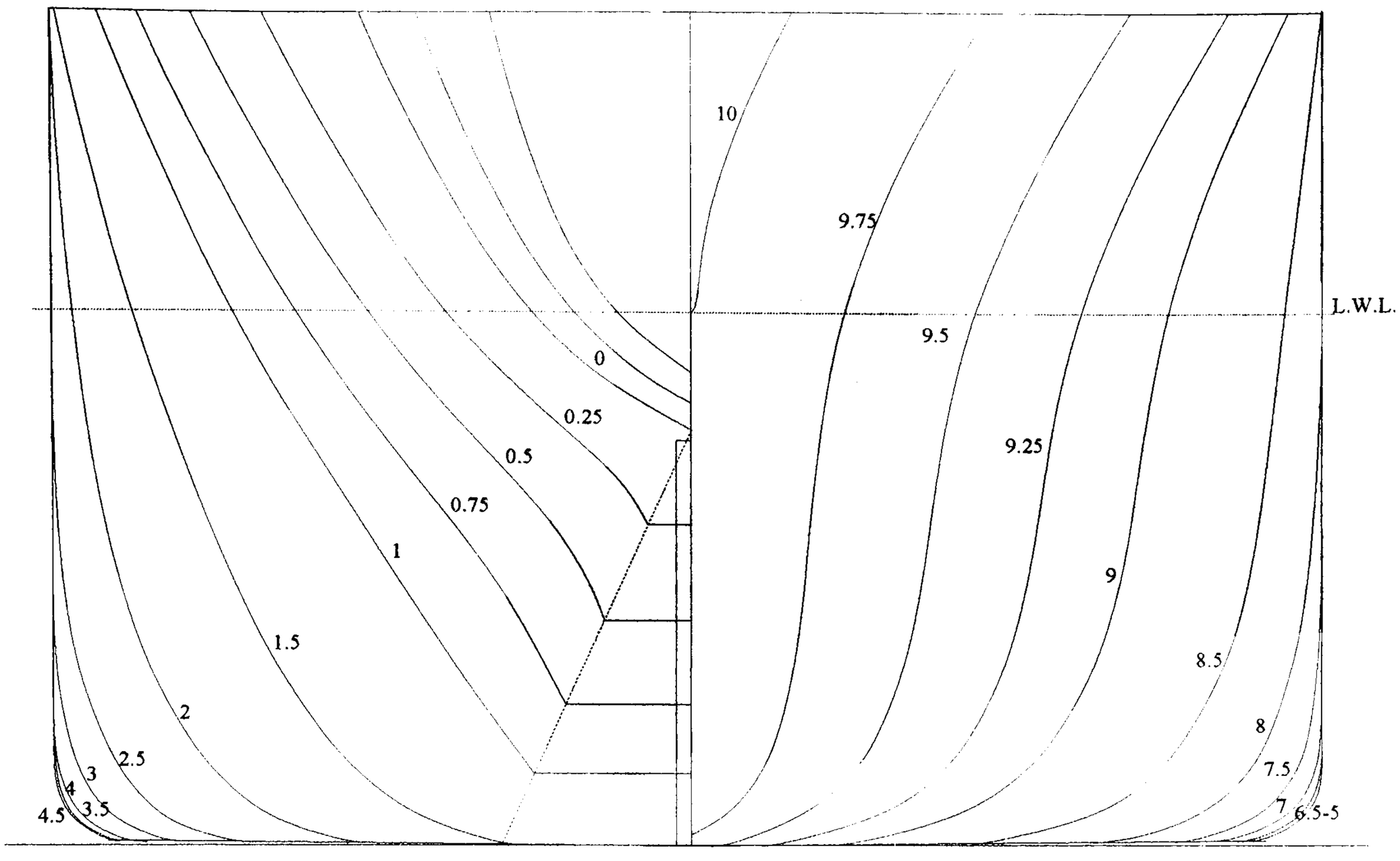

Figure 3.5 Body Plan of British Bombardier with Modified Conventional Stern

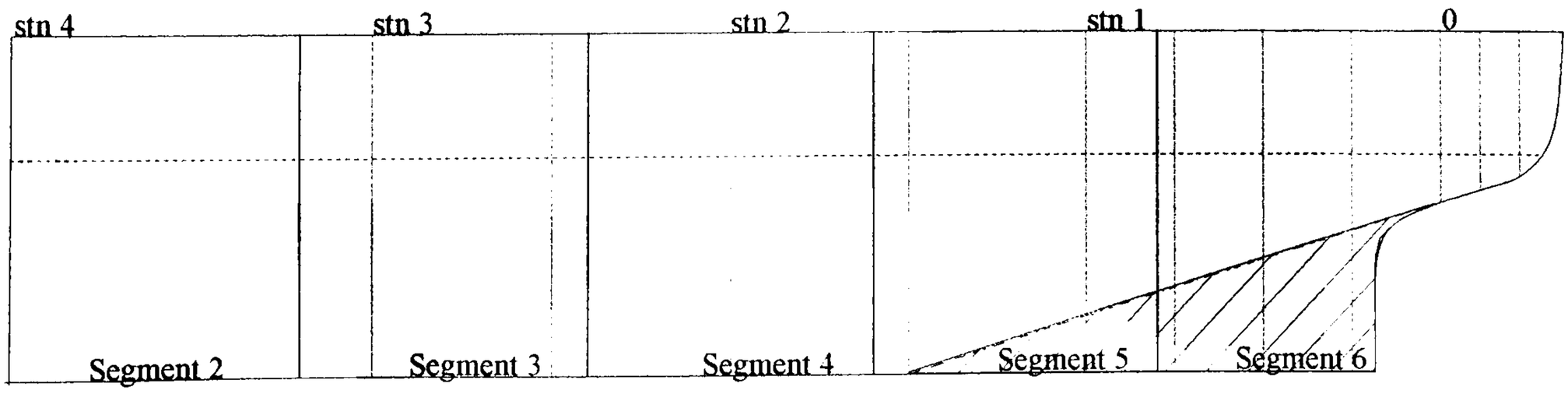

Figure 3.6 Centreline Profile of British Bombardier with Modified Conventional Stern

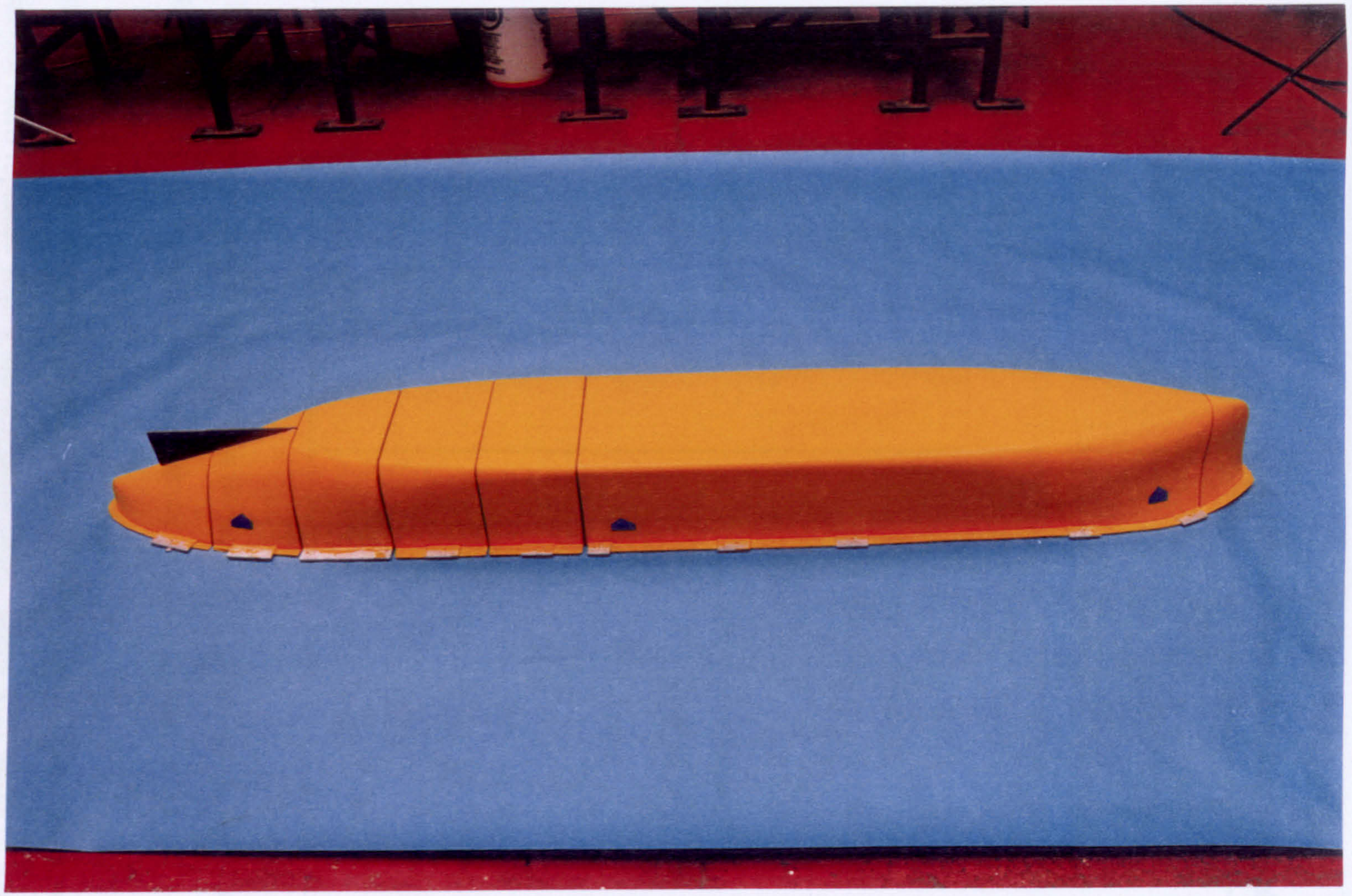

Figure 3.7 GRP Model of British Bombardier with Modified Conventional Stern.

would be largely lost, although it is thought that their position and strength would be largely unchanged since the geometry of the separation zones remains the same.

Removal of the skeg is difficult, however, because it is difficult to define a piece of the hull that could reasonably be called the skeg but which, upon removal, leaves a hydrodynamically smooth shape. The criteria proposed by Della Loggia [59] involve taking the body sections near the stern and fitting a spline through points of reverse curvature to isolate a skeg. When applied to the stern of the British Bombardier this procedure failed because a satisfactory way could not be found of terminating the removed portion without leaving a large step in the modified hull. The solution to this problem has been to simply remove a wedge of material containing the skeg to leave a flat inclined triangular surface at the stern of the hull: this hull was tested as the British Bombardier conventional stern (no skeg). It is assumed that the hard edges produced by this modification lie in the same direction as the flow and so produce little in the way of separation effects. If this is the case, the vortex strength should remain the same as the parent hull form

The model was then fitted with a skeg of the same centreline profile as the removed portion but made as a thin flat plate. In terms of vortex influence there should be little difference between this and the British Bombardier conventional stern: hull forces may change slightly due change of added mass of sections.

The principal particulars of these two models are given in Table 3.2 and a body plan and stern centreline profile of the hull form are shown in Figure 3.5 and Figure 3.6 respectively. The completed GRP model of the British Bombardier conventional stern (no skeg with plate) is illustrated in Figure 3.7. It is important to note that the only difference between these two models is the addition of a thin flat plate of PVC of the same centreline profile as the skeg removed from the conventional British Bombardier.

Table 3.2 Principal Particulars of the British Bombardier with Modified Conventional Stern

Model	**British Bombardier Cruiser Stern (no skeg with plate)**
Length between perpendiculars (m)	221.0
Breadth (m)	29.6
Draught, Forward (m)	12.5
Draught, Aft (m)	12.5 (2.7)*
Draught, Mean (m)	12.5
Trim (by stern) (m)	0.0
Displacement (tonnes)	67457
LCG (+ Forward) (m)	3.1
Model Designation	bbconsp (bbcons)*
Model Scale	1/88.39
Number of Segments	6
Rudder Fitted	No
Screw Fitted	No
Ship Speed (knots)	15.6
Model Speed (m/sec)	0.857

*Note that the entries in the brackets refer to the hull form, which is not fitted with the PVC flat plate skeg, otherwise the values given are common to both hulls.

As part of the MOSES programme, Glasgow tested the British Bombardier with the conventional stern replaced with a modern pram stern. Ships with sterns of this shape are known to have poor directional stability. It has been conjectured that this because of the ineffectiveness of a skeg below a rectangular stern section and because of the sense of rotation of stern vortices further diminishes the side force generated by the skeg. A segmented model of the British Bombardier fore body with a pram stern was tested with and without a flat plate skeg to investigate these hypotheses. The principal

particulars of these two models are given in Table 3.3 and a body plan and stern centreline profile of the hull form are shown in Figure 3.8 and Figure 3.9 respectively. The completed GRP model of the British Bombardier pram stern (with skeg) is illustrated in Figure 3.10. Again note that the only difference between these two models is the addition of a thin flat plate of PVC.

Table 3.3 Principal Particulars of the British Bombardier with Pram Stern

Model	**British Bombardier Pram Stern (with plate)**
Length between perpendiculars (m)	221.0
Breadth (m)	29.6
Draught, Forward (m)	12.5
Draught, Aft (m)	12.5 (2.4)*
Draught, Mean (m)	12.5
Trim (by stern) (m)	0.0
Displacement (tonnes)	66945
LCG (+ Forward) (m)	2.4
Model Designation	bbps (bbpns)*
Model Scale	1/88.39
Number of Segments	6
Rudder Fitted	No
Screw Fitted	No
Ship Speed (knots)	15.6
Model Speed (m/sec)	0.857

*Note that the entries in the brackets refer to the hull form, which is not fitted with the PVC flat plate skeg, otherwise the values given are common to both hulls.

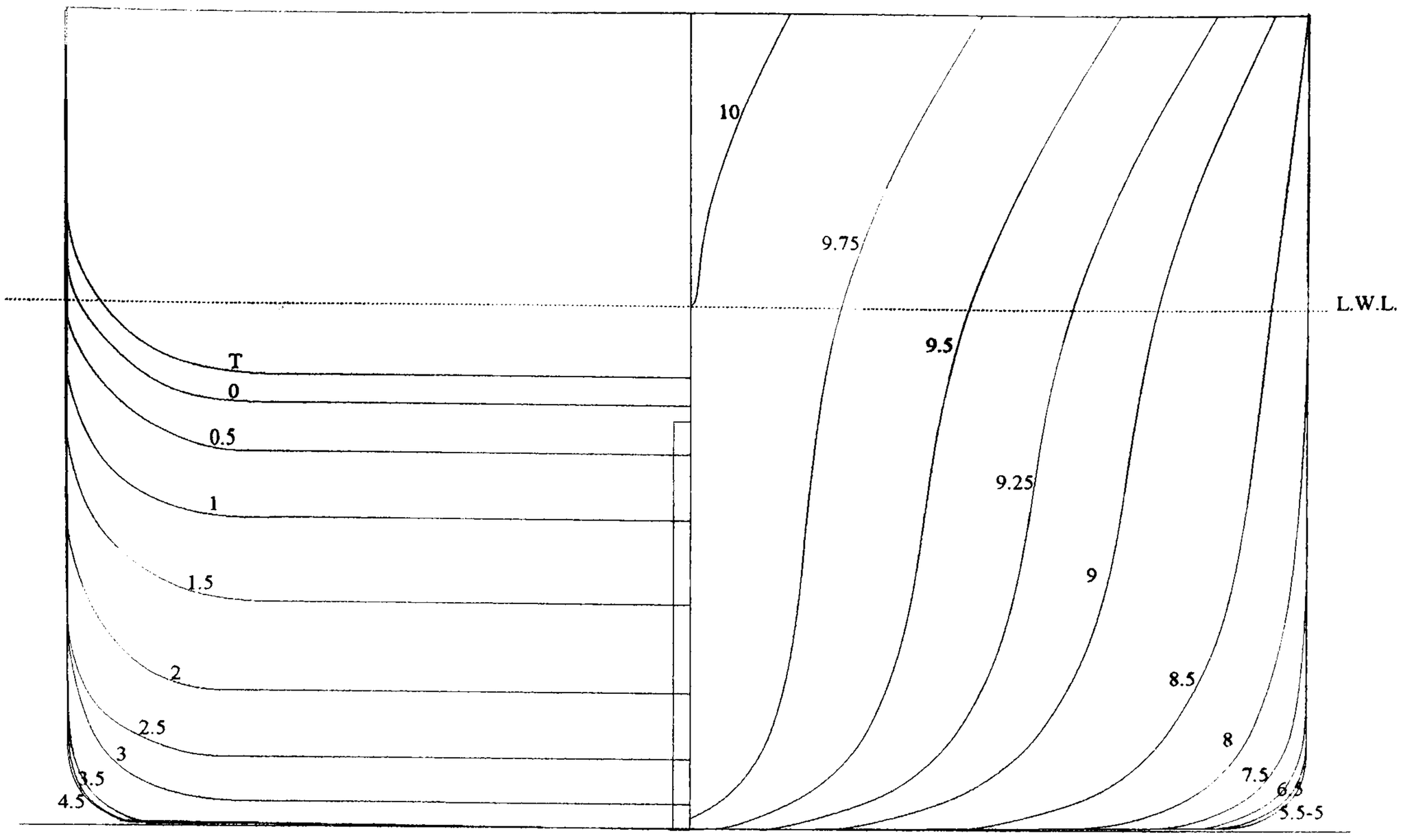

Figure 3.8 Body Plan of British Bombardier with Pram Stern

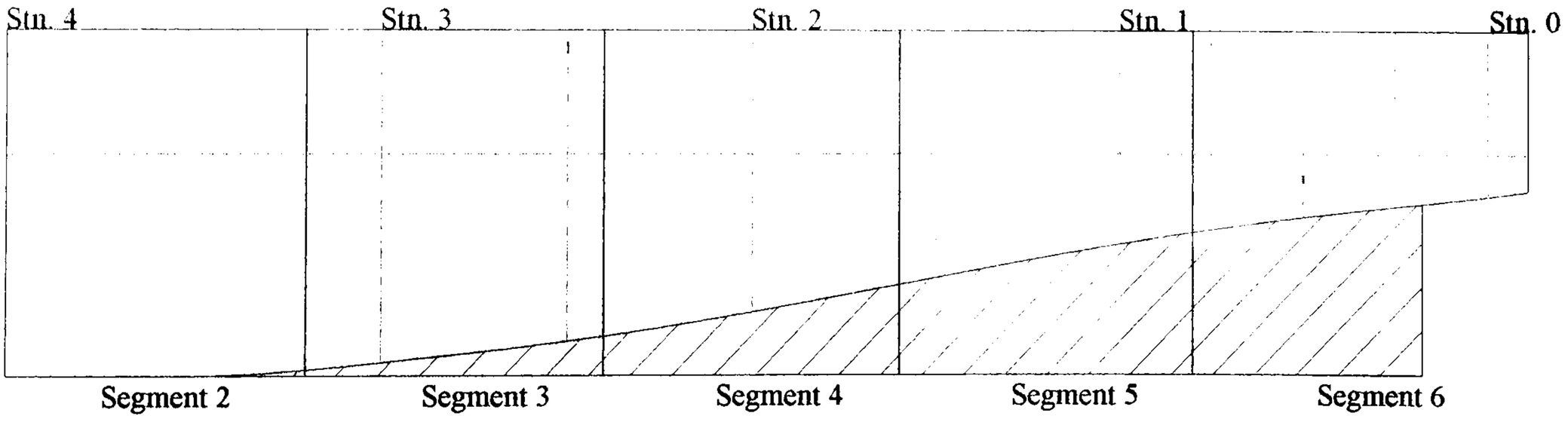

Figure 3.9 Centreline Profile of British Bombardier with Pram Stern

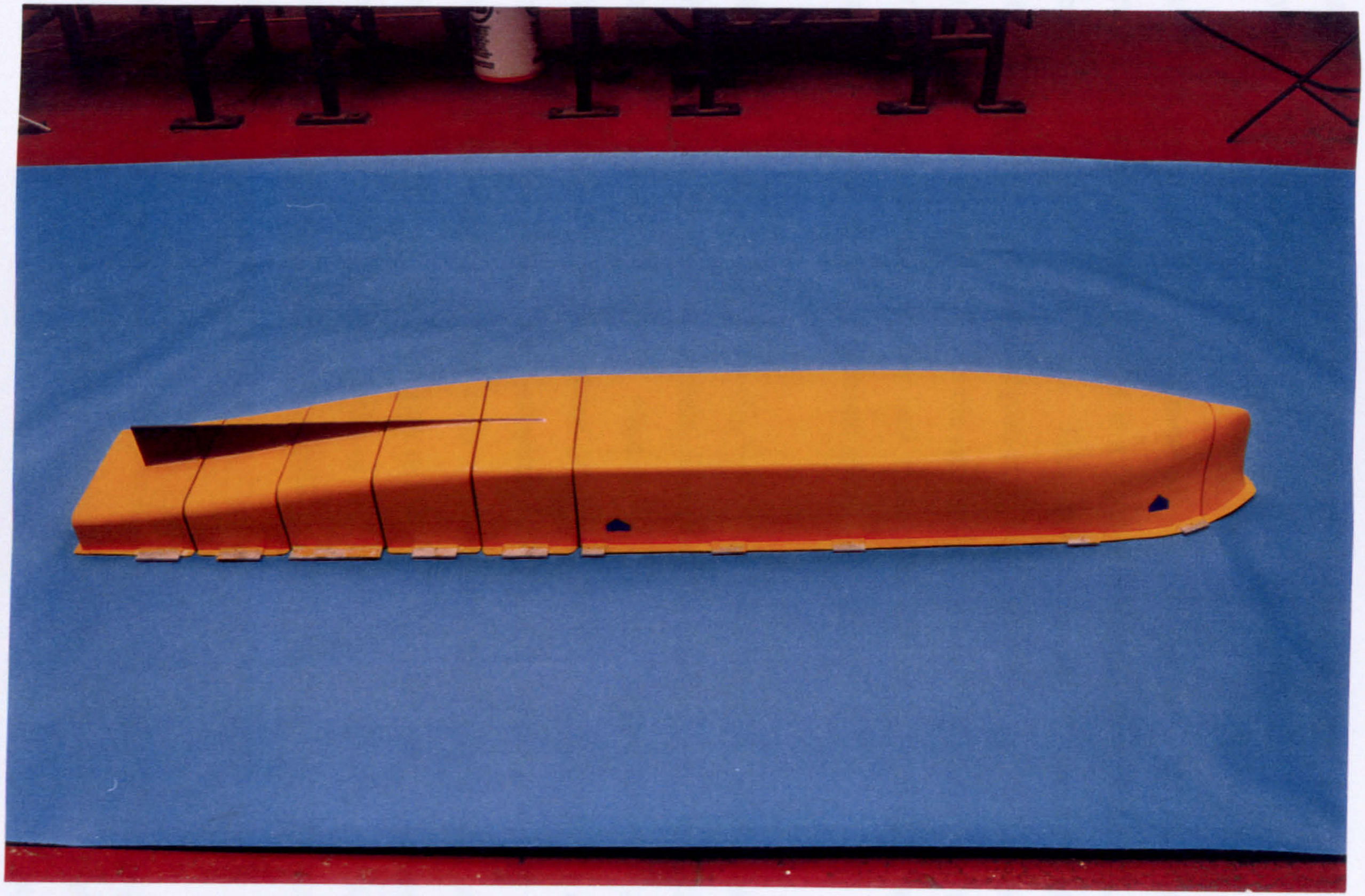

Figure 3.10 GRP Model of British Bombardier with Pram Stern.

3.4.2 Elliptic Hull Form

If the vortex influence theory is correct then the manoeuvring derivatives of a hull form that does not produce trailing vortices should closely match that predicted by potential flow slender-body theory. The two elliptic models were designed with the aim of directly testing this hypothesis.

The basic assumption about the mechanism of vortex generation in the stern region is requirement of a separation region: this is a region towards the stern of the hull, which has areas of high geometric curvature. The work of Tanaka [54] has shown that for conventional vessels this separation region is on the bilge where the flat bottom of the hull turns upward to form the skeg. In the case of the pram stern it is postulated that the separation zones are actually on the hull sides, thus leading to vortices rotating in opposite sense to those of the conventional stern.

The elliptic hull form is a fine form (C_B = 0.47) but has the same length, beam and draught as the British Bombardier models. The model is based on a hull form tested at the Davidson Laboratory [16], ETT Model 842. In the elliptic hull the original centreline profile and waterline have been preserved, but the body sections are all now elliptic. This has two effects: the horizontal added mass coefficient for an elliptic section is unity; the fineness of the ends together with these elliptic body sections produces a hull without any areas of high curvature. In consequence, it is postulated that this hull shape will generate little or no trailing vorticity and therefore the hydrodynamic manoeuvring derivatives should conform closely to those predicted by slender-body theory.

The model has been tested in two forms, with and without a flat plate skeg. The principal particulars of these two models are given in Table 3.4 and a body plan and stern centreline profile of the hull form are shown in Figure 3.11 and Figure 3.12 respectively. The completed GRP model of the elliptic hull form (without skeg) is illustrated in Figure 3.13.

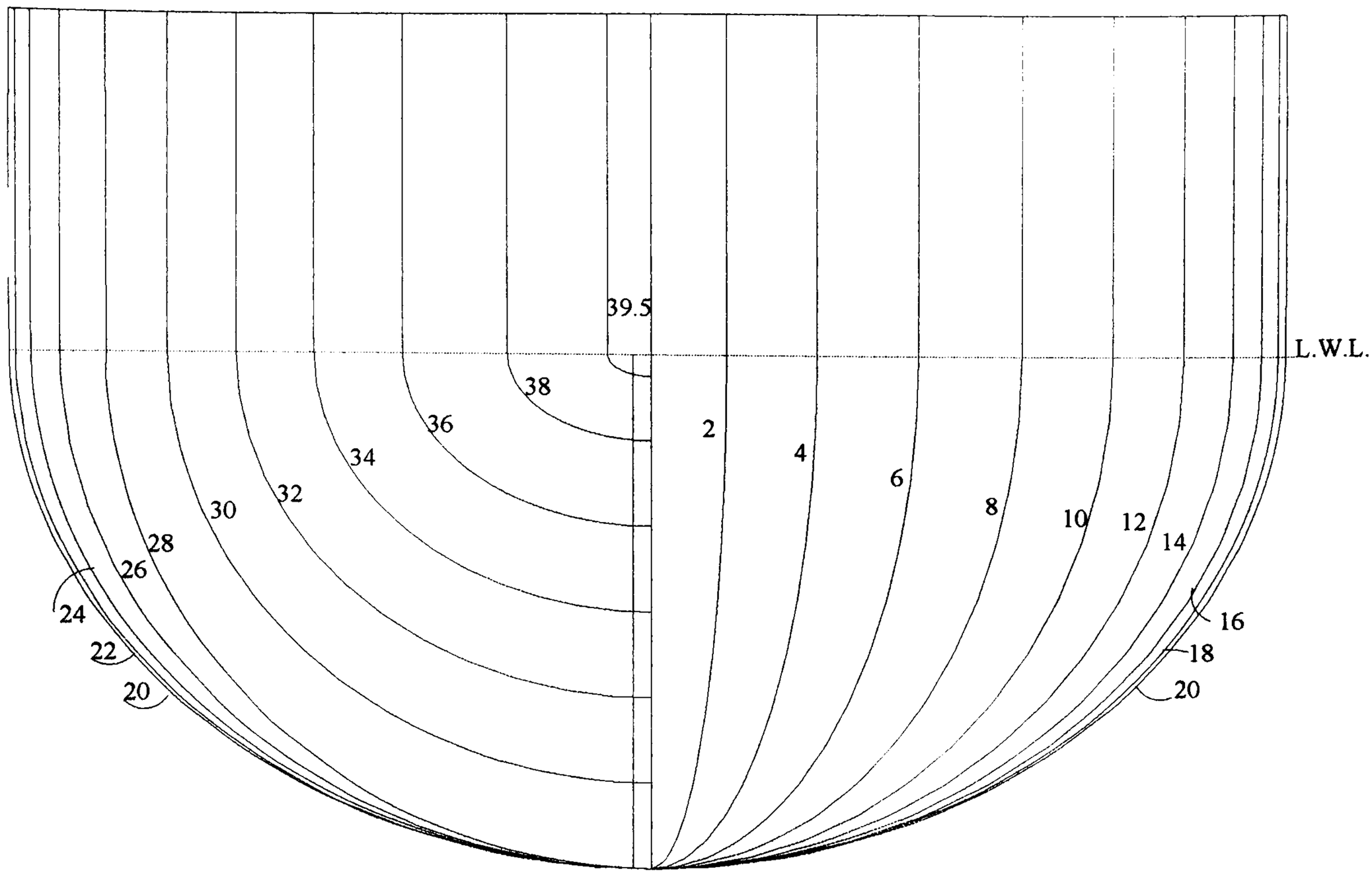

Figure 3.11 Body Plan of Elliptic Hull Form

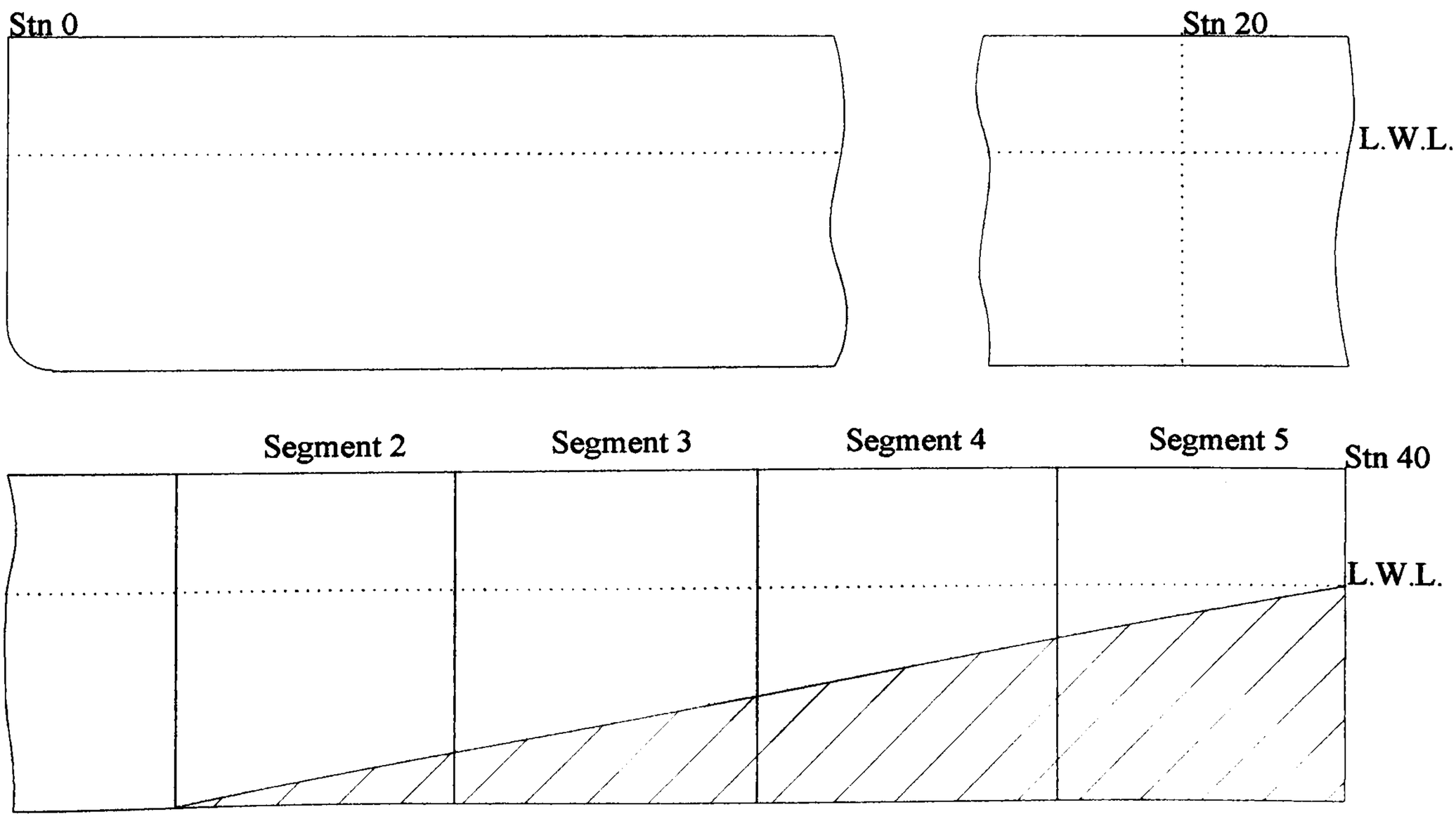

Figure 3.12 Centreline Profile of Elliptic Hull Form

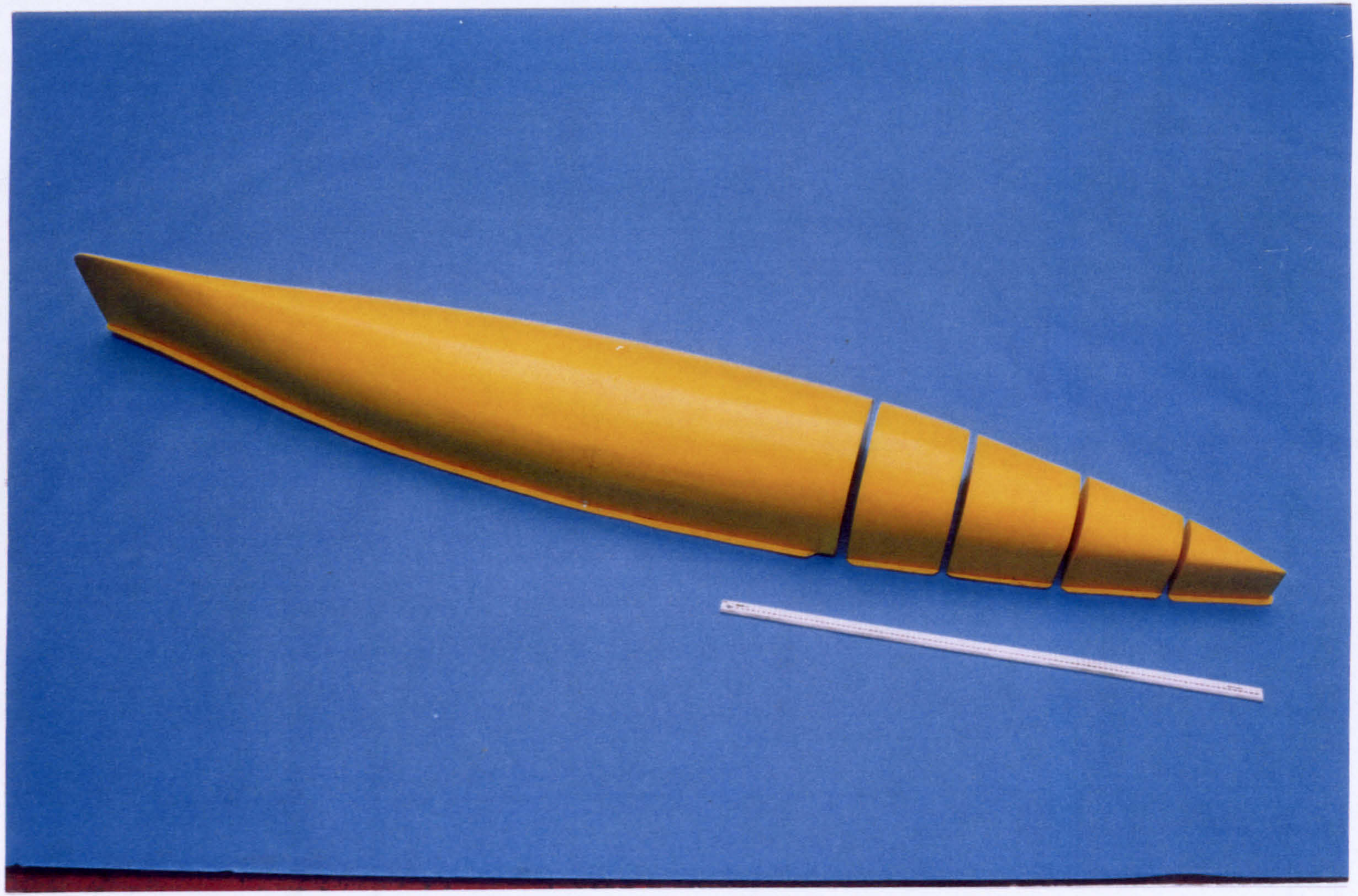

Figure 3.13 GRP Model of Elliptic Hull Form.

Table 3.4 Principal Particulars of the Elliptic Hull Form

Model	**Elliptic Hull Form (with skeg)**
Length between perpendiculars (m)	2.5
Breadth (m)	0.335
Draught, Forward (m)	0.141
Draught, Aft (m)	0.141 (0.0)*
Draught, Mean (m)	0.141
Trim (by stern) (m)	0.0
Displacement (kg)	55.5
LCG (+ Forward) (m)	0.03
Model Designation	ells (ellns)*
Model Scale	1
Number of Segments	5
Rudder Fitted	No
Screw Fitted	No
Ship Speed (knots)	-
Model Speed (m/sec)	0.857

*Note that the entries in the brackets refer to the hull form, which is not fitted with the PVC flat plate skeg, otherwise the values given are common to both hulls.

3.5 Some Experimental Considerations

Previous segmented model experiments [23], [52] carried out on the British Bombardier and Mariner hull forms used models, of approximately 5 metres in length, in oblique towing and rotating arm tests. Recent testing of the same hull forms to measure the strength and position of stern vortices at Glasgow University [29] has been carried out on models of 2.5 metres in length. The scale of the models was selected to have the largest model available, so to reduce scale effects, while avoiding the effects of tank

blockage. The towing tank at Glasgow University is 77 metres long by 4.6 metres wide and 2.4 metres deep.

In selecting the scale of the models to be tested at Newcastle University, the effects of tank blockage were considered. The towing tank at Newcastle is 32 metres long by 3.97 metres wide and 1.05 metres deep. With the aid of modern data acquisition systems the length of a towing tank is not as important as it used to be. At Newcastle, the model only needs to be towed in a steady state for approximately 10 seconds for the required data to be collected and so the tank length was not a limiting factor.

The proposed experiments are primarily concerned with the effects of flow separation and vortex formation, phenomena that are critically dependent on the behaviour of the boundary layer. These viscous effects are known to be important in towing tank experiments [52]. Comparison between experiments of various scales relies on similarity of the flow conditions in those experiments. In towing experiments it is possible to satisfy the inertia similarity by towing the model at the appropriate Froude number. However, similarity in viscous effects, as measured by the Reynolds number, could only be simultaneously satisfied for models of 1:1 scale. It was decide that for the Newcastle experiments the models used would be of the same scale as those tested at Glasgow. In this way the scale effects are the same for Glasgow and Newcastle models. It was not expected that blockage effects would be a problem for the towing speed of 0.857m/s, and the veracity of this could be assessed in a direct comparison of results from Glasgow.

3.6 Construction of Segmented Models

The following section briefly describes the three-stage process in producing a segmented, glass reinforced plastic (GRP) model, and the fitting out of that model for experimental use.

The model construction starts with a 1:1 scale set of waterlines at 1 cm spacing along the vertical axis and from these a wax plug is cut mechanically and finish by hand. Next this plug is laminated to form a female GRP mould. The mould is extended to a large

lip around the topsides of the plug, which can be used as a datum plane to ensure that the attachment of the rail system is parallel with the model waterline. At this stage a considerable amount of stiffening was bonded to the outside of the mould to guarantee that there could be no distortion of the shape when the mould was removed form the plug.

The segmented models were produced by subdividing the female moulds with a set of PVC bulkheads of 4.5 mm thick. These bulkheads were inserted before laminating and so all subsequent processes were carried out on, effectively, several compartments within a larger mould. In this way the model was composed of a large fore body and a set of separate watertight compartments which formed a smooth, continuous stern region. During laminating, the return edge of the model was extended over the lip of the mould so that the original top surface of the wax plug, which was parallel to the load waterplane, was faithfully transferred to the final model.

Before removal from the mould, the model was stiffened with plywood bulkheads and longitudinal stringers. The top edges of these bulkheads were fitted with a length of aluminium L-profile that extends the full beam of the model, and is aligned with the datum return edge. These profiles form a plane surface, parallel to the load waterline, to which the measurement system was attached. The models could then be released from the mould and finished to a smooth mat surface before the marking of the waterline. The details of the internal structure can be clearly seen in Figure 3.14 and Figure 3.15.

A wire of 0.9144 mm (0.036 inches) diameter was glued to the each model at station 1/2 to act as a turbulence generator. Before assembly on the force measuring system, each segment of the models were ballasted to their own waterline, to ensure that they all would float independently at the correct draught. Cross-flow between the segments was prevented by the 4.5 mm gap being sealed by a self adhesive foam strip, of the kind used to seal off draughts in household situations. These elements of the construction can be seen in Figure 3.16.

The models fitted with flat plate skegs were first assembled as described above. The skegs were made from 6 mm thick PVC, which was then bonded to the model as one

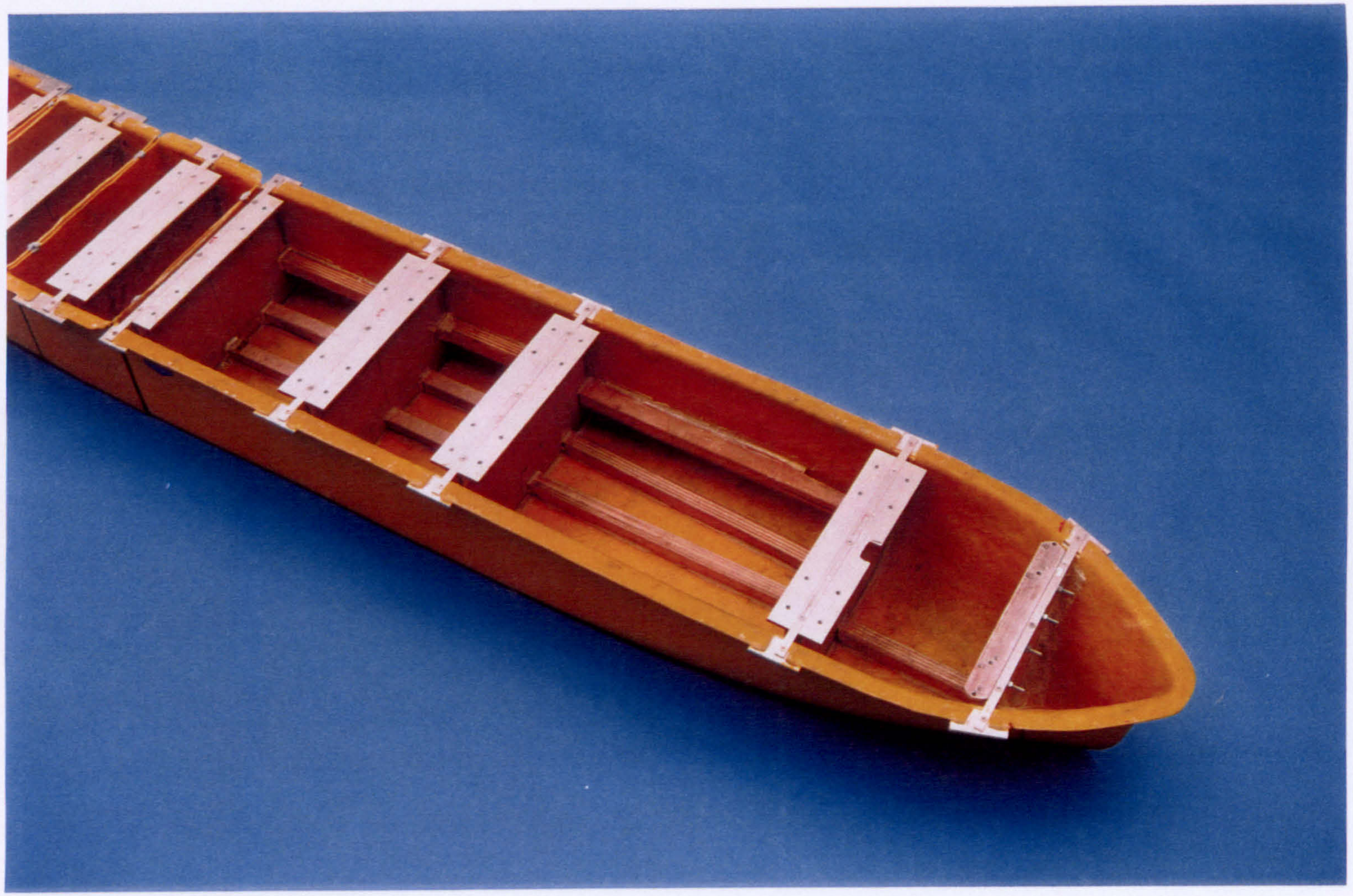

Figure 3.14 Internal Structure of GRP Models at the Bow.

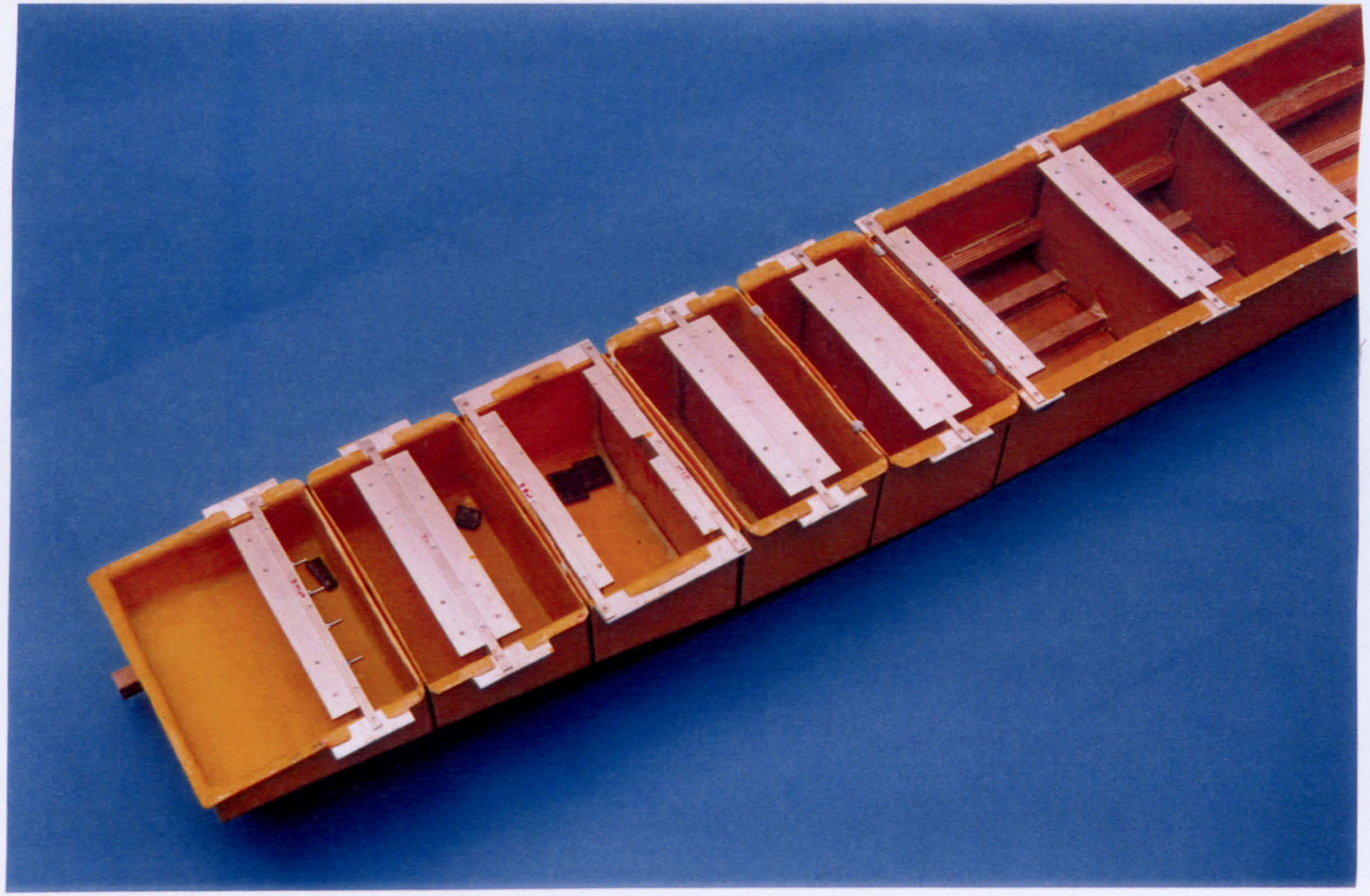

Figure 3.15 Internal Structure of GRP Models at the Stern.

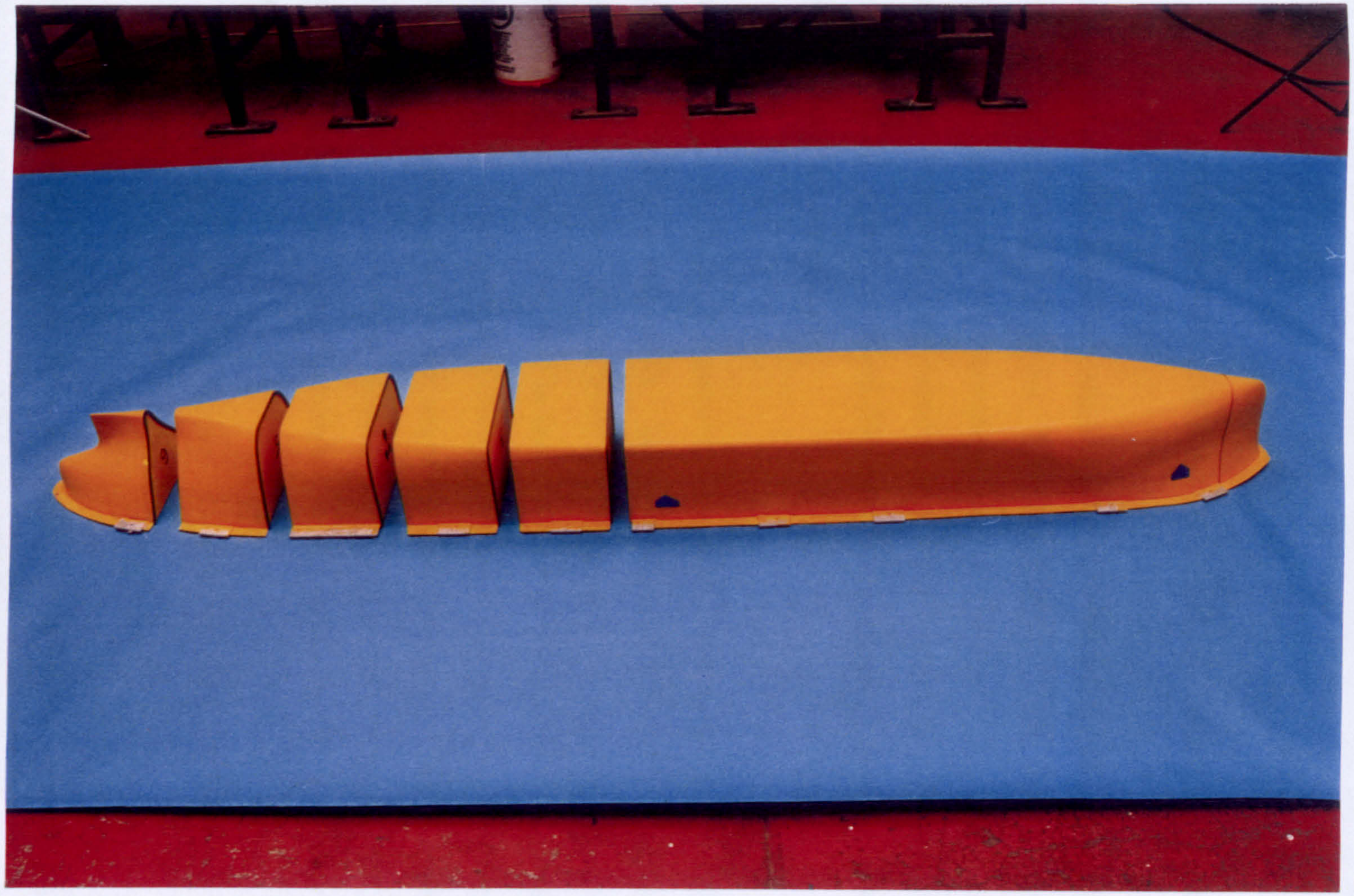

Figure 3.16 Foam Strip at the Interface of Model Sections.

piece and then slit at the appropriate longitudinal positions coincident with the gaps between, segments. This procedure was adopted to obtain perfect alignment of the flat plate skeg pieces. No attempt was made to seal the gap between skeg plates because it was considered that the slits were sufficiently narrow (less than 0.8 mm) so that their effect on the fluid flow could be neglected.

3.7 Design and Construction of Force Measuring System

The aim of the experiment was to evaluate the vortex influence addition to slender-body prediction of manoeuvring derivatives. The experimental method used to accomplish this aim was the measurement of elemental forces on the stern sections of a variety of different models. In this way, the distribution of force in the region of the hull, which showed greatest discrepancy between potential theory and previous segmented model experiments, could be established.

The requirements for the force measuring apparatus could have been satisfied by a number of mechanical arrangements. Initially, a system was considered that would have resembled a comb, with the teeth extending into the segments of the various models. This design was discarded in favour of the double rail system similar to that used at A.E.W. [52] because it was thought that the setting up of each of the models onto the comb measuring apparatus would be time consuming. Also, a double rail system could be used on a wide range of model types and sizes, whereas a comb arrangement would have to be constructed to a specific model size and segment distribution.

3.7.1 Development of Collar System

The first attempt was a system based on an existing dynamometer. In this dynamometer the forces placed upon the footplate of the apparatus are registered by a set of four force gauges arranged in a crucifix.

A collar and frame were constructed which were attached to the towing post to hold the set of outer rails; these rails are 'earth' since any force transmitted to them would be

exerted on the towing post via the collar and frame and would therefore not be measured. An aluminium box was constructed; the floor of which held the foot of the dynamometer on a plate that could be set at different angles in the horizontal plane. The 'live' set of rails were bolted onto this box; anything attached to these inner rails would transmit force to the foot of the dynamometer and could therefore be measured. The various angles of yaw required in the towing experiments were set by fixing the inner and outer rails together, loosening the collar arrangement on the towing post, and then using the graduated plate in the bottom of the box to set an angle. The collar was then tightened again and the rails decoupled.

This system failed to work satisfactorily. The main reason for this failure was that the dynamometer was not stiff enough in torsion to maintain the segments of the model in reasonable alignment, despite the positioning of the towing point well forward in the model to reduce the magnitude of the moments applied to the apparatus.

It was for these reasons that this first system was discarded and new pair of modular force cells was constructed to measure the forces between the rails directly.

3.7.2 Development of Modular Force Cell System

The modular force cell system is similar in design to that developed at A.E.W. Haslar [52] and consists of two pairs of parallel rails, which were connected by a pair of modular force cells. In operation, this arrangement is suspended in a plane parallel to the water surface beneath the towing carriage via a set of articulated counter balanced levers. The entire weight of the measuring mechanism is therefore borne by the carriage, and not the model. The third element of the system is the towing post, the footplate of which is fixed to the inner rails by an aluminium box. The base of the towing post is articulated fore and aft and the towing post tube is sleeved with roller bearings on the carriage: thus the model is free in heave and pitch, but is fixed in all other modes.

The various angles of yaw to which the models are set during experimentation can be fixed at the towing post base plate in increments of 2 degrees to port and starboard.

The towing arrangement, like the force gauges, can be placed at any point along the rails, as long as there is space inside the model. It was found that placing the towing arrangement as far forward in the model as possible, to reduce the moment acting on the single towing point, helps to keep the model fixed at the correct yawing angle and reduces the oscillations about the towing post. The general arrangement of system is shown in Figure 3.17 and Figure 3.18.

During experimentation, the segments of the models are attached to one of the two sets of parallel rails. The inner set of rails is connected rigidly to the towing post and therefore the towing carriage by the aluminium towing box. The hydrodynamic forces exerted on any segments of the model attached to these inner rails are transmitted to the carriage without being measured. The outer set of rails are connected to the inner rails by two modular force gauges, and these can be positioned at any point along the rails. In practise, the force cells are placed as far apart as the internal geometry of the models allow and this resulted in different locations for the elliptic hull form and British Bombardier models.

The experimental measurement of the forces and moments acting on the segmented models depends upon correlating the strain sampled on the surface of elements within the modular force cells with the hydrodynamic forces and moments transmitted to the outer rails. The active component within the modular force cells is an aluminium box section, the sidewalls of which have been machined down to thin flexures.

The complete measuring system is suspended from the towing carriage by two sets of levers and counter weights. The attachment point for these levers has to be on one set of rails only so that the inner and outer rails are only connected together via the force cells. In the configuration selected, the inner rails are connected to the carriage, which means that the weight of the outer rails and the outer box of the force cells is suspended from the active flexures. The flexures are thus operating under tension. The alternative configuration, with the outer rail connected to the towing carriage would have meant that the flexures would have been under compression and therefore in a statically unstable system with the consequent risk of hysteresis in the measuring system.

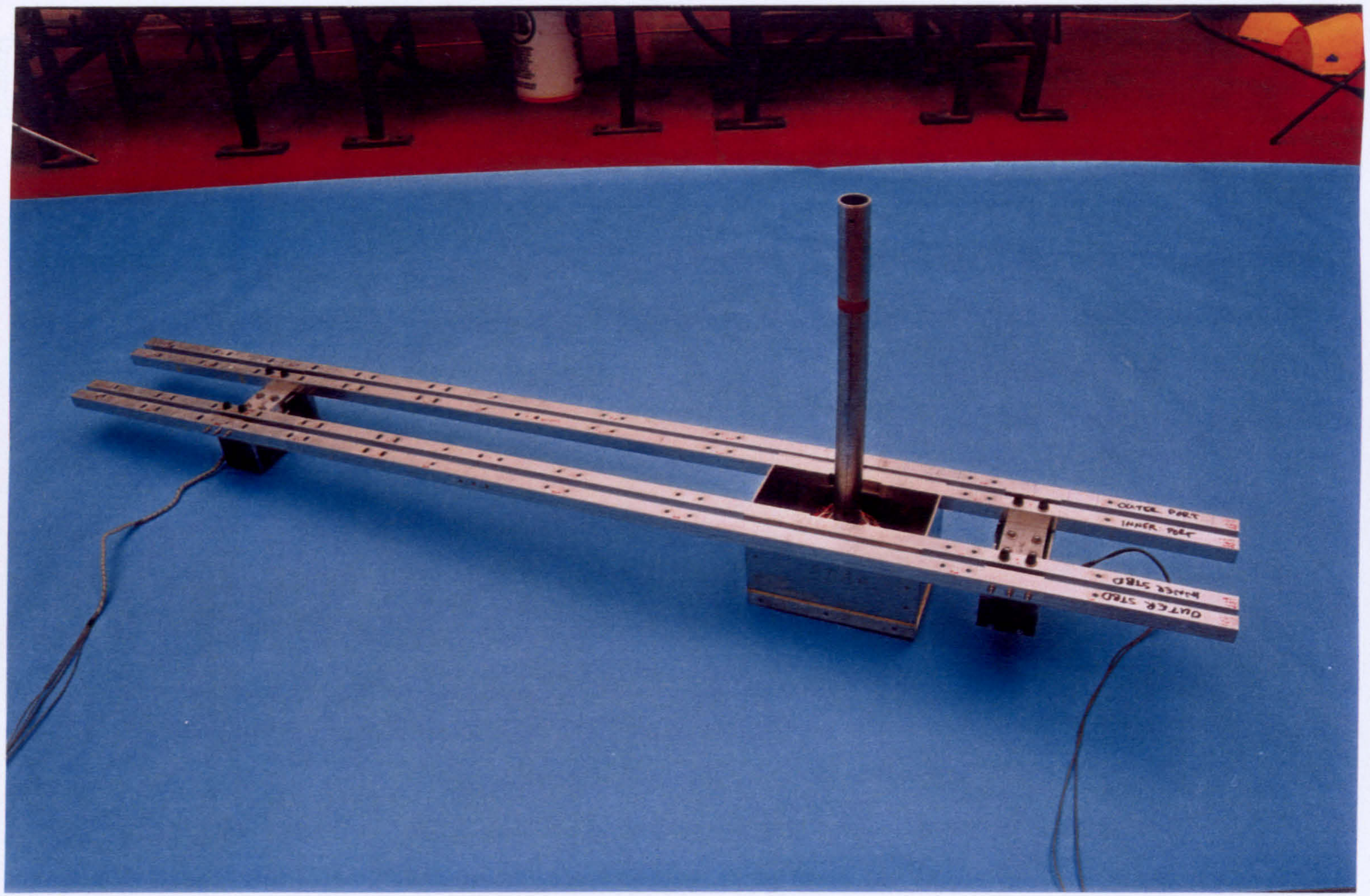

Figure 3.17 Assembled Rail Measuring System.

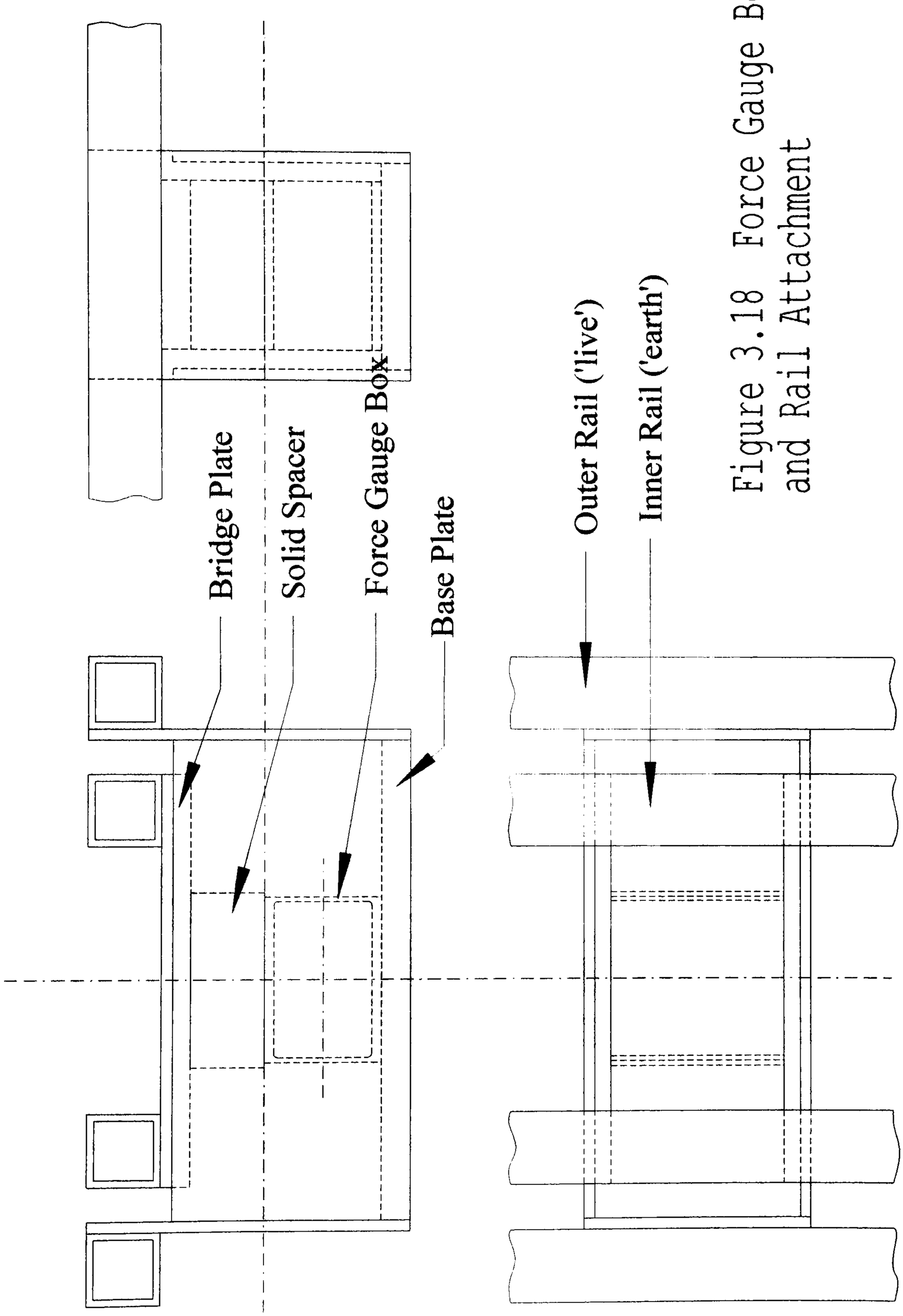

Figure 3.18 Force Gauge Box and Rail Attachment

The system is required to exhibit selective response only in the y-direction of the model reference frame, therefore, the modular force cells must be compliant in this mode, but rigid in all other modes. The active element of the modular force cell is essentially compliant in shear. The modular force cells are arranged so that the horizontal centreline of the flexures as near as possible to the line of action of sway hydrodynamic forces. Any misalignment in the z-direction will result in a rolling moment on the force cells. This moment can only be resisted by tension and compression loads in the thin flexures, a situation that may complicate the strain field within the strain gauge area and therefore complicate the response of the force cells.

During experimentation, the models were accelerated up to test speed and allowed to settle, before the measurement phase took place. The active flexures have to be sufficiently robust to with stand the loads applied under model acceleration. In general, the natural frequency of the spring element should be as high as possible, consistent with the specific sensitivity requirements, and this implies a rigid, low-compliance design. This is of particular importance in the segmented model measuring system because it is essential that the deflection of the spring element is small enough so that it is reasonable to assume the model acts as a single unit from the hydrodynamic point of view.

Within the gauge area there must be sufficient strain to allow accurate measurement and the strain in this region should be uniformly distributed. The gauged component should be the highest strain level, anywhere in the system since this will help to ensure freedom for creep and frictional losses at joints, which would lead to hytheresis. The gauge box itself is machined from aluminium box section so that the spring elements are rigidly connected to the rest of the structure.

3.7.3 Gauging and Calibration of Gauge Boxes

The gauge boxes can be considered as a pair of cantilevered spring elements. The function of these spring elements is to serve as he reaction for the applied hydrodynamic load. It is desirable that the effect of the load is focused into an isolated, preferably uniform, strain field where strain gauges can be fixed for load measurement.

The implicit assumption in the use of strain gauging is that the strain level in the gauged area of the spring element responds in a linear-elastic manner to the applied load.

The dimensions of the gauge boxes were set to satisfy the mechanical requirements described above, but also to provide appropriate strain levels in the gauged area of the spring elements. In practise, the main variable used in engineering the strain levels was the wall thickness of the spring elements. The necessary strain level was set in the range 1000 to 1700 $\mu\varepsilon$. With a four gauge fully active bridge circuit, 1500 $\mu\varepsilon$ will produce a nominal output signal of 3 mV / V of bridge excitation, based on a gauge factor of 2.0. Treating the problem as a set of rigidly connected cantilevered beams the strain requirements were used to calculate a wall thickness of approximately 1 mm.

The gauge boxes are made by machining down the walls of an extruded aluminium box to the required thickness and glue strain gauges in positions shown in Figure 3.19. Since the maximum allowable strain level in the gauge region limits the electrical output of the load cell, this strain level should exist uniformly over the entire area of the gauge grids to maximise the signal. Figure 3.20 shows the deformation of the gauge box under shear, thus the gauge positions coincide with the regions of maximum strain. Note that the gauges are glued onto the inside surface of the gauge box. This is done to prevent accidental damage to the gauges and to allow the possibility of removing material from the outside of the spring elements if on testing necessary signal levels could not be obtained.

The calibration of the cells was done by applying an accurately known load and recording the response. The result of the calibration was recorded in the data acquisition program so that the output from the experiment could be recorded directly as forces in Newtons. The bridge is then 'loaded' with a strain level of say 160 $\mu\varepsilon$ and the response recorded. With the entire system assembled and placed in the towing tank, this procedure was then used periodically to check that the calibration of the cells was unchanged.

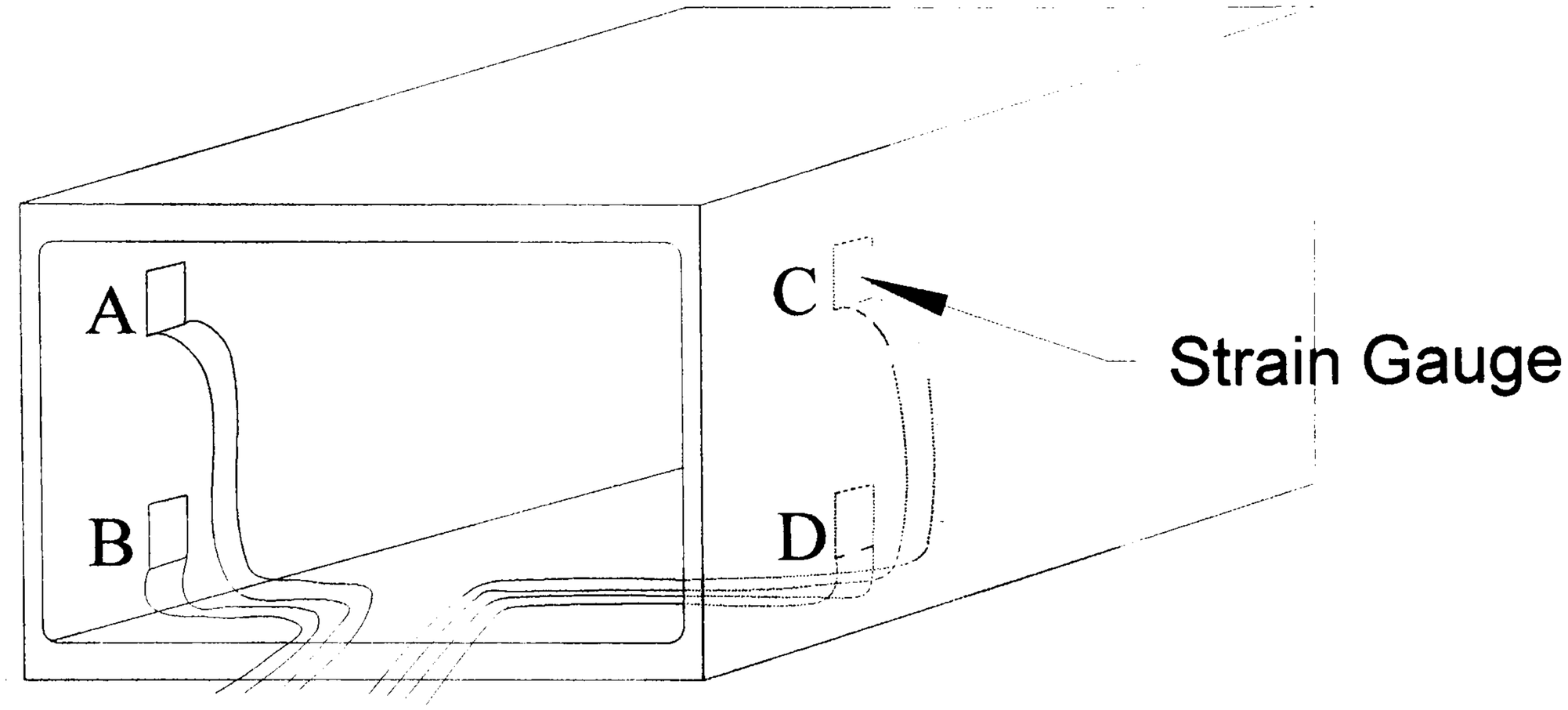

Figure 3.19 Force Gauge Box with Details of Strain Gauges

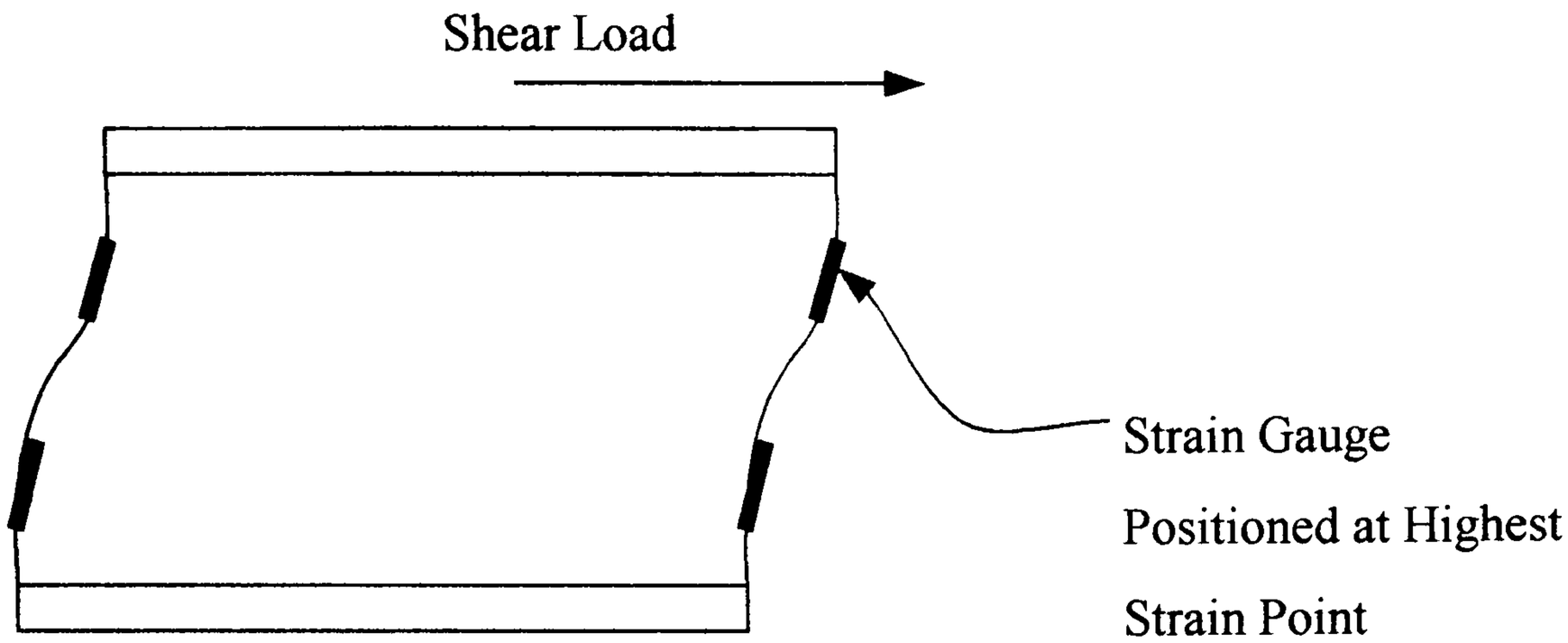

Figure 3.20 Deformations of Force Gauges

3.8 EXPERIMENTAL PROCEDURES

The following procedures were used in order to ensure that the experiment was carefully controlled.

All the segments of each model were ballasted to their individual waterlines and the required ballast recorded. The complete measuring apparatus including bolts for securing the model segments was suspended in a frame prior to installation so that the counter balance weights could be adjusted for correct attitude of the rails. The models were assembled on the rail system with foam strip in the gap between segments, where upon, the complete arrangement was transferred to the towing tank. With all segments ballast and counter balances attached all the spacers from the inner rail were removed to leave the model fixed to the 'live' outer rail at correct draught and trim.

The angle of yaw of the model was set at the foot plate of the towing mechanism. This area consisted of two flat plates, which pivoted about the centre of the towing post in the horizontal plane. The upper plate is delineated in an arc so that a yawing angle may be set to port or starboard in increments of $\pm 2^{\circ}$. The lower plate is bolted to the base of the towing box by four caphead bolts, and these bolts sit in slots which allow adjustment of the model to set a straight ahead condition. With the upper plate set at zero yaw angle the model is towed down the tank and the resulting side force recorded. The yaw angle was adjusted with the lower plate until the side force is zero and this is the defined as the straight ahead towing condition from which all other angles are set. In practise, a side force of less than 0.05 N was accepted as straight-ahead condition. Therefore, in some cases, the zero angle readings have a small residual side force, which was recorded and used in subsequent analysis.

Once the models were set up, data acquisition and recording was a semi-automatic process. The towing carriage and the control room are connected via an umbilical that stretches the full length of the tank. Electrical signals from the fore and aft force gauge boxes are amplified and the processed by computer equipped with data acquisition hardware and software. Before each experimental run, the amplifiers were adjusted so that the fore and aft forces read approximately zero; this adjustment is simply a shifting

of reference origin which is made for convenience. The remaining residual forces are then recorded for a period of 100 seconds, at a sample rate of 1 per second. The mean of these time series were recorded as the residual for and aft forces.

The model was then accelerated down the tank until the test speed of 0.857 m/s was reached, and the data acquisition equipment continually samples the carriage velocity until difference between consecutive values reaches a certain tolerance. The outputs from the fore and aft gauges were then sampled for 10 seconds at a sample rate of 100 readings per second and the resulting time series were stored with the mean and r.m.s. values displayed. All the readings from the force gauges were corrected with their respective calibration factors within the computer software, so that all outputs were displayed directly in Newtons.

After the model was returned to the start position and the tank had settled, the residuals now registered by the amplifiers were compared with the previous values. Generally, the residual values remained less than ± 0.05 N for consecutive experiments. Any greater change in the residual values usually indicated a fault in the system and the affected runs were repeated once this fault had been identified. Thus, any interference between the inner and outer rails was easily detected through the examination of the residual values.

The testing of each model was carried out in the following way. Initially, all the segments of the hull are attached to the outer rail and so were all measured. In the case of the British Bombardier models this was segments 1 to 6. Once the straight-ahead condition had been established, three separate runs are made in each condition, starting at zero degrees yaw angle, then $\pm 2^{\circ}$, $\pm 4^{\circ}$ and $\pm 6^{\circ}$, a total of 21 runs for the complete hull. At this stage the aft most segment, segment 6, was transferred to the inner rail by first bolting the segment to the inner rail and then releasing it form the outer, thus preserving the alignment of the hull. The yaw angle was then set to zero degrees and the experimental procedure repeated for segments 1 to 5, although the straight-ahead condition of the complete model is maintained throughout testing of all model segments.

The experiment proceeded until segment 1 remained on the outer rails and was tested alone, all other segments having been transferred to the inner rail. This successive transferring of segments from the live rails to the earthed rails makes it possible to measure the distribution of side force and yawing moment along the stern region of the various models. The complete experimental programme is summarised in Table 3.5.

Table 3.5 Summary of Experimental Programme.

Models	Number of Segments	Model Speed (m/s)	Yaw Angles (degrees)
Elliptic hull form (with flat plate skeg)	5	0.857	0,±2,±4,±6
Elliptic hull form (no skeg)	5	0.857	0,±2,±4,±6
British Bombardier cruiser stern (conventional stern shape)	6	0.857	0,±2,±4,±6
British Bombardier cruiser stern (no skeg)	6	0.857	0,±2,±4,±6
British Bombardier cruiser stern (no skeg with flat plate)	6	0.857	0,±2,±4,±6
British Bombardier pram stern (with flat plate skeg)	6	0.857	0,±2,±4,±6
British Bombardier pram stern (no skeg)	6	0.857	0,±2,±4,±6

3.9 Initial Testing of the Measuring System

The first model to be tested was the elliptic hull form with a flat plate skeg. This model was based in part on the model tested by Tsakonas [16], with the sections changed to elliptic sections. It was expected that the forces and moments measured would be similar to those presented by Tsakonas, but with the possibility of lower side forces. The results of the first experiments were surprising since the measured side

forces were higher than those of Tsakonas and the measured moments were considerably lower.

The system was removed from the towing tank and set up on a test bench in a way that simulated the tank situation as closely as possible. A series for experiments were carried out in which known masses were suspended from the outer rail over a pulley wheel so that the line of action of force was horizontal. These simple tests showed that the sway forces applied, and the output of the system were in reasonable agreement, although a little too high as was suspected. However, the distribution of the forces between the cells and therefore the calculated moment values were between 10% and 250% in error, depending on the point of application of the force along the rail!

3.10 Correction of Measured Forces and Moments

This section summaries the causes of the observed error and lists some of the methods considered for solving the problem, including experimental and semi-analytical approaches. The final solution procedure involves a combination of physical changes to the apparatus and a graphical method of correcting the measurements. Full details are given in Appendix A1.

As a first step, the apparatus was bench tested with a 200 gram mass applied at a series of points along the rails. The total side force shown in Table 3.6 was calculated by summing the forces recorded at the forward, F_1 and aft, F_2 modular force gauges,

$$\text{Total Side Force} = F_1 + F_2 . \tag{3.1}$$

The moments were calculated by summing the moment contribution of the forces recorded at each modular force gauge. Note that for the elliptic hull, the modular force gauge separation was 0.7 m and moments were taken about a midpoint,

$$\text{Total Moment} = x_1 . F_1 + x_2 . F_2 , \tag{3.2}$$

where $x_1 = 0.35$, and $x_2 = -0.35$.

The calculation of forces and moment in this way rests on the implicit assumption that the structure of the rail is simply connected. The bench test results showed that this assumption was not valid. In reality a considerable fraction of the load applied at the forward modular force gauge is transferred to the aft modular force gauge, and vice-versa. It is this transfer of load that leads to the underestimate of the applied moment.

The degree of fixity between the gauge boxes and the rails means that lateral displacement of one box necessarily results in a lateral displacement of the other, and angular displacement on both. This distorts the readings in the strain gauge bridges.

Several methods were devised to try and correct the torsional effects of the gauge boxes on the measured moments, including the following.

- Semi-Analytical Methods – the force gauges were idealised as a pair of thin flexures to obtain a correction factor.
- Alternative Gauge Configurations – the strain gauges were repositioned to make insensitive to the torsional effects.

These methods were unsuccessful and so a direct graphical method of mapping the experimental outputs of the forward and aft gauges with values for forward and aft forces that correspond to the simply connected structure. These mapped values were used to calculate the corrected total side force and total moment.

This proved satisfactory in correcting experimental results reliably and accurately. However, the disadvantage was that any change in the position of the modular force gauges required another calibration experiment to be carried in order to construct the appropriate contour diagrams, and this was quite lengthy process. Bench testing results indicated that the side forces could be measured to approximately 1% accuracy. Calculated moments were accurate to less than 5%

3.11 Concluding Remarks

In the first part of this chapter a review of the literature has shown that there is experimental evidence to suggest that the strength and sense of rotation of stern vortices is dependent on certain features of the stern geometry. The generalised slender-body theory predicts that vortex strength and sense of rotation have a significant effect on the side force generated by the stern of a ship.

An experiment has been suggested which uses segmented models with a variety of stern geometry to investigate the generalised slender-body theory. This experiment is similar to that carried out previously [52] to test the early development of the slender-body theory and produces the distribution of the manoeuvring force and moment derivatives along the hull. However, unlike the previous experiment, here only the stern end of the models has been segmented since it has already been established that the greatest discrepancy between theory and experiment exists at the stern.

A description has been given of the double rail system, which was made to measure the forces and moments on the segmented models. Initially the system proved to be inaccurate in measuring the moments, despite careful calibration of the active components.

The problem with the rail system has been fully investigated and a number of methods of correcting the errors were tried. The most successful of these was a graphical method, which allowed the measurements from the experiment to be adjusted to provide accurate the force and moment outputs.

4. RESULTS OF SEGMENTED MODEL EXPERIMENTS

4.1 INTRODUCTION

The aim of the experimental programme was to investigate the influence of stern vortices on ship manoeuvring. A theoretical examination of the problem by Clarke and Hearn [28] has been tested with data from previous segmented model experiments. The experiments undertaken at Newcastle concentrate on segmented stern sections to further test the theoretical results and improve understanding of the physical problem.

Chapter 3 described in detail the construction and use of a double rail measuring system. This apparatus was used to measure the longitudinal force and moment distributions in segmented models, which were based on two hull forms. The first set of two models was based on an elliptic hull form and differed only in the provision of a flat plate skeg; the second set of five models was based on the British Bombardier model with a variety of stern geometries.

In the following chapter, the results of these experiments are presented. The first section describes the adjustments made to the data to non-dimensional form. The forces and moments measured for the British Bombardier with conventional stern shape are compared with previous experiments [23], [29] in order to validate the experimental method. The Sections 4.4 and 4.5 give details of the determination of force and moment derivatives by regression analysis. Some discussion is given to the effect of the limited drift angle range on the fitted derivative values.

4.2 ADJUSTMENT OF EXPERIMENTAL DATA

The experimental programme consisted of a total of 826 separate towing tank runs which each yielded a pair of force measurements from the fore and aft modular force gauges. These force data were adjusted to obtain non-dimensional force and moment coefficients. For each experimental run, the mean force recorded at the modular force

gauges was adjusted for the residual gauge reading and then calibrated using the appropriate contour calibration diagram as described in Chapter 3. The total side force and total moment were then calculated using these calibrated force data, the moments being taken about the longitudinal centroid the model, Equations 4.1 and 4.2.

$$\text{Total Side Force}, Y = Y_F + Y_A, \tag{4.1}$$

$$\text{Total Moment}, N = x_F . Y_F + x_A . Y_A . \tag{4.2}$$

The force and moment data are then non-dimensionalised using the length between perpendiculars and model speed, Equations 4.3 and 4.4.

$$Y' = \frac{Y}{\frac{1}{2}\rho U^2 L^2} \tag{4.3}$$

$$N' = \frac{N}{\frac{1}{2}\rho U^2 L^3} \tag{4.4}$$

The resulting non-dimensional total side force and total moment coefficients are presented in Tables 4.1 to 4.36. Each Table corresponds to a model test at the towing angles $0^\circ, \pm 2^\circ, \pm 4^\circ, \pm 6^\circ$ for a given number of active model segments. For example, Table 4.15 presents the results for the test of the British Bombardier conventional stern model with segments 1 to 5 connected to the live rails. Table 4.16 contains the force and moment coefficients of the British Bombardier conventional stern for segments 1 to 6 which is the complete model. Consistent with the adopted reference frame, side forces are positive to starboard and moments are positive in the clockwise sense. The force and moment coefficients have all been multiplied by a factor of 1000 to enhance the clarity of presentation.

The first model to be tested was the elliptic hull form with flat plate skeg. For each experimental condition five repeat runs were carried out to obtain a larger sample and therefore more confidence in the estimated values in data analysis. The precision of the experiment was such that this number of runs was thought excessive and for succeeding

models, all other experimental conditions were repeated three times, making a total of 21 data points for a given number of segments.

Plots of the non-dimensionalised forces for the elliptic hullform (with plate) for segments 1 to 1 and 1 to 5 are shown in Figures 4.1 and 4.2 respectively.

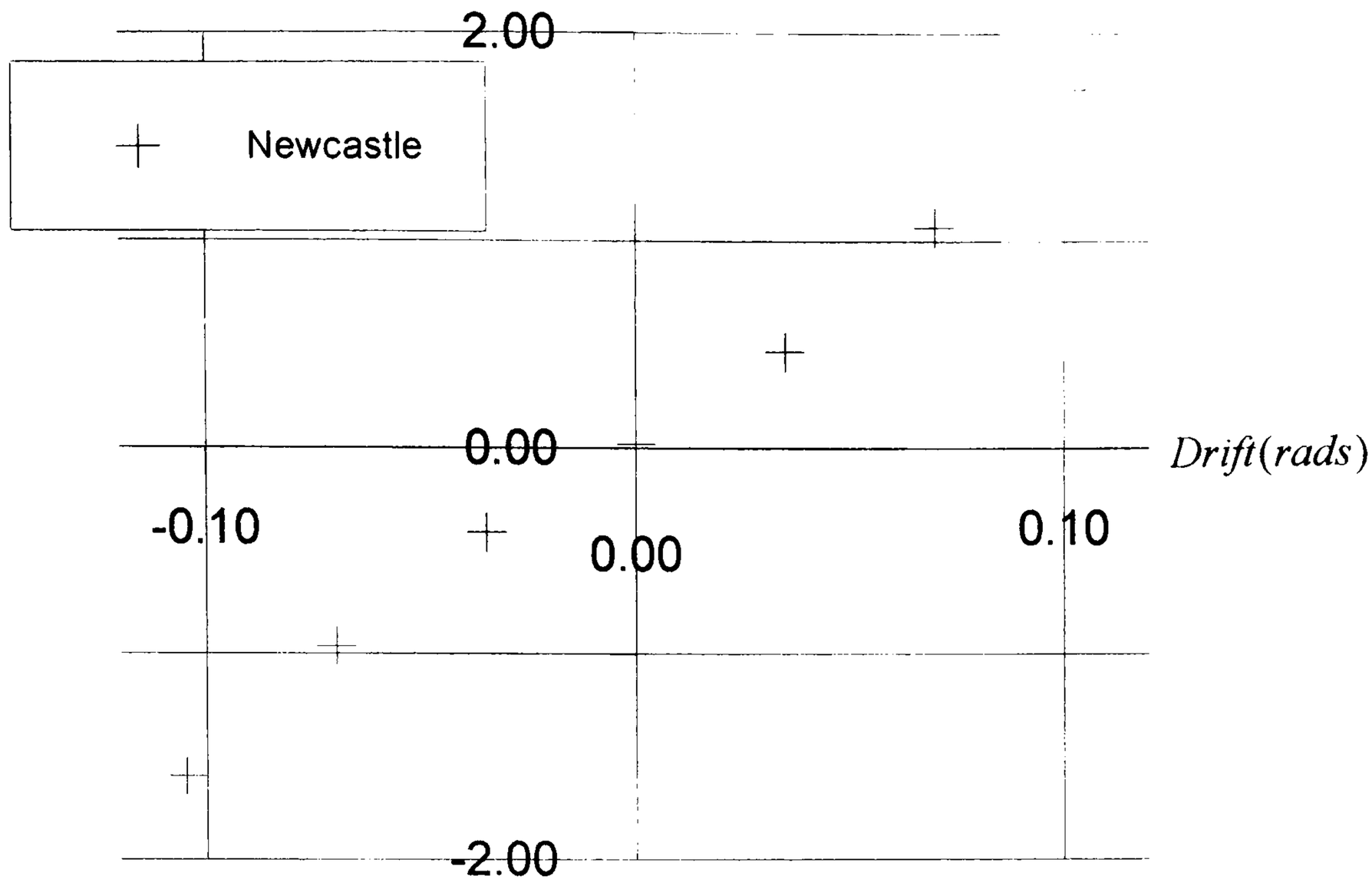

Figure 4.1 Plot of Non-Dimensionalised Side Force, Y', Measured for Segments 1 to 1 of the Elliptic (With Plate) Model.

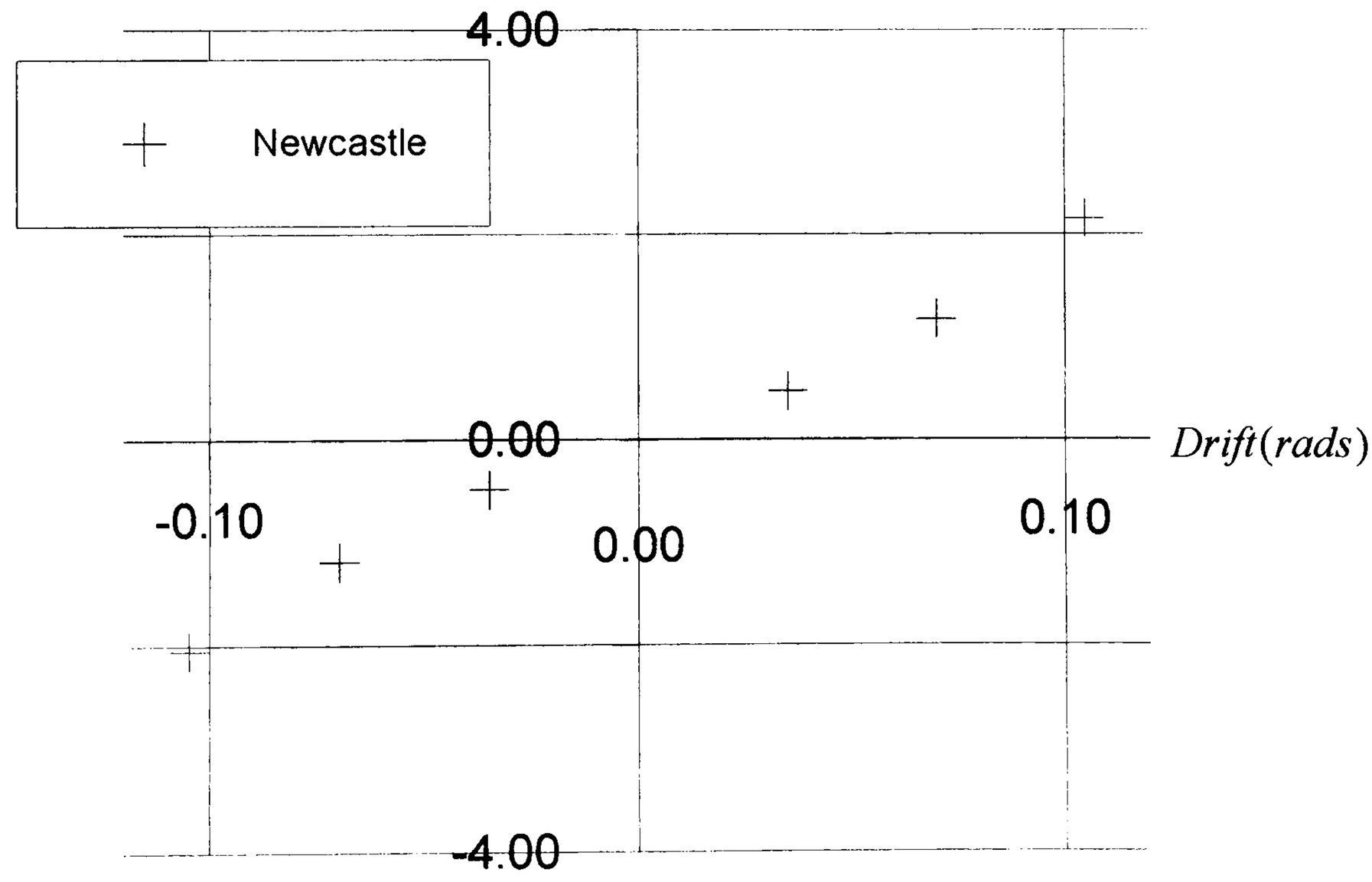

Figure 4.2 Plot of Non-Dimensionalised Side Force, Y', Measured for Segments 1 to 5 of the Elliptic (With Plate) Model.

Table 4.1 Experimental Results for Elliptic Form (With Plate)

Model: Elliptic Form (with plate)			Dimensionless Force and Moment Coefficients			Number of Segments 1 to 1	
Towing Angle (degrees)	**6°S**	**4°S**	**2°S**	**0°**	**2°P**	**4°P**	**6°P**
Side Force Y' $\times 10^3$ (+ S)	1.7320	1.0682	0.4660	0.0198	-0.4088	-0.9627	-1.5957
	1.7496	1.0374	0.4528	0.0437	-0.4176	-0.9100	-1.6133
	1.7672	1.0242	0.5319	0.0434	-0.4484	-0.9891	-1.5693
	1.7232	1.0594	0.5231	0.0264	-0.4396	-0.9451	-1.6045
	1.7232	1.0814	0.5231	0.0371	-0.3649	-0.9671	-1.6045
Moment N' $\times 10^3$ (+ CW)	0.4645	0.2931	0.1374	-0.0025	-0.1460	-0.3048	-0.4647
	0.4634	0.2877	0.1333	0.0004	-0.1516	-0.2983	-0.4685
	0.4647	0.2861	0.1442	-0.0003	-0.1558	-0.3043	-0.4651
	0.4577	0.2900	0.1436	-0.0020	-0.1539	-0.2973	-0.4690
	0.4577	0.2935	0.1460	-0.0012	-0.1439	-0.3008	-0.4629

Table 4.2 Experimental Results for Elliptic Form (With Plate)

Model: Elliptic Form (with plate)			Dimensionless Force and Moment Coefficients			Number of Segments 1 to 2	
Towing Angle (degrees)	**6°S**	**4°S**	**2°S**	**0°**	**2°P**	**4°P**	**6°P**
Side Force Y' $\times 10^3$ (+ S)	1.6485	0.9363	0.3605	0.0474	-0.4264	-0.8924	-1.6177
	1.6836	0.9056	0.3737	-0.0256	-0.4660	-0.9715	-1.6001
	1.6309	0.9495	0.4176	0.0518	-0.4352	-0.9187	-1.5518
	1.5518	0.8792	0.4132	-0.0367	-0.4528	-0.9187	-1.6265
	1.6177	0.9056	0.3605	0.0095	-0.3561	-0.8880	-1.5869
Moment N' $\times 10^3$ (+ CW)	0.4846	0.3065	0.1442	0.0050	-0.1658	-0.3179	-0.4891
	0.4947	0.3060	0.1470	-0.0050	-0.1706	-0.3264	-0.4816
	0.4882	0.3130	0.1516	0.0041	-0.1677	-0.3224	-0.4712
	0.4601	0.3016	0.1531	-0.0055	-0.1678	-0.3175	-0.4861
	0.4842	0.3109	0.1491	-0.0007	-0.1519	-0.3170	-0.4714

Table 4.3 Experimental Results for Elliptic Form (With Plate)

Model: Elliptic Form (with plate)			Dimensionless Force and Moment Coefficients			Number of Segments 1 to 3	
Towing Angle (degrees)	**6°S**	**4°S**	**2°S**	**0°**	**2°P**	**4°P**	**6°P**
Side Force Y' $\times 10^3$ (+ S)	1.7584	0.9803	0.4132	-0.0045	-0.4572	-0.9935	-1.7715
	1.6924	0.9187	0.4176	0.00227	-0.4088	-0.9891	-1.7891
	1.7408	0.9715	0.4176	-0.0292	-0.4792	-0.9715	-1.6836
	1.7759	0.9583	0.4704	-0.0371	-0.4835	-0.9715	-1.7188
	1.7320	0.9275	0.4088	-0.0175	-0.4923	-1.0374	-1.6353
Moment N' $\times 10^3$ (+ CW)	0.4653	0.3061	0.1568	0.0044	-0.1613	-0.2991	-0.4570
	0.4523	0.2978	0.1491	0.0036	-0.1521	-0.2994	-0.4571
	0.4590	0.3067	0.1639	-0.0009	-0.1599	-0.2993	-0.4393
	0.4654	0.2965	0.1716	-0.0010	-0.1596	-0.2944	-0.4493
	0.4485	0.2948	0.1595	-0.0005	-0.1652	-0.3000	-0.4363

Table 4.4 Experimental Results for Elliptic Form (With Plate)

Model: Elliptic Form (with plate)			Dimensionless Force and Moment Coefficients			Number of Segments 1 to 4	
Towing Angle (degrees)	**6°S**	**4°S**	**2°S**	**0°**	**2°P**	**4°P**	**6°P**
Side Force Y' $\times 10^3$ (+ S)	2.0089	1.1781	0.3912	0.0295	-0.4220	-1.0990	-1.9474
	1.9869	1.0506	0.4616	-0.0342	-0.4528	-1.0067	-1.9606
	1.9606	1.1473	0.4748	0.0123	-0.4660	-1.0198	-1.8902
	1.9474	1.1210	0.3956	0.0127	-0.4044	-1.0814	-2.0045
	1.8902	1.0638	0.5011	-0.0113	-0.4835	-1.0726	-1.9122
Moment N' $\times 10^3$ (+ CW)	0.4011	0.2897	0.1471	0.0025	-0.1513	-0.2862	-0.4051
	0.3988	0.2721	0.1487	-0.0040	-0.1555	-0.2737	-0.4018
	0.3956	0.2855	0.1553	0.0000	-0.1559	-0.2753	-0.3940
	0.4041	0.2786	0.1382	0.0007	-0.1512	-0.2848	-0.4113
	0.3817	0.2700	0.1560	-0.0034	-0.1596	-0.2879	-0.4061

Table 4.5 Experimental Results for Elliptic Form (With Plate)

Model: Elliptic Form (with plate)			Dimensionless Force and Moment Coefficients			Number of Segments 1 to 5	
Towing Angle (degrees)	**6°S**	**4°S**	**2°S**	**0°**	**2°P**	**4°P**	**6°P**
Side Force Y' $\times 10^3$ (+ S)	2.1496	1.1693	0.4660	-0.0134	-0.4879	-1.1869	-2.0485
	2.0837	1.1297	0.4616	0.0113	-0.5055	-1.2001	-2.1100
	2.1188	1.0902	0.4967	-0.0008	-0.4923	-1.1649	-2.1056
	2.1188	1.2968	0.4396	-0.0050	-0.4923	-1.1429	-2.0705
	2.1760	1.2089	0.4484	-0.0096	-0.4616	-1.1957	-2.1452
Moment N' $\times 10^3$ (+ CW)	0.3650	0.2459	0.1472	0.0019	-0.1409	-0.2497	-0.3530
	0.3557	0.2374	0.1426	0.0033	-0.1521	-0.2526	-0.3503
	0.3584	0.2400	0.1465	0.0009	-0.1382	-0.2376	-0.3506
	0.3596	0.2673	0.1428	0.0019	-0.1406	-0.2366	-0.3528
	0.3645	0.2557	0.1459	0.0027	-0.1303	-0.2479	-0.3530

Table 4.6 Experimental Results for Elliptic Form (No Skeg)

Model: Elliptic Form (no skeg)			**Dimensionless Force and Moment Coefficients**			**Number of Segments 1 to 1**	
Towing Angle (degrees)	**6°S**	**4°S**	**2°S**	**0°**	**2°P**	**4°P**	**6°P**
Side Force Y'	1.6252	1.0021	0.5403	0.0217	-0.4662	-0.9869	-1.6339
$\times 10^3$ **(+ S)**	1.7254	1.0239	0.5795	0.0235	-0.4096	-0.9803	-1.6448
	1.7254	1.0326	0.4793	-0.0076	-0.4248	-0.9803	-1.6469
Moment N'	0.4248	0.2783	0.1458	-0.0049	-0.1518	-0.2963	-0.4547
$\times 10^3$ **(+ CW)**	0.4501	0.2757	0.1457	-0.0035	-0.1493	-0.3004	-0.4595
	0.4574	0.2787	0.1314	-0.0068	-0.1495	-0.2955	-0.4612

Table 4.7 Experimental Results for Elliptic Form (No Skeg)

Model: Elliptic Form (no skeg)			**Dimensionless Force and Moment Coefficients**			**Number of Segments 1 to 2**	
Towing Angle (degrees)	**6°S**	**4°S**	**2°S**	**0°**	**2°P**	**4°P**	**6°P**
Side Force Y'	1.5446	0.9084	0.4096	0.0012	-0.4030	-0.9019	-1.5990
$\times 10^3$ **(+ S)**	1.5467	0.9498	0.4618	0.0005	-0.4008	-0.9019	-1.5642
	1.5990	0.9542	0.4444	-0.0026	-0.4096	-0.9150	-1.5642
Moment N'	0.4770	0.3124	0.1444	-0.0030	-0.1534	-0.3164	-0.4960
$\times 10^3$ **(+ CW)**	0.4896	0.3195	0.1533	-0.0028	-0.1572	-0.3177	-0.4970
	0.4826	0.3180	0.1568	-0.0022	-0.1578	-0.3229	-0.4848

Table 4.8 Experimental Results for Elliptic Form (No Skeg)

Model: Elliptic Form (no skeg)			**Dimensionless Force and Moment Coefficients**			**Number of Segments 1 to 3**	
Towing Angle (degrees)	**6°S**	**4°S**	**2°S**	**0°**	**2°P**	**4°P**	**6°P**
Side Force Y'	1.4792	0.8257	0.3529	-0.0244	-0.3573	-0.8801	-1.4857
$\times 10^3$ **(+ S)**	1.4857	0.8583	0.3616	-0.0372	-0.3398	-0.8453	-1.4966
	1.5489	0.8278	0.3878	-0.0070	-0.4104	-0.8736	-1.4596
Moment N'	0.5141	0.3360	0.1566	-0.0055	-0.1612	-0.3276	-0.5070
$\times 10^3$ **(+ CW)**	0.5131	0.3351	0.1597	-0.0043	-0.1611	-0.3225	-0.5020
	0.5218	0.3249	0.1580	-0.0012	-0.1712	-0.3231	-0.4977

Table 4.9 Experimental Results for Elliptic Form (No Skeg)

Model: Elliptic Form (no skeg)			**Dimensionless Force and Moment Coefficients**			**Number of Segments 1 to 4**	
Towing Angle (degrees)	**6°S**	**4°S**	**2°S**	**0°**	**2°P**	**4°P**	**6°P**
Side Force Y'	1.2788	0.7407	0.3268	-0.0286	-0.3442	-0.7864	-1.3463
$\times 10^3$ (+ S)	1.3027	0.7973	0.3181	-0.0050	-0.3224	-0.8191	-1.3485
	1.2962	0.7712	0.3115	-0.0055	-0.3442	-0.8278	-1.3681
Moment N'	0.5319	0.3500	0.1644	-0.0030	-0.1730	-0.3635	-0.5379
$\times 10^3$ (+ CW)	0.5432	0.3573	0.1650	-0.0002	-0.1732	-0.3694	-0.5341
	0.5253	0.3529	0.1672	-0.0021	-0.1730	-0.3786	-0.5390

Table 4.10 Experimental Results for Elliptic Form (No Skeg)

Model: Elliptic Form (no skeg)			**Dimensionless Force and Moment Coefficients**			**Number of Segments 1 to 5**	
Towing Angle (degrees)	**6°S**	**4°S**	**2°S**	**0°**	**2°P**	**4°P**	**6°P**
Side Force Y'	1.3028	0.7886	0.3355	0.0091	-0.3486	-0.7952	-1.3594
$\times 10^3$ **(+ S)**	1.3006	0.7777	0.3094	0.0210	-0.3290	-0.8148	-1.3289
	1.2679	0.7363	0.3486	0.0071	-0.3028	-0.7472	-1.3550
Moment N'	0.5310	0.3481	0.1736	0.0042	-0.1703	-0.3544	-0.5395
$\times 10^3$ **(+ CW)**	0.5335	0.3525	0.1631	00028	-0.1740	-0.3526	-0.5305
	0.5204	0.3344	0.1789	0.0040	-0.1757	-0.3411	-0.5349

Table 4.11 Experimental Results for British Bombardier Conventional Stern

Model: British Bombardier Conventional Stern			**Dimensionless Force and Moment Coefficients**			**Number of Segments 1 to 1**	
Towing Angle (degrees)	**6°S**	**4°S**	**2°S**	**0°**	**2°P**	**4°P**	**6°P**
Side Force Y'	1.7112	1.0819	0.5306	-0.0500	-0.6417	-1.2587	-1.8346
$\times 10^3$ **(+ S)**	1.6989	1.0983	0.5101	-0.0641	-0.6540	-1.2587	-1.7935
	1.6948	1.0695	0.5306	-0.0683	-0.6623	-1.2258	-1.7976
Moment N'	0.6241	0.4144	0.2144	0.0000	-0.1978	-0.4029	-0.6065
$\times 10^3$ **(+ CW)**	0.6195	0.4177	0.2123	-0.0069	-0.2051	-0.4048	-0.5967
	0.6208	0.4125	0.2116	-0.0057	-0.2082	-0.3989	-0.5983

Table 4.12 Experimental Results for British Bombardier Conventional Stern

Model: British Bombardier Conventional Stern			**Dimensionless Force and Moment Coefficients**			**Number of Segments 1 to 2**	
Towing Angle (degrees)	**6°S**	**4°S**	**2°S**	**0°**	**2°P**	**4°P**	**6°P**
Side Force Y'	1.6783	1.0777	0.5018	-0.0616	-0.6211	-1.2094	-1.7112
$\times 10^3$ **(+ S)**	1.6907	1.1436	0.5306	-0.0590	-0.6623	-1.2217	-1.7030
	1.6742	1.1024	0.5018	-0.0850	-0.6582	-1.2423	-1.7112
Moment N'	0.6146	0.4128	0.2092	-0.0076	-0.2039	-0.4039	-0.5688
$\times 10^3$ **(+ CW)**	0.6165	0.4263	0.2116	-0.0082	-0.2165	-0.4112	-0.5658
	0.6131	0.4193	0.2064	-0.0125	-0.2177	-0.4161	-0.5688

Table 4.13 Experimental Results for British Bombardier Conventional Stern

Model: British Bombardier Conventional Stern			**Dimensionless Force and Moment Coefficients**			**Number of Segments 1 to 3**	
Towing Angle (degrees)	**6°S**	**4°S**	**2°S**	**0°**	**2°P**	**4°P**	**6°P**
Side Force Y'	1.6166	1.0325	0.4566	-0.0807	-0.6335	-1.1929	-1.7606
$\times 10^3$ **(+ S)**	1.6207	1.0202	0.4772	-0.0868	-0.6705	-1.2094	-1.7359
	1.6043	1.0819	0.4895	-0.0922	-0.6499	-1.2011	-1.7400
Moment N'	0.6801	0.4789	0.2587	0.0102	-0.1975	-0.4060	-0.5928
$\times 10^3$ **(+ CW)**	0.6788	0.4632	0.2636	0.0059	-0.2030	-0.4094	-0.5919
	0.6810	0.4835	0.2654	0.0053	-0.1981	-0.4036	-0.5879

Table 4.14 Experimental Results for British Bombardier Conventional Stern

Model: British Bombardier Conventional Stern			**Dimensionless Force and Moment Coefficients**			**Number of Segments 1 to 4**	
Towing Angle (degrees)	**6°S**	**4°S**	**2°S**	**0°**	**2°P**	**4°P**	**6°P**
Side Force Y'	1.5220	0.9955	0.4278	-0.0464	-0.5800	-1.0366	-1.6043
$\times 10^3$ **(+ S)**	1.5467	0.9749	0.4319	-0.0481	-0.5759	-1.0531	-1.6084
	1.5014	0.9708	0.4443	-0.0724	-0.5841	-1.0613	-1.6207
Moment N'	0.7609	0.5204	0.2562	-0.0077	-0.2853	-0.5108	-0.7225
$\times 10^3$ **(+ CW)**	0.7563	0.5155	0.2605	-0.0087	-0.2810	-0.5142	-0.7212
	0.7366	0.5139	0.2624	-0.0146	-0.2869	-0.5090	-0.7286

Table 4.15 Experimental Results for British Bombardier Conventional Stern

Model: British Bombardier Conventional Stern			**Dimensionless Force and Moment Coefficients**			**Number of Segments 1 to 5**	
Towing Angle (degrees)	**6°S**	**4°S**	**2°S**	**0°**	**2°P**	**4°P**	**6°P**
Side Force Y'	1.6207	1.0284	0.4977	-0.0264	-0.5759	-1.0901	-1.6577
$\times 10^3$ **(+ S)**	1.6084	1.0243	0.5018	-0.0181	-0.5882	-1.0695	-1.6865
	1.6166	1.0119	0.4772	-0.0509	-0.5923	-1.0777	-1.6907
Moment N'	0.6927	0.4801	0.2353	-0.0131	-0.2672	-0.4921	-0.6733
$\times 10^3$ **(+ CW)**	0.6908	0.4924	0.2424	-0.0061	-0.2718	-0.5010	-0.6702
	0.6911	0.4657	0.2304	-0.0162	-0.2733	-0.4930	-0.6800

Table 4.16 Experimental Results for British Bombardier Conventional Stern

Model: British Bombardier Conventional Stern			Dimensionless Force and Moment Coefficients			Number of Segments 1 to 6	
Towing Angle (degrees)	**6°S**	**4°S**	**2°S**	**0°**	**2°P**	**4°P**	**6°P**
Side Force Y'	1.7688	1.1641	0.5430	0.0086	-0.6006	-1.1888	-1.7976
$\times 10^3$ **(+ S)**	1.7853	1.1106	0.5594	-0.0086	-0.5882	-1.1765	-1.8305
	1.7894	1.1106	0.6047	-0.0141	-0.6170	-1.2094	-1.8511
Moment N'	0.5599	0.4091	0.1914	-0.0054	-0.2377	-0.4432	-0.5817
$\times 10^3$ **(+ CW)**	0.5688	0.3975	0.1837	-0.0156	-0.2442	-0.4441	-0.5801
	0.5703	0.4002	0.1978	-0.0137	-0.2438	-0.4370	-0.5878

Table 4.17 Experimental Results for British Bombardier Conventional Stern (No Skeg)

Model: British Bombardier Conventional Stern (no skeg)			**Dimensionless Force and Moment Coefficients**			**Number of Segments 1 to 3**	
Towing Angle (degrees)	**6°S**	**4°S**	**2°S**	**0°**	**2°P**	**4°P**	**6°P**
Side Force Y'	1.7770	1.1353	0.5553	-0.0185	-0.5759	-1.1250	-1.7359
$\times 10^3$ (+ S)	1.7709	1.1970	0.5985	0.0004	-0.5615	-1.1065	-1.7380
	1.8198	1.1888	0.5985	-0.0048	-0.5656	-1.1230	-1.7606
Moment N'	0.6625	0.4523	0.2513	0.0285	-0.1539	-0.3351	-0.5228
$\times 10^3$ (+ CW)	0.6699	0.4739	0.2687	0.0319	-0.1568	-0.3310	-0.5249
	0.6801	0.4708	0.2646	0.0322	-0.1528	-0.3357	-0.5292

Table 4.18 Experimental Results for British Bombardier Conventional Stern (No Skeg)

Model: British Bombardier Conventional Stern (no skeg)			**Dimensionless Force and Moment Coefficients**			**Number of Segments 1 to 4**	
Towing Angle (degrees)	**6°S**	**4°S**	**2°S**	**0°**	**2°P**	**4°P**	**6°P**
Side Force Y'	1.5816	1.0572	0.5121	0.0477	-0.4525	-0.9214	-1.5097
$\times 10^3$ **(+ S)**	1.5487	1.0263	0.5060	0.0666	-0.4401	-0.9153	-1.5241
	1.5775	1.0284	0.4854	0.0472	-0.4134	-0.8967	-1.4665
Moment N'	0.7776	0.5600	0.2821	0.0254	-0.2102	-0.4403	-0.6678
$\times 10^3$ **(+ CW)**	0.7640	0.5416	0.2854	0.0324	-0.2056	-0.4352	-0.6649
	0.7692	0.5230	0.2832	0.0290	-0.2080	-0.4366	-0.6656

Table 4.19 Experimental Results for British Bombardier Conventional Stern (No Skeg)

Model: British Bombardier Conventional Stern (no skeg)			Dimensionless Force and Moment Coefficients			Number of Segments 1 to 5	
Towing Angle (degrees)	**6°S**	**4°S**	**2°S**	**0°**	**2°P**	**4°P**	**6°P**
Side Force Y'	1.3575	0.9441	0.4175	0.0112	-0.4237	-0.8289	-1.3883
$\times 10^3$ (+ S)	1.3677	0.9502	0.4401	0.0253	-0.4031	-0.8021	-1.3821
	1.3863	0.9502	0.4401	0.0379	-0.3970	-0.7816	-1.3739
Moment N'	0.8530	0.6242	0.3616	0.0412	-0.2188	-0.5094	-0.7525
$\times 10^3$ (+ CW)	0.8554	0.6279	0.3659	0.0421	-0.2166	-0.5064	-0.7475
	0.8623	0.6141	0.3686	0.0451	-0.2129	-0.4904	-0.7472

Table 4.20 Experimental Results for British Bombardier Conventional Stern (No Skeg)

Model: British Bombardier Conventional Stern (no skeg)			**Dimensionless Force and Moment Coefficients**			**Number of Segments 1 to 6**	
Towing Angle (degrees)	**6°S**	**4°S**	**2°S**	**0°**	**2°P**	**4°P**	**6°P**
Side Force Y'	1.3801	0.9132	0.4155	-0.0070	-0.4237	-0.9050	-1.4356
$\times 10^3$ (+ S)	1.4212	0.9255	0.4401	0.0122	-0.4216	-0.8680	-1.4171
	1.4253	0.9605	0.4545	0.0197	-0.4175	-0.8659	-1.4171
Moment N'	0.8434	0.6113	0.3456	0.0362	-0.2326	-0.4728	-0.7287
$\times 10^3$ (+ CW)	0.8477	0.6187	0.3493	0.0437	-0.2332	-0.4521	-0.7273
	0.8520	0.6096	0.3408	0.0434	-0.2331	-0.4665	-0.7204

Table 4.21 Experimental Results for British Bombardier Conventional Stern (No Skeg With Plate)

Model: British Bombardier Conventional Stern (no skeg with plate)			Dimensionless Force and Moment Coefficients			Number of Segments 1 to 3	
Towing Angle (degrees)	**6°S**	**4°S**	**2°S**	**0°**	**2°P**	**4°P**	**6°P**
Side Force Y'	1.7014	1.1306	0.5446	-0.0230	-0.5337	-1.1328	-1.7014
$\times 10^3$ (+ S)	1.7079	1.1590	0.5686	-0.0244	-0.5207	-1.1306	-1.7058
	1.7624	1.1807	0.5512	-0.0180	-0.5403	-1.1568	-1.7123
Moment N'	0.7060	0.4947	0.2850	0.0270	-0.1624	-0.3872	-0.6035
$\times 10^3$ (+ CW)	0.7026	0.5023	0.2764	0.0320	-0.1487	-0.3805	-0.5949
	0.7317	0.5134	0.2772	0.0352	-0.1721	-0.4005	-0.5944

Table 4.22 Experimental Results for British Bombardier Conventional Stern (No Skeg With Plate)

Model: British Bombardier Conventional Stern (no skeg with plate)			**Dimensionless Force and Moment Coefficients**			**Number of Segments 1 to 4**	
Towing Angle (degrees)	**6°S**	**4°S**	**2°S**	**0°**	**2°P**	**4°P**	**6°P**
Side Force Y'	1.6252	1.0914	0.4945	-0.0230	-0.4575	-0.8104	-1.4030
$\times 10^3$ (+ S)	1.6121	1.1067	0.5250	-0.0244	-0.4531	-0.8692	-1.4073
	1.6535	1.1503	0.5054	-0.0180	-0.4379	-0.8845	-1.4117
Moment N'	0.8284	0.5957	0.2912	0.0270	-0.2511	-0.4675	-0.7148
$\times 10^3$ (+ CW)	0.8191	0.6058	0.2997	0.0320	-0.2538	-0.4748	-0.7252
	0.8228	0.6045	0.2909	0.0352	-0.2569	-0.4878	-0.7166

Table 4.23 Experimental Results for British Bombardier Conventional Stern (No Skeg With Plate)

Model: British Bombardier Conventional Stern (no skeg with plate)			**Dimensionless Force and Moment Coefficients**			**Number of Segments 1 to 5**	
Towing Angle (degrees)	**6°S**	**4°S**	**2°S**	**0°**	**2°P**	**4°P**	**6°P**
Side Force Y'	1.5947	1.0675	0.5185	0.0073	-0.4248	-0.9368	-1.5162
$\times 10^3$ (+ S)	1.5620	1.0762	0.5076	0.0554	-0.4183	-0.9781	-1.4836
	1.6056	1.0326	0.5054	0.0439	-0.4357	-0.9150	-1.5162
Moment N'	0.7555	0.5590	0.3163	0.0209	-0.2447	-0.4927	-0.6955
$\times 10^3$ (+ CW)	0.7653	0.5637	0.3078	0.0326	-0.2408	-0.4949	-0.6980
	0.7742	0.5548	0.2997	0.0270	0.2429	-0.4875	-0.6941

Table 4.24 Experimental Results for British Bombardier Conventional Stern (No Skeg With Plate)

Model: British Bombardier Conventional Stern (no skeg with plate)			**Dimensionless Force and Moment Coefficients**			**Number of Segments 1 to 6**	
Towing Angle (degrees)	**6°S**	**4°S**	**2°S**	**0°**	**2°P**	**4°P**	**6°P**
Side Force Y'	1.7755	1.1350	0.5577	0.0524	-0.4727	-1.0413	-1.7363
$\times 10^3$ (+ S)	1.7450	1.1415	0.5403	0.0431	-0.4793	-1.1045	-1.7210
	1.7058	1.1611	0.5969	0.0569	-0.4793	-0.9934	-1.7428
Moment N'	0.6780	0.5036	0.2957	0.0405	-0.1762	-0.3970	-0.5785
$\times 10^3$ (+ CW)	0.6769	0.5105	0.2951	0.0360	-0.1787	-0.3971	-0.5699
	0.6696	0.5046	0.3016	0.0434	-0.1757	-0.3806	-0.5765

Table 4.25 Experimental Results for British Bombardier Pram Stern (With Plate)

Model: British Bombardier Pram Stern (with plate)			Dimensionless Force and Moment Coefficients			Number of Segments 1 to 1	
Towing Angle (degrees)	**6°S**	**4°S**	**2°S**	**0°**	**2°P**	**4°P**	**6°P**
Side Force Y'	1.6099	1.0348	0.4553	-0.1583	-0.7821	-1.2548	-1.8888
$\times 10^3$ (+ S)	1.5663	1.0348	0.4553	-0.1513	-0.7472	-1.2818	-1.8613
	1.5968	1.0370	0.4531	-0.1595	-0.7908	-1.2788	-1.8670
Moment N'	0.6265	0.4165	0.2224	-0.0140	-0.2184	-0.3814	-0.6178
$\times 10^3$ (+ CW)	0.6103	0.4150	0.2180	-0.0098	-0.2068	-0.3953	-0.5996
	0.6187	0.4188	0.2202	-0.0139	-0.2201	-0.3947	-0.6067

Table 4.26 Experimental Results for British Bombardier Pram Stern (With Plate)

Model: British Bombardier Pram Stern (with plate)			**Dimensionless Force and Moment Coefficients**			**Number of Segments 1 to 2**	
Towing Angle (degrees)	**6°S**	**4°S**	**2°S**	**0°**	**2°P**	**4°P**	**6°P**
Side Force Y'	1.6862	1.0740	0.5546	-0.0715	-0.5926	-1.1459	-1.6870
$\times 10^3$ **(+ S)**	1.6469	1.1067	0.5381	-0.0919	-0.6078	-1.1241	-1.6404
	1.6295	1.1720	0.5276	-0.0667	-0.6261	-1.1633	-1.6448
Moment N'	0.5993	0.3814	0.1921	-0.0346	-0.2355	-0.4623	-0.6582
$\times 10^3$ **(+ CW)**	0.5847	0.3862	0.1889	-0.0411	-0.2471	-0.4542	-0.6481
	0.5811	0.4106	0.1791	-0.0317	-0.2554	-0.4688	-0.6556

Table 4.27 Experimental Results for British Bombardier Pram Stern (With Plate)

Model: British Bombardier Pram Stern (with plate)			**Dimensionless Force and Moment Coefficients**			**Number of Segments 1 to 3**	
Towing Angle (degrees)	**6°S**	**4°S**	**2°S**	**0°**	**2°P**	**4°P**	**6°P**
Side Force Y'	1.5010	0.9803	0.4279	-0.1022	-0.5926	-1.0849	-1.5860
$\times 10^3$ (+ S)	1.4640	0.9424	0.4631	-0.1129	0.5917	-1.0871	-1.6339
	1.4400	0.9760	0.3930	-0.0891	-0.5817	-1.1219	-1.6077
Moment N'	0.7338	0.4826	0.2151	-0.0380	-0.2619	-0.5333	-0.7523
$\times 10^3$ (+ CW)	0.7156	0.4690	0.2341	-0.0380	-0.2856	-0.5224	-0.7643
	0.6993	0.4839	0.2051	-0.0226	-0.2783	-0.5418	-0.7458

Table 4.28 Experimental Results for British Bombardier Pram Stern (With Plate)

Model: British Bombardier Pram Stern (with plate)			Dimensionless Force and Moment Coefficients			Number of Segments 1 to 4	
Towing Angle (degrees)	**6°S**	**4°S**	**2°S**	**0°**	**2°P**	**4°P**	**6°P**
Side Force Y'	1.3812	0.9019	0.3900	-0.0765	-0.5228	-0.9694	-1.5119
$\times 10^3$ (+ S)	1.4117	0.9063	0.3747	-0.0682	-0.4902	-1.0195	-1.5947
	1.3855	0.8888	0.3812	-0.538	-0.4758	-0.9564	-1.5655
Moment N'	0.8165	0.5851	0.2815	-0.0041	-0.2828	-0.5429	-0.7627
$\times 10^3$ (+ CW)	0.8220	0.5955	0.2978	-0.0004	-0.2852	-0.5587	-0.8024
	0.8240	0.5949	0.3017	0.0003	-0.2807	-0.5483	-0.7950

Table 4.29 Experimental Results for British Bombardier Pram Stern (With Plate)

Model: British Bombardier Pram Stern (with plate)			Dimensionless Force and Moment Coefficients			Number of Segments 1 to 5	
Towing Angle (degrees)	**6°S**	**4°S**	**2°S**	**0°**	**2°P**	**4°P**	**6°P**
Side Force Y'	1.4204	0.8692	0.3769	-0.0443	-0.4932	-0.9978	-1.5655
$\times 10^3$ (+ S)	1.3899	0.9215	0.3246	-0.0234	-0.4967	-0.9542	-1.5511
	1.4008	0.8453	0.3921	-0.0353	-0.4749	-1.0043	-1.6121
Moment N'	0.7520	0.5363	0.2884	-0.0043	-0.2834	-0.5154	-0.7116
$\times 10^3$ (+ CW)	0.7641	0.5485	0.2820	-0.0027	-0.2876	-0.5065	-0.7071
	0.7667	0.5347	0.2940	0.0002	-0.2678	-0.5208	-0.7210

Table 4.30 Experimental Results for British Bombardier Pram Stern (With Plate)

Model: British Bombardier Pram Stern (with plate)			**Dimensionless Force and Moment Coefficients**			**Number of Segments 1 to 6**	
Towing Angle (degrees)	**6°S**	**4°S**	**2°S**	**0°**	**2°P**	**4°P**	**6°P**
Side Force Y'	1.5555	0.8954	0.4858	-0.0271	-0.4671	-0.9259	-1.6339
$\times 10^3$ **(+ S)**	1.5903	0.9760	0.4422	-0.0185	-0.4557	-0.9738	-1.5860
	1.5598	0.9760	0.4836	-0.0146	-0.4845	-0.9999	-1.7119
Moment N'	0.6531	0.4729	0.2441	-0.0083	-0.2707	-0.4916	-0.6472
$\times 10^3$ **(+ CW)**	0.6661	0.4824	0.2381	-0.0064	-0.2694	-0.4831	-0.6527
	0.6635	0.4956	0.2623	-0.0132	-0.2714	-0.5045	-0.6678

Table 4.31 Experimental Results for British Bombardier Pram Stern (No Skeg)

Model: British Bombardier Pram Stern (no skeg)			Dimensionless Force and Moment Coefficients			Number of Segments 1 to 1	
Towing Angle (degrees)	**6°S**	**4°S**	**2°S**	**0°**	**2°P**	**4°P**	**6°P**
Side Force Y'	1.8449	1.2053	0.5779	-0.0663	-0.6602	-1.2053	-1.8182
$\times 10^3$ (+ S)	1.8716	1.1826	0.5923	-0.0327	-0.6397	-1.2073	-1.8099
	1.8449	1.2053	0.5800	-0.0189	-0.6520	-1.1950	-1.7997
Moment N'	0.5731	0.3857	0.2141	0.0126	-0.1425	-0.3083	-0.4926
$\times 10^3$ (+ CW)	0.5817	0.3856	0.2181	0.0212	-0.1403	-0.3105	-0.4882
	0.5744	0.3857	0.2107	0.0256	-0.1422	-0.3073	-0.4857

Table 4.32 Experimental Results for British Bombardier Pram Stern (No Skeg)

Model: British Bombardier Pram Stern (no skeg)			Dimensionless Force and Moment Coefficients			Number of Segments 1 to 2	
Towing Angle (degrees)	**6°S**	**4°S**	**2°S**	**0°**	**2°P**	**4°P**	**6°P**
Side Force Y'	1.7976	1.2053	0.5594	0.0243	-0.5574	-1.1148	-1.6536
$\times 10^3$ (+ S)	1.8202	1.2032	0.6067	0.0057	-0.5656	-1.1230	-1.6907
	1.8079	1.2053	0.6294	-0.0028	-0.5656	-1.0839	-1.7194
Moment N'	0.5527	0.3940	0.2030	0.0229	0.2180	00139	-0.1556
$\times 10^3$ (+ CW)	0.5597	0.3933	0.2096	0.0191	0.0229	-0.1511	-0.3285
	0.5579	0.3982	0.2180	0.0139	0.0191	-0.1542	-0.3316

Table 4.33 Experimental Results for British Bombardier Pram Stern (No Skeg)

Model: British Bombardier Pram Stern (no skeg)			**Dimensionless Force and Moment Coefficients**			**Number of Segments 1 to 3**	
Towing Angle (degrees)	**6°S**	**4°S**	**2°S**	**0°**	**2°P**	**4°P**	**6°P**
Side Force Y'	1.6290	1.0942	0.5265	0.0323	-0.4628	-0.9667	-1.4973
$\times 10^3$ **(+ S)**	1.6207	1.0860	0.5718	0.0320	-0.4689	-0.9482	-1.4891
	1.6207	1.0983	0.5430	0.0492	-0.4772	-0.9790	-1.4624
Moment N'	0.6570	0.4826	0.2516	0.0357	-0.1684	-0.3742	-0.5693
$\times 10^3$ **(+ CW)**	0.6567	0.4795	0.2629	0.0299	-0.1748	-0.3784	-0.5772
	0.6484	0.4813	0.2660	0.0364	-0.1737	-0.3802	-0.5700

Table 4.34 Experimental Results for British Bombardier Pram Stern (No Skeg)

Model: British Bombardier Pram Stern (no skeg)			**Dimensionless Force and Moment Coefficients**			**Number of Segments 1 to 4**	
Towing Angle (degrees)	**6°S**	**4°S**	**2°S**	**0°**	**2°P**	**4°P**	**6°P**
Side Force Y'	1.2834	0.8597	0.3682	-0.0112	-0.4031	-0.7569	-1.2073
$\times 10^3$ **(+ S)**	1.2690	0.8618	0.3682	-0.0186	-0.3908	-0.7240	-1.1950
	1.2772	0.8823	0.3949	-0.0058	-03826	-0.7425	-1.2053
Moment N'	0.8323	0.6135	0.3197	0.0218	-0.2498	-0.5157	-0.7431
$\times 10^3$ **(+ CW)**	0.8380	0.5991	0.3252	0.0169	-0.2563	-0.5035	-0.7496
	0.8493	0.6192	0.3241	0.0202	-0.2532	-0.5104	-0.7451

Table 4.35 Experimental Results for British Bombardier Pram Stern (No Skeg)

Model: British Bombardier Pram Stern (no skeg)			**Dimensionless Force and Moment Coefficients**			**Number of Segments 1 to 5**	
Towing Angle (degrees)	**6°S**	**4°S**	**2°S**	**0°**	**2°P**	**4°P**	**6°P**
Side Force Y'	1.0592	0.7219	0.3353	0.0048	-0.3270	-0.6479	-0.9749
$\times 10^3$ (+ S)	1.0675	0.6582	0.3209	-0.0113	-0.3311	-0.6458	-0.9770
	1.1065	0.6746	0.3147	-0.0134	-0.3435	-0.6684	-1.0099
Moment N'	0.9284	0.6686	0.3738	0.0280	-0.3002	-0.5981	-0.8472
$\times 10^3$ (+ CW)	0.9384	0.6531	0.3684	0.0245	-0.2962	-0.5946	-0.8493
	0.9516	0.6551	0.3827	0.0258	-0.2898	-0.5878	-0.8436

Table 4.36 Experimental Results for British Bombardier Pram Stern (No Skeg)

Model: British Bombardier Pram Stern (no skeg)			**Dimensionless Force and Moment Coefficients**			**Number of Segments 1 to 6**	
Towing Angle (degrees)	**6°S**	**4°S**	**2°S**	**0°**	**2°P**	**4°P**	**6°P**
Side Force Y'	1.0489	0.6253	0.2921	-0.0172	-0.2777	-0.6129	-0.9811
$\times 10^3$ (+ S)	1.0345	0.6540	0.2735	-0.0090	-0.2859	-0.6170	-0.9543
	1.0498	0.6705	0.2797	0.0056	-0.3065	-0.6253	-0.9420
Moment N'	1.0268	0.7113	0.3853	0.0219	-0.3122	-0.6155	-0.9214
$\times 10^3$ (+ CW)	1.0311	0.7193	0.3936	0.0273	-0.3070	-0.6087	-0.9086
	1.0271	0.7144	0.3890	0.0322	-0.3091	-0.6063	-0.9151

4.3 Comparison of Forces and Moment Estimates

To validate the experimental results presented in Section 4.2 it is necessary to make comparisons with previous measurements of the forces and moments on the same hull forms. These comparisons are made by directly examining the force and moment measurements at a number of experimental conditions. In Section 4.4 the same hull forms are compared by examining the derivative values obtained from the fitting of the data points. The British Bombardier model has been tested at Newcastle and elsewhere [23], [29] and will be used here to assess the accuracy of the experiments.

The non-dimensional force and moment data for the British Bombardier complete model are plotted in Figures 4.5 and 4.6. This compares the experimental results obtained by Clarke [23], Glasgow [29] and those presented in Table 4.11.

The results from Newcastle cover drift angles $6^\circ S, 4^\circ S, 2^\circ S, 0^\circ, 2^\circ P, 4^\circ P, 6^\circ P$; the results from Clarke [23] cover drift angles $4^\circ S, 0^\circ, 2^\circ P, 4^\circ P, 6^\circ P, 8^\circ P, 12^\circ P$; the results from Glasgow cover drift angles $0^\circ, 2^\circ P, 4^\circ P, 6^\circ P, 8^\circ P, 10^\circ P, 12^\circ P, 15^\circ P$. However, we are only concerned here with comparison up to the drift angles measured at Newcastle. As is normal practise [16], since models are usually only tested to either port or starboard, the omitted drift angles are obtained by reflecting the results about the straight-ahead condition. It may be recalled that the Newcastle models could only be set to a maximum drift angle of six degrees, due to a physical constraint of the experimental set-up, and so results were recorded to port and starboard to increase the sample size for analysis.

Figure 4.5 shows the comparison for the non-dimensionalised side force, Y' measured for the British Bombardier complete model. The agreement between Newcastle and Clarke and Hearn [28] is very good, although there is some difference between these measurements and those of Glasgow [29]. Figure 4.6 shows similar comparisons for the non-dimensional yaw moment, N'. In this case the moments measured at Newcastle tend to be at the lower end of the range when compared with the other sources [28],

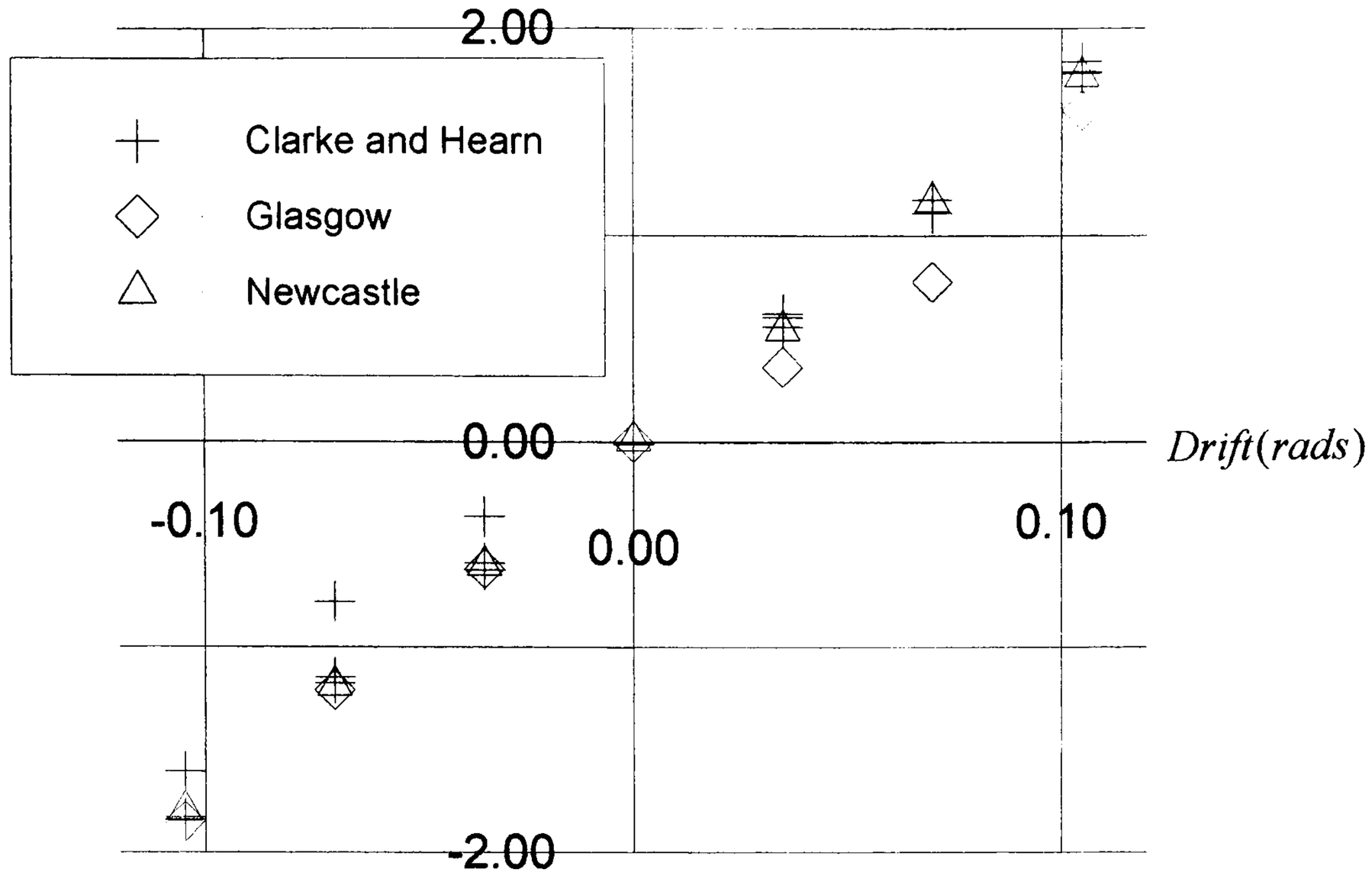

Figure 4.3 Comparison of Non-Dimensionalised Side Force, Y', Measured for the British Bombardier Complete Model

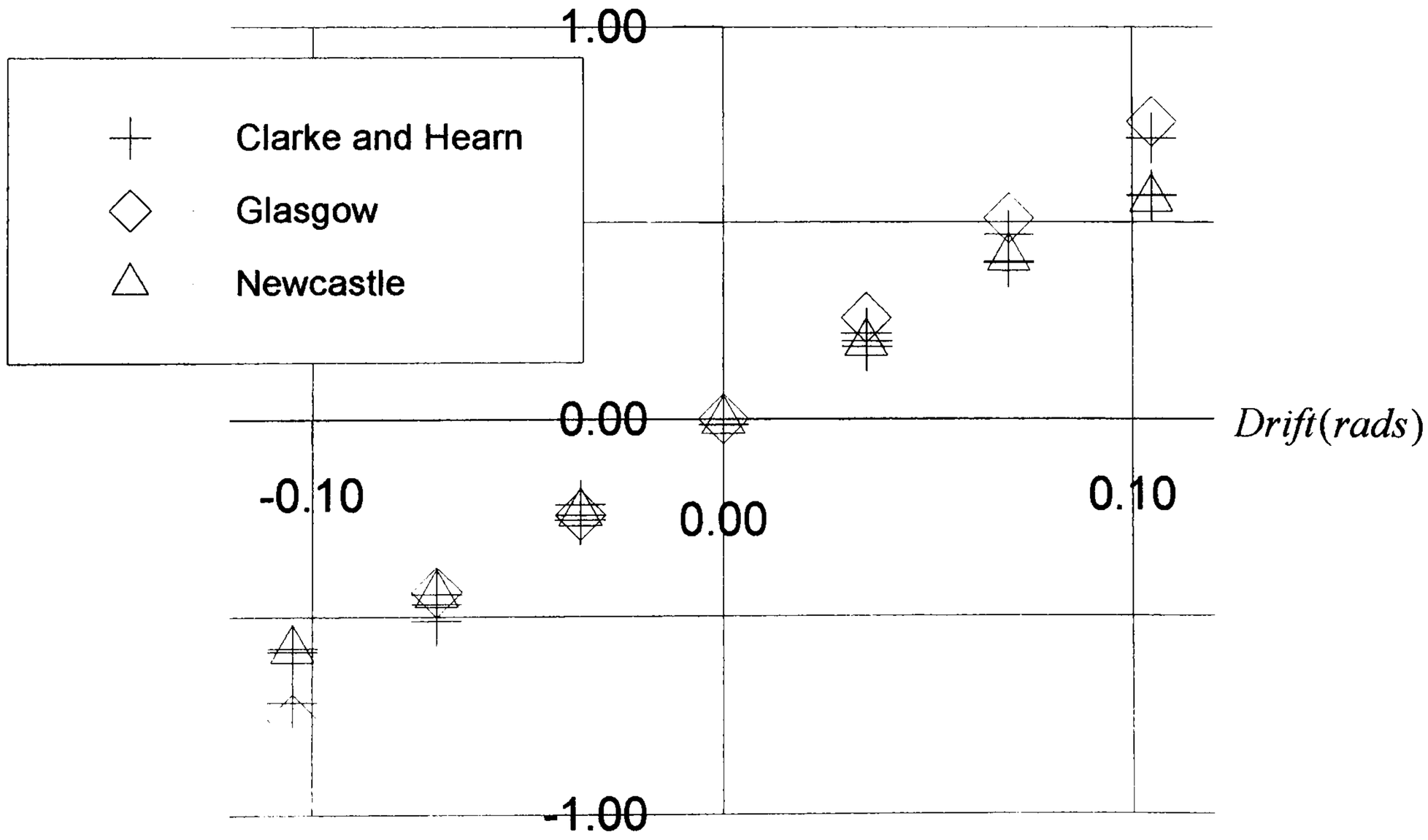

Figure 4.4 Comparison of Non-Dimensionalised Yaw Moment, N', Measured for the British Bombardier Complete Model.

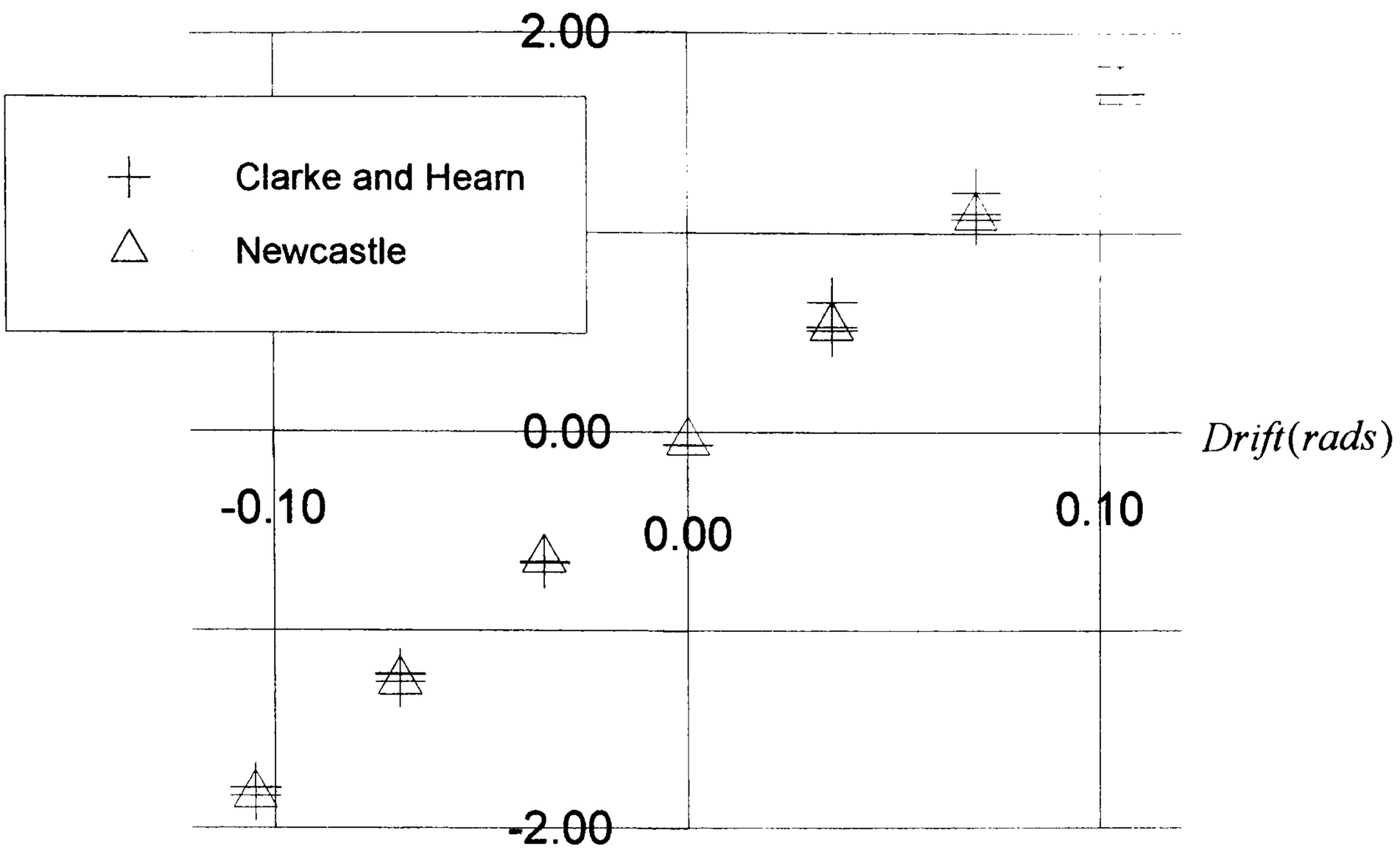

Figure 4.5 Comparison of Non-Dimensionalised Side Force, Y', Measured for the British Bombardier Model up to Station 4.0

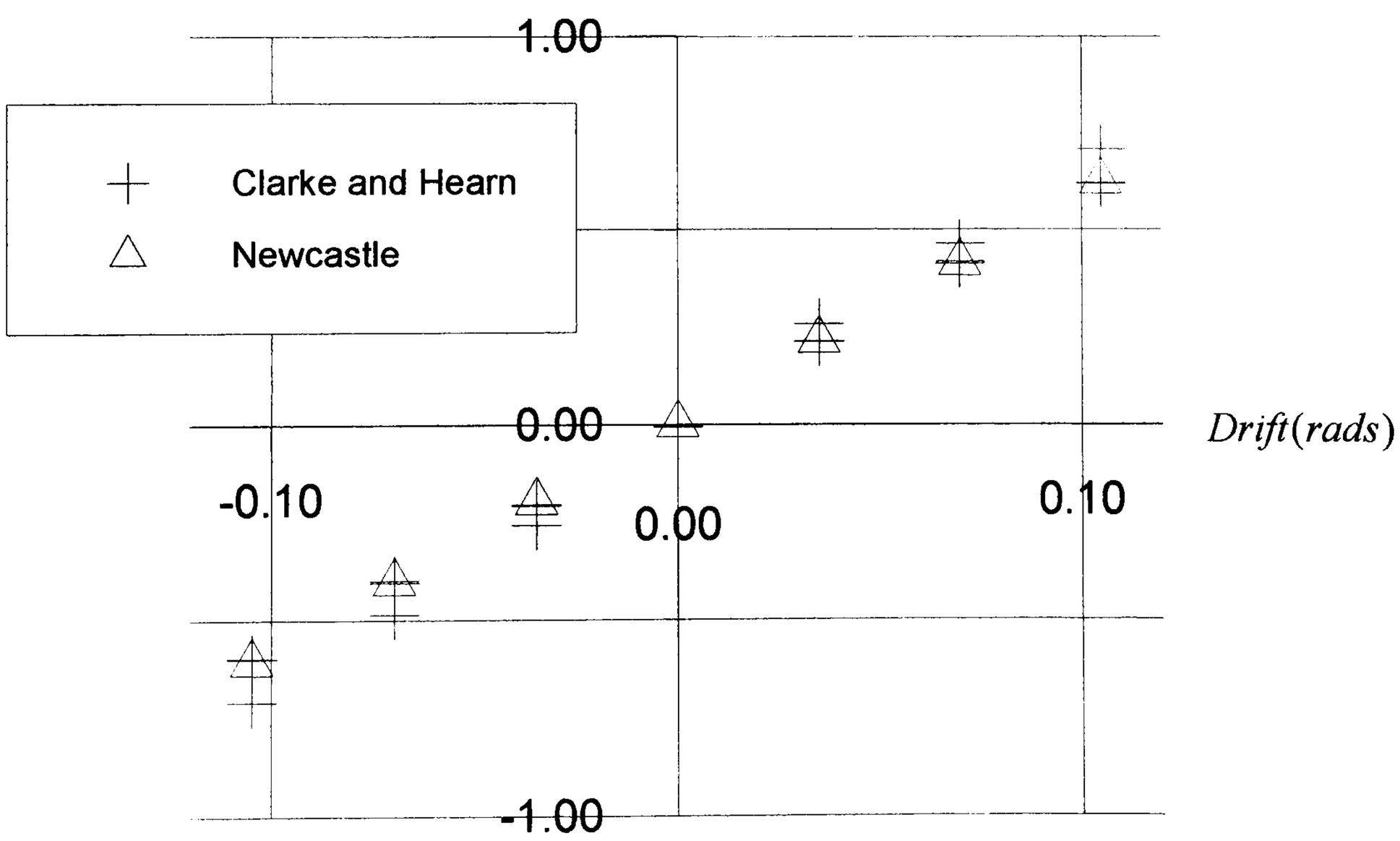

Figure 4.6 Comparison of Non-Dimensionalised Yaw Moment, N', Measured for the British Bombardier Model up to Station 4.0

[29], although still showed very good agreement with those presented by Clarke and Hearn [28]

The experiments carried out by Clarke [23] were on a segmented British Bombardier model. There is a corresponding segment between Clarke and Hearn [28] and Newcastle at Station 4 on this model and the non-dimensionalised forces and moments for the British Bombardier from the F.P. to Station 4 are compared in Figure 4.5 and 4.6.

Figure 4.5 shows the comparison for the non-dimensionalised side force, Y' measured at Station 4 of the British Bombardier model. Again, the agreement between Newcastle and Clarke and Hearn [28] is very good. Figure 4.6 shows similar comparisons for the non-dimensional yaw moment, N'.

The above comparisons demonstrate that the side forces measured at Newcastle are accurate for the complete model and at an intermediate segmented point, and can therefore be compared with theoretical predictions with confidence. The original concerns over the possible effects of scale and blockage on the experimental results have not been detected in these results.

It is interesting to note that the measured side forces on the complete British Bombardier model from Glasgow [29] as illustrated in Figure 4.5 shows a significant difference to those of Newcastle and Clarke and Hearn [28]. In the experiments conducted by Clarke [23] the model was free in heave, pitch and roll, but constrained in all other modes as was the case for the experiments at Newcastle

4.4 Comparison for Fitted Derivative Values

The experimental data presented in Section 4.2 describes the measured distribution of force and moment along the length of the seven models tested. Each Table gives the cumulative force and moment, from the bow to a particular section in the model for various drift angles. It is now possible to fit polynomial expressions to the measured

forces and moments in order to obtain an estimate of the derivative values for the models tested.

The method used to obtain the cumulated hydrodynamic derivatives at each station is exactly the same as that used for analysis of complete model data. The data is fitted with a polynomial expression using linear regression and the coefficients of the resulting fit are the required hydrodynamic derivatives. As discussed in Chapter 1, the most appropriate mathematical form of this polynomial expression is, to date, the subject of some debate [11]. Historically, a third order expression has been used although this is simply a consequence of expanding hydrodynamic force and moment derivatives using a Taylor series expansion. Other experimental facilities, notably Lyngby, have favoured the use of a second order form on the grounds that some physical aspects of the manoeuvring ship hydrodynamics can more readily identified with a cross flow drag which is described by such an expansion.

The appropriateness of the chosen polynomial expressions can be evaluated with reference to statistical measures of goodness of fit, the measure used here being the standard deviation of the sum of the residuals, s. An alternative analysis of previous segmented model data [28] has used the goodness of fit to examine the most appropriate order of fit where non-integer powers of the sway velocity were used. This analysis has lead to some tentative conclusions about the most appropriate mathematical form of the data fitting polynomial in the light of vortex influence considerations. This aspect of the work will be discussed it detail in Section 4.6.

The experimental force and moment data was fitted with both second and third order polynomial expressions. For oblique towing tests, the second and third order expansions of the hydrodynamic side force in terms of sway velocity are given in Equations 4.5 and 4.6 respectively.

$$Y(x) = Y_0 + Y_v v + Y_{v|v|} v|v| \tag{4.5}$$

$$Y(x) = Y_0 + Y_v v + Y_{vvv} v^3 \tag{4.6}$$

Polynomial expressions for the total moment arising from oblique towing tests can be obtained by simply replacing Y with N in Equations 4.5 and 4.6.

The only element of these expressions that require further explanation is the inclusion of a constant term which implies an asymmetry in the experiment. The models tested were symmetrical about the longitudinal centre plane and were not fitted with propeller or rudder and should therefore show no asymmetry when towed to port or starboard. However, due to the limited range of drift angles $0^\circ, \pm 2^\circ, \pm 4^\circ, \pm 6^\circ$, the models were tested to both port and starboard and in the straight ahead condition in order to obtain a reasonable sample size.

Setting the zero angle for each model was done by making a series of runs down the tank and making adjustments until the total measured side force was ≤ 0.05 Newtons. Three experimental runs were recorded at zero drift angle in the same way as any other angle to measure the small but finite asymmetry introduce by the experimental design. The zero heading force and moment data was therefore included in the linear regression analysis, although the estimated values for the constant terms were found to be insignificant. If zero heading readings had been ignored, the regression line would have been forced through the origin which was theoretically correct, but for which there were no experimental data points.

Comparison of the derivative estimates from this least squares method for the British Bombardier have been made between the Newcastle and Clarke and Hearn [28] experiments. Tables 4.37 and 4.38 show the results for the sway force derivative distribution from Newcastle and Clarke respectively using a second order fit. Note that only the Clarke results for the aft end of the hull from Station 4 have been reproduced. Table 4.39 and 4.40 show the corresponding comparison for the third order fit.

Table 4.37 Newcastle. Sway Force Derivatives for British Bombardier with Conventional Stern Using a Second Order Fit

Number of Segments	X'	$-Y_v'/\pi(T/L)^2$		$-Y_{v\|v\|}'/\pi(T/L)^2$	
		Value	Stn. Dev.	Value	Stn. Dev.
1 to 1	-0.1	1.6756	0.0238	0.003	0.2579
1 to 2	-0.1818	1.7244	0.0415	-0.9705	0.4496
1 to 3	-0.2636	1.6183	0.0239	-0.1259	0.289
1 to 4	-0.3454	1.4045	0.0276	0.8683	0.2987
1 to 5	-0.4272	1.4567	0.0268	1.0609	0.2897
1 to 6	-0.5	1.6034	0.0321	1.1090	0.3479

Table 4.38 Clarke and Hearn [28]. Sway Force Derivatives for British Bombardier with Conventional Stern Using a Second Order Fit.

Number of Segments	X'	$-Y_v'/\pi(T/L)^2$		$-Y_{v\|v\|}'/\pi(T/L)^2$	
		Value	Stn. Dev.	Value	Stn. Dev.
1 to 6	-0.1	1.5102	0.0845	2.4218	0.4961
1 to 7	-0.3	1.3632	0.0165	2.7250	0.0967
1 to 8	-0.4	1.2970	0.0464	2.8035	0.2724
1 to 9	-0.5	1.4207	0.0530	3.2704	0.3111

Table 4.39 Newcastle. Sway Force Derivatives for British Bombardier with Conventional Stern Using a Third Order Fit

Number of Segments	X'	$-Y_v'/\pi(T/L)^2$		$-Y_{vvv}'/\pi(T/L)^2$	
		Value	Stn. Dev.	Value	Stn. Dev.
1 to 1	-0.1	1.6744	0.0152	0.1792	1.6569
1 to 2	-0.1818	1.6939	0.0260	-6.6312	2.8378
1 to 3	-0.2636	1.6139	0.0153	0.08065	1.6626
1 to 4	-0.3454	1.4328	0.0172	5.8247	1.8774
1 to 5	-0.4272	1.4879	0.0156	7.5273	1.7014
1 to 6	-0.5	1.6380	0.0197	7.6169	2.1431

Table 4.40 Clarke and Hearn [28]. Sway Force Derivatives for British Bombardier with Conventional Stern Using a Third Order Fit.

Number of Segments	X'	$-Y_v'/\pi(T/L)^2$		$-Y_{vvv}'/\pi(T/L)^2$	
		Value	Stn. Dev.	Value	Stn. Dev.
1 to 6	-0.1	1.6532	0.0367	8.5600	1.1090
1 to 7	-0.3	1.5391	0.0238	9.1176	0.7179
1 to 8	-0.4	1.4757	0.0316	9.4579	0.9558
1 to 9	-0.5	1.6250	0.0208	11.1770	0.6298

Examining these Tables a direct comparison can be made between equivalent Stations on the hull. These points are segments 1 to 1 and 1 to 6 for the Newcastle data and segments 1 to 1 and 1 to 9 for the Clarke and Hearn data respectively corresponding to Station 4.0 and the complete model. A comparison of the linear derivatives show that the fitted estimates derived from the Newcastle data are approximately 10% greater than those obtained by Clarke for the second order fit, but match very closely for the

third order fit. Comparison on the non-linear derivatives shows that the Newcastle derivatives are a considerable under estimate of those derived by Clarke.

The Newcastle experiments were conducted at various drift angles not exceeding $\pm 6^{\circ}$ and this is small in comparison to other oblique towing tests [23], [16]. Initial regression of the force and moment data showed that a linear fitting of the data resulted in high values for 's' when compared with non-linear fitting, a fact which justifies the use of non-linear polynomials. This was generally found to be the case, except in a few instances. It can be seen from Table 4.37 and 4.39 that where a negative estimate of the non-linear derivative is indicated the simple linear fit would be more appropriate.

It was concluded that the small drift angles were insufficient to provide a reliable estimate of non-linear effects. In addition, the low values for the non-linear derivative estimates produces an over estimate of the linear derivative as a consequence of the fitting method. This fitting artefact is similar to that observed when comparing the linear derivative estimates arising from second and third order fitting of the same set of experimental data. Note that the effect on estimated linear derivatives of fitting artefacts is dependent on non-linearity of the experimental points. It was observed that models equipped with flat plate skegs showed more non-linear effects at lower drift angles than did those models with more rounded underwater sections. The discrepency between previous results [28] and Newcastle cannot therefore be easily corrected since it is model dependent.

Comparison of fitted moments with previous experiments [28] is illustrated for the linear moment derivative estimates arising from a second order fit, shown in Tables 4.41 and 4.42.

Table 4.41 Newcastle. Yaw Moment Derivatives for British Bombardier with Conventional Stern Using a Second Order Fit

Number of Segments	X'	$-N_v'/\pi(T/L)^2$	
		Value	Stn. Dev.
1 to 1	-0.1	0.5981	0.0081
1 to 2	-0.1818	0.6380	0.0182
1 to 3	-0.2636	0.6858	0.0176
1 to 4	-0.3454	0.8096	0.0168
1 to 5	-0.4272	0.7757	0.0168
1 to 6	-0.5	0.6832	0.0138

Table 4.42 Clarke and Hearn [28]. Yaw Moment Derivatives for British Bombardier with Conventional Stern Using a Second Order Fit.

Number of Segments	X'	$-N_v'/\pi(T/L)^2$	
		Value	Stn. Dev.
1 to 6	-0.1	0.6242	0.0276
1 to 7	-0.3	0.7291	0.0311
1 to 8	-0.4	0.7623	0.0100
1 to 9	-0.5	0.6690	0.0012

Generally, Newcastle moment values show good agreement with those estimated by Clarke and Hearn [28]. The Newcastle values are derived from the moment data which has been shown above to be at the lower end of the range compared to other results for the British Bombardier [23], [29]. With the effect of fitting on estimating of linear derivatives, it is thought that these errors nullify each other to produce more accurate results than was expected.

4.5 SEGMENTAL FORCE AND MOMENT DERIVATIVES

The results of the regression analysis are presented for the seven models considered in Table 4.43 to 4.58. For each model there are two Tables for the second and third order data fitting respectively. The Tables contain the linear hydrodynamic force and moment derivatives for a given number of model segments and the station to which that number of segments corresponds. The standard deviation of these derivative estimates is included as a measure of the experimental precision. Where measures of goodness of fit indicate that linear fitting would be more appropriate, these values are shown in Table 4.57 and 4.58 used in subsequent analysis.

In addition to the usual non-dimensionalisation of the force and moment data prior to regression analysis, the tabulated derivative values have been normalised with the factor $-\pi(T/L)^2$. This was found to be the common factor arising from the slender body theoretical analysis discussed in Chapter 2, and is used to adjust the experimental derivatives here so that they may be more easily be compared with theoretical results in Chapter 5.

4.5.1 British Bombardier Conventional Stern

Table 4.43 Linear Force and Moment Sway Derivatives for British Bombardier with Conventional Stern Using a Second Order Fit

Number of Segments	X'	$-Y_v'/\pi(T/L)^2$		$-N_v'/\pi(T/L)^2$	
		Value	Stn. Dev.	Value	Stn. Dev.
1 to 1	-0.1	1.6756	0.0238	0.5981	0.0081
1 to 2	-0.1818	1.7244	0.0415	0.6380	0.0182
1 to 3	-0.2636	1.6183	0.0239	0.6858	0.0176
1 to 4	-0.3454	1.4045	0.0276	0.8096	0.0168
1 to 5	-0.4272	1.4567	0.0268	0.7757	0.0168
1 to 6	-0.5	1.6034	0.0321	0.6832	0.0138

Table 4.44 Linear Force and Moment Sway Derivatives for British Bombardier with Conventional Stern Using a Third Order Fit.

Number of Segments	X'	$-Y_v'/\pi(T/L)^2$		$-N_v'/\pi(T/L)^2$	
		Value	Stn. Dev.	Value	Stn. Dev.
1 to 1	-0.1	1.6744	0.0152	0.5927	0.0052
1 to 2	-0.1818	1.6939	0.0260	0.6149	0.0114
1 to 3	-0.2636	1.6139	0.0153	0.6587	0.0114
1 to 4	-0.3454	1.4328	0.0172	0.7733	0.0111
1 to 5	-0.4272	1.4879	0.0156	0.7355	0.0105
1 to 6	-0.5	1.6380	0.0197	0.6410	0.0078

4.5.2 British Bombardier Conventional Stern (no skeg)

Table 4.45 Linear Force and Moment Sway Derivatives for British Bombardier with Conventional Stern (no skeg) Using a Second Order Fit

Number of Segments	X'	$-Y_v'/\pi(T/L)^2$		$-N_v'/\pi(T/L)^2$	
		Value	Stn. Dev.	Value	Stn. Dev.
1 to 1	-0.1	-	-	-	-
1 to 2	-0.1818	-	-	-	-
1 to 3	-0.2636	1.5950	0.0312	0.5937	0.0216
1 to 4	-0.3454	1.2693	0.0291	0.7220	0.0159
1 to 5	-0.4272	1.1444	0.0470	0.8737	0.0167
1 to 6	-0.5	1.1782	0.0287	0.8423	0.0181

Table 4.46 Linear Force and Moment Sway Derivatives for British Bombardier with Conventional Stern (no skeg) Using a Third Order Fit.

Number of Segments	X'	$-Y_v'/\pi(T/L)^2$		$-N_v'/\pi(T/L)^2$	
		Value	Stn. Dev.	Value	Stn. Dev.
1 to 1	-0.1	-	-	-	-
1 to 2	-0.1818	-	-	-	-
1 to 3	-0.2636	1.6223	0.0194	0.5845	0.0139
1 to 4	-0.3454	1.3348	0.0185	0.7109	0.0101
1 to 5	-0.4272	1.2015	0.0301	0.8385	0.0106
1 to 6	-0.5	1.2387	0.0189	0.8087	0.0122

4.5.3 British Bombardier Conventional Stern (no skeg with plate)

Table 4.47 Linear Force and Moment Sway Derivatives for British Bombardier with Conventional Stern (no skeg with plate) Using a Second Order Fit

Number of Segments	X'	$-Y_v'/\pi(T/L)^2$		$-N_v'/\pi(T/L)^2$	
		Value	Stn. Dev.	Value	Stn. Dev.
1 to 1	-0.1	-	-	-	-
1 to 2	-0.1818	-	-	-	-
1 to 3	-0.2636	1.5819	0.0318	0.6491	0.0180
1 to 4	-0.3454	1.3342	0.0851	0.8260	0.0264
1 to 5	-0.4272	1.3089	0.0291	0.8480	0.0084
1 to 6	-0.5	1.4021	0.0435	0.7281	0.0116

Table 4.48 Linear Force and Moment Sway Derivatives for British Bombardier with Conventional Stern (no skeg with plate) Using a Third Order Fit.

Number of Segments	X'	$-Y_v'/\pi(T/L)^2$		$-N_v'/\pi(T/L)^2$	
		Value	Stn. Dev.	Value	Stn. Dev.
1 to 1	-0.1	-	-	-	-
1 to 2	-0.1818	-	-	-	-
1 to 3	-0.2636	1.6089	0.0208	0.6431	0.0114
1 to 4	-0.3454	1.3739	0.0543	0.7977	0.0166
1 to 5	-0.4272	1.3700	0.0197	0.7987	0.0049
1 to 6	-0.5	1.4887	0.0279	0.6845	0.0074

4.5.4 British Bombardier Pram Stern (with skeg)

Table 4.49 Linear Force and Moment Sway Derivatives for British Bombardier with Pram Stern (with skeg) Using a Second Order Fit

Number of Segments	X'	$-Y_v'/\pi(T/L)^2$		$-N_v'/\pi(T/L)^2$	
		Value	Stn. Dev.	Value	Stn. Dev.
1 to 1	-0.1	1.7391	0.0355	0.6068	0.0168
1 to 2	-0.1818	1.6882	0.0472	0.6411	0.0114
1 to 3	-0.2636	1.4719	0.0325	0.7365	0.0172
1 to 4	-0.3454	1.2023	0.0363	0.8845	0.0183
1 to 5	-0.4272	1.1393	0.0403	0.8636	0.0159
1 to 6	-0.5	1.1599	0.0533	0.8193	0.0142

Table 4.50 Linear Force and Moment Sway Derivatives for British Bombardier with Pram Stern (with skeg) Using a Third Order Fit.

Number of Segments	X'	$-Y_v'/\pi(T/L)^2$		$-N_v'/\pi(T/L)^2$	
		Value	Stn. Dev.	Value	Stn. Dev.
1 to 1	-0.1	1.7020	0.0235	0.5956	0.0109
1 to 2	-0.1818	1.6533	0.0301	0.6259	0.0072
1 to 3	-0.2636	1.4739	0.0207	0.7281	0.0107
1 to 4	-0.3454	1.2746	0.0240	0.8484	0.0110
1 to 5	-0.4272	1.2377	0.0268	0.8091	0.0107
1 to 6	-0.5	1.2761	0.0314	0.7571	0.0084

4.5.5 British Bombardier Pram Stern (no skeg)

Table 4.51 Linear Force and Moment Sway Derivatives for British Bombardier with Pram Stern (no skeg) Using a Second Order Fit

Number of Segments	X'	$-Y_v'/\pi(T/L)^2$		$-N_v'/\pi(T/L)^2$	
		Value	Stn. Dev.	Value	Stn. Dev.
1 to 1	-0.1	1.7244	0.0411	0.4945	0.0124
1 to 2	-0.1818	1.6469	0.0384	0.5308	0.0103
1 to 3	-0.2636	1.4491	0.0262	0.6540	0.0109
1 to 4	-0.3454	1.0749	0.0466	0.8753	0.0179
1 to 5	-0.4272	0.9136	0.0377	1.0015	0.0133
1 to 6	-0.5	0.7789	0.0340	1.0171	0.0166

Table 4.52 Linear Force and Moment Sway Derivatives for British Bombardier with Pram Stern (no skeg) Using a Third Order Fit.

Number of Segments	X'	$-Y_v'/\pi(T/L)^2$		$-N_v'/\pi(T/L)^2$	
		Value	Stn. Dev.	Value	Stn. Dev.
1 to 1	-0.1	1.7269	0.0261	0.4975	0.0078
1 to 2	-0.1818	1.6532	0.0245	0.5243	0.0066
1 to 3	-0.2636	1.4615	0.0168	0.6329	0.0065
1 to 4	-0.3454	1.1135	0.0299	0.8372	0.0107
1 to 5	-0.4272	0.9375	0.0240	0.9499	0.0095
1 to 6	-0.5	0.8425	0.0226	0.9847	0.0112

4.5.6 Elliptic Hull Form (with skeg)

Table 4.53 Linear Force and Moment Sway Derivatives for Elliptic Hull Form (with skeg) Using a Second Order Fit

Number of Segments	X'	$-Y_v'/\pi(T/L)^2$		$-N_v'/\pi(T/L)^2$	
		Value	Stn. Dev.	Value	Stn. Dev.
1 to 1	-0.194	1.2245	0.0313	0.4195	0.0048
1 to 2	-0.266	0.9811	0.0423	0.4652	0.0088
1 to 3	-0.345	1.0505	0.0444	0.4764	0.0085
1 to 4	-0.424	1.0194	0.0457	0.4808	0.0071
1 to 5	-0.5	1.0323	0.0038	0.4152	0.0008

Table 4.54 Linear Force and Moment Sway Derivatives for Elliptic Hull Form (with skeg) Using a Third Order Fit.

Number of Segments	X'	$-Y_v'/\pi(T/L)^2$		$-N_v'/\pi(T/L)^2$	
		Value	Stn. Dev.	Value	Stn. Dev.
1 to 1	-0.194	1.3805	0.0201	0.4357	0.0028
1 to 2	-0.266	1.1961	0.0261	0.4722	0.0056
1 to 3	-0.345	1.2771	0.0253	0.4679	0.0055
1 to 4	-0.424	1.3417	0.0305	0.4542	0.0049
1 to 5	-0.5	1.3661	0.0043	0.3866	0.0009

4.5.7 Elliptic Hull Form (no skeg)

Table 4.55 Linear Force and Moment Sway Derivatives for Elliptic Hull Form (no skeg) Using a Second Order Fit

Number of Segments	X'	$-Y_v'/\pi(T/L)^2$		$-N_v'/\pi(T/L)^2$	
		Value	Stn. Dev.	Value	Stn. Dev.
1 to 1	-0.194	1.2073	0.0475	0.3937	0.0103
1 to 2	-0.266	1.0178	0.0302	0.44310	0.0060
1 to 3	-0.345	0.8430	0.0354	0.4470	0.0084
1 to 4	-0.424	0.8195	0.0259	0.5002	0.0102
1 to 5	-0.5	0.8000	0.0341	0.4830	0.0082

Table 4.56 Linear Force and Moment Sway Derivatives for Elliptic Hull Form (no skeg) Using a Third Order Fit.

Number of Segments	X'	$-Y_v'/\pi(T/L)^2$		$-N_v'/\pi(T/L)^2$	
		Value	Stn. Dev.	Value	Stn. Dev.
1 to 1	-0.194	1.3229	0.0281	0.4044	0.0003
1 to 2	-0.266	1.1759	0.0177	0.4432	0.0039
1 to 3	-0.345	1.0373	0.0227	0.4582	0.0053
1 to 4	-0.424	0.9751	0.0211	0.5073	0.0067
1 to 5	-0.5	0.9577	0.0241	0.4909	0.0052

4.5.8 Appropriate Linear Fitting

Examination of measurement goodness of fit, s, shows that in some cases a linear or first order fit would be more appropriate than second or third order fitting. These instances are shown in Tables 4.57 and 4.58 below along with the new estimate of the linear derivatives.

Table 4.57 Linear Force Sway Derivatives for British Bombardier Conventional Using a First Order Fit

Number of Segments	X'	$-Y_v'/\pi(T/L)^2$	
		Value	Stn. Dev.
1 to 2	-0.1818	1.6373	0.01067
1 to 3	-0.2636	1.6070	0.00551

Table 4.58 Linear Force Sway Derivatives for British Bombardier Pram (with skeg) Using a First Order Fit

Number of Segments	X'	$-Y_v'/\pi(T/L)^2$	
		Value	Stn. Dev.
1 to 1	-0.1	1.6620	0.00919
1 to 2	-0.1818	1.5970	0.0119
1 to 3	-0.32636	1.4720	0.0074

4.6 Effect of Vortices on Goodness of Fit

An alternative to the usual second or third order fitting was used in the re-analysis of the British Bombardier and Mariner segmented model data [28], which employed measures of goodness of fit to experimental data to determine the appropriate order of polynomial expression. Taking the sway force, a general non-linear expression of the form,

$$Y'(x) = Y_v' v' + Y_{v|v'^{n-1}|}' v' \left| v'^{n-1} \right|$$

was used with the index ranging between n=2.0 and n=3.0, in increments of 0.1, to fit the experimental data. The merit of a particular index was decided on the estimate of the standard error, s, which was used as a measure of goodness of fit.

Table 4.59 Clarke and Hearn [28]. Standard Error, s, on Fitting of Sway Force Experimental Data for British Bombardier with Conventional Stern.

Number of Segments	X'	Standard Error, s, for the Second Order Fit, n=2	Standard Error, s, for the Third Order Fit, n=3
1 to 5	0.1	39.03	44.6
1 to 6	-0.1	77.96*	51.57
1 to 7	-0.2	15.20	33.39
1 to 8	-0.4	42.81	44.46
1 to 9	-0.5	48.89	29.29

*Note that this value was ignored since it was considered abhorant.

It was tentatively concluded from the results of this analysis that the natural order of fit was second order from the bow to Station 4.0 [28]. At this point, the stern vortices are generated and this has the effect on the fitting that can be seen in the goodness of fit measure, s. The natural order of fit grows linearly from n=2.0 at Station 4.0 to n=3.0 at A.P.

A similar set of measures for the British Bombardier derived from the Newcastle data is given in Table 4.60

Table 4.60 Newcastle. Standard Error, s, on Fitting of Sway Force Experimental Data for British Bombardier with Conventional Stern.

Number of Segments	X'	Standard Error, s, for the Second Order Fit, n=2	Standard Error, s, for the Third Order Fit, n=3
1 to 1	0.1	1.793	1.793
1 to 2*	-0.1818	3.124	3.070
1 to 3*	-0.2636	1.799	1.799
1 to 4	-0.3454	2.031	2.054
1 to 5	-0.4272	2.014	1.841
1 to 6	-0.5	2.418	2.319

Comparing Table 4.59 and 4.60, it may be noted that the values for s arising from the Newcastle experiments are an order of magnitude less than those produced from the Clarke data. This is a reflection of the number of repeat runs carried out in the Newcastle experiments, resulting in a larger number of data points. From the Newcastle data, comparison of goodness of fit indicated by s, show that the third order fitting equations more closely match the data from Segments 1 to 5 and 1 to 6, which is in agreement with Clarke and Hearn. However, it should be noted that the difference between the s values for n=2.0 and n=3.0 are much smaller in these experiments than that seen in the Clarke and Hearn analysis. This reflects the small non-linear component in the Newcastle experimental data.

The measures of goodness of fit for Segments 1 to 2 and 1 to 3 marked * indicate data sets which would be more appropriately fitted with a linear equation. The analysis of Clarke and Hearn was based on the assumption that the natural order of it for the experimental data would lie between n=2.0 and n=3.0. It is therefore concluded that these experiments cannot be used to corroborate the tentative conclusions of Clarke and Hearn [28].

4.7 CONCLUDING REMARKS

In the preceding Chapter the forces and moments measured on a series of segmented models have been presented. These measurements are compared with other experiments [23], [29] on the British Bombardier with conventional stern, and it was found that the side forces and monents were in very good agreement with those previously established.

Comparison of the fitted force derivatives for the British Bombardier existing segmented model data [23] showed that there was reasonable agreement for the linear derivatives, but that the estimates of the non-linear derivatives were inaccurate. It has been shown that this error was due to the comparatively small drift angles possible in the experiments. The low estimates for the non-linear derivatives force the estimates for the linear derivatives up, although this effect cannot be quantified. The derivative estimates for the linear derivatives are 10% higher in these experiments than those estimated for the segmented model experiment, which includes a greater range of drift angles [23]. This fitting artefact is similar to that seen when comparing estimates of linear derivatives from second and third order polynomials.

Comparison of fitted moment derivatives for the British Bombardier with previous segmented model data [23] showed that there was good agreement for the linear derivatives.

In the next Chapter, these experimental results are compared with theoretical results and some of the implications of the vortex influence theory, with respect to the effect of stern geometry, are discussed. Although the force derivative have been shown to be an over-estimate compared with previously established values [28], useful comparison of the experimental measurements can still be made because the design of the experiment relies on differencing between hull forms of similar geometry, rather than accurate measurement of absolute quantities.

5. DISCUSSION OF SEGMENTED MODEL EXPERIMENTS

5.1 INTRODUCTION

The aim of the segmented model experiments was to examine a number of implications of the generalised slender-body theory.

In the previous chapter the results of the segmented model experiments were analysed to determine the distributed force and moment sway derivatives of the tested hull forms. Comparison of the force measurements for the British Bombardier with a conventional stern shape with previous experiments [28] validated the method and the accuracy of the results. However, comparison of the derivatives showed that these experiments consistently over estimated the distributed sway force derivatives. It was concluded that this was due to the effect of fitting of data to a set that included a more limited range of drift angles than in other experiments.

This discrepancy has been considered in comparisons of the experimental and theoretical results. In the original design of the experiment, the hull forms were chosen that were specific variations in geometry. Differencing results from variations in geometry can therefore be used in examining the generalised slender-body theory. This treatment is valid if it is assumed that the effects of low drift angles on the determination of derivatives are similar in the various model results.

5.2 COMPARISON OF EXPERIMENTAL RESULTS WITH SLENDER-BODY THEORY

Plots of the experimental results for distributed sway force and moment derivatives for the various hull forms are given in Figures 5.1 to 5.14 below. Each plot shows the experimental and theoretical results. The theoretically determined added mass values for the slender-body predictions come from close fitting techniques where available [28], or from Lewis Section results [51].

Figure 5.1 shows the results for the sway force derivative distributed along the British Bombardier. In addition to the experimental and slender-body results, the re-analysed results of Clarke and Hearn [28] are given. It can be seen that the second order derivatives determined from the current set of experiments are a consistent small over-estimate compared with the previous results, of the order of 10%. It is interesting to note however that the third order fit of Clarke and Hearn for this data set corresponds very closely with the current results. The difference between the current experimental second order fit and that of Clarke and Hearn is approximately the same as the difference in second and third order fitting with the same experimental data.

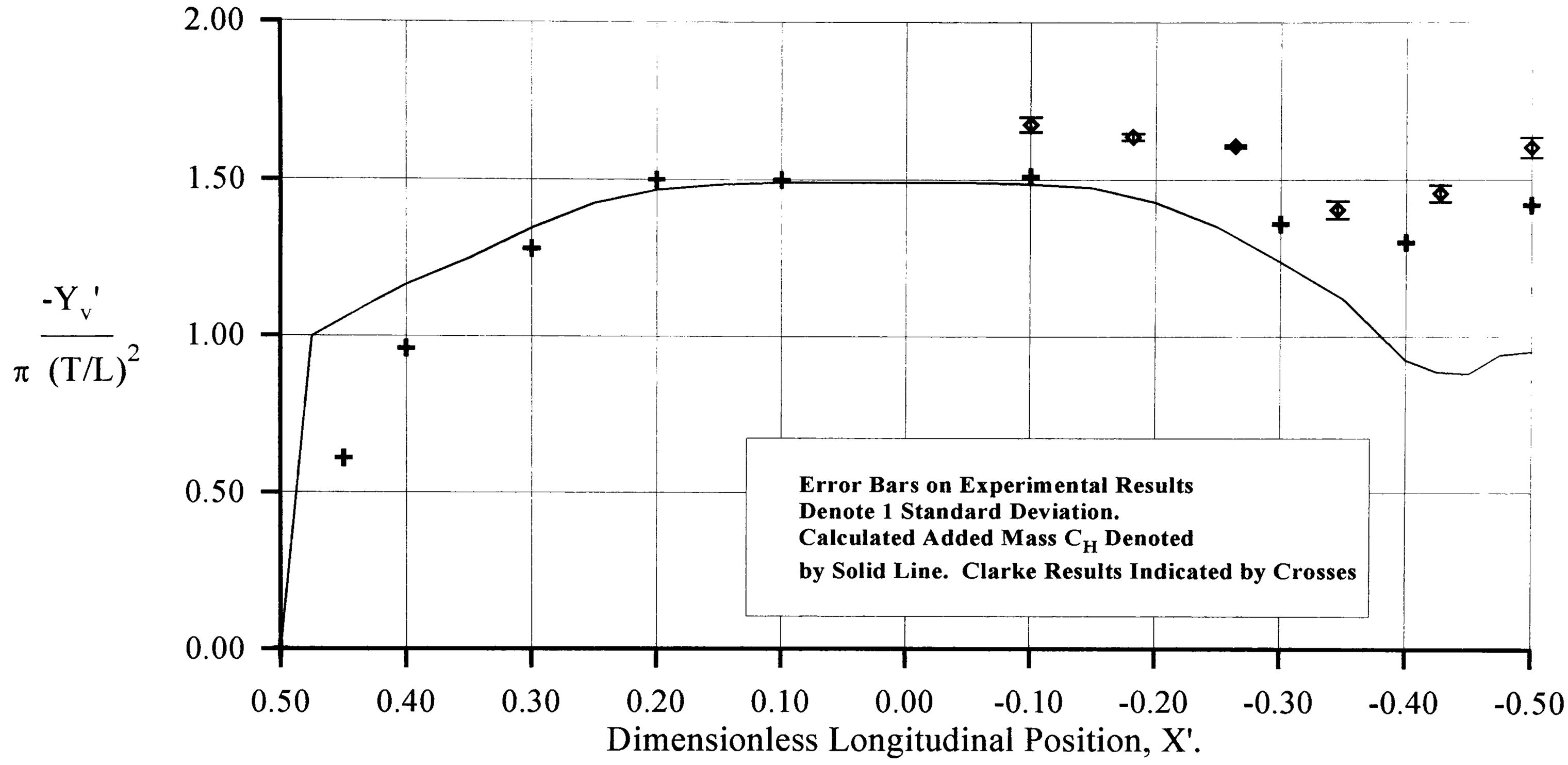

Figure 5.1 British Bombardier Conventional Stern. Longitudinal Variation of Y_{vT}' and C_H. Second Order Fit.

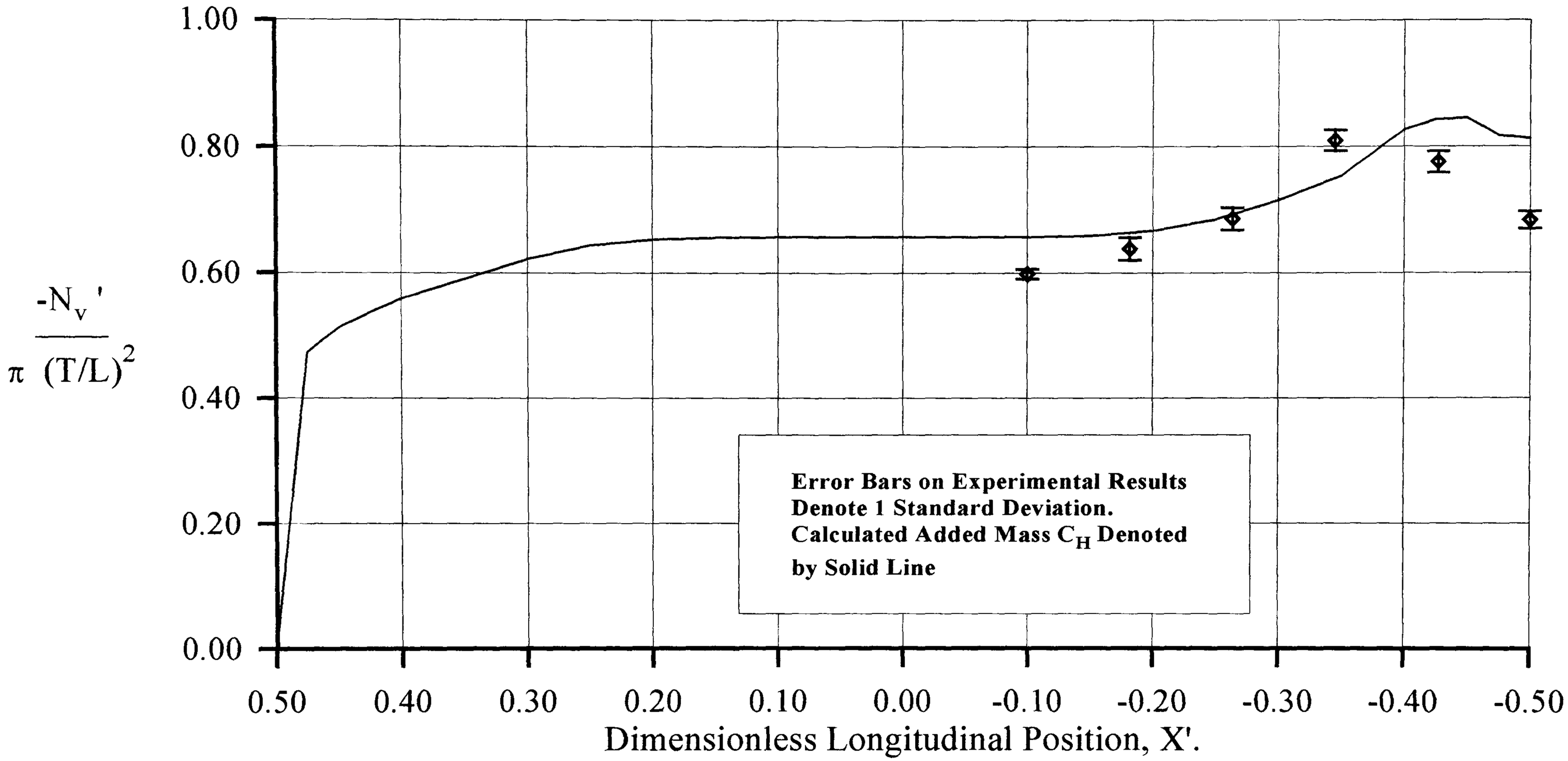

Figure 5.2 British Bombardier Conventional Stern. Longitudinal Variation of N_{vT}' and C_H. Second Order Fit.

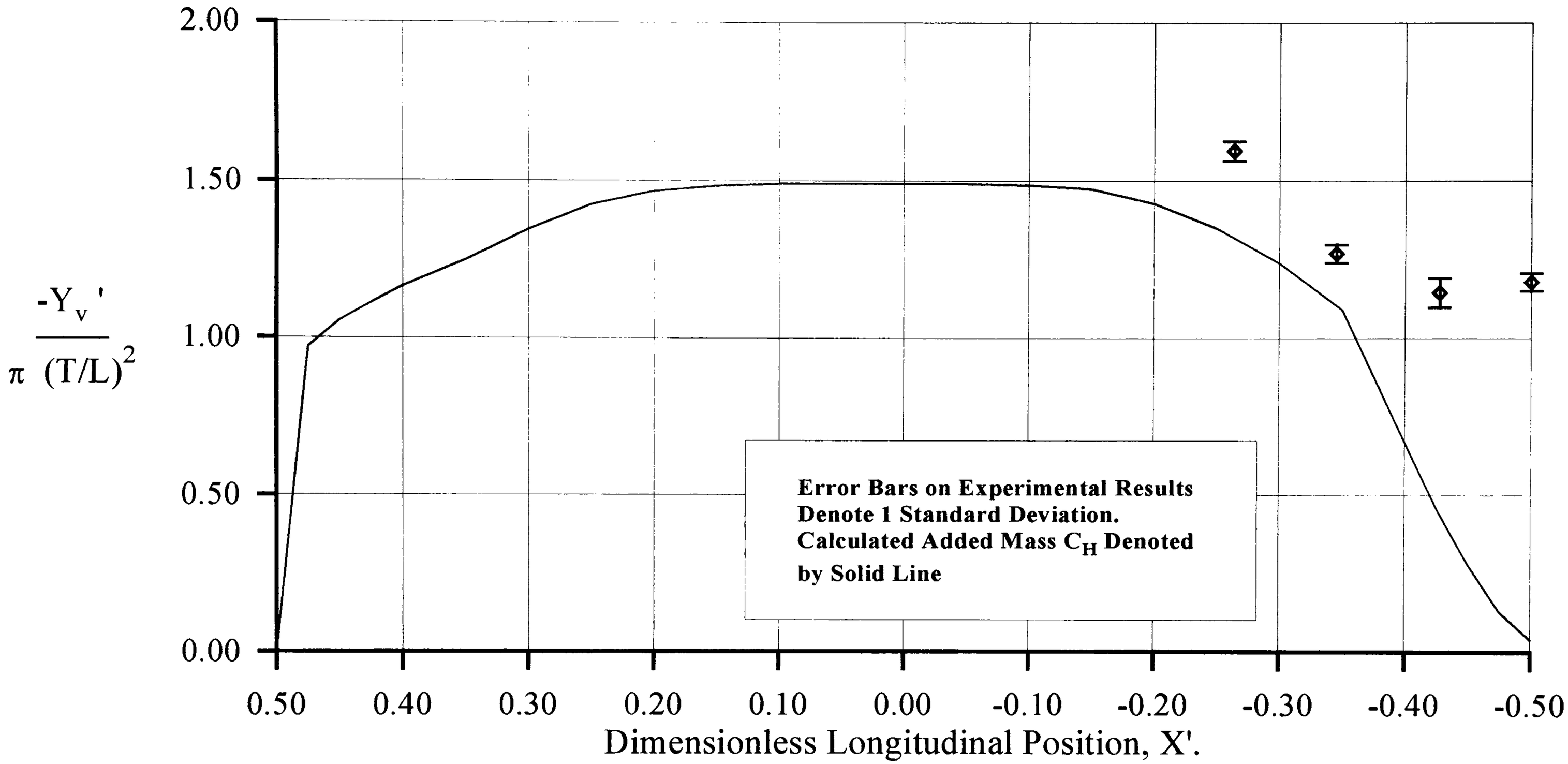

Figure 5.3 British Bombardier Conventional Stern (no skeg). Longitudinal Variation of Y_{vT}' and C_H. Second Order Fit.

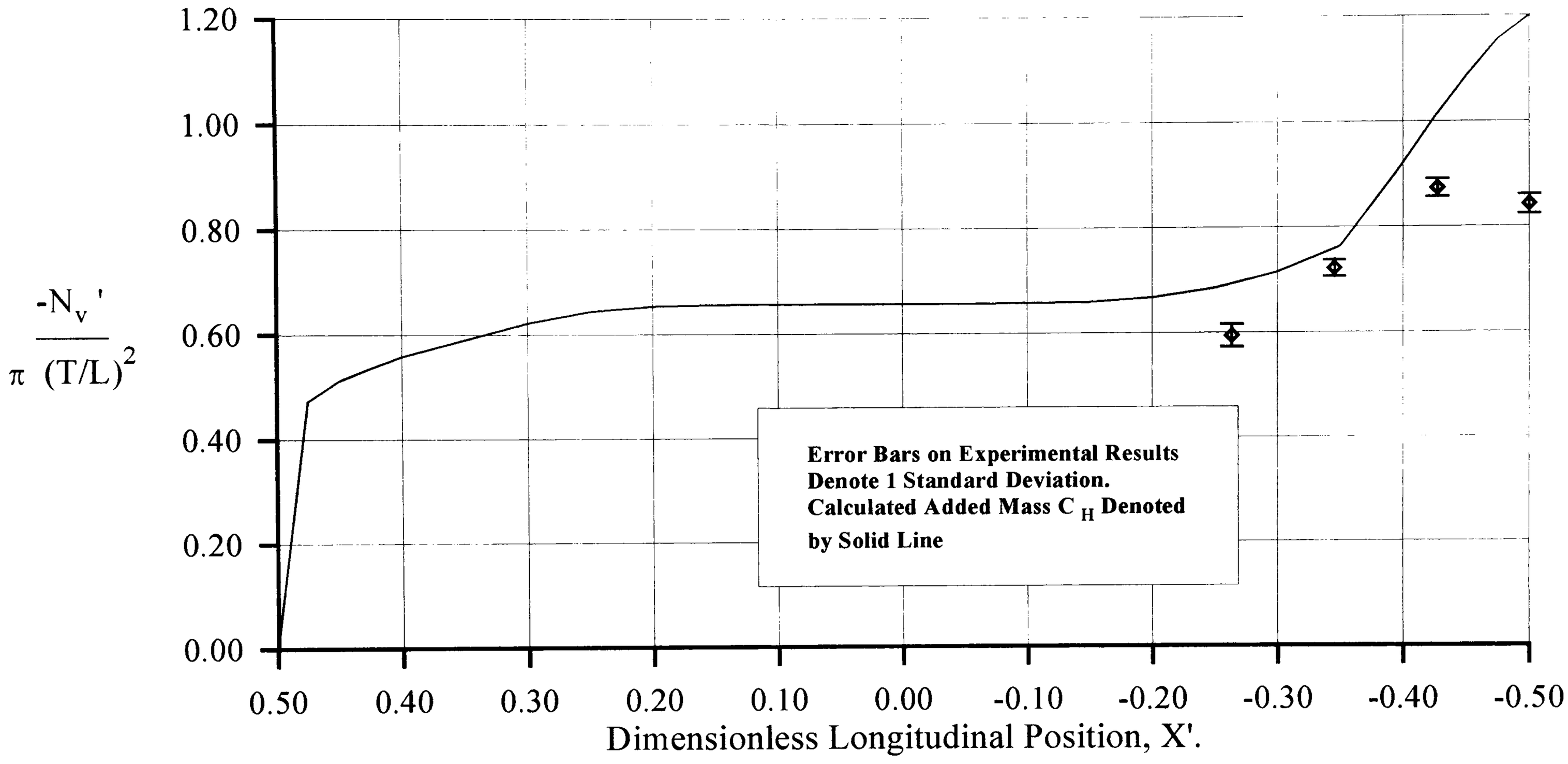

Figure 5.4 British Bombardier Conventional Stern (no skeg). Longitudinal Variation of N_{vT}' and C_H. Second Order Fit.

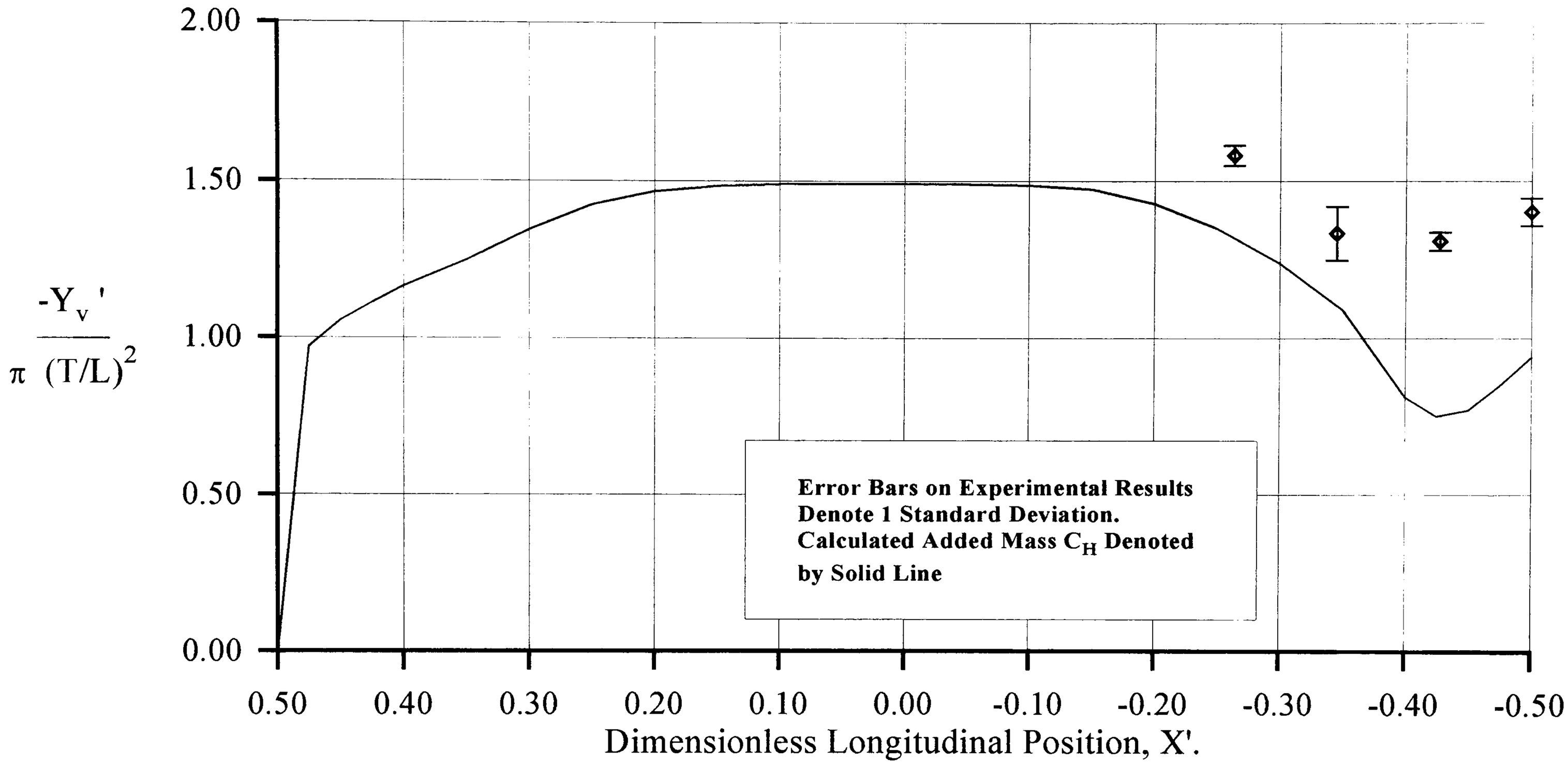

Figure 5.5 British Bombardier Conventional Stern (no skeg with plate). Longitudinal Variation of Y_{vT}' and C_H. Second Order Fit.

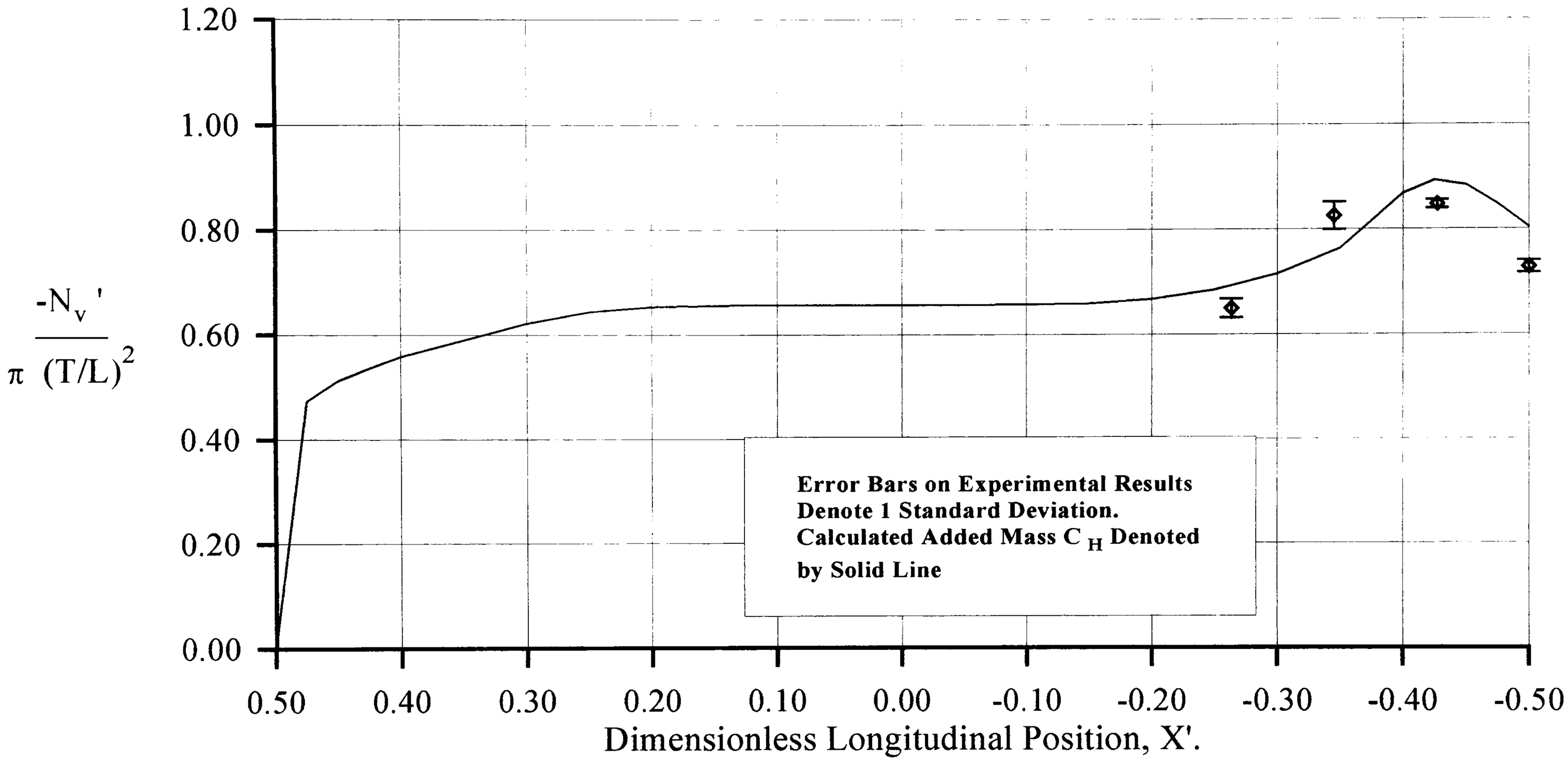

Figure 5.6 British Bombardier Conventional Stern (no skeg with plate). Longitudinal Variation of N_{vT}' and C_H. Second Order Fit.

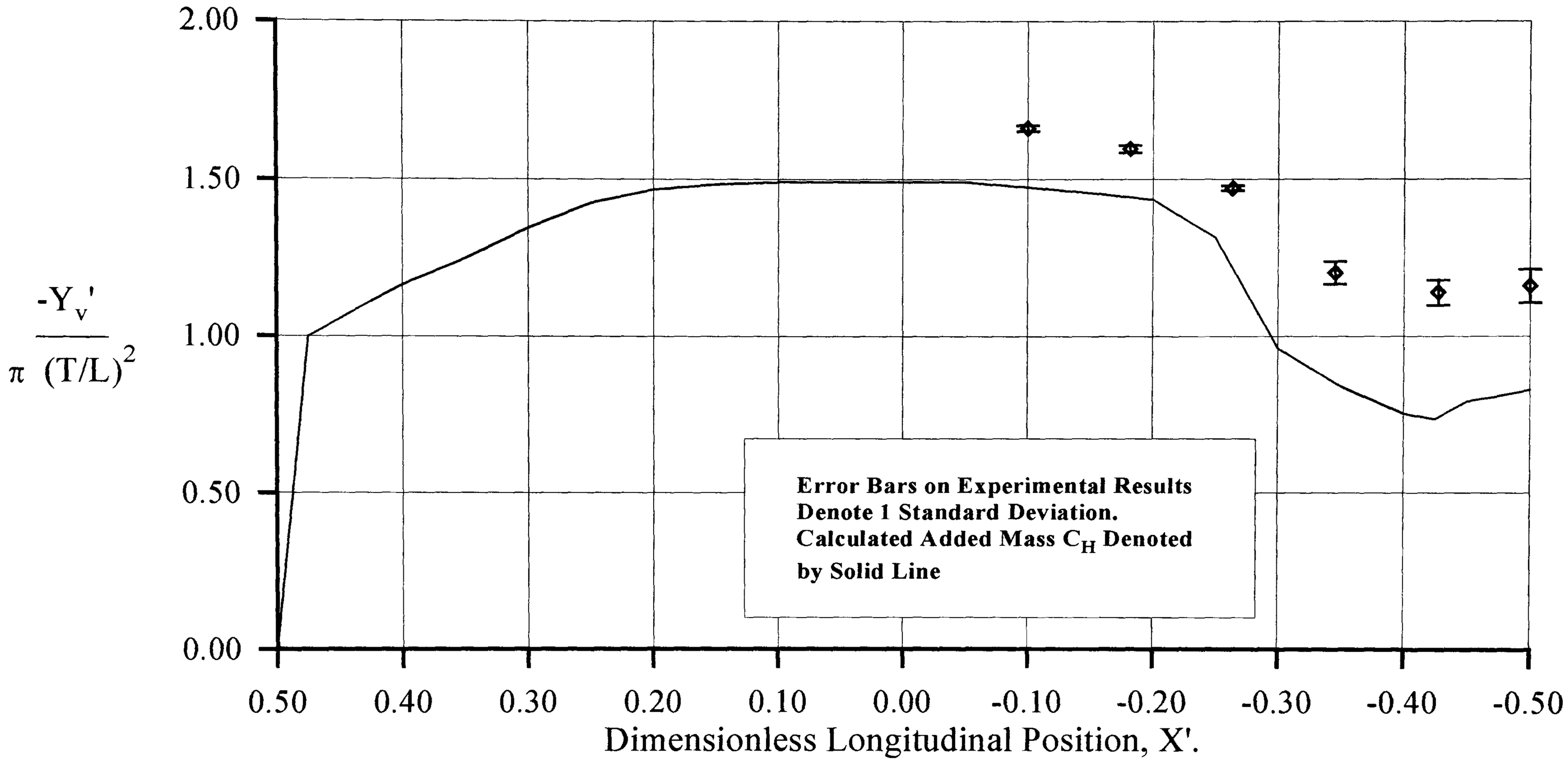

Figure 5.7 British Bombardier Pram Stern (with skeg). Longitudinal Variation of Y_{vT}' and C_H. Second Order Fit.

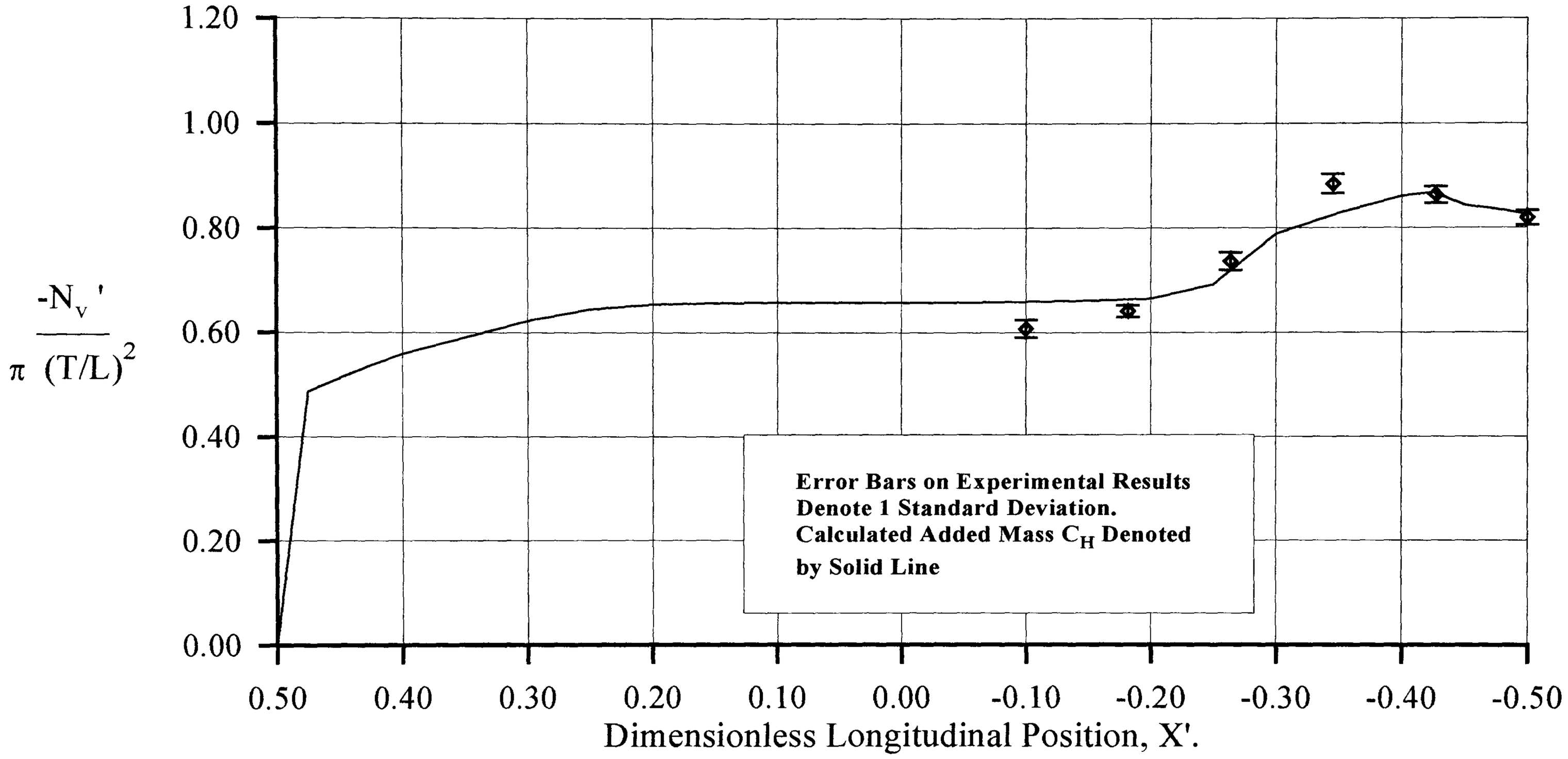

Figure 5.8 British Bombardier Pram Stern (with skeg). Longitudinal Variation of N_{vT}' and C_H. Second Order Fit.

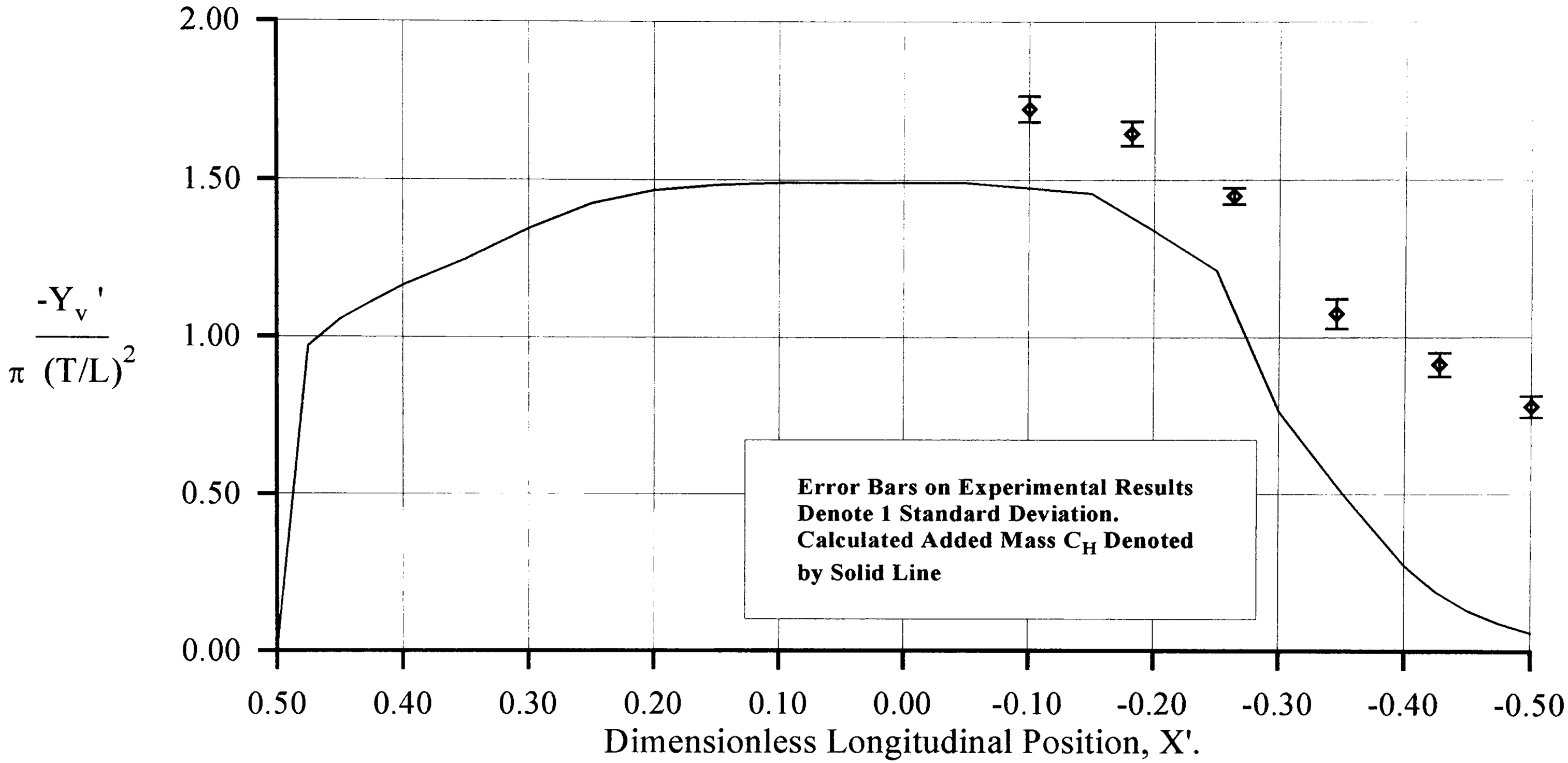

Figure 5.9 British Bombardier Pram Stern (no skeg). Longitudinal Variation of Y_{vT}' and C_H. Second Order Fit.

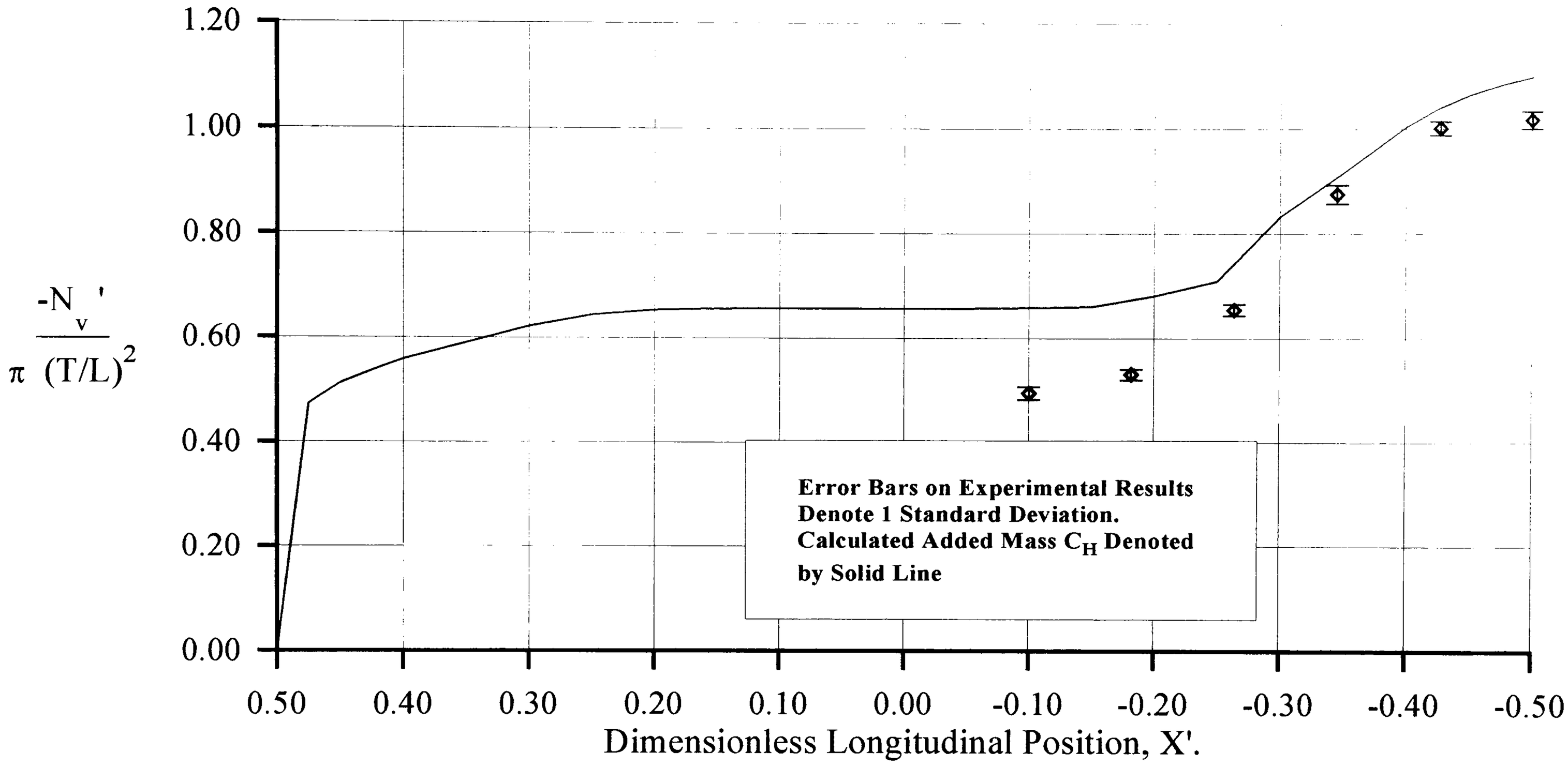

Figure 5.10 British Bombardier Pram Stern (no skeg). Longitudinal Variation of N_{vT}' and C_H. Second Order Fit.

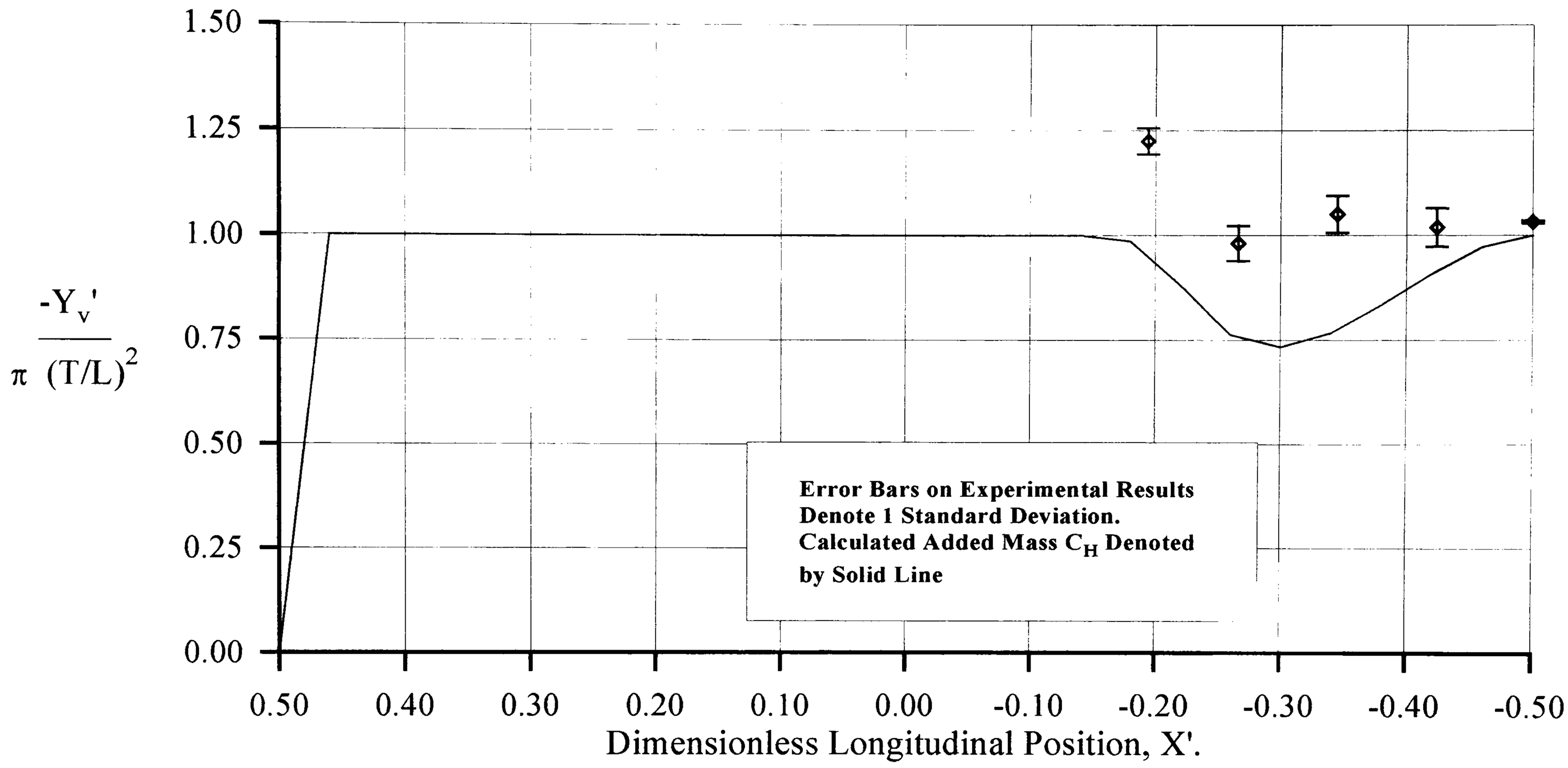

Figure 5.11 Elliptic Hull Form (with skeg). Longitudinal Variation of Y_{vT}' and C_H. Second Order Fit.

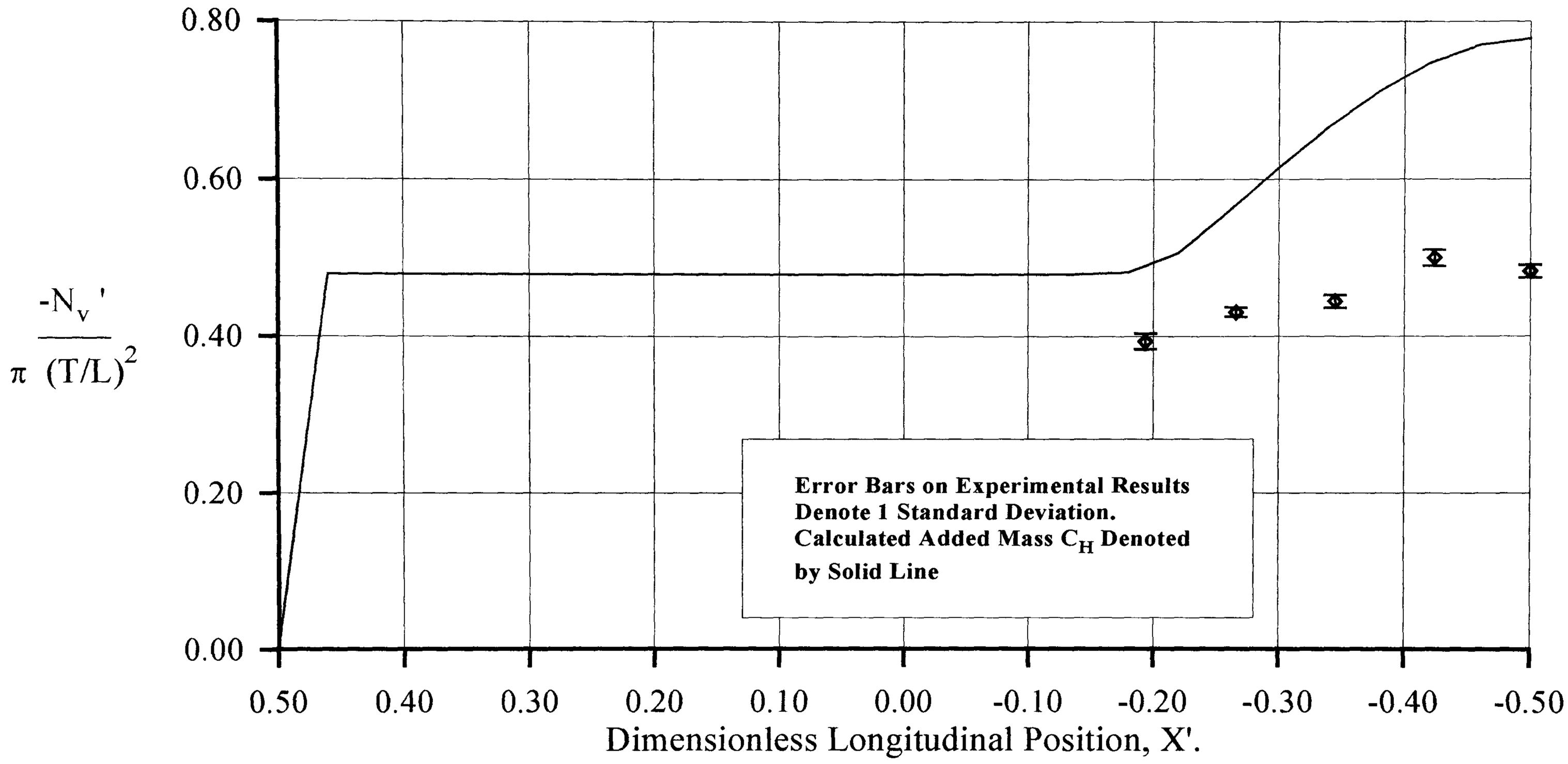

Figure 5.12 Elliptic Hull Form (no skeg). Longitudinal Variation of N_{vT}' and C_H. Second Order Fit.

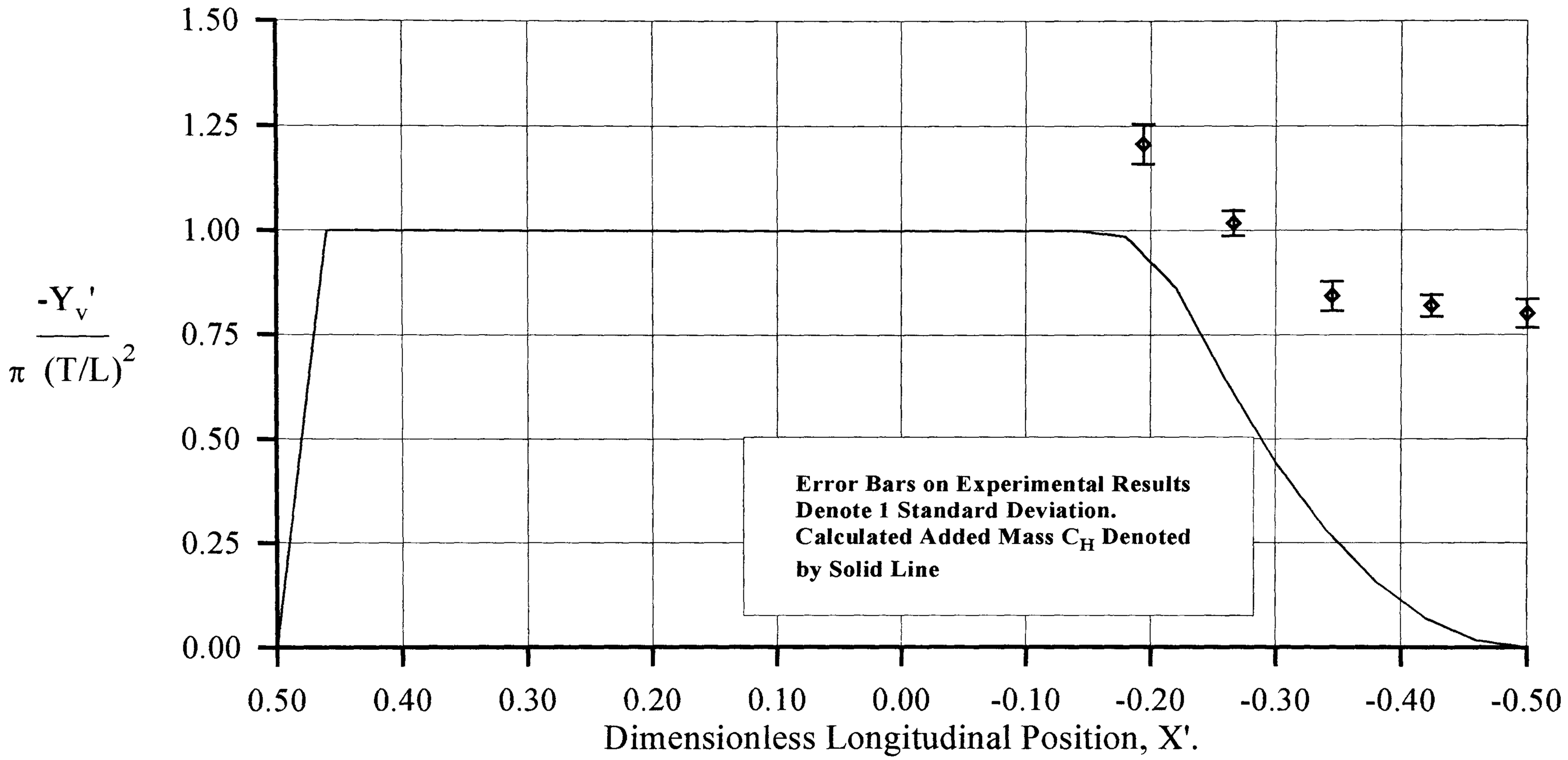

Figure 5.13 Elliptic Hull Form (no skeg). Longitudinal Variation of Y_{vT}' and C_H. Second Order Fit.

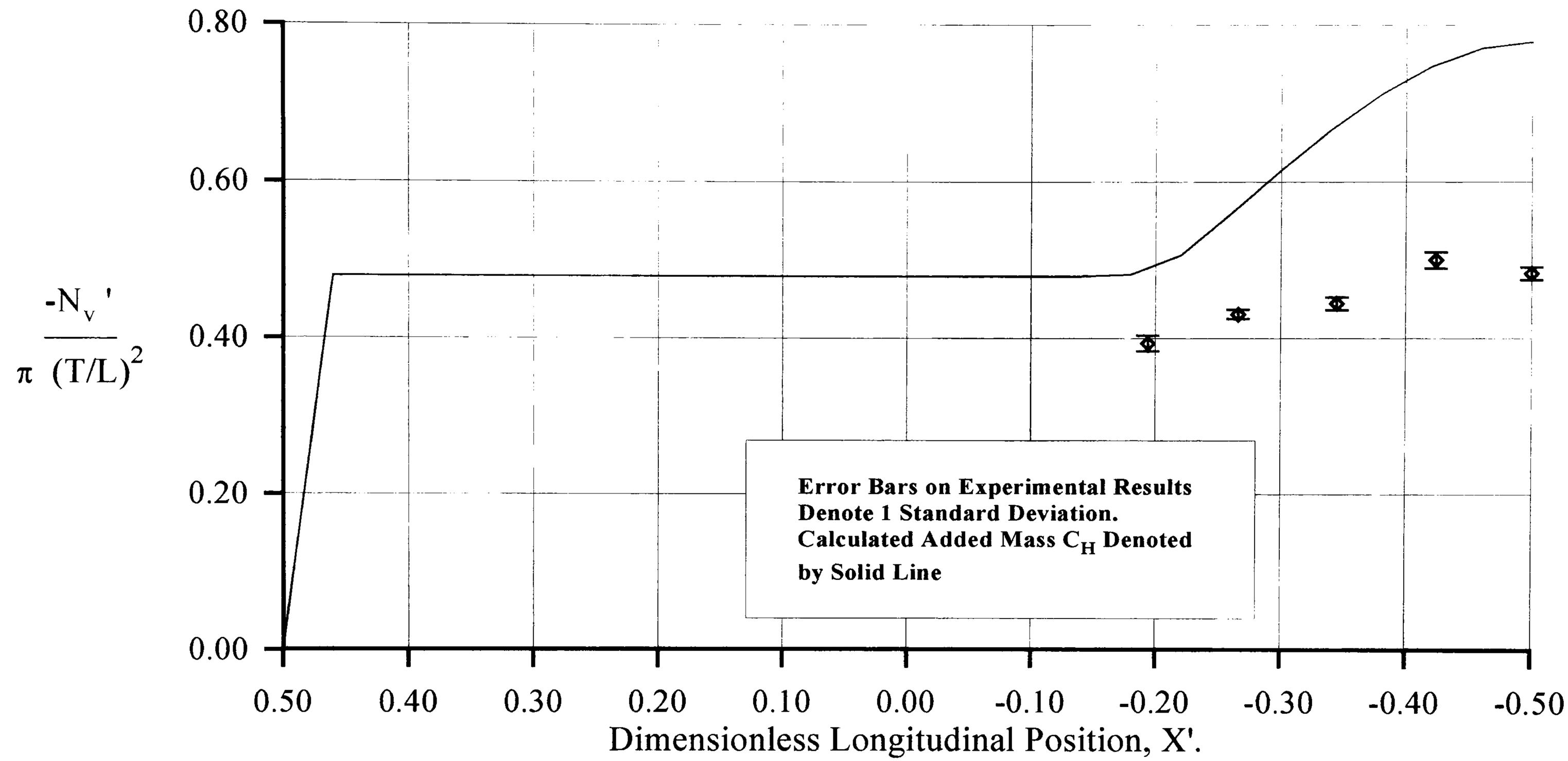

Figure 5.14 Elliptic Hull Form (no skeg). Longitudinal Variation of N_{vT}' and C_H. Second Order Fit.

5.3 Comparison of Experimental Results with Generalised Slender-Body Theory

The generalised slender-body theory accounts for the discrepancy between the slender-body theory and experimental determined sway force derivatives by the inclusion of a vortex impulse derivative. This impulse is generated by the effect of a pair of vortices passing near the stern sections of a hull when under sway or yaw motion. The magnitude of the impulse is dependent on the strength of the vortices and the proximity to the hull. The sign of the impulse is dependent on the sense of rotation of the vortices.

For a conventional hull form, the stern vortex pair is generated at the bilge and results in a counter-rotating pair with the port vortex rotating in an clockwise direction. This is supported by experimental evidence [29], [30]. It is postulated that [32] in the case of the pram stern vortex shedding takes place from the sides of the vessel and the generated vortex pair would have a lower circulation and may even rotate in the opposite sense compared with those shed from an conventional stern. If this is the case, then the side force generated by a pram stern would be less than that predicted for the conventional stern, in which case it would appear as if a virtual fin is being removed from the ship with the pram stern.

The corollary to these hypotheses is that a hull form, which generates no vortices, will have distributed sway force derivatives similar to those predicted by slender-body theory with no vortex impulse. The elliptic hull form was considered to be a geometry that would not produce trailing vortices.

To test these implications, consider the sway force derivatives, Y_{v1}' and Y_{v2}' for two vessels which differ only in stern configuration. From the generalised slender-body theory, the difference in the side force derivatives generated by these vessels under sway velocity, $\Delta Y_v'$ may be deduced from Equation (2.43) as,

$$\frac{\Delta Y_v{}'}{\pi\left(\frac{T}{L}\right)^2} = \frac{Y_{v1}{}'}{\pi\left(\frac{T}{L}\right)^2} - \frac{Y_{v2}{}'}{\pi\left(\frac{T}{L}\right)^2} = \left[C_{H1} + I_{H1}\right]_S - \left[C_{H2} + I_{H2}\right]_S \qquad (5.1)$$

If the horizontal added mass coefficients C_{H1} and C_{H2} of the two vessels for the after most sections are similar then the difference in the generated side force between the two vessels can be attributed to the difference in the vortex influence coefficient, I_H. That is,

$$\Delta Y_{vT}{}' = \frac{\Delta Y_v{}'}{\pi\left(\frac{T}{L}\right)^2} = \frac{Y_{v1}{}'}{\pi\left(\frac{T}{L}\right)^2} - \frac{Y_{v2}{}'}{\pi\left(\frac{T}{L}\right)^2} = \left[I_{H1} - I_{H2}\right]_S. \qquad (5.2)$$

The subscript T has been introduced here to the common hydrodynamic derivative notation to indicate non-dimensionalisation with the factor $\pi(T/L)^2$.

Alternatively, the difference between the two vessels can be expressed as,

$$\frac{\Delta Y_v{}'}{\pi\left(\frac{T}{L}\right)^2} = \frac{Y_{v1}{}'}{\pi\left(\frac{T}{L}\right)^2} - \frac{Y_{v2}{}'}{\pi\left(\frac{T}{L}\right)^2} = \left[I_{H1} - I_{H2}\right]_S + \left[C_{H1} - C_{H2}\right]_S \qquad (5.3)$$

Where the second term in Equation 5.3 is the difference between the calculated added mass of the vessels. Examining the relative magnitude of the experimental derivative difference and the calculated added mass difference can therefore isolate the effect of the vortex influence coefficient. This procedure eliminates the problem of over-estimation of the derivative values.

Figure 5.15 shows a plot of the differenced experimental results for the British Bombardier with conventional stern and the conventional stern with the skeg removed. The derivatives have been determined using second order and third order fitting of the force data respectively. It can be seen that the small over-estimates of the derivatives introduced by the fitting process are nullified by the differencing procedure. This

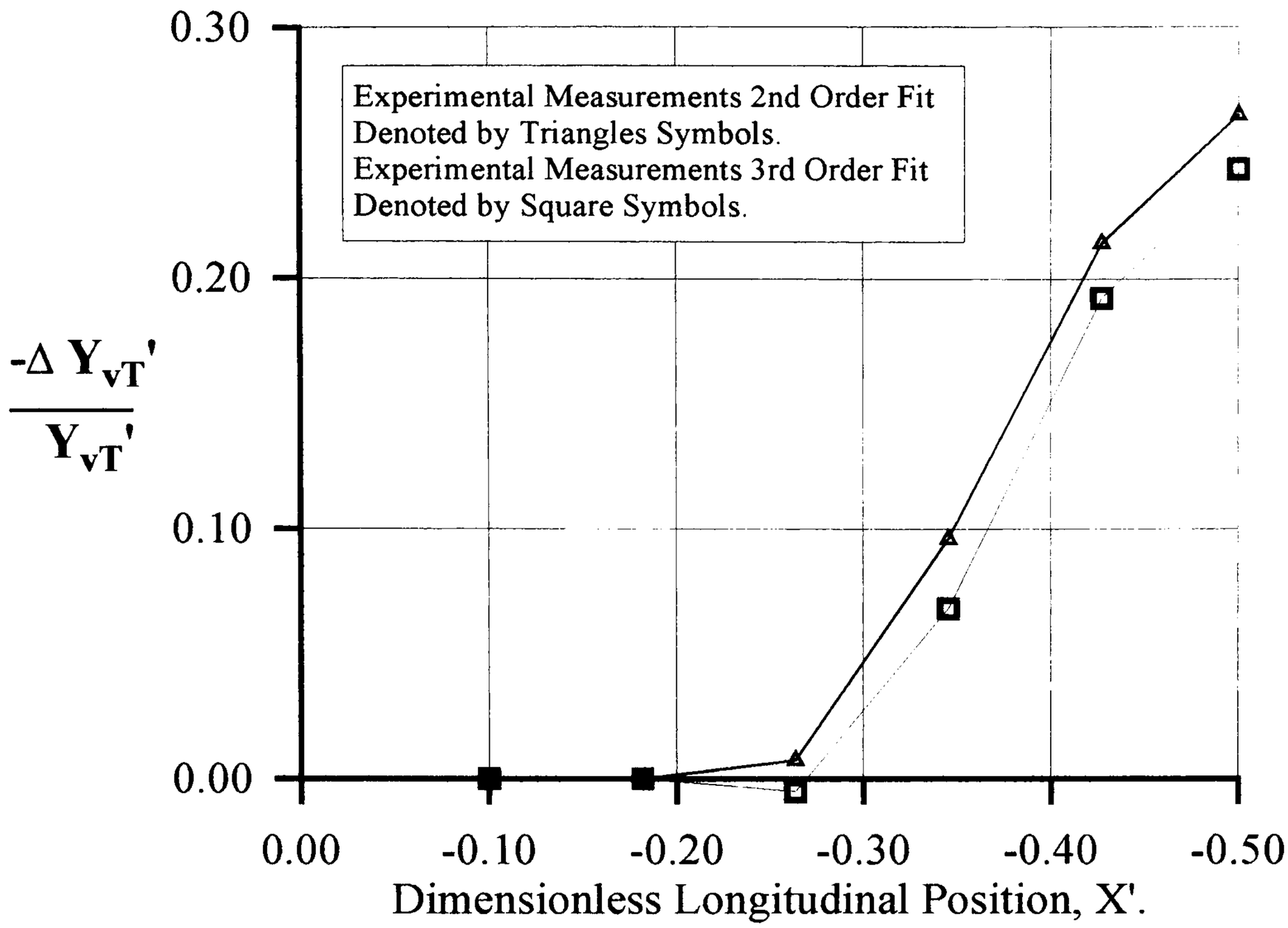

Figure 5.15 Differenced Experimental Measurements with Second and Third Order Fit for the British Bombardier Conventional Stern with and without Skeg.

confirms that, using the differencing approach, the conclusions drawn from the results of the experiment will not be affected by choice of either second order or third order fitting method or low drift angles.

Figures 5.16 to 5.21 show plots of the difference between experimental sway force derivatives and those calculated from added mass for pairs of vessels.

Figure 5.19 compares the British Bombardier with a conventional stern and a pram stern. The experimental derivative difference and the calculated added mass difference agree reasonable well until Station 2.0, where the plots diverge. It can be concluded that this divergence is due to the difference in the vortex influence coefficients of the two vessels.

Figure 5.20 shows the experimental and theoretical differencing for the pram stern vessel with and without a flat plate skeg. With reference to the terms in Equation 5.1, it has been postulated that $I_{H1}{}'$ is approximately zero or less than zero and that $I_{H2}{}'$ is equal to zero since the vortices generated from the pram stern with no skeg have no proximity to the hull horizontally and therefore cannot generate an impulse. In this case, if the theoretical results are extracted from the experimental results, then the remaining term will be $I_{H1}{}'$. This will be zero or negative if the hypotheses are correct.

This is indeed the case, as the experimental derivatives and the calculated added mass diverge, with the calculated added mass being large in magnitude.

However, the conclusion that this supports the hypothesis that the vortices generated from this pram stern rotate in the opposite sense to those from the conventional stern is not safe. Examining Figure 5.9, the comparison of the experimental sway force derivatives and the slender-body theory show a divergence which accounts for the divergence in the differenced results. Figure 5.7 shows the comparison of the experimental derivatives and the calculated added mass for the pram stern with a flat plate. If the effect of the fitting over-estimate is of the same magnitude as those noted

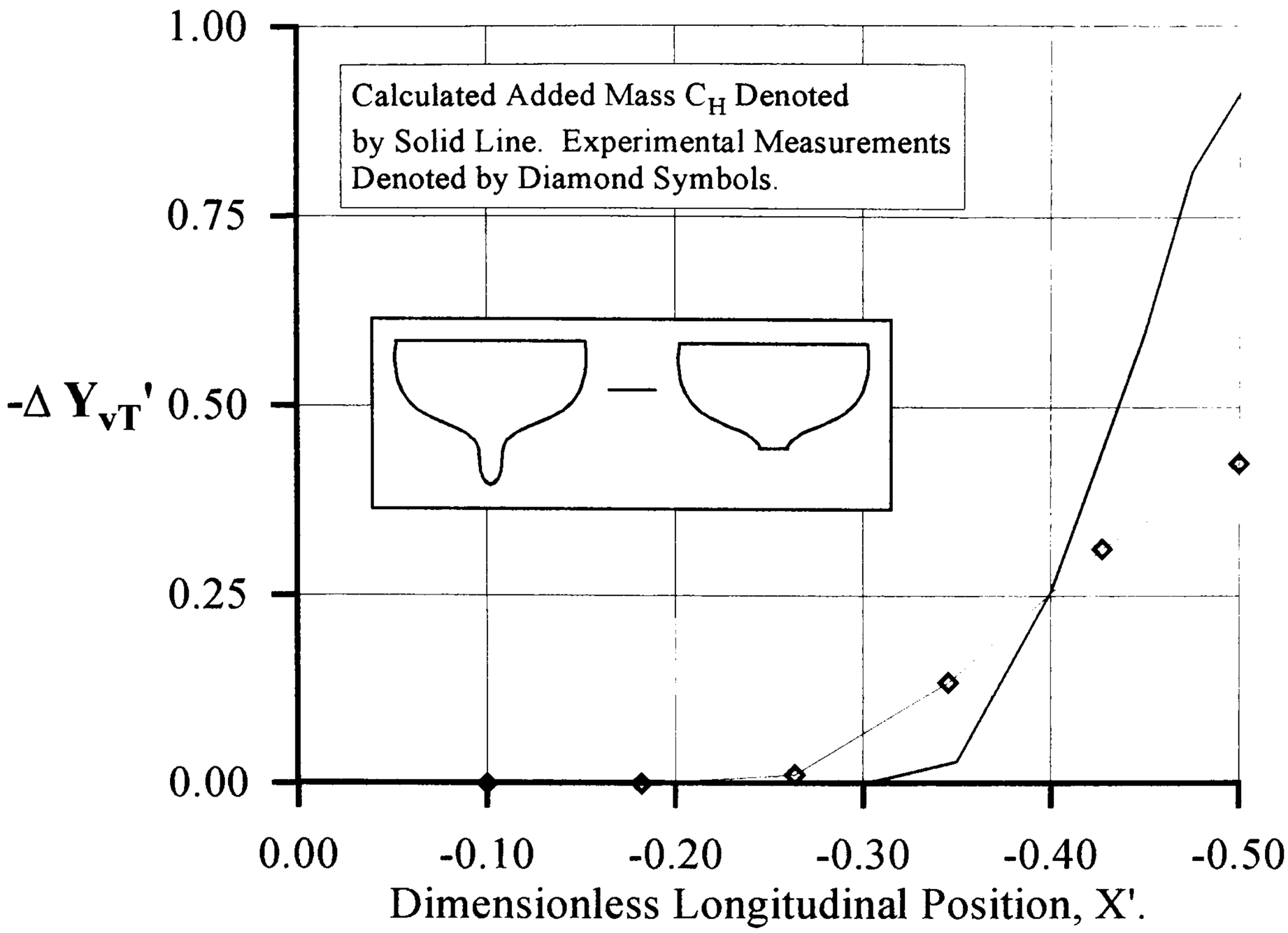

Figure 5.16 Differenced Added Mass and Experimental Measurements for the British Bombardier Conventional Stern with and without Skeg

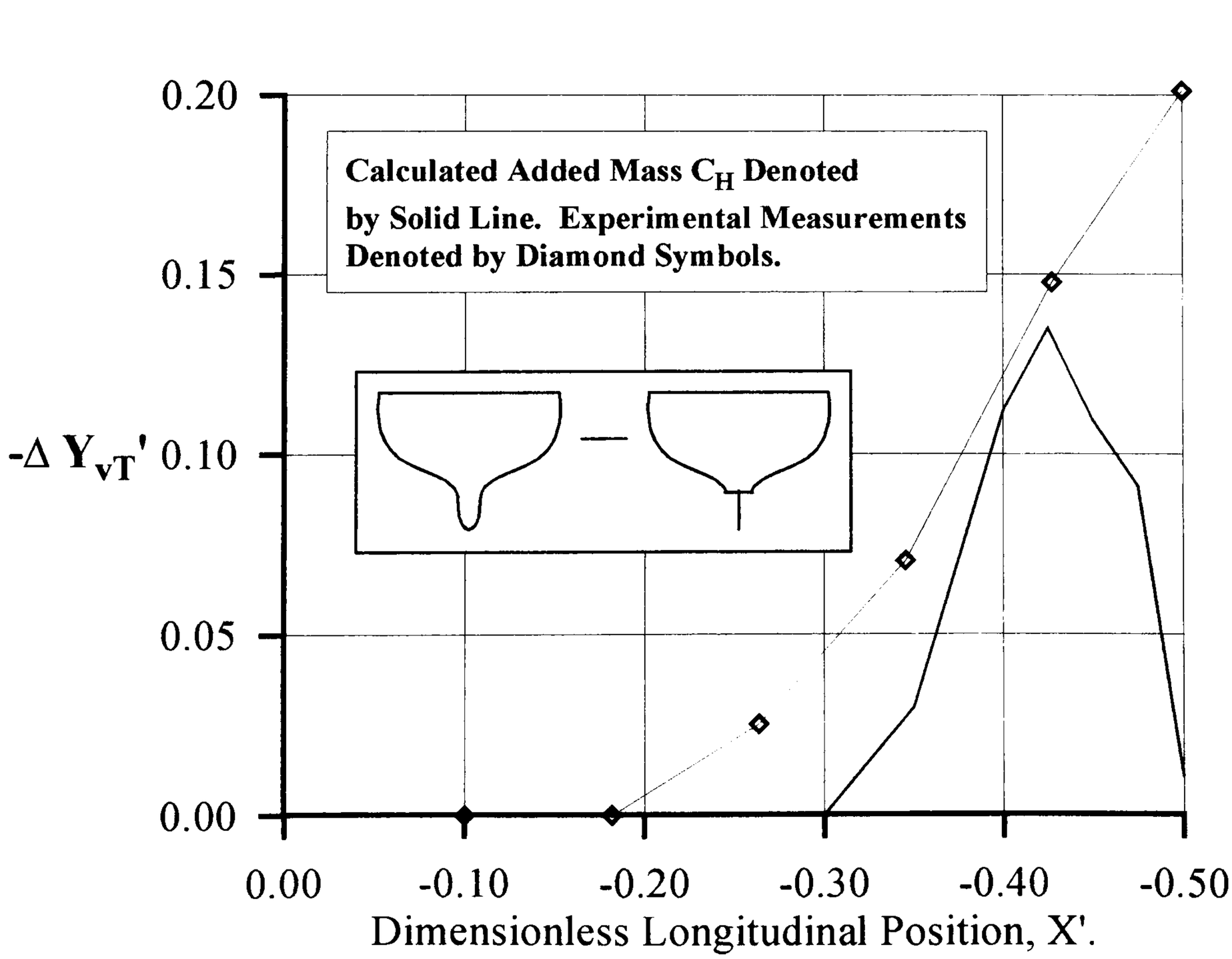

Figure 5.17 Differenced Added Mass and Experimental Measurements for the British Bombardier Conventional Stern and Skeg Replaced with a Plate

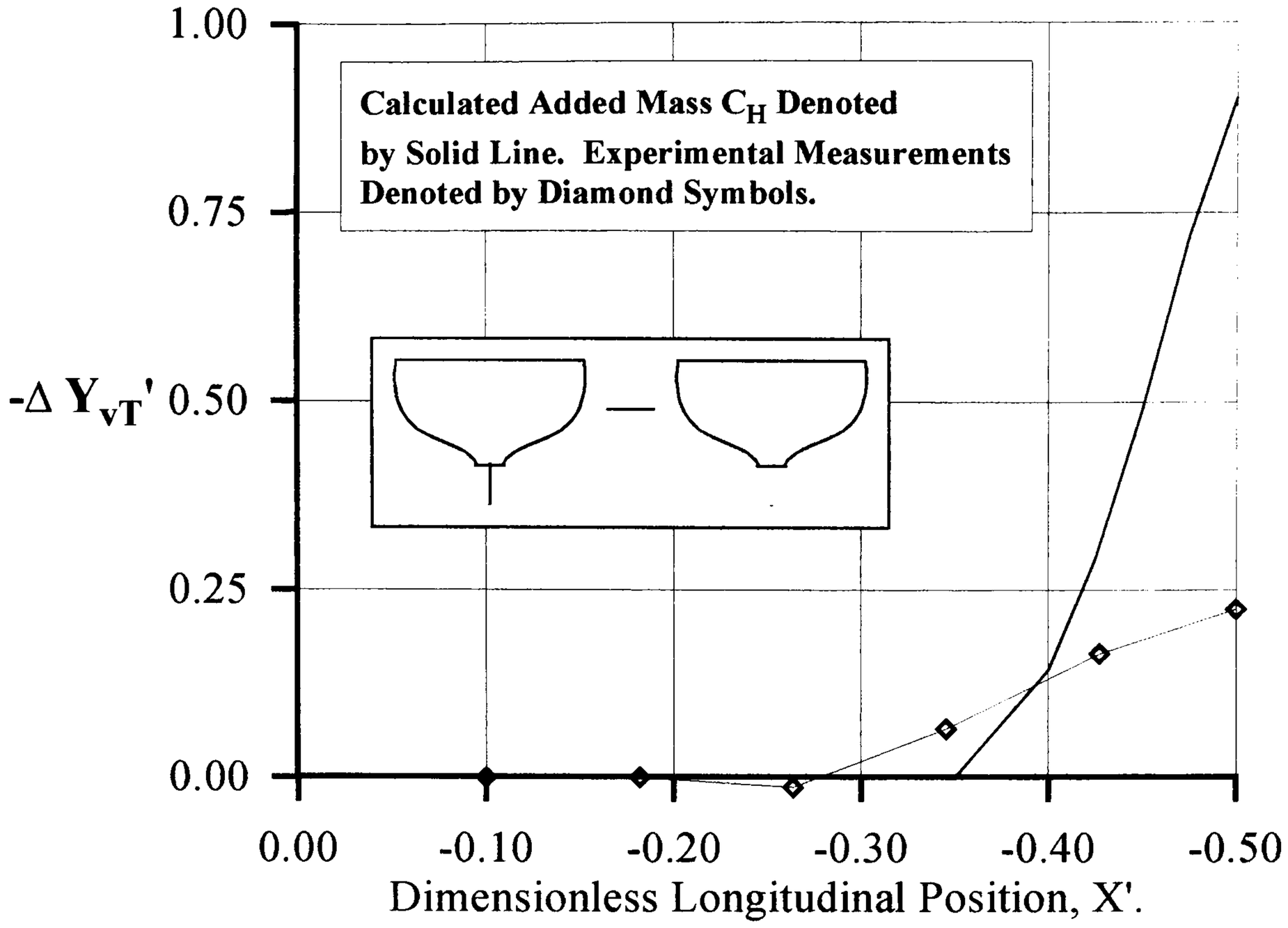

Figure 5.18 Differenced Added Mass and Experimental Measurements for the British Bombardier Conventional Stern with Plate and with No Skeg

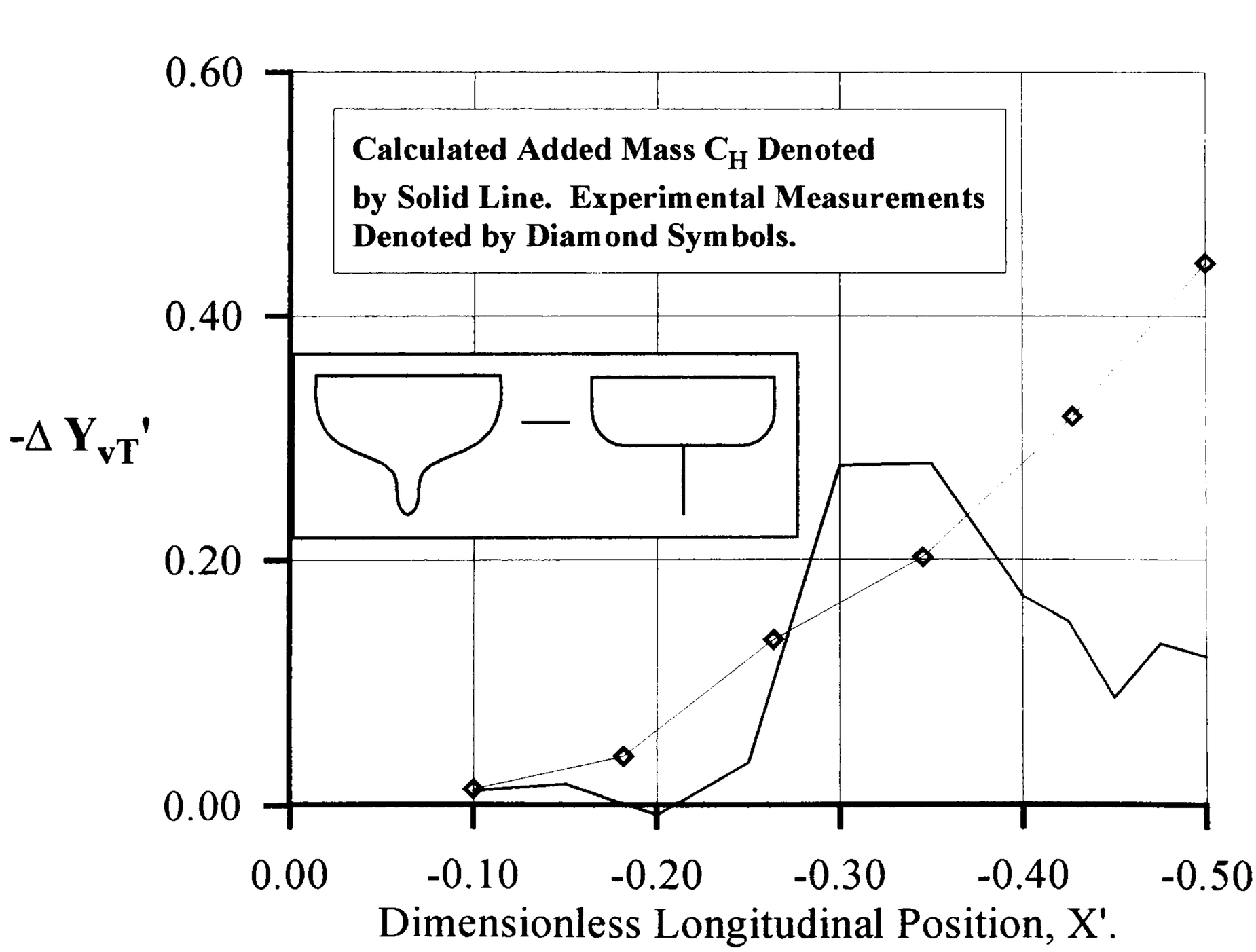

Figure 5.19 Differenced Added Mass and Experimental Measurements for the British Bombardier Conventional Stern and Pram Stern

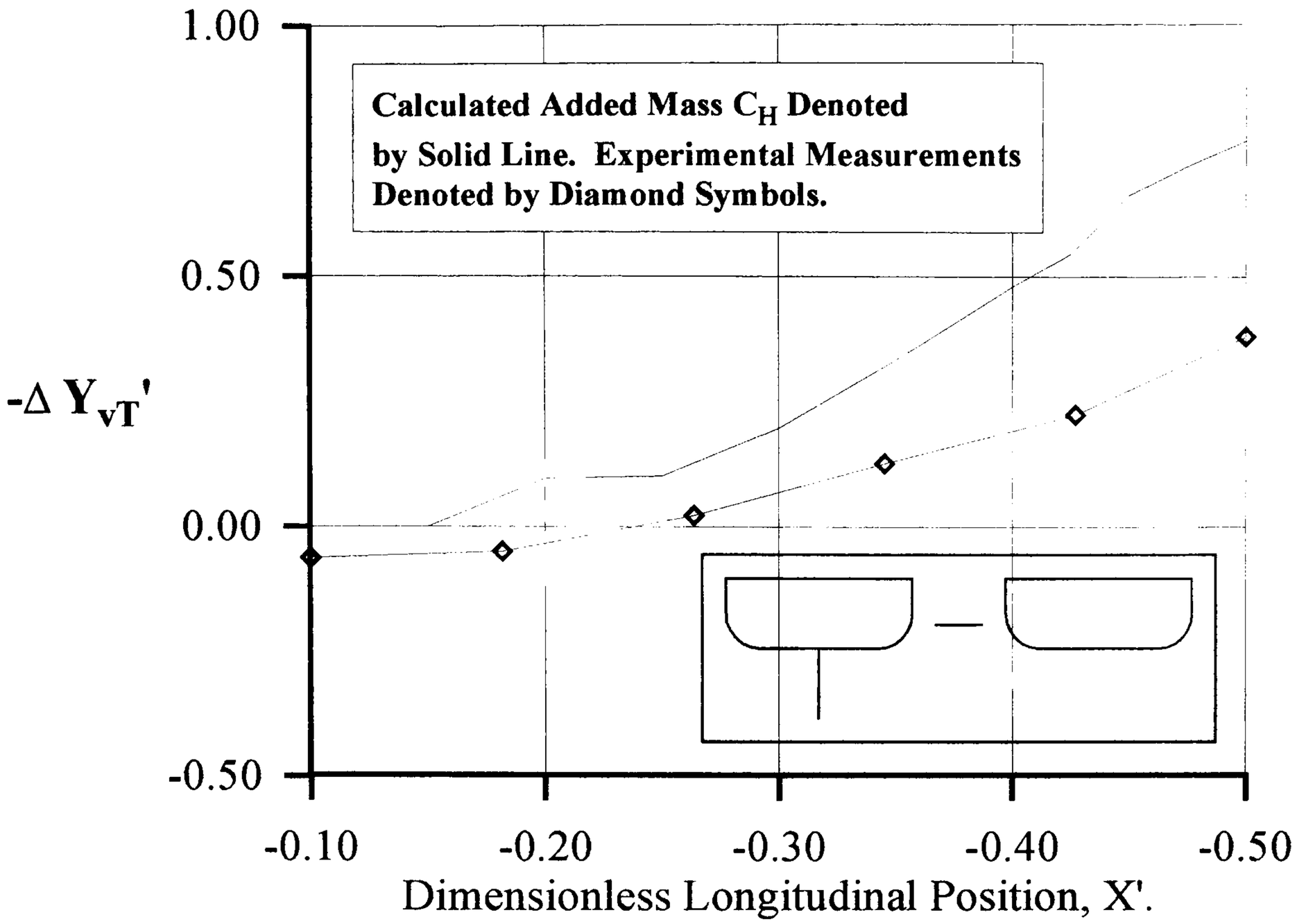

Figure 5.20 Differenced Added Mass and Experimental Measurements for the British Bombardier Pram Stern with and without Skeg

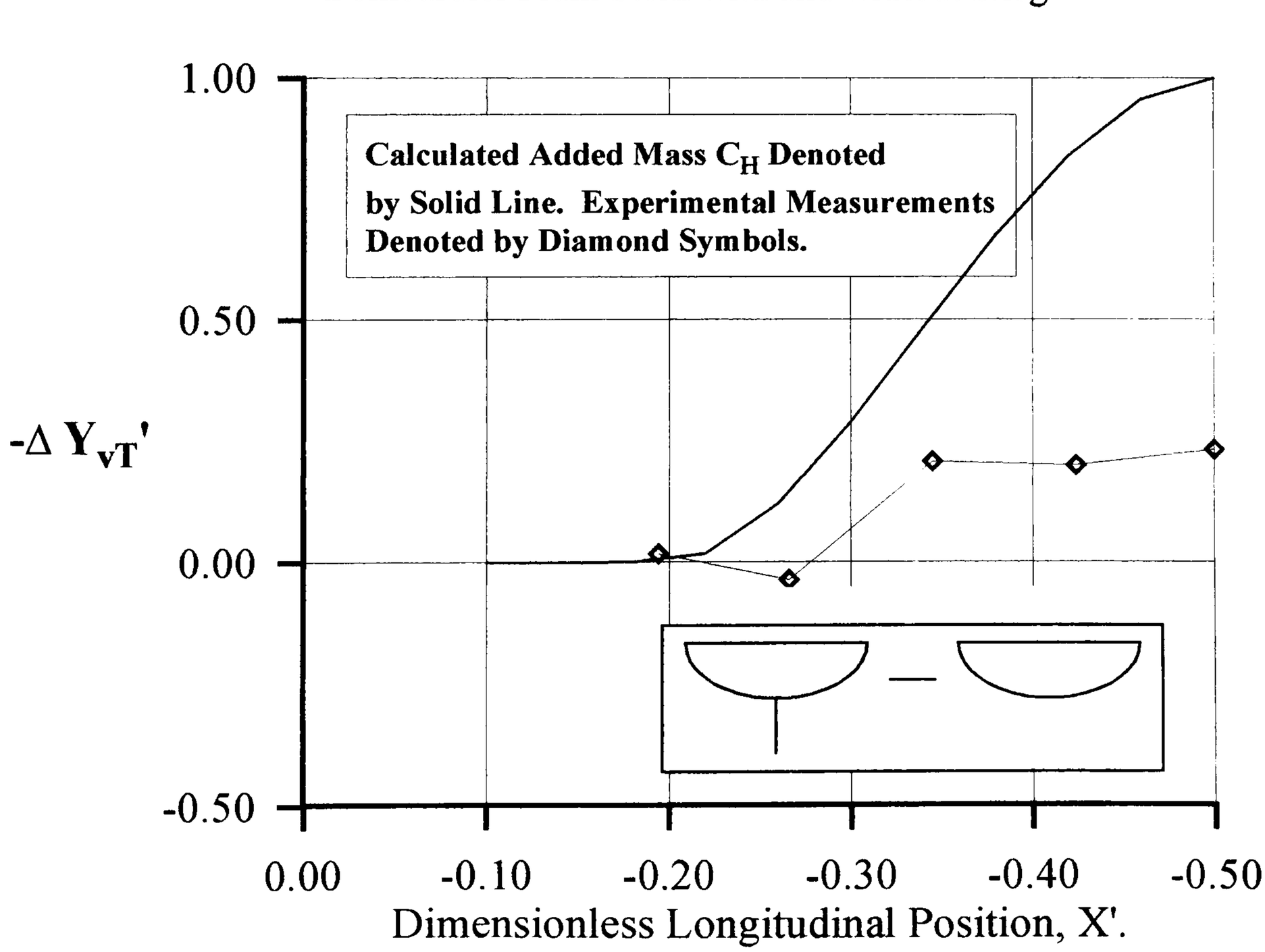

Figure 5.21 Differenced Added Mass and Experimental Measurements for the Elliptic Hull Form with and without Skeg.

on the British Bombardier with a conventional stern, then it can tentatively be concluded that the vortices shed from the pram stern hull are approximately zero.

The divergence seen between the experimental and calculated added mass derivatives for the pram stern without a skeg can also be seen in the same comparison for the elliptic hull form without a skeg. Differencing of the results for the elliptic hull form, with and with out a skeg are show in Figure 5.21. If, as had been postulated, the elliptic hull form does not shed vortices, then the expected result would be that the experimental difference and the added mass difference would follow each other closely.

As with the pram stern with a skeg, it is tentatively concluded that the close comparison of slender body theory and experimental derivatives for the elliptic hull form with a flat plate skeg show that the elliptic form does not shed vortices.

The divergence of the calculated added mass and the experimental derivatives can be seen in all the geometries tested which have a rapidly up sweeping stern shape. These instances are the British Bombardier with the skeg removed and with the pram stern without skeg as well as the elliptic model without skeg, as shown in Figures 5.3, 5.9 and 5.13 respectively.

It is possible that the presence of an adverse pressure gradient, particularly near the keel of these shapes leads to the growth of the boundary layer, leading to an apparent increase in the size of the stern sections. This would lead to an increase in the added mass of the sections. This effect is significant for those vessels where the stern geometry is not dominated by a large skeg or fin plate.

Figure 5.22 shows a comparison of the non-dimensionalised sway force derivatives for all the full model hullforms together. In each case the theoretical results predicted by slender-body theory have been put alongside the experimental results. Figure 5.23 is essentially the same as Figure 5.22, but the results have been further non-dimensionalised using the British Bombardier conventional stern experimental sway force derivative. This allows a comparison to made of the percentage effect, of each hullform change, over the parent hull.

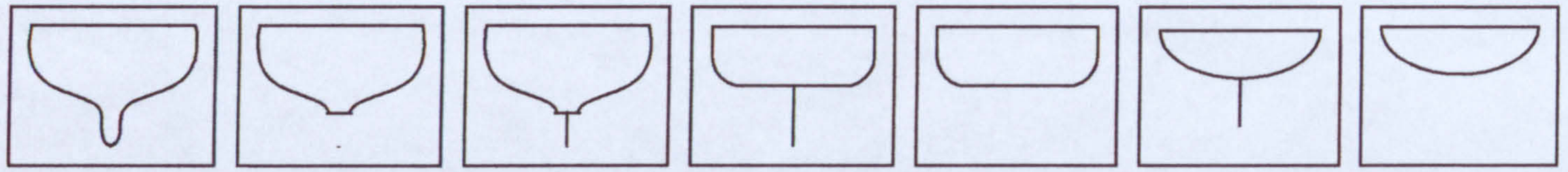

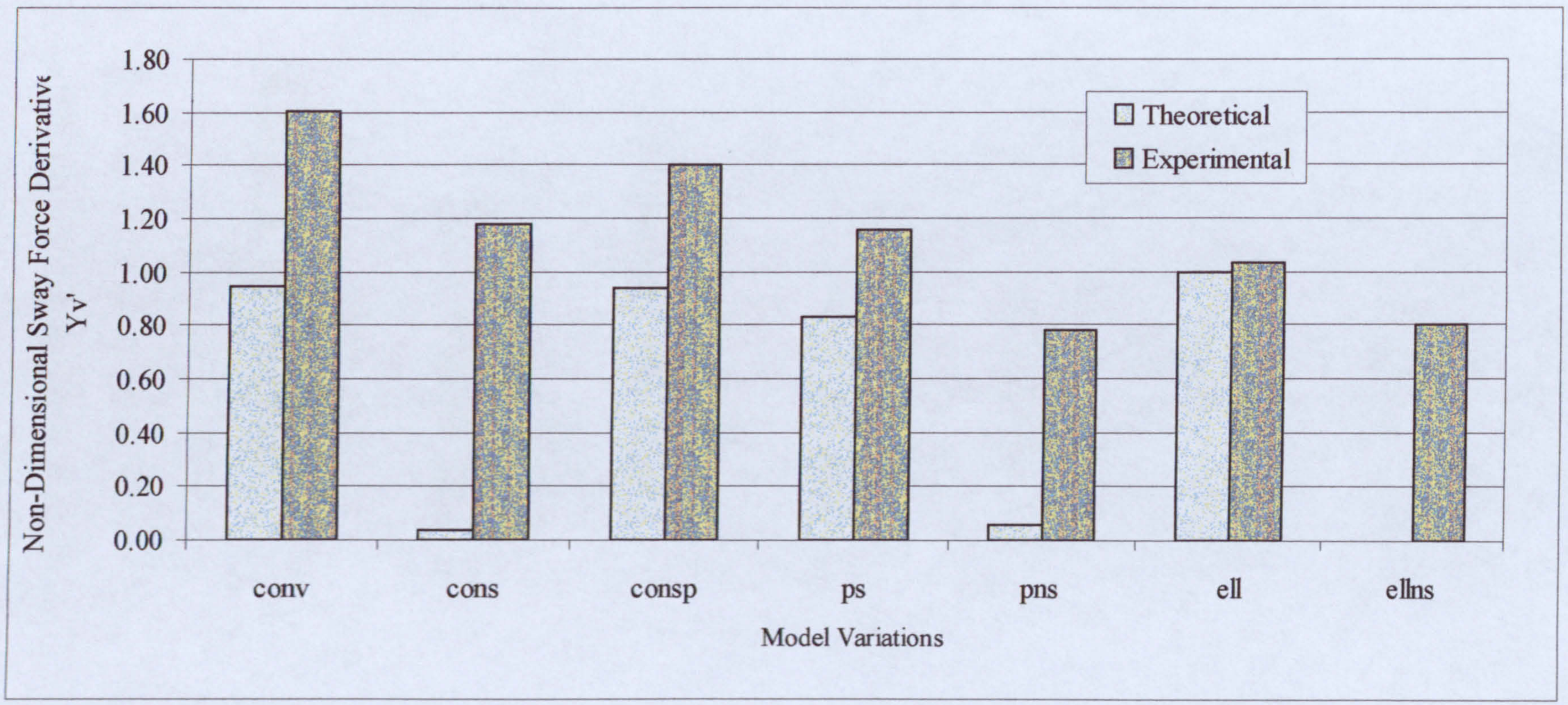

Figure 5.22 Absolute Comparison of Experimental and Theoretical Sway Force Derivatives for 7 Model Variations. Bombardier Conventional (conv), Without Skeg (cons), With Plate (consp), Bombardier Pram (ps), Without Skeg (pns), Ellipse (ell), Without Skeg (ellns).

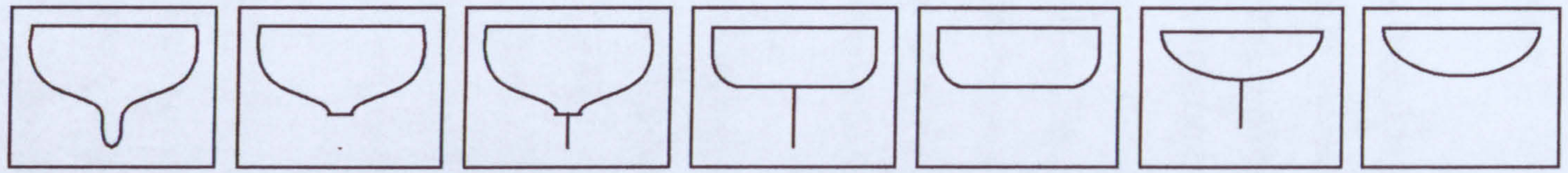

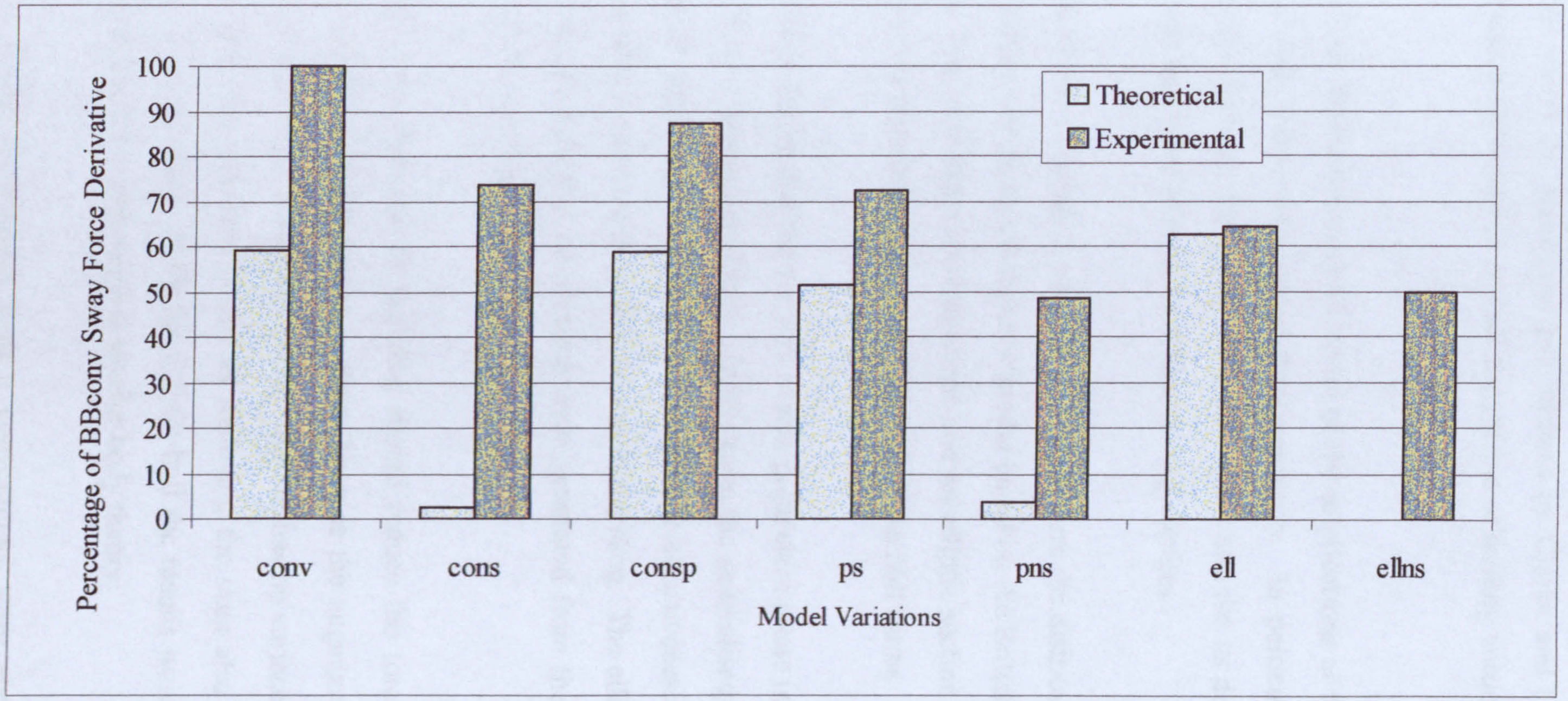

Figure 5.23 Percentage Comparison of Experimental and Theoretical Sway Force Derivatives for 7 Model Variations. Bombardier Conventional (conv), Without Skeg (cons), With Plate (consp), Bombardier Pram (ps), Without Skeg (pns), Ellipse (ell), Without Skeg (ellns).

5.4 CONCLUSIONS

In this section of the thesis the arguments put forward by Clarke and Hearn [28] in generalising the slender body theory to include the effects of trailing vortices have been rehearsed.

An experiment has been devised to examine some of the implications of this theory by testing a number of hull forms with varied stern geometry. In particular the basic theoretical relationships between the vortex influence effect and the its dependence on the strength, proximity and sense of rotation of the trailing vortices.

The experiment described in Chapter 3 was devised to measure the distribution of force and moment sway derivatives along a 6 segment model based on the British Bombardier with a conventional and pram stern configurations and an elliptic section model. The segments of these models were concentrated at the stern of the hull forms.

There is experimental evidence that the vortices from a pram stern rotate in the opposite sense to those shed from a conventional stern. In this case, the generalised slender body theory predicts that the presence of vortices will reduce the effectiveness of the skeg. Conventional form vortices augment the effectiveness of the skeg. The elliptic hull was chosen because it was thought that no vortices were generated from the stern. This model, as with the others, was run with and without a skeg.

For the conventional form, removal of the skeg should reduce the force derivatives more than the original slender body theory predicts because the augmenting effect of the trailing vortices is also lost because the vortex impulse has no surface on which to act. For the pram stern the converse is true as removing the skeg also removes the diminishing effects of the vortices. With the elliptic hull the results were expected to closely follow those predicted by the original slender body theory.

Comparison of the British Bombardier with a conventional stern and the British Bombardier with a pram stern confirms that the difference between the sway force derivatives of these hull forms is greater than could be accounted for by the change in

original slender body theory predictions. This finding supports the generalised slender body theory.

Comparing the British Bombardier with a pram stern, with and without a flat plate skeg, the conclusions are not as clear since the sway force derivatives for the pram stern without a skeg shows divergence between the original slender body theory and experiment. This is thought to be due to the growth of the boundary layer near the up sweeping stern sections.

A similar pattern is evident for the elliptic model, with and without a flat plate skeg. However, in both the case of the elliptic and the pram sterns with a skeg, where the skeg dominates, agreement between experiment and slender body thoery is close enough to conclude that vortices trailing from these forms have much less effect than those from a conventional stern. This supports the original hypothesis of the generalised slender body theory.

6. SEMI-EMPIRICAL ESTIMATION OF LINEAR HYDRODYNAMIC MANOEUVRING DERIVATIVES.

6.1 INTRODUCTION

The adoption of IMO Resolution A.751(18) has meant that there is a requirement to address the manoeuvring behaviour of a ship at an early design stage. The theoretical developments tested experimentally in the previous chapters show that the generalised slender-body, which includes the effects of stern vortices, can be used to explain experimentally derived linear hydrodynamic derivatives. However, there still remains the problem of predicting the start point and subsequent development of the stern trailing vortices, which are necessary components for a complete theoretical manoeuvring prediction.

Experimental measurements of model hulls, coupled with simulations of the manoeuvres, offers an accurate means of predicting manoeuvring characteristics of a vessel. However, this approach is not usually considered at an early design stage due to the cost of model testing.

A variety of semi-empirical methods have been used to calculate the necessary manoeuvring derivatives from hull parameters available at an early design stage and this approach remains a reasonable alternative. In many cases, these methods have used theoretical results to help formulae predictors, which are then used to regress available experimental results to derive equations for the derivatives.

The aim of the work presented in this chapter is to investigate whether the new physical insights provided by the generalised slender-body theory can be used to select meaningful predictors that will more adequately encapsulate the experimental derivative data.

The remainder of the chapter begins by considering previous developments in this area. The underlying statistical theory is rehearsed and the available data examined.

A previously published set of regression equations are re-analysed with this data to provide a baseline for comparison of the new analysis [36]. Two approaches to the regression analysis are then compared. The first uses the physical insight provided by the generalised slender-body theory and other theoretical results to presume a form for the regression equations. This is then compared for goodness of fit with a simplified approach.

6.2 Development of Semi-Empirical Methods

The need to predict the hydrodynamic manoeuvring derivatives by means other than experiment has given rise to a variety of semi-empirical methods. This section contains a review of some of these empirical prediction methods. Details which are of particular interest are, the source and range of the data set used, any underlying theory that may dictate the form of the equations and estimates of the success of the resulting equation in explaining variability in the data.

The various methods may easily be compared if all the equations are expressed in the same form. The standard adopted here was used by Clarke [36] and means the equations may be expressed generally as follows,

$$\text{ITTC Standard Derivative} = -\pi\left(\frac{T}{L}\right)^2\left[f\left(L,B,T,C_B\right)\right]. \qquad (6.1)$$

Where the function of the ship variates length, beam, draught and block coefficient, f must contain only dimensionless combinations of these quantities. This type of expression was chosen to reflect the functional form of the slender body theory predictions.

If the Jones [19] low aspect ratio wing theory is applied to ships, where the wing is turned on its side to become a flat plate with a draught of half the maximum wing span, the linear derivatives can be expressed as follows.

$$
\begin{aligned}
Y_{\dot{v}}' &= -\pi(T/L)^2(1) & Y_{\dot{r}}' &= -\pi(T/L)^2(0) \\
N_{\dot{v}}' &= -\pi(T/L)^2(0) & N_{\dot{r}}' &= -\pi(T/L)^2(1/12) \\
Y_{v}' &= -\pi(T/L)^2(1) & Y_{r}' &= -\pi(T/L)^2(-1/2) \\
N_{v}' &= -\pi(T/L)^2(1/2) & N_{r}' &= -\pi(T/L)^2(1/4)
\end{aligned}
\qquad (6.2)
$$

Early attempts to calculate derivatives made the simplifying assumption that the hull of the ship may be considered to be a low aspect ratio wing and made use of the Jones results.

Two studies by Wagner-Smitt [33] and Norrbin [34], were carried out at about the time, on the same data set. The data set contains approximately 30 observations of the velocity derivatives obtained from PMM tests of 'normal ship form models with normal-sized rudders propelled at medium Froude numbers on even keels'.

The results of Wagner-Smitt [33] were presented in the form of a constant multiplying $(T/L)^2$. If a factor of π is extracted from these constants, then the empirical formulae are as follows.

$$
\begin{aligned}
Y'_v &= -\pi(T/L)^2(1.59) \\
Y'_r &= -\pi(T/L)^2(-0.32) \\
N'_v &= -\pi(T/L)^2(0.62) \\
N'_r &= -\pi(T/L)^2(0.21)
\end{aligned}
\qquad (6.3)
$$

Norrbin developed regression equations in his 'Bis' nondimensionalising system. As an example, the Jones equation for Y'_v given in Equation (6.1), has the equivalent form in this notation of,

$$
Y''_{uv} = -\frac{\pi}{2}\frac{LT^2}{\nabla} \qquad (6.4)
$$

Norrbin fitted a simple linear equation with a constant using this $\pi/2\left(LT^2/\nabla\right)$ factor as the predictor variable; the Y''_{uv} derivative formula is,

$$Y''_{uv} = -(1.69)\frac{\pi}{2}\frac{LT^2}{\nabla} - (0.04) \tag{6.5}$$

Norrbin produced similar equations for the remaining velocity derivatives with intercepts for the moment derivatives chosen in a -1:2 ratio with their corresponding force derivatives.

A measure of goodness-of-fit of the regression equations is given as the percentage of the data points that appear within ±20% of the fitted line. These values are 100, 67, 86 and 79 percent for Y'_v, Y'_r, N'_v and N'_r respectively. Norrbin noted that the scatter of data in a plot of Y''_{uv} versus the variable LT^2/∇ is smaller than the scatter of Y'_v against aspect ratio $2T/L$.

The empirical formulae for the velocity derivatives in studies by Inoue et al [35] are presented as part of a mathematical description of a modular manoeuvring prediction method. The data set regressed in each case came from a coherent series of experiments. Inoue tested ten models of widely varying hull form on oblique tow and rotating arm experiments at various draughts to produce 24 observations of bare hull velocity derivatives in all.

In common with Wagner Smitt and Norrbin, Inoue et al [35] uses low aspect ratio wing theory to dictate the form of the regression equations. They also attempted a correlation of the velocity derivatives with hullform parameters and also covered the effects of trim. The equations in the standard form can be expressed as,

$$\begin{aligned} Y_v' &= -\pi(T/L)^2\left(1.0 + \frac{1.4}{\pi}C_B\frac{B}{T}\right) & Y_r' &= -\pi(T/L)^2\left(-\frac{1}{2}\right) \\ N_v' &= -\pi(T/L)^2\left(\frac{2.0}{\pi}\right) & N_r' &= -\pi(T/L)^2\left(\frac{1.04}{\pi} - \frac{4.0}{\pi}\frac{T}{L}\right) \end{aligned} \tag{6.6}$$

The appearance of the factor $C_B B / T$ in the equation for Y'_v is included by design as a 'form factor'. The form of the equation for N'_r allows better agreement with the experimental data. Kijima et al [60] and later Kose et al [61] have elaborated on the work of Inoue et al [35], using the same basic form applied in the original work, but including additional terms to improve the accuracy of estimation.

The empirical estimates so far considered have come from the regression of data sets originating from individual experimental facilities. The analysis carried out by Clarke et al [36] developed regression equations on a pool of 72 observations of velocity derivatives and 36 of acceleration derivatives gathered from the open literature.

It was noted that the variety of opinion in the literature about the prediction of the velocity derivatives was due, at least in part, to the systematic differences between experimental facilities. These differences include the type of experiment, data reduction techniques as well as scale effects. Collecting data from the open literature and carrying out a meta-analysis means that the variability between facilities will be present in addition to that due to differences in ship hydrodynamics. However, the bias in the regression equations towards any particular facility will be reduced. One problem with pooling the data in this way is that observations from complete self propelled models and bare hulls are amalgamated. While this doesn't matter for the acceleration derivatives, the velocity derivatives are significantly affect by the presence of a rudder and so the bare hull and complete model derivatives are, in a sense, drawn from different populations.

Clarke used the extension to the slender body strip theory [23] to provide the form for the regression equations. The velocity and acceleration derivatives, normalised by the $-\pi(T/L)^2$ factor are regressed with a set of nondimensional predictor variables form from combinations of L, B, T and C_B. The predictors chosen are those which tend to zero as B tends to zero and the equation is fitted with a preassigned constant so that the derivatives approach the correct intercept of the flat plate solution. The formulae for velocity and acceleration derivatives are as follows.

$$-Y'_v/\pi(T/L)^2 = 1+0.40C_B B/T$$
(9.6)

$$-Y'_r/\pi(T/L)^2 = -1/2+2.2B/L-0.080B/T$$
(5.2) (4.1)

$$-N'_v/\pi(T/L)^2 = 1/2+2.4T/L$$
(0.6)

$$-N'_r/\pi(T/L)^2 = 1/4+0.039B/T-0.56B/T$$
(3.4) (2.2)

$$-Y'_{\dot{v}}/\pi(T/L)^2 = 1+0.16C_B B/T$$
(5.0)

$$-Y'_{\dot{r}}/\pi(T/L)^2 = -1/2+2.2B/L-0.080B/T$$
(5.2) (4.1)

$$-N'_{\dot{v}}/\pi(T/L)^2 = 1/2+2.4T/L$$ (6.8)
(0.6)

$$-N'_{\dot{r}}/\pi(T/L)^2 = 1/4+0.039B/T-0.56B/T$$
(3.4) (2.2)

Clarke gave a complete set of statistics characterising the equations, which are reviewed in the re-analysis of this regression.

Ankudinov [37] has developed a set of formulae for the velocity derivatives to be used in a modular manoeuvring simulation program. The data used in the analysis comes from PMM tests conducted at the Hydronautics Ship Model Basin and consists of over 40 experiments. The data for complete models has been adjusted to estimate the bare hull derivatives where possible.

Ankudinov adopted a mathematical form for the regression equations similar to that used by Clarke, although an attempt has been made to reduce the number of possible predictor variables by 'an exploratory analytical treatment'. Thus the velocity

derivatives are all expressed in terms of only three predictor variables, x_1, x, y. These variables are defined below along with the resulting empirical formulae which are given in the standard form.

$$x_1 = (T/L)^2\left[1+1.5C_B B/T\right]$$

$$x = (T/L)^2\left[1+0.5C_B B/T\right]$$

$$y = BT/L^2$$

$$Y'_v = -\pi(T/L)^2\left[\frac{1}{2}\left(1+1.5C_B\frac{T}{B}\right)+\frac{0.8}{\pi}\frac{B}{T}\right]$$

$$Y'_r = \pi(T/L)^2\left[\frac{0.54}{\pi}C_B\left(1+0.5C_B\frac{T}{B}\right)+\frac{0.25}{\pi}C_B\frac{B}{T}\right]$$

$$-N'_v = -\pi(T/L)^2\left[\frac{1}{4}\left(1+0.5C_B\frac{T}{B}\right)+\frac{0.41}{\pi}\frac{B}{T}\right]$$

$$-N'_r = -\pi(T/L)^2\left[\frac{0.4}{\pi}C_B\left(1+0.5C_B\frac{T}{B}\right)+\frac{0.175}{\pi}C_B\frac{B}{T}\right] \quad (6.9)$$

No statistical measures for goodness-of-fit are presented, but scatter plots for the experimental versus predicted derivatives are given and Ankudinov states that residual variability is about the same as that found by Clarke.

6.3 Regression Theory

In this section the mathematical derivation of regression is rehearsed. The following discussion is concerned with the hypothesis of a linear model. If Y is the dependent variable which is to be predicted, and x is the explanatory variable, then a set of observations may be modelled as

$$Y_i = \beta_0 + \beta_1 x_i + \varepsilon_i . \tag{6.10}$$

This is a straight line probabilistic model where ε_i are the random errors associated with the experimental observations. The normal assumptions that are made about the nature of these random errors are,

1. The mathematical expectation of the errors is zero, $E[\varepsilon_i] = 0$,
2. The ε_i are independent of the x_i,
3. The ε_i are independent of each other,
4. The ε_i all have the same variance, σ^2,
5. The ε_i are normally distributed.

The unknown parameters of the model are estimated by least squares. The estimate to the regression line is,

$$\hat{y} = \hat{\beta}_0 + \hat{\beta}_1 x \tag{6.11}$$

The least square estimators $\hat{\beta}_0$ and $\hat{\beta}_1$ are the values of β_0 and β_1 which minimise Ψ, where,

$$\Psi = \sum \varepsilon_i^{\,2} = \sum (Y_i - (\beta_0 + \beta_1 x))^2 . \tag{6.12}$$

It is interesting to consider the basis for believing that the least squares estimator gives the best fit of the data. We are trying to get the best estimate for the statistical model from which the observations we have were drawn. So the question changes from the probability that a particular estimated regression line is correct to one of the likelihood of these observations arising, given a particular estimated line.
"The probability of the data given the parameters is identified as the likelihood of the parameters given the data. This identification is entirely based on intuition." [62]

Once this identification has been made, then the problem becomes one of parameter estimation by maximum likelihood estimation. The least squares fit is a maximum

likelihood estimation of the fitted regression parameters if the errors are independent and normally distributed with constant variance.

The estimated regression line is the line such that the sum of squared vertical distances from the data points to the line is a minimum. The residuals are the best estimates of the errors and are defined as,

$$r_i = y_i - (\hat{\beta}_0 + \hat{\beta}_1 x_i). \tag{6.13}$$

Thus the minimum value of Ψ is $\sum r_i^2$. The values of the parameters in the regression equation are obtained in terms of the data by partial differentiation of Ψ with respect to each parameter in turn and equating to zero.

$$\hat{\beta}_1 = \frac{\sum_{i=1}^{n}(x_i - \bar{x})(y_i - \bar{y})}{\sum_{i=1}^{n}(x_i - \bar{x})^2} = \frac{SS_{xy}}{SS_{xx}}$$
$$\hat{\beta}_0 = \bar{y} - \hat{\beta}_1 \bar{x} \tag{6.14}$$

Given the assumptions about the nature of the errors, the probability distribution of ε_i would be completely specified if the variance were known. The best estimate of the errors are the residuals and these can be used to make an estimate of the variance of the error,

$$s^2 = \frac{\sum r_i^2}{(n-2)}. \tag{6.15}$$

the number of degrees of freedom associated with the error is n minus the number of estimates made from the sample, $\hat{\beta}_0$ and $\hat{\beta}_1$.

6.4 DATA

The data used in this analysis is available in the open literature and comes from a number of different types of experimental facility including rotating arm (Inoue et al [35], Jacobs [24], Clarke [23]), planar motion mechanism (Berlekom and Goddard [63], Brummer et al [64], Wagner Smitt and Chislett [34],[65], van Leeuwan [66], [67], Cox and Motter [68], Fujino [69], Gerritsma et al [70], Gerritsma [71], Glansdorp and Pijfers [72], Matsmoto and Suemitsu [73]), and circulating water channel, (Gill and Price [74], Kashiwadani [75]). The type of model used also varies: bare hull, hull and rudder, complete self-propelled model. These models also vary in scale, trim, ballast condition and degrees of tow freedom. The experimental results are reduced to the nondimensional hydrodynamic derivatives using different fitting methods and nondimensionalising systems.

Carrying out a meta-analysis, in which data from a number of different sources is used, provides as large a data set as is available, although it has a number of possible weaknesses associated with it. These weaknesses arise from consideration of whether the data from different sources can be treated as observations drawn from the same population, or whether systematic differences in experimental methods and experimental data reduction techniques mean that the observations are drawn from different populations.

An attempt has been made here to reduce these problems by the following means.

1. The data was analysed using a relational database to remove duplicate entries: for example, the same experiment presented in two different references.
2. Only those data for hull only experiments were used. An attempt was made to use empirical methods [37] to remove the rudder effects from derivative values, but this approach was rejected on the ground that no means of validating the resulting derivatives was available.

This process reduced the number of derivative observation that could be used to a subset of 52 observations. The summary statistics for this subset are given below, Table 6.1.

Table 6.1. Summary Statistics for the Hull Only Data Subset.

Variable	Mean	Standard deviation	Minimum	Maximum
B/T	3.57	1.08	2.07	6.25
L/T	22.03	6.40	13.66	40.11
L/B	6.26	0.88	4.00	8.68
C_B	0.67	0.11	0.49	0.85
$Y'_v.10^5$	-1436	603	-3583	-490
$Y'_r.10^5$	312	189	67	845
$N'_v.10^5$	-524	271	-1029	-125
$N'_r.10^5$	-231	96	-477	-75

These data contain variability associated with the systematic differences between facilities. Therefore, it is not possible, even in principle, to create regression equations that will completely explain all the variability in the data using details of hull geometry. However, the possible bias created by analysis of a single source data set is prevented by a meta-analysis.

6.5 Non-Dimensionalisation of Derivatives

The customary ITTC standard non-dimensionalising factors are initial forward speed, U and ship length between perpendiculars, L. Thus, in ITTC standard notation the non-dimensional side force is expressed as,

$$Y' = \frac{Y}{\frac{1}{2}\rho U^2 L^2}. \tag{6.16}$$

It is important to note that the choice of L as the non-dimensionalising term is entirely arbitrary, although convenient since the duration of any ship manoeuvres can be expressed in terms of ship lengths travelled. Alternatively, we could use LT which has an equivalence in the aeronautical practice of using wing planform area.

In the original paper by Jones [19], the lift generated by a thin delta wing was found to be proportional to the square of the span of the wing. In identifying a ship as an instance of a low aspect ratio wing, the side force on the ship would be a function only of the square of the maximum draught of the vessel, if it were a thin flat plate. It has been shown in the generalised slender-body theory how the geometry of a ship hull form influences the side force generated by a manoeuvring vessel.

In the slender-body formulation, the appearance of the factor $-\pi(T/L)^2$ is essentially an artifice. The draught appears as a natural consequence of the slender-body approach, while the length of the vessel appears because of the ITTC standard notation. The presentation of these equations may be simplified considerably by non-dimensionalising the ITTC derivatives by $-\pi(T/L)^2$.

Thus we can define a set of linear velocity derivatives as follows,

$$\begin{aligned} Y_{vT}' &= Y_v' \Big/ -\pi(T/L)^2 & Y_{rT}' &= Y_r' \Big/ -\pi(T/L)^2 \\ N_{vT}' &= N_v' \Big/ -\pi(T/L)^2 & N_{rT}' &= N_r' \Big/ -\pi(T/L)^2 \end{aligned} . \tag{6.17}$$

6.6 Re-Analysis of Previous Equations

The work of Clarke et al [36] has been revisited to provide a benchmark for comparison.

The pooled data set described above was used in a multiple regression analysis with the same predictor variables as before and the following results for the velocity derivatives were obtained,

$$Y_{vT}{}' = 1 + 0.422\, C_B \frac{B}{T} \qquad Y_{rT}{}' = -\frac{1}{2} + 7.87\ B/L - 0.062\ B/T$$
(8.9) (3.9) (2.9)

$$N_{vT}{}' = -\frac{1}{2} + 2.97\ T/L \qquad N_{rT}{}' = -\frac{1}{4} + 0.039\frac{B}{T} - 0.56\frac{B}{L} \tag{6.18}$$
(2.2) (4.1) (2.3)

Following the format of the original paper, the values in brackets are the t-statistics associated with that term which are all significant at the 5% confidence level, including now the $N_{vT}{}'$ equation. Strictly, the t-statistic is not applicable to equations with a pre-assigned constant and only one term and the values given for $Y_{vT}{}'$ and $N_{vT}{}'$ are those for a regression with fitted constant. Measure of statistical merit for Equation (6.18) given by Clarke et al [36] are reproduced in Table 6.2. These are values for the standard derivation of the dependent variable (SD), the estimated standard derivation of the errors (s) or equivalently, residual error (RE) and the percentage reduction in error (PR) expressed as $100(SD - RE)/SD$.

The latter statistics, PR, is given as an alternative measure of goodness-at-fit to the multiple correlation coefficient, R, since the latter is not applicable to equations with pre-assigned constants.

By comparison similar results for the re-analysed equations are given in Table 6.2.

The results of the re-analysis are very similar to those presented originally [36] which is not surprising since the data used are similar. The equation for $N_{vT}{}'$ has improved with the T/L term now significant. The variety of opinion seen in the literature about the predictors used in regressions is highlighted with this re-analysis. Even small changes in the data set lead to some modifications of the 'best fit' equations. The problem with developing semi-empirical equations in this way is that not enough is known about true forms of the predictors to limit their inclusion and so this choice can only be made on statistical grounds.

Table 6.2. Comparison of Statistical Measures of Merit for Re-Appraised Regression Equations.

Variable	(SD)	(RE)	(PR)	(R)	(SD_{ITTC})
Original Results of Clarke et al [36]					
Y_{vT}'	0.582	0.387	33.5	0.75	0.330
Y_{rT}'	0.181	0.164	9.4	0.45	0.072
N_{vT}'	0.177	0.177	0.0	0.07	0.056
N_{rT}'	0.104	0.097	6.7	0.37	0.040
Re-Analysis of Clarke et al [36]					
Y_{vT}'	0.597	0.391	34.5	0.78	-
Y_{rT}'	0.174	0.161	7.5	0.40	-
N_{vT}'	0.108	0.103	4.6	0.30	-
N_{rT}'	0.073	0.066	9.6	0.52	-

Clarke also includes the standard deviation (SD_{ITTC}) of sets of derivatives obtained for a Mariner Class hull, from the ITTC Standard Captive-Model Tests [76]. The results gathered by the ITTC came from standardised experiments carried out by ten experimental facilities around the world. Any empirical formulae based on ship variates L, B, T and C_B could not, even in principal, explain the variability in derivative values between experimental facilities, observed by the ITTC study. So, if the estimated standard deviation of the errors, RE about a regression fit approaches the SD_{ITTC}, then this indicates that the regression formula is explaining most of the variability in the data attributable to differences in ships.

6.7 Vortex Influence Theory

6.7.1 An Appropriate Form for I_H

As reviewed in Chapter 2, the result of including the effects of stern vortices in a slender body treatment of a ship hull gives rise to the following equations for the linear derivatives, restating Equation (2.43)

$$Y_v' = \pi \left(\frac{T}{L}\right)^2 \left[C_H + I_H\right]_S^B \qquad N_v' = \pi \left(\frac{T}{L}\right)^2 \left\{\left[\left(C_H + I_H\right)X'\right]_S^B - \int_S^B \left(C_H + I_H\right)dX'\right\}$$

$$Y_r' = \pi \left(\frac{T}{L}\right)^2 \left[\left(C_H + I_H\right)X'\right]_S^B \qquad N_r' = \pi \left(\frac{T}{L}\right)^2 \left\{\left[\left(C_H + I_H\right)X'^2\right]_S^B - \int_S^B \left(C_H + I_H\right)X'\,dX'\right\} \tag{6.19}$$

Restating Equation (2.44), the vortex influence coefficient I_H may be expressed in terms of the rate of change of impulse, with lateral displacement y', of the two-dimensional cross section, as follows,

$$I_H = -\frac{1}{\pi\left(T/L\right)^2}\frac{\partial I'}{\partial y'}\frac{\partial y'}{\partial V'}. \tag{6.20}$$

where $\partial I'/\partial y'$ is the impulse position derivative and $\partial y'/\partial V'$ is the position sway derivative.

It has been shown (Equation 2.64) that the impulse position derivative may be expressed as

$$\frac{\partial I'}{\partial y'} = \pi \left(\frac{T}{L}\right)^2 \left[\frac{8\Gamma' r'^2 \xi'\eta'}{\pi\left(\xi'^2 + \eta'^2\right)^2}\right] \Re\left(f'(x)\right) \tag{6.21}$$

where the external vortices of strength Γ' are at points $\left(\xi', \eta'\right)$ and $\left(-\xi', \eta'\right)$ in the circle σ-plane. The position sway derivative may be deduced by making simple assumptions about the motion of the shed vortices (Equation 2.65). If the vortices leave the body at location X_O' It can be simply shown that,

$$\left(\frac{\partial y'}{\partial V'}\right)_{r'=0} = \frac{L}{T}X'\left(1 - \frac{X_O'}{X'}\right) \tag{6.22}$$

Recent developments in hull design have given rise to what has been called the pram stern. These buttock flow sterns have proved to be more efficient in terms of resistance and propulsion performance but have exhibited a tendency towards directional instability. Part of the reason for this behaviour was explained by Clarke [31], who showed that the side force generated by a skeg attached to a rectangular section, characteristic of pram sterns, was less than that generated by a skeg attached to a triangular section, more characteristic of conventional stern designs.

In addition, Kuiper [32] pointed out that there is experimental evidence which shows that the vortices shed from pram sterns rotate in the opposite sense to those shed from a conventional stern. The sign of the vortex influence coefficient I_H is dependent on the sense of rotation of the trailing vortices. In the case of conventional sterns, I_H is positive and therefore augments the side force generated by the stern sections. If the direction of rotation of the trailing vortices is reversed, then I_H is a negative quantity and so diminishes the side force generated by the stern sections. For the pram stern, this effect further reduces the effectiveness of the skeg and may explain some of the problems reported from ships with this type of pram stern.

It would therefore be desirable to devise a predictor for I_H that changes sign in the case of a pram stern. The aim was to devise new predictors that would reflect the new physical insight gained from the generalised slender-body theory. In addition, any new empirical formulae should have the same attributes as those devised by Clarke et al [36]; that is reduce to the Jones constant values in the limiting case of a thin flat plate.

Take as the starting point the equation for $Y_v' \big/ -\pi(T/L)^2$ from the generalised slender-body theory.

$$\frac{Y_v'}{-\pi(T/L)^2} = \left[C_H + I_H\right]_S^B \tag{6.23}$$

The value for horizontal added mass, C_H at the stern of each vessel in the data set was determined by simplifying the shape to a triangle, an ellipse or a rectangle attached to the thin skeg. The value of C_H was then obtained by analytic methods [31]. From the

expression for I_H Equation (6.20), the aim is to obtain a predictor variable that emulates the behaviour of this function, in terms of L, B, T and C_B.

One important result from the theoretical work [28] comes from plots of $\partial I'/\partial y'$ for a vortex of unit strength in the domain around stern like sections. These plots show that the value of impulse position derivative, for a unit vortex, is reasonably constant in the regions in which trailing vortices have been detected in experimental observations. This result implies that the position of the vortex is not critical to the evaluation of this term, but that vortex strength is important, that is

$$\frac{\partial I'}{\partial y'} \propto \Gamma' \tag{6.24}$$

Accordingly the problem is reduced to obtaining a function of L, B, T and C_B, which is proportional to the strength of trailing vortices. In experimental studies, Tanaka et al [54] have related the strength of trailing stern vortices to a parameter dependent upon the flat bottom area of the ship hull.

For a conventional stern ship, the geometry can be grossly simplified to that shown in Figure 6.1.

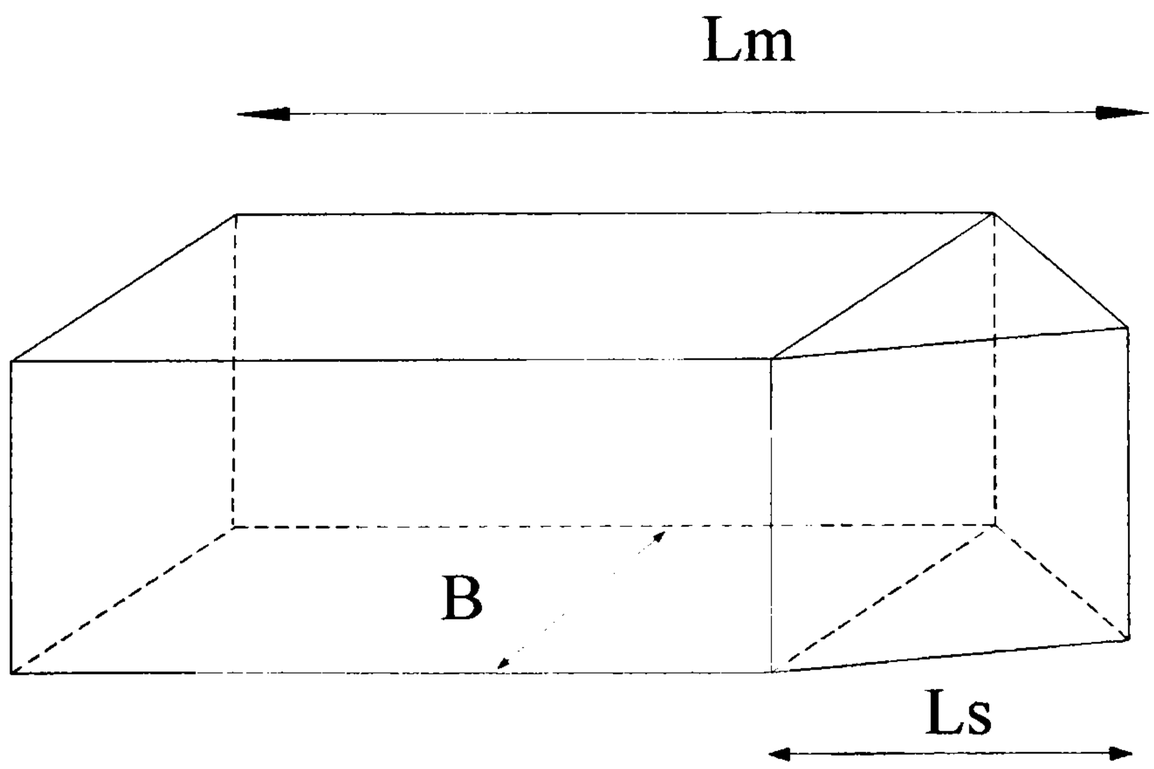

Figure 6.1. Simplified Stern Shape.

From Tanaka [54], the flat bottom area coefficient A_{FBA}, can be shown to be

$$A_{FBA} = \frac{2A}{BL} = \frac{2BL(1-L_s/L)}{2BL} = \left(1-\frac{L_s}{L}\right) = 1-\frac{1}{2}\left(1-\frac{L_m}{L}\right) = 1-\frac{1}{2}.2(1-C_B) = C_B, \tag{6.25}$$

for this simplified geometry.

Now, for pure sway motion, the position sway derivative is given by Equation (6.22). Which at the aft perpendicular, and assuming vortices are generated at the end of the middle body, becomes,

$$\frac{\partial y'}{\partial V'} \propto \left(\frac{L}{T}\frac{L_s}{L}\right) \tag{6.26}$$

We have shown that $L_s / L = (1-C_B)$, so that collecting all these terms we find that,

$$I_H \propto C_B{}^n \frac{L}{T}(1-C_B) \tag{6.27}$$

where, the power curve $C_B{}^n$ was introduced to fit the Tanaka curve [54].

An alternative simplification leads to another possible predictor. Referring to Figure 6.1, we see that at the aft end of a conventional ship, vortices are generated by flat bottom shape, which can be likened to a delta wing moving in reverse.

The hypothetical lift acting on the stern can be calculated from this assumption, using the Jones low aspect ratio theory [19],

$$C_{Ls} = \frac{\pi}{2}AR \quad \text{and} \quad AR = \frac{2B}{L_S} \tag{6.28}$$

$$C_{Ls} = \pi\frac{B}{L_S} \tag{6.29}$$

The lift is defined by $\text{Lift} = \frac{1}{2}\rho U^2 \text{ Area } \pi\frac{B}{L_S}$

(19)

$$= \frac{1}{2}\rho U^2 L^2 \frac{\pi}{2}\frac{B^2}{L^2} \tag{6.30}$$

The lifting line theory gives, $\text{Lift} = \rho U \Gamma B$

So on combining the expressions for lift and non-dimensionalising Γ by UT, we have $\frac{\Gamma}{UT} = \frac{\pi}{4}\frac{B}{T}$. This term was introduced into the predictor for I_H, which also included a term for the results of Tanaka [54]. By examining the requirements for a formula, it was found that a term of the form $\frac{B}{T}\frac{1}{1-C_B}$ was the simplest form and fitted the data with least vertical error.

6.7.2 Regression for Velocity Derivatives.

The general approach to developing the linear velocity derivatives was to use the predictors from the theoretical considerations to obtain an equation for $Y_{vT}{}'$. The predicted values of $Y_{vT}{}'$ for each data point, have then been used, in combination with other variates to produce regression equations for $Y_{rT}{}', N_{vT}{}' \text{ and } N_{rT}{}'$.

For $Y_{vT}{}'$ the alternative predictors were both regressed.

$$Y_{vT}{}' = (C_H)_S + 0.629 C_B{}^{3.5}\frac{L}{T}(1 - C_B) \tag{6.31}$$

(7.49)

where n=3.5 was obtained by trial and error to find the index which showed least residual error.

The second form determined by the theoretical considerations above yields the following equation,

$$Y_{vT}{}' = (C_H)_s + 0.17\left(\frac{B}{T}\right)^{1.4}\left(\frac{1}{1-C_B}\right)^{0.2} \tag{6.32}$$

(9.85)

The approach for $Y_{rT}{}'$,was to regress the following ratio to produce an expression for the lever arm, in terms of polynomial combinations of L, B, T and C_B .

$$\frac{Y_{rT}{}'}{Y_{vT}{}'} = \text{lever arm.}$$

$$Y_{rT}{}' = \left(-\frac{1}{2} + 1.73\frac{B}{L}\right).Y_{vT}{}' \tag{6.33}$$

(4.41)

The equation for $N_{vT}{}'$ was determined in a similar manner, but first an estimate was made of the Munk Moment generated by the hull form from empirical formulae used by Ankudinov [37]. Thus,

$$\frac{N_{vT}{}' - N_{vT(Munk)}{}'}{Y_{vT}{}'} = lever\ arm \tag{6.34}$$

The final expression is,

$$N_{vT}{}' = \left[0.97C_B\frac{B}{L} - \frac{1}{2}\left(1-\frac{T}{L}\right)\right].Y_{vT}{}' + N_{vT(Munk)}{}' \tag{6.35}$$

The derivative N_{rT}' was difficult to obtain an expression in terms of Y_{vT}'. The following combination produced the least residual error.

$$N_{rT}' = \underset{(7.89)}{\frac{1}{4}} + \underset{(7.89)}{0.08Y_{vT}'} - \underset{(-5.15)}{0.983C_B\frac{B}{L}} \tag{6.36}$$

Table 6.3 shows the statistical measures of these new formulae compared with the 'bench mark' values of the re-analysed Clarke et al [36] regression.

Table 6.3 shows that some improvement as been achieved in the predictive accuracy of the velocity derivative regression equation except in the case of N_{vT}' where no expression could derived which was better than the mean value. Scatter plots for each of these empirical equations are given in Figures 6.2, 6.3, 6.4 and 6.5.

Table 6.3. Comparison of Statistical Measures of Merit for Regression Equations with New Predictors.

Variable	(SD)	(RE)	(PR)	(R)	(SD_{ITTC})
Re-Analysis of Clarke et al [36]					
Y_{vT}'	0.597	0.391	34.5	0.78	0.330
Y_{rT}'	0.174	0.161	7.5	0.40	0.072
N_{vT}'	0.108	0.103	4.6	0.30	0.056
N_{rT}'	0.073	0.066	9.6	0.52	0.040
New Predictors Based on Vortex Theory					
Y_{vT}' (6.31)	0.597	0.394	34.0	0.73	-
Y_{vT}' (6.32)	0.597	0.331	44.5	0.81	-
Y_{rT}'	0.174	0.152	12.7	0.53	-
N_{vT}'	0.108	-	-	-	-
N_{rT}'	0.073	0.053	27.4	0.70	-

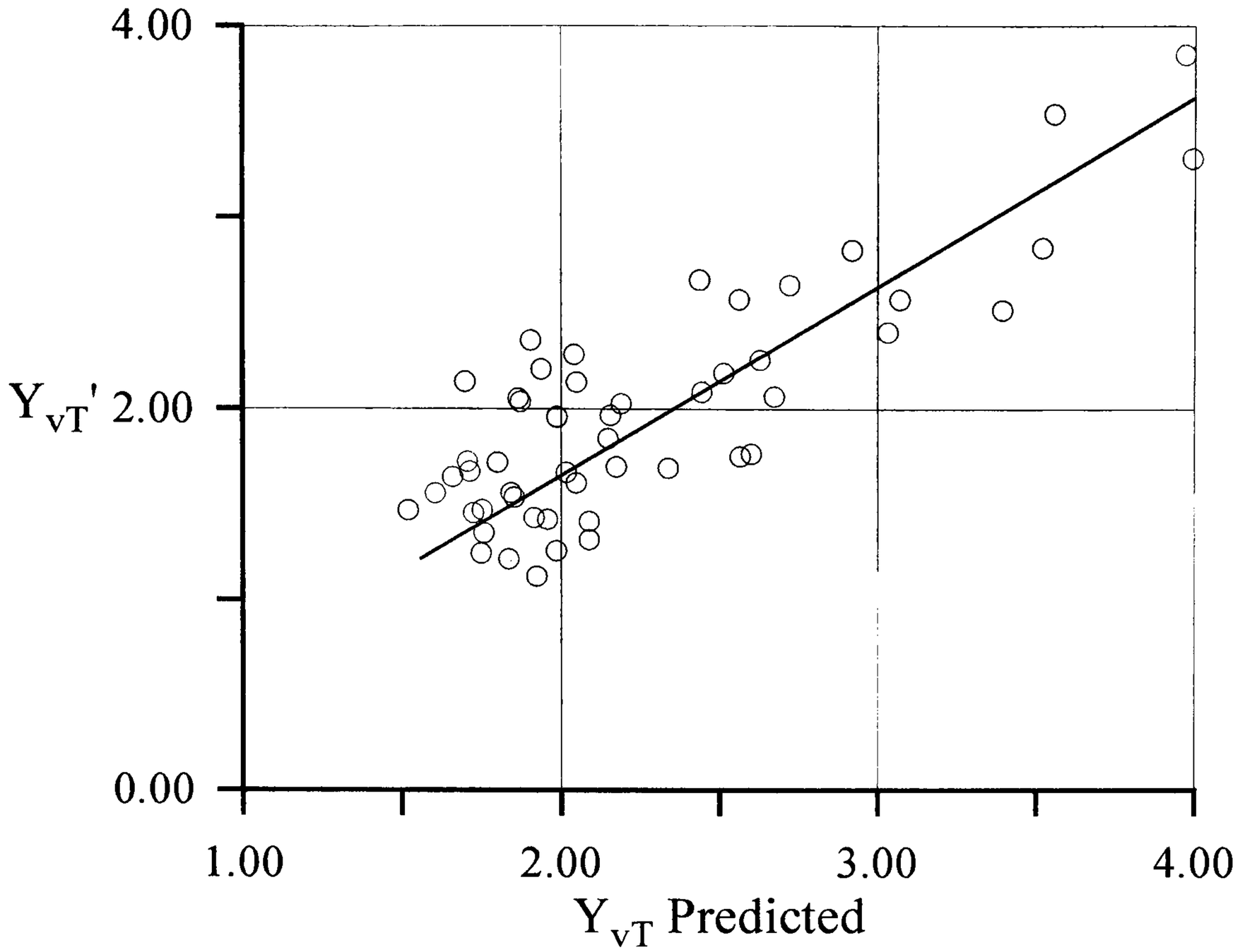

Figure 6.2 Scatter Plot of Y_{vT}' Using New Predictors.

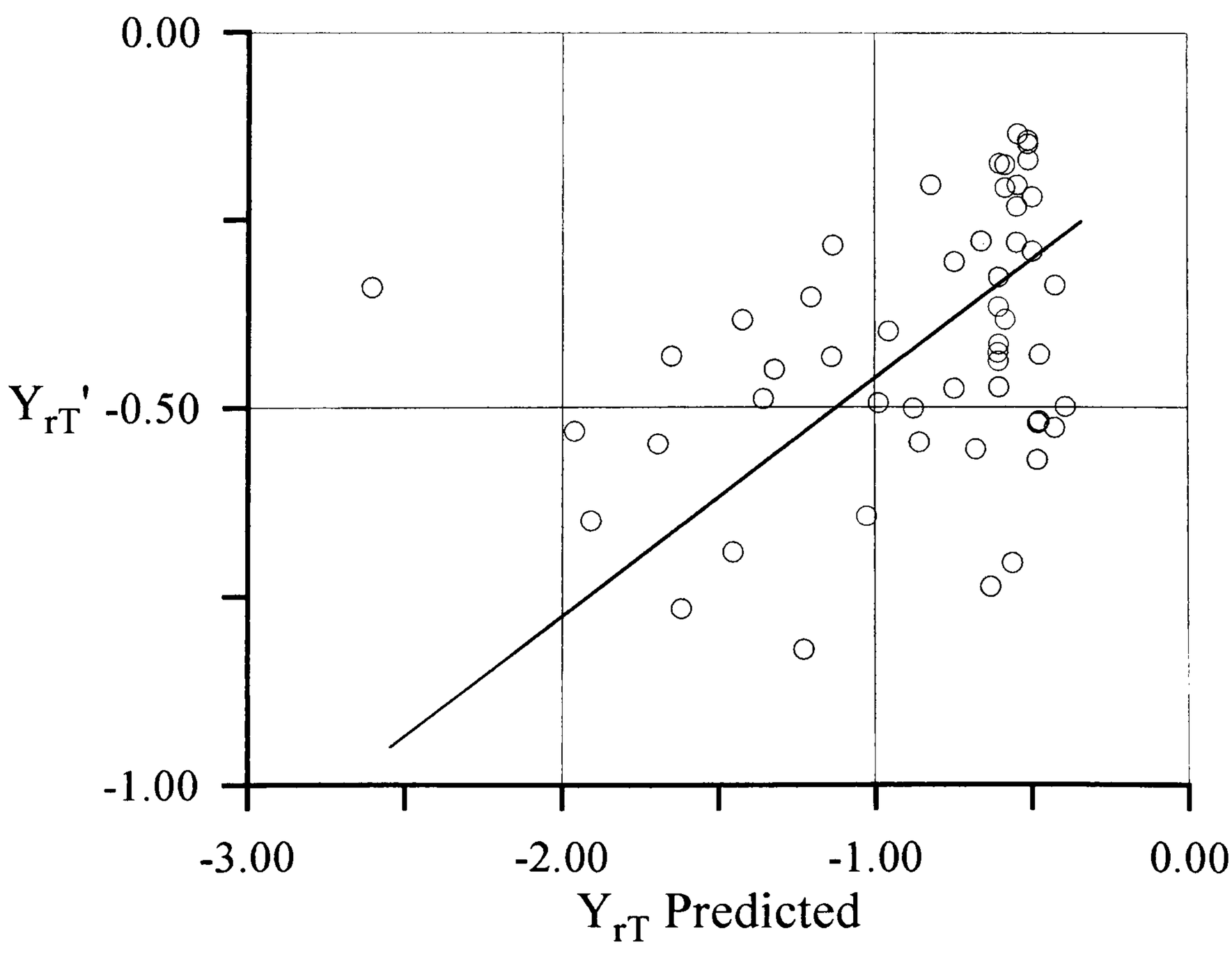

Figure 6.3 Scatter Plot of Y_{rT}' Using New Predictors.

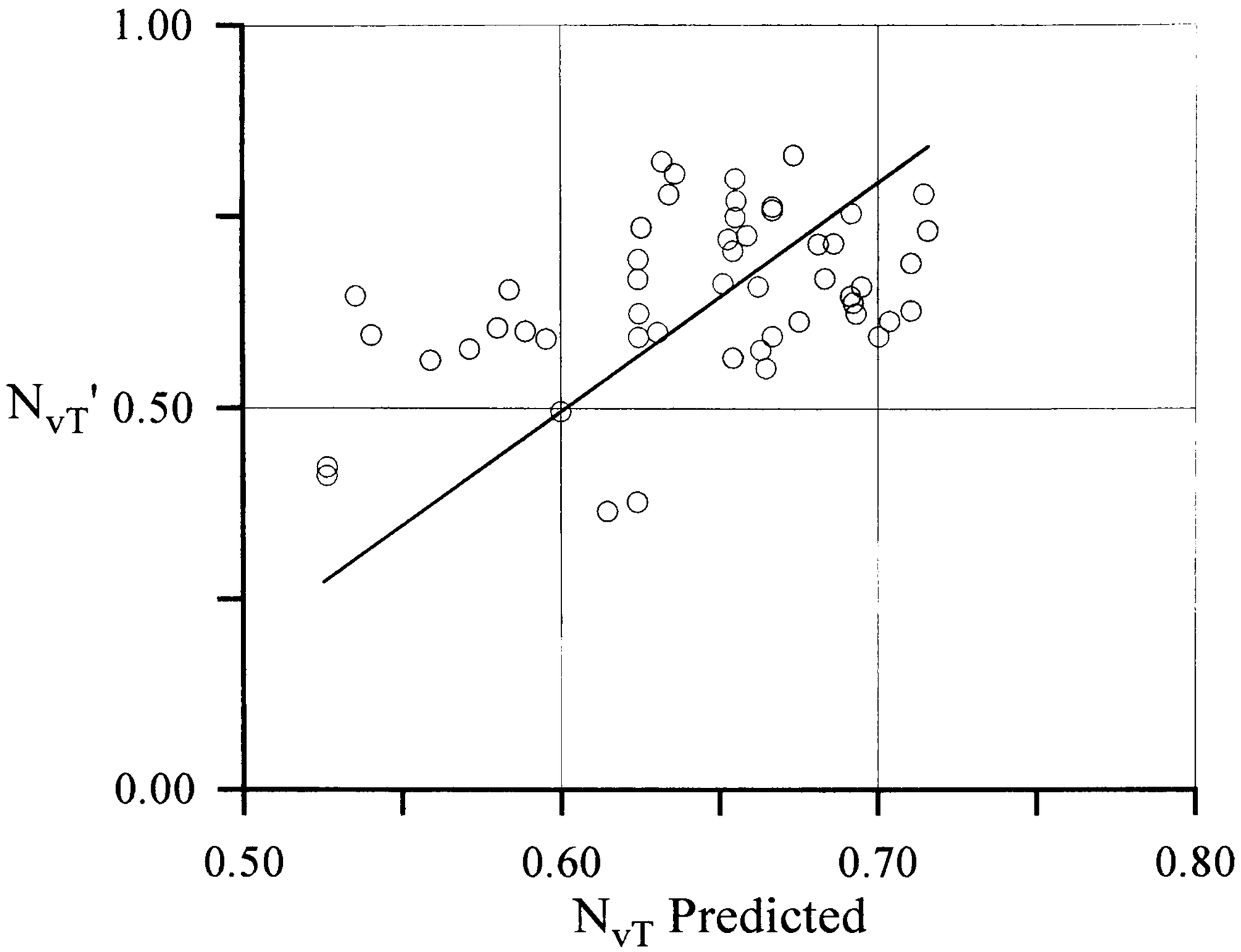

Figure 6.4 Scatter Plot of N_{vT}' Using New Predictors.

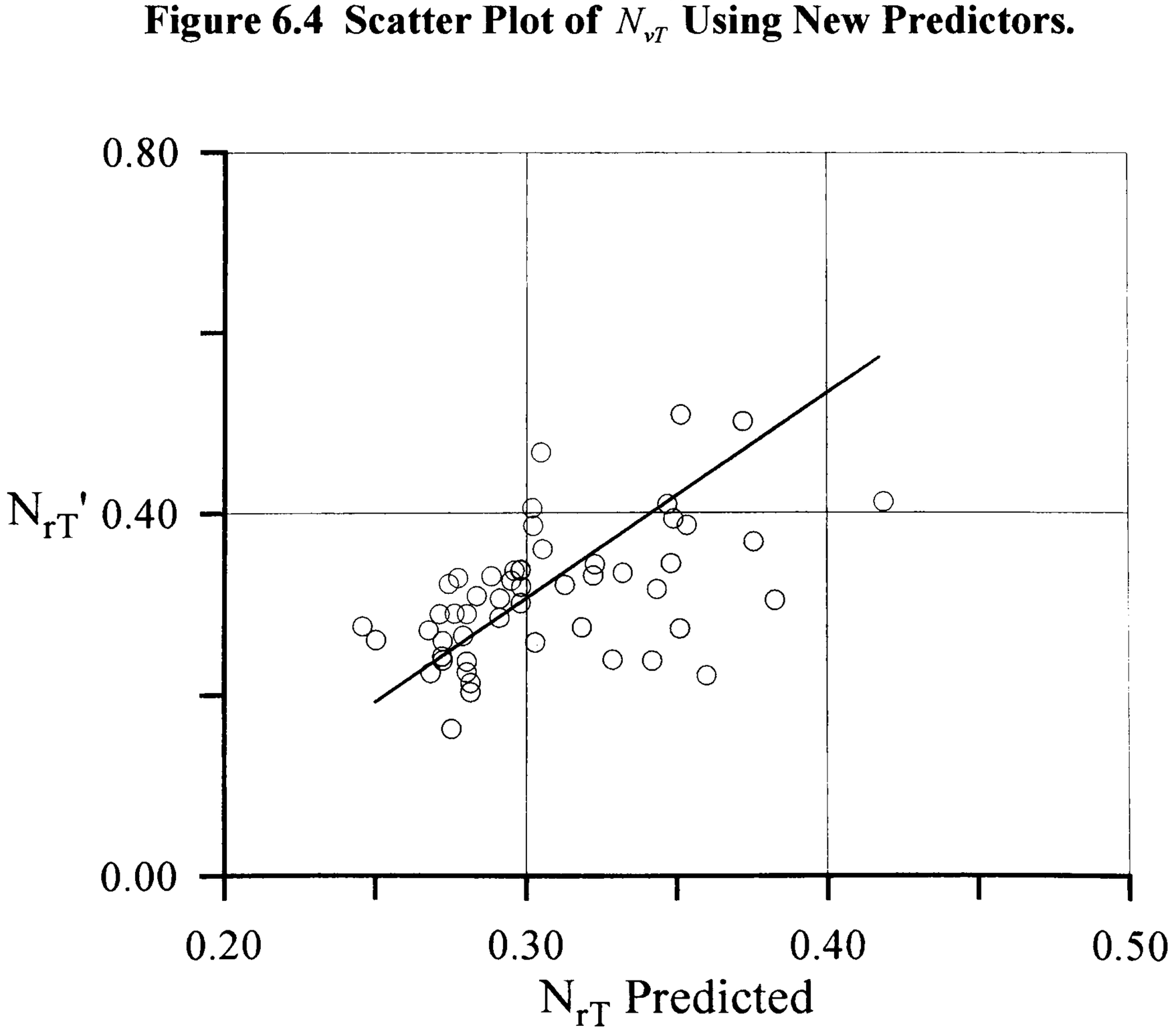

Figure 6.5 Scatter Plot of N_{rT}' Using New Predictors.

6.8 T-SPACE

The use of generalised slender body theory and other theoretical results to presume the form of the regression equations extends the previous approaches, in which first Jones [19] low aspect wing theory and then slender body theory have been used to restrict the predictors in the regression equations as much as possible.

From a statistical point of view, one weakness of this approach is that by forcing an intercept in the equations, we are in fact forcing the regression equations to span two distinct data sets. These data set are the ship model derivative data and the single experimental point for a thin flat plate; taken as the limiting case for the ship hull as the beam tends to zero. It could be argued that there are many experimental point for the thin flat plate result, but only one is admissible for the same reasons that duplicate hull experiments were removed from the derivative database. Multiple observations can only be used to improve the confidence in a given result, they cannot make that observation carry any more weight.

An alternative approach presented here is to apply a strictly statistical basis for the regression and to confine the equations to the available data by using a free intercept.

In the previous analysis, the velocity derivatives, normalised by the $-\pi(T/L)^2$ factor are regressed with a set of nondimensional predictor variables formed from combinations of L, B, T and C_B. It has been noted that the appearance of the factor $-\pi(T/L)^2$ is essentially an artifice. Continuing with this line of reasoning, the predictors used in this polynomial regression have all been non-dimensionalised with T as follows.

$$L_T = \frac{L}{T}, \text{ and } B_T = \frac{B}{T} \tag{6.37}$$

and,

$$C_B = \frac{\nabla}{LBT} = \frac{\nabla}{\frac{L}{T}\frac{B}{T}\frac{T}{T}} \cdot \frac{1}{T^3}.$$

Therefore,

$$C_{T3} = C_B \frac{B}{T}\frac{L}{T}. \tag{6.38}$$

These variables were used in polynomial terms fitting with a free intercept to create the following regression equations for the linear velocity derivatives.

$$\underset{(4.6)}{Y_{vT}'} = \underset{}{1.03} + \underset{(6.6)}{0.0026 B_T C_{T3}} + \underset{(2.3)}{0.0026 L_T^{\,2}} - \underset{(-2.7)}{0.000075 L_T^{\,3}}$$

$$\underset{(-1.5)}{Y_{rT}'} = \underset{}{-0.173} - \underset{(-1.1)}{0.00014 C_{T3}} - \underset{(-1.7)}{0.00096 L_T^{\,2}} - \underset{(1.4)}{0.000014 L_T^{\,3}}$$

$$\underset{(10.8)}{N_{vT}'} = \underset{}{0.966} - \underset{(-2.5)}{0.106 B_T} + \underset{(3.0)}{0.0038 C_{T3}} - \underset{(-1.5)}{0.00715 L_T}$$

$$\underset{(4.6)}{N_{rT}'} = \underset{}{0.193} + \underset{(3.0)}{0.00876 L_T} + \underset{(-1.3)}{0.0218 B_T} \tag{6.39}$$

The statistical measures of goodness of fit are given in Table 6.4, together with repeated results from Table 6.3 for ease of comparison. It can be seen that the T-space equations show a small improvement in explaining the variability in the data than the re-analysis of Clarke [36]. In comparison with the new predictors, the T-space equation for Y_{vT}' shows a small improvement, although the equations for the other derivatives are worse. Scatter plots for each of these T-space empirical equations are given in Figures 6.6, 6.7, 6.8 and 6.9.

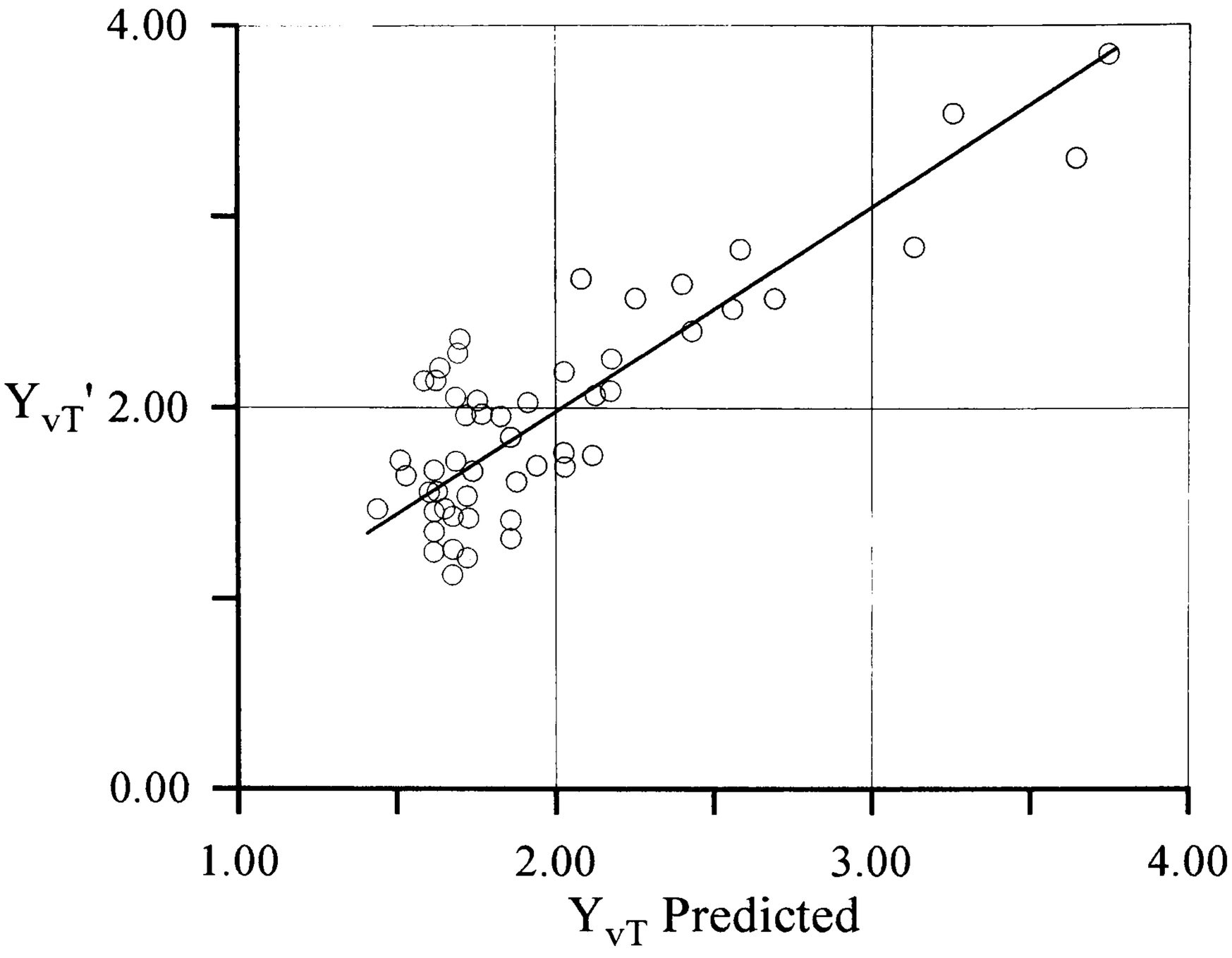

Figure 6.6 Scatter Plot of Y_{vT}' Using T-Space Predictors.

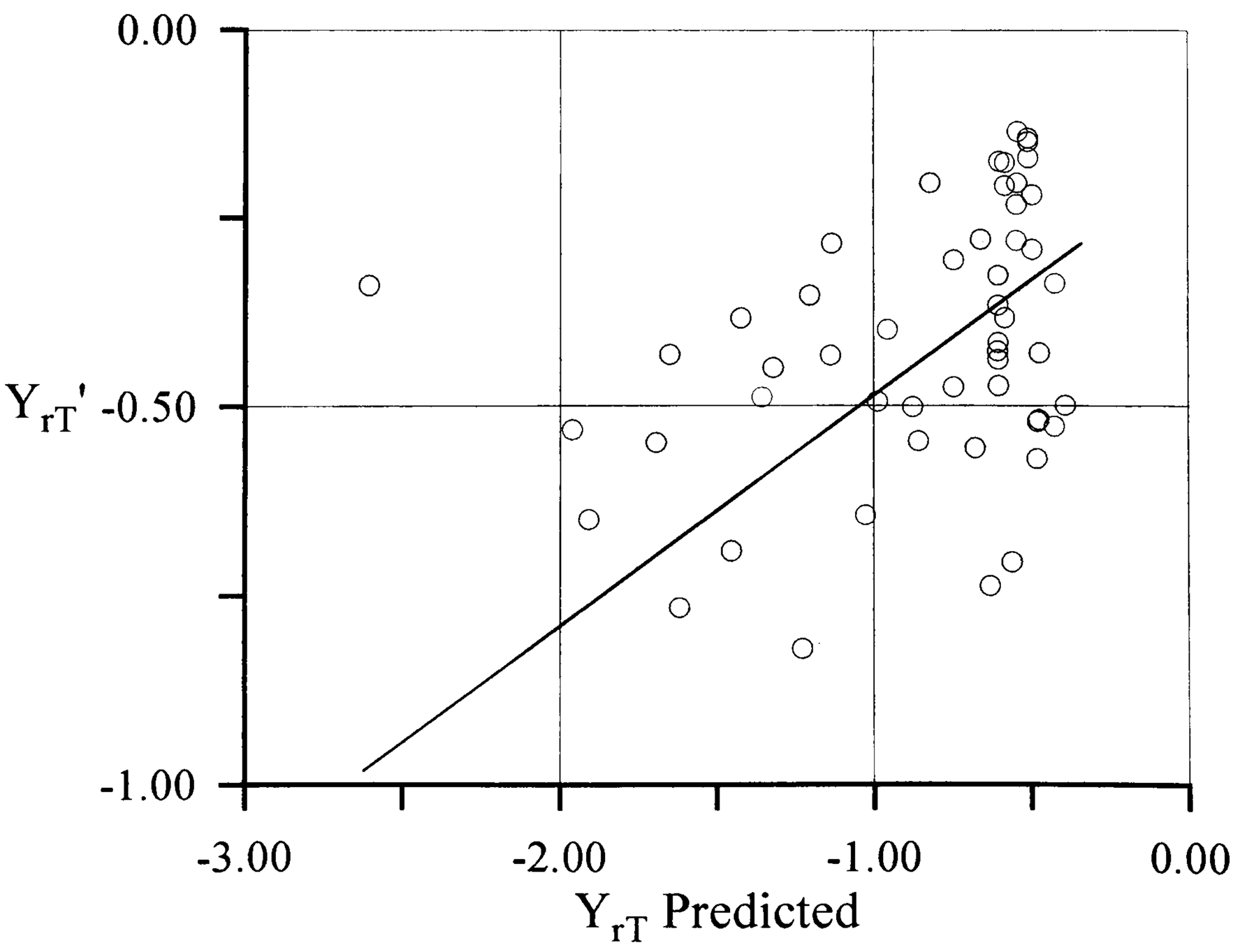

Figure 6.7 Scatter Plot of Y_{rT}' Using T-Space Predictors.

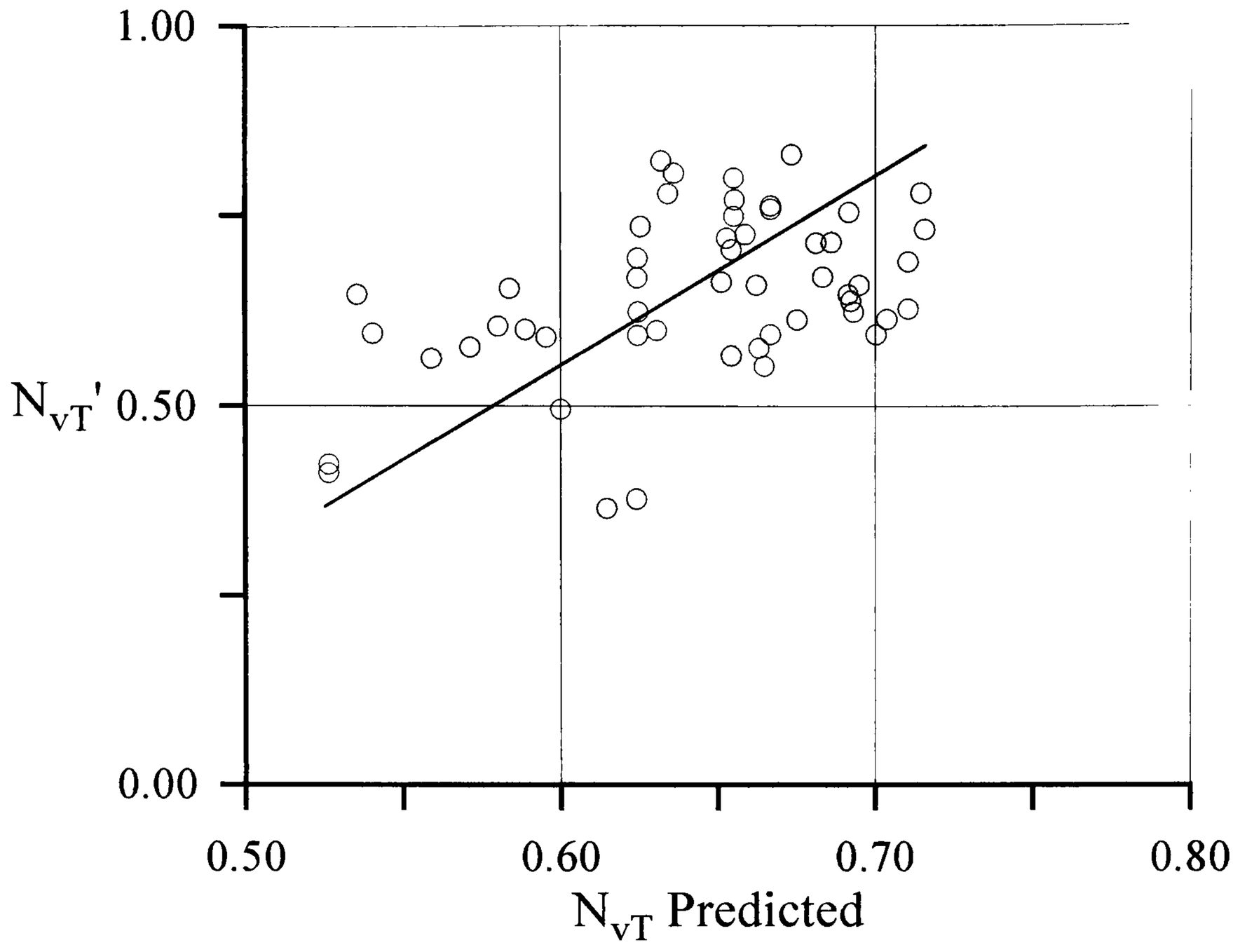

Figure 6.8 Scatter Plot of N_{vT}' Using T-Space Predictors.

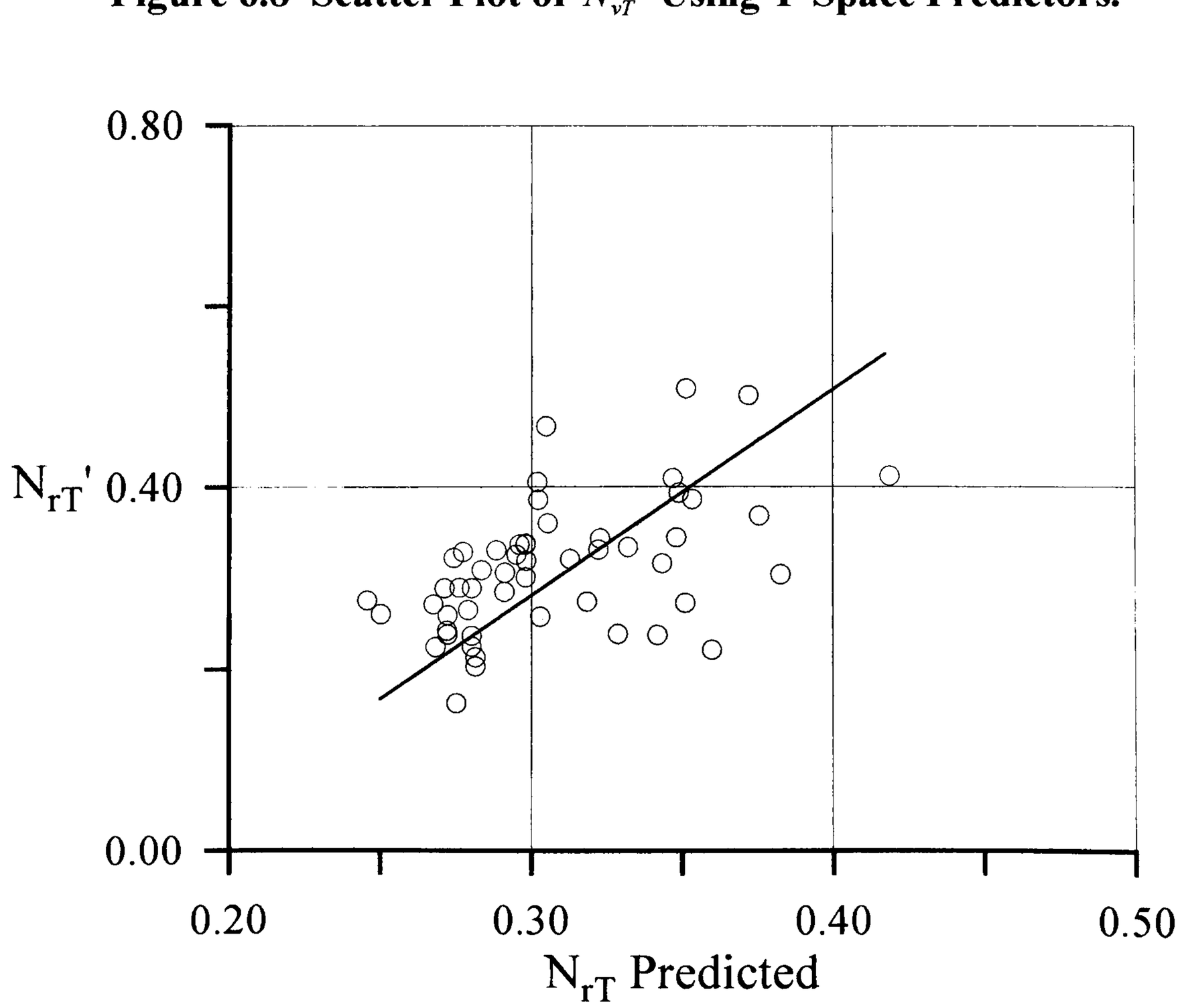

Figure 6.9 Scatter Plot of N_{rT}' Using T-Space Predictors.

Table 6.4. Comparison of Statistical Measures of Merit for Regression Equations with T-Space Predictors.

Variable	(SD)	(RE)	(PR)	(R)	(SD_{ITTC})
Re-Analysis of Clarke et al [36]					
Y_{vT}'	0.597	0.391	34.5	0.78	0.330
Y_{rT}'	0.174	0.161	7.5	0.40	0.072
N_{vT}'	0.108	0.103	4.6	0.30	0.056
N_{rT}'	0.073	0.066	9.6	0.52	0.040
New Predictors Based on Vortex Theory					
Y_{vT}' (6.31)	0.597	0.394	34.0	0.73	-
Y_{vT}' (6.32)	0.597	0.331	44.5	0.81	-
Y_{rT}'	0.174	0.152	12.7	0.53	-
N_{vT}'	0.108	-	-	-	-
N_{rT}'	0.073	0.053	27.4	0.70	-
T Space Predictors					
Y_{vT}'	0.597	0.328	45.1	0.85	-
Y_{rT}'	0.174	0.156	9.9	0.55	-
N_{vT}'	0.108	0.099	8.7	0.46	-
N_{rT}'	0.073	0.064	12.4	0.51	-

6.9 CONCLUSIONS

In this chapter an assessment has been made as to whether the generalised slender body theoretical forms could be used to create more accurate semi-empirical formulae for the prediction of linear hydrodynamic velocity derivatives.

In previous work [36] the theoretical form of the slender body theory has been used to define the form and limit of the regression equations to a thin flat plate, the predictors being generated from the basic hull parameters.

This theme has been continued to define predictor variables which have a theoretical basis again being generated from the basic hull parameters and with the inclusion of the horizontal zero frequency sectional added mass at the stern instead of the thin flat plate constants. In addition, an attempt has been made to recognise the interdependency of the linear derivatives.

The resulting regression equations show some improvement in the predictive accuracy when compared with previous analysis.

In a separate analysis, an attempt was made to simplify the form of the regression equations by nondimensionalising the predictors in the same way as the derivatives themselves. This second analysis was undertaken to see if the use of the constrained theoretical approach could be improved upon by a strictly statistical approach. Comparison of the predictive accuracy showed that overall the regression based the theoretical knowledge was more accurate.

The simplified polynomial regression was undertaken to establish whether a formulation where the predictors were selected purely on 'goodness of fit' criteria would improve on the formulations using a theoretical backdrop. In this instance, the theoretical approach proved more satisfactory, although with a different data set, this may not have been the case. The problem with selecting predictors purely on 'goodness of fit' is that the preferred predictors can change with the data set used. In the author's opinion, this is an unsatisfactory situation and it is on these grounds that it is argued that the theoretical approach, in formulating the predictors, is superior.

7. CONCLUSIONS AND FURTHERWORK

7.1 CONCLUDING DISCUSSION

Recent theoretical developments extend slender-body theory to generalised slender-body theory to include stern vortices. Experimental evidence from testing of the British Bombardier and Mariner has shown that this vortex addition explains the discrepancy between distributed forces and measurements on hull and slender-body theory calculations. The theory is limited at this time by the fact that no complete satisfactory theoretical means has been established for determining the start point, downstream path and strength of these shed vortices.

A number of developments in hullform design have seen the emergence of the pram stern. There is evidence that these stern shapes are less directionally stable than are conventional sterns. This finding is partially explained by the fact that skegs attached to rectangular sections are less effective in generating side force than are skegs attached to elliptic and triangular sections [31]. In addition to this, it has been found that hullforms with rectangular sections generate stern vortices that rotate in the opposite sense to those vortices generated by conventional hullforms. The generalised slender-body can be used to explain the effect of this observation. Stern vortices rotating in the sense typical of conventional hullforms augment the effectiveness of the skeg, while those rotating in the opposite sense diminish the effectiveness of the skeg.

The aim of the first part of this thesis was to test these predictions directly by testing a variety of models with segmented stern sections, based on the British Bombardier and an Elliptic hullform. The details of this experiment are given in Chapter 3.

The hullforms were chosen to provide a range of geometries which generated strong vortices rotating in a sense that augments the effectiveness of the skeg (British Bombardier conventional stern); weak or no vortices in the case of the elliptical form and weak vortices rotating in a sense that diminishes the effectiveness of the skeg

(British Bombardier pram stern). In each case the models were equipped with a thin flat plate skeg that could be removed.

It was postulated that in the case of the conventional stern, removing the skeg would diminish the side force generated by the section by an amount that could be explained by a slender-body theory treatment of the difference in the shapes. This difference being due to the loss of the stabilising vortex impulse, which acts mainly on the skeg because of the position of the vortex. Conversely removal of the skeg from a pram stern would reduce the side force less than would be expected because of the diminishing influence of the vortex.

These models were tested by towing them at a set of oblique angles to port and starboard. To obtain the distribution of forces over the stern sections a special apparatus was made consisting of two pairs of rails with force cells measuring the force between them. By progressively moving sections from the 'live' to the 'earth' rails the forces and moments acting on the hull were obtained for distributions along the stern sections.

Some difficulties were encountered with the experimental apparatus in the accurate measurement of the forces and moments. It was found that, although the force cells were accurately calibrated, the geometry of the apparatus and the degree of fixity of the cells to the rails resulted in a rather complicated combination of forces and moments being applied to the force cells. The assumption in the analysis had been that the connection between the force cells and the rails could be treated as a simple pair of pin joints.

A number of attempts were made to correct this problem, first by alterations to the apparatus, then by deriving some corrective factor. These methods did not prove adequate so an experiment was carried out to create a contour map of the response of the apparatus to a range of known loads. This was used to correct the measured forces.

The re-mapping of the measurements was a laborious task and could be eliminated by improving the design of the force cells; for example by mounting the bearing surfaces so that the pin jointed assumption applied.

The results for the seven combinations of hull forms were analysed to first obtain total forces and moments for each variation. The results were validated by comparing the results with forces and moments for the complete British Bombardier hullform from Clarke [23] and Glasgow [29]. The agreement for the forces and moments were very good, Figures 4.1 and 4.2. A comparison was also made with Clarke [23] for the distributed forces at a point where the longitudinal segments were coincident, Figures 4.3 and 4.4. Again the comparison shows that the forces and moments were in very good agreement. These comparisons validated the experimental procedures.

It was concluded that the experiments were valid for both the total forces and moments and also that the segmented results were valid across all the results presented in Tables 4.1 to 4.36.

As is normal practice, the experimental results were fitted with second and third order fits to obtain the linear and second and third order sway derivatives. The debate about the correct form for this analysis has continued for a number of years. There are arguments that the second order fit is more appropriate on the grounds that it has a physical basis in cross flow drag. Clarke and Hearn [28] have tentatively put forward the idea that the underlying physical form is affected by the presence of the vortices. Therefore in more forward sections the cross flow drag is more appropriate whereas in the aft sections the vortex presence means that a third order is more appropriate.

In analysing the results of the experiments described here it was found that comparison of the distributed linear sway force derivatives derived by third order fitting showed good agreement with those of Clarke [23] as shown in Tables 4.39 and 4.40. However second order were slightly higher than Clarke, Tables 4.37 and 4.38.

This discrepancy between the linear force derivatives using the second order fit was of the same order of magnitude as the difference between second and third order fitting of

Clarke [23] data alone. It is concluded that this discrepancy is a fitting artifice. The origin of this is a limitation of the experiment due to restrictions of the towing tank means that only drift angles up to six degrees could be tested. This affected the fitting and therefore the linear derivatives. The derivative fits are shown in Tables 4.43 to 4.56.

Those models with a sharp edge thin flat plate (skeg) showed a greater degree of non-linearity in the forces that the more rounded sections. However the difference is small and therefore, since the experiment design depends on differencing, this over estimate does not affect the findings. This latter point was demonstrated by comparing the differencing of the British Bombardier conventional stern and with the skeg removed with second order fitting and third order fitting, Figure 5.15.

The comparison of predicted distributed force and moment sway derivatives using slender-body theory are compared with the experimental estimates in Figures 5.1 to 5.14. To review these results against the original hypothesis, the experimental and slender-body theory values are differenced for pairs of hulls. These plots are shown in Figures 5.16 to 5.21.

The comparison of the British Bombardier conventional with the British Bombardier pram is given in Figure 5.19. From Equation 5.3, if the generalised slender-body theory is correct and the sense of vortices for the pram stern diminishes the effectiveness of the skeg while the vortices effect in the conventional hull, rotating in the opposite sense augment the effect, then the difference in experimental values should still be greater than that predicted by slender-body theory alone. This is indeed the case. It is therefore concluded that the initial hypothesis is correct.

This conclusion is further strengthened by comparison of the pram stern with and without flat plate skeg, Figure 5.20. This comparison should indicate that the slender-body theory differences are greater than those measured experimentally since when we remove skeg here, we loose the added mass of skeg, but also remove the diminishing effect of vortex influence. However, close examination of the absolute plots for experiment versus slender-body theory for the pram stern with and without skeg in

Figures 5.7 and 5.9 show this evidence cannot be used to verify hypothesis since the measured experimental values for the model without the skeg are higher than expected and this can be attributed to some of the difference. The comparison for this and the other hull pairs where flat plate skegs have been removed in British Bombardier and elliptical forms are also unclear for the same reason.

Given the earlier validation of the experimental results, it is concluded that the experimental estimates for the models without skegs are accurate within the limitations of the experiment already stated. It is tentatively suggested that the discrepancy between slender-body theory and experimental results for these hull forms where skeg has been removed is due to boundary layer growth in the adverse gradient created by the upflowing turned shapes of these sterns. It may be that this boundary layer growth has been increased by the presence of the gaps between the segments of the model sterns. It also indicates that for these more extreme shapes, the generalised slender-body is not a complete description of flow phenomenon at stern that may effect the manoeuvring characteristics.

Comparison of theoretical and experimental results of all the full model hullforms together is given in Figures 5.22 and 5.23. Figure 5.22 shows the absolute values of the sway force derivative compared with slender-body prediction. In Figure 5.23 the results have been nondimensionalised with the experimental value for the British Bombardier conventional stern, sway force derivative. This shows the relative effects of modifications to the stern form, from the parent hull. This comparison provides useful design information about the relative stabilising effects of changes in the stern geometry.

The second part of the work presented in this thesis is concerned with the use of semi-empirical methods to determine equations for the linear derivatives using an existing body of experimental data available in the open literature.

This type of approach has been used by a number of authors [33], [34], [35], [36], [37]. The aim here was to determine whether the new physical insight provided by the

generalised slender-body theory could be used to improve the predicted accuracy of these semi-empirical equations.

As a first step the data available in the open literature was collected in a relational database. In contrast to some previous analyses, the subset of data chosen in this meta-analysis were those results relating to hull only experiments. This was done on the grounds that inclusion of complete hull and rudder would introduce a systematic variability in the data that could not be explained by basic hull geometry.
A previous analysis by Clarke et al [36], in which the form of the equations for the linear derivatives were constrained to a form which complied with the slender-body theory, was analysed to provide a benchmark for comparison. One point highlighted by Clarke et al [36] was that the choice of nondimensional predictors formed from basic hull parameters of length, beam, draught, relative block coefficient was somewhat arbitrary and likely to change for different data sets.

This point is highlighted by a simple polynomial analysis of predictor based on what is referred to here as T space variable. In this analysis the derivative nondimensionalised and variable nondimensionalising factor were chosen as draught, thus eliminating draught as a variable. Table 6.4 shows that these variables can be used to create arbitrary collections of predictors, which are an improvement over the re-analysed Clarke predictors.

Considering Equation 6.19, the form of the equation for side force sway derivative was determined by a set of predictors for the vortex influence coefficient based on a simplified analysis of the physical situation. In addition, the horizontal added mass coefficient was evaluated for the data set. These predictors were regressed to provide Equations 6.27 and 6.28, these showed a significant improvement over previous equations.

Following Ankudinov [37], an attempt was made to encapsulate the relationship between the derivative equations by including known components such as Munk moment, which could be evaluated by other means, and then regressing the equations to find the necessary coefficients. The resulting equations show an improvement over

previous analysis. However, the variability remaining unexplained in the data is still larger than could be attributed to systematic differences between experiment facilities. The measure of this being the ITTC standard deviation.

One limitation of this semi empirical analysis is that it has not been possible to include terms which could be used to account for differences between conventional and pram sterns. This was due to the fact that very little data exists for the pram stern hull forms.

7.2 CONCLUSIONS

The conclusions of this thesis can be summarised in the following points.

- The experiment described in Chapter 3 has provided accurate measures of the distributed forces and moments along the stern sections of 7 hullforms, presented in Chapter 4 and 5.

- Differencing of the results for similar hullforms supports the hypothesis that the inclusion of the effects of stern vortices within the slender-body theory properly accounts for difference in manoeuvring characteristics of conventional and pram stern hullforms.

- The generalised slender-body theory is not a complete description of the flow phenomena around strongly up-swept sterns where boundary layer growth significantly affects the theoretical predictions.

- The semi-empirical equations, which encapsulate the mathematical form of the generalised slender-body theory, more accurately explain the variability in the experimentally determined manoeuvring derivatives available in the open literature than do those based on slender-body theory alone.

7.3 FURTHERWORK

There are a number of ways in which the work presented here could be developed further. Considering the further development of the generalised slender-body theory more broadly, there are a number of possible options.

It has been possible to successfully include the effect of vortices with the framework of the slender-body theory. However, there is as yet no theoretical means of determining the start point, strength and path of the stern vortices. The problem with determining these necessary inputs is that they are dependent on small-scale geometric characteristics of the hullform. Hitherto, these types of problems have been successfully resolved in aeronautics, but here the geometry is dominated by wings and fins. It has therefore been possible to identify the start point of vortices and estimate the strength of the vortices accurately.

In the opinion of the author, it seems unlikely that an analytical method of solving this problem for ships will be available without recourse to computational fluid dynamics methods. It is therefore possible that a semi-empirical approach to this problem may be the most fruitful in the shorter term.

In the work presented here, the experimental comparison of some of the hullform pairs with and without skegs proved inconclusive because other flow phenomena masked the effects that were under investigation. To progress this area of the work further it is suggested that one possibility would be to conduct a set of experiments that in general would be similar to those presented here. However in this new set of experiments a series of hullforms would be generated that had much smaller variations in geometry than those tested thus far.

The aim would be to design an experimental series that could be used to tie the two parts of this work more closely. One of the main points of interest is to investigate what geometrical features of the stern shape lead to a given vortex strength and sense of rotation. For this approach to be successful, it would be necessary to characterise the elements of the geometry important to whether the vortices were going to be generated

from the flat bottom area or from the side wall as simply as possible. Coefficients that varied with flat bottom area and sidewall area might be appropriate.

The results of this work could be used in two ways. Firstly, to provide systematic data necessary for further development of the theoretical determination of the vortex start point and strength. Secondly, to provide the necessary data to include the effect of pram sterns in the existing body of experimental results used in the semi-empirical analysis of the manoeuvring derivatives. If this data were available, then it might be possible to include coefficients that would encapsulate the diminishing effect of shed vortices on the skeg for pram sterns.

The type of experimental programme suggested here would be costly and time consuming. One possible short cut to much of the information required is available through the work of Inoue et al [35]. The results presented in this experimental testing were carried out with a variety of hullforms, and, if combined with more recent pram stern results, could form an excellent basis for a preliminary study. However, the problem with this is that the published data from Inoue does not include the necessary body plans for the hullforms considered. The first step would therefore be to obtain this information.

References

1. KEMPF, G., 'Measurements of the Propulsive and Structural Characteristics of Ships', Trans. Soc. Nav. Archit. Mar. Engrs, N. Y. (40), 1932.
2. DIEUDONNE, J., 'Collected French Papers on the Stability of Route of Ships at Sea', David, W. Taylor Model Basin, Translation 246, 1953.
3. BECH, M., 'Alternative Procedure for Carrying Out Spiral Tests', Scandinavian Ship Technical Symposium, Malmo, 1966.
4. DAVIDSON, K. S. M., and SCHIFF, L. I., 'Turning and Course Keeping Qualities', Trans. Soc. Nav. Archit. Mar. Engrs, N. Y. (54), 1946.
5. BRYAN, G. H., 'Stability in Aviation', Macmillan, London, 1911.
6. BISHOP, R. E. D., BURCHER, R. K., and PRICE, W. G., 'On the Linear Representation of Flud Forces and Moments in Unsteady Flow: The Fifth Annual Fairey Lecture', J. Sound and Vibration, 1973.
7. BURCHER, R. K., 'Studies into the Validity of Quasi-Steady Prediction Techniques', Proc. Fourteenth I.T.T.C., Ottawa, 1975.
8. ABKOWITZ, M. A., 'Lectures on Ship Hydrodynamics, Steering and Manoeuvrability', Hy A Rept Hy – 5, 1964.
9. GOODMAN, A., and GERTLER, M., 'Analytical and Experimental Techniques Used at HSMB for Surface-Ship Directional Stability and Control Studies', Hydronautics Inc. Report 7500-1, 1965.
10. GOODMAN, A., GERTLER, M., ROBERT, K., 'Experimental Techniques and Methods of Analysis Used at Hydronautics, for Surface-Ship Manoeuvring Predictions', Proc. Eleventh ONR Symposium, April 1976.
11. HAGEN, G.R., 'A Catalogue of Existing Mathematical Models of Manoeuvring', Proceedings of 20th American Towing Tank Conference, Stevens Institute of Technology, August 1983.
12. THIEME, H., 'Inclined Towing Tests with a Straignt and a Curved Model of a Habour Launch', Schif Hafen, 1956.
13. SUAREZ, A. 'The Davidson Laboratory Rotating-Arm Facility', Davidson Laboratory Note 597, 1960.

14. GERTLER, M., 'The D.T.M.B. Planar Motion Mechanism System', Proc. Symposium on Towing Tank Facilities, Instrumentation and Measuring Techniques, Zagreb, Yugoslavia, 1959.
15. GOODMAN, A., 'Experimental Techniques and Methods of Analysis Ised in Submerged Body Research', Proc. Third Symposium on Naval Hydrodynamics, Scheveningen, Netherlands, 1960.
16. TSAKONAS, S., 'Effect of Appendage and Hull Form on the Hydrodynamic Coefficients of Surface Ships', Davidson Laboratory Report No. 740, 1959.
17. INOUE, S., 'On the Turning of Ships', Memoirs, Faculty of Engineering, Kyushu University, 1956.
18. BRARD, R., 'The Manoeuvring of Ships in Deep Water, in Shallow Water and in Canals' Trans. Soc. Nav. Archit. Mar. Engrs., N.Y., 1951.
19. JONES, R.T., 'Properties of Low-Aspect Ratio Pointed Wings at Speeds Below and Above the Speed of Sound', NACA Report No. 835, 1946.
20. FEDYAEVSKY, K.K. and SOBOLEV, G.V 'Application of the Results of Low Aspect Ratio Wing Theory to the Solution of Some Steering Problems', Proc. Netherlands Ship Model Basin, Symposium of Ships in a Seaway, Wageningen, 1957.
21. FEDYAEVSKY, K.K. and SOBOLEV, G.V., 'The Handling Qualities of Ship', Sudpromgiz, Leningrad, 1963.
22. MUNK, M., 'The Aerodynamic Forces an Airship Hulls', NACA Report No. 184, 1924.
23. CLARKE, D., 'A Two-dimensional Strip Method for Surface Ship Hull Derivatives: Comparison of Theory with Experiments on a Segmented Tanker Model', Journal of Mechanical Engineering Science, Vol. 14, No. 7, (Supplementary Issue), 1972.
24. JACOBS, W. R., 'Estimation of Stability Derivatives and Indices of Various Ship Forms, and Comparison with Experimental Results.', Journal of Ship Research, 1966, Vol. 10, No. 3.
25. JACOBS, W. R., 'Methods of Predicting Course Stability and Turning Qualities of Ships', Int. Shipbiulding Prog., No. 121, 1964.

26. BRYSON, A.E., 'Stability Derivatives for a Slender Missile with Application to a Wing-Body-Vertical-Tail Configuration', Journal of the Aeronautical Sciences, Vol. 20, No. 5, pp. 297-308, May 1953.
27. NIELSEN, J.N., 'Missile Aerodynamics', McGraw Hill, New York, 1960, pp. 96-101.
28. CLARKE, D., HEARN, G.E. 'A Fundamental Investigation of the Hydrodynamics of a Manoeuvring Ship', MOSES Managed Programme, University of Newcastle upon Tyne, Department of Marine Technology, 1994, 350 p.
29. VARYANI, K.S., INCECIK, A. and HANNAH, S.T., 'Experimental Investigation on the Hydrodynamic Forces and Vortices around a Cargo and Tanker Vessel for Linear Drift Angles', University of Glasgow, Department of Naval Architecture and Ocean Engineering, Report NAOE, 94-16, March 1994.
30. CHAN, H.S., VARYANI, K.S. and INCECIK A., 'Experimental Investigation of the Hydrodynamics of a Ship Moving at a Drift Angle', University of Glasgow, Department of Naval Architecture and Ocean Engineering, Report NAOE, 93-25, 1993.
31. CLARKE, D., 'The Effect of Skegs and Stern Shape on the Dynamic Stability of Ships', Proceedings of Second International Conference on Manoeuvring and Control of Marine Craft, University of Southampton, 14-17 July 1992.
32. KUIPER, G., 'Resistance and Propulsion of Ships', TU Delft, Report 847-K, January 1994.
33. WAGNER SMITT, L., 'Steering and Manoeuvring Full Scale and Model Tests. (Parts 1 and 2).', European Shipbuilding 1970 (19) No. 6 and 1971 (2) No. 1.
34. NORRBIN, N.H., 'Theory and Observation on the Use of a Mathematical Model for Ship Manoeuvring in Deep and Confirmed Waters.', Meddelanden SSPA No. 68, 1971 (Sweden).
35. INOUE, S., HIRANO, M., KIJIMA, K., 'Hydrodynamic Derivatives on Ship Manoeuvring.', International Shipbuilding Progress Vol. 28, No. 321, May 1981.
36. CLARKE, D., GEDLING, P., HINE, G., 'The Application of Manoeuvring Criteria in Hull Design Using Linear Theory.', Trans RINA, 1983, Vol. 125, pp. 45-68.
37. ANKUDINOV, V., KAPLAN, P., JACOBSEN, B. K., 'Assessment and Principal Structure of the Mathematical Model for Manoeuvrability Prediction and Real-

Time Manoeuvring Simulations.', International Conference on Marine Simulation and Ship Manoeuvrability, 1993, Vol. 2, pp. 661.

38. LAMB, H., 'Hydrodynamics', Cambridge University Press, London, 6th Edition, 1932.
39. GLAUERT, H., 'The Elements of Aerofoil and Airscrew Theory', Cambridge University Press, 1959.
40. WARD, G.N., 'Supersonic Flow past Slender Pointed Bodies', Quarterly Journal of Mechanics and Applied Mathematics, Vol. 2, Pt. 1, 1949.
41. TSIEN, H.S., 'Supersonic Flow over an Inclined Body of Revolution', Journal of the Aeronautical Sciences, Vol. 5, No. 12, October 1938.
42. BRYSON, A.E., 'Evaluation of the Inertia Coefficients of the Cross Section of a Slender Body', Journal of the Aeronautical Sciences, Vol. 21, No. 6, pp. 424, 1954.
43. KIRCHOFF, G., 'Uber die Bewegung eines Rotationskorpers in eines Flussigkeit', Crelle, Vol. 71, p.237, 1869.
44. SUMMERS, R.G., 'On Determining the Additional Apparent Mass of a Wing-Body-Vertical-Tail Cross Section', Journal of the Aeronautical Sciences, Vol. 20, No. 12, p. 856, 1953.
45. LEWIS, F.M., 'The Inertia of the Water Surrounding a Vibrating Ship', Transactions of the Society of Naval Architects and Marine Engineers, Vol. 37, New York, 1929.
46. LANDWEBER, L. and MACAGNO, M.C., 'Added Mass of Two-Dimensional Forms Oscillating in a Free Surface', Journal of Ship Research, Vol. 1, No. 3, pp. 20-30, November 1957.
47. LANDWEBER, L. and MACAGNO, M.C., 'Added Mass of a Three-Parameter family of Two-Dimensional Forms Oscillating in a Free Surface', Journal of Ship Research, Vol. 2, No. 4, pp. 36-44, March 1959.
48. LANDWEBER, L. and MACAGNO, M.C., 'Added Mass of Two-Dimensional Forms by Conformal Mapping', Journal of Ship Research, Vol. 11, No. 2, June 1967.
49. MILNE-THOMPSON, L.M., 'Theoretical Hydrodynamics', 4th Edition, Macmillan, London, 1960.
50. KOBER, H., 'Dictionary of Conformal Representations', Dover Publications, New York, 1957.

51. CLARKE, D., 'Some Aspects of the Dynamics of Ship Steering', Ph.D. Thesis, University of London, July 1976.
52. BURCHER, R.K., 'Developments in Ship Manoeuvrability', Transactions of the Royal Institution of Naval Architects, Vol. 114, 1992.
53. BURCHER, R.K., 'Captive Model Tests with a Segmented Mariner Hull Form', Proceedings 13th ITTC, Berlin-Hamburg, pp. 107-120, 1972.
54. TANAKA, H., KAWAKAMI, Y., UEDA, T., TAKAHASHI, K., and YANAGIHARA, T.Y., 'Experimental Studies on Trailing Vortices of Ship', Proceedings of the 2nd International Symposium on Practical Design in Shipbuilding, pp. 295-302, 1983.
55. BROWN, C.E., MICHAEL, W.H., 'Effect of Leading-Edge Separation on the Lift of a Delta Wing', Journal of the Aeronautical Sciences, pp. 690-706, 1954.
56. GATZER, H., 'Vortices and Vortex Effects on Ships', Siptechnic, Vol. 5, 1985, Department of Ship Technology, University of Cochin.
57. OH, C.D., TANAKA, I, BABA, T. and LING, M.C., 'A Study on Separation Vortices Around a Full Ship Model', Journal of Kansai Society of Naval Architects, No. 171, December 1978.
58. NONAKA, K., FUWA, T. and NIMARA, T., 'Measurement of Wake Flow and Hydrodynamic Forces Distribution on a Ship Model with Drift Angle', Journal of Kansai Society of Naval Architects, No. 58, May 1991.
59. DELLA LOGGIA, B., LAURO, G., MASSA, L., 'Afterbody Hull Form Design: A Rational Approach and Related First Experimental Results', CETENA, Italian Ship Research Centre, 1989.
60. KIJIMA, K., TANAKA, S., FURUKAWA, Y., HORI, T., 'On a prediction method of ship manoeuvring characteristics.', International Conference on Marine Simulation and Ship Manoeuvrability, 1993, Vol. 1, pp. 285-294.
61. KOSE, K., MISIAG, W. A., 'A systematic procedure for predicting manoeuvring performance.', International Conference on Marine Simulation and Ship Manoeuvrability, 1993, Vol. 1, pp. 331-340.
62. PRESS, FLANNERY, TEUKOLSKY, VETTERLING, 'Numerical Recipies.', Cambridge University Press, 1986, ~400 p.
63. VAN BERLEKOM, W. B., GODDARD, T. A., 'Manoeuvring of large tankers.', Trans SNAME, 1972, Vol.81.

64. BRUMMER, G. M. A. ET AL., 'Simulation of the steering and manoeuvring characteristics of a second generation container ship.', Netherlands Research Centre, 1972, TNO Report, No. 170S.
65. WAGNER SMITT, L., CHISLETT, M. S., 'Large amplitude PMM tests and manoeuvring predictions for a 'Mariner' class vessel.', Proceedings 10th Symposium on Naval Hydrodynamics, 1974, Boston.
66. VAN LEEUWEN, G. JOURNEE, J. M. J., 'Prediction of ship manoeuvrability.', Netherlands Research Centre, 1972, TNO Report, No. 158S.
67. VAN LEEUWEN, G., ,Damping and added mass of an oscillating ship model.', Netherlands Research Centre, 1964, TNO Report, No. 64S.
68. COX, G. G., MOTTER, L. E., 'Prediction of standard manoeuvring characteristics for a Naval Auxiliary Oiler (AO177).', NSRDC, 1975, Report SPD-624-01.
69. FUJINO, M., 'Experimental studies on ship manoeuvrability in restricted waters.', International Shipbuilding Progress, 1968, Vol. 15, No. 168.
70. GERRITSMA, J., BEUKELMAN, W., GLANSDORP, C. C., 'The effects of beam on the hydrodynamic characteristics of ship hulls.', Proceedings 10th Symposium on Naval Hydrodynamics, 1974, Boston.
71. GERRITSMA, J., 'Hydrodynamic derivatives as a function of draught and speed.', Technical Hogeschool, Delft, 1979, Report No. 477.
72. GLANSDORP, C. C., PIJFERS, J. G. L., 'Effect of design modifications on the natural course stability of full tanker models.', Journal of Mechanical Engineering Science, 1972, Vol. 14, No. 7, Paper 22.
73. MATSMOTO, N., SUEMITSU, K., 'The prediction of manoeuvring performance by captive model tests.', J. Kansai Socirty of Naval Architects, !980, No. 176.
74. GILL, A. D., PRICE, W. G., 'Determination of the derivatives of a ship model using horizontal PMM in a circulating water channel.', Trans RINA, 1977, Vol. 119.
75. KASHIWADANI, T. ET AL., 'Experimental studies on the hydrodynamic forces acting upon full-bodied ships with relation to their course stability.', J. Kansai Society of Naval Architects, !977, No. 167.
76. GERTLER, M., 'Final Analysis of First Phase of ITTC Standard Captive Model Test Programme', Proc. of Twelth ITTC, Rome, 1969.

77. TIMOSHENKO, S. and MACCULLOUGH, G. H., 'Elements of Strength of Material', 3rd Edition, D. van Nostrand Company Inc., 1949.

A1. APPENDIX A1 – CORRECTION OF MEASURED FORCES AND MOMENTS

A1.1 INTRODUCTION

This Appendix describes the causes of the observed error and examines some of the possible methods of solving the problem including experimental and semi-analytical approaches. The final solution procedure is explained in detail and this method involves a combination of physical changes to the apparatus and a graphical method of correcting the measurements.

A1.2 INITAIL INVESTIGATION

As a first step the port and starboard outer rails were removed and a known load was applied to each of the modular force gauges in turn. The load had to be applied horizontally and simply attaching a fine nylon string to the modular gauge box and then passing it over a free running pulley to a balance pan did this. The resulting forces were measured in a similar way to the model experiments by first recording a residual and then applying the load. The testing of the fore and aft modular force gauges individually established that the original calibration of the gauge boxes, before assembly, was still valid. The modular force gauges accurately measured the masses placed in the balance pan, when in isolation.

The measuring apparatus was then re-assembled and a load of 1.9622 N (200 grams) was applied at three points on the outer rail: at the centre of the forward modular force gauge, at the centre of the aft modular force gauge, and at the mid point between these two positions. The results of the experiment are shown in Table 3.6 together with force and moment actually applied. Note that for simplicity, the moments are taken about the mid-point between the modular force gauges although this is not coincident with either the midpoint of the rails or the midpoint of the elliptic hull form.

Table 3.6 Comparison of Measured and Applied Load on the Rail Apparatus.

Load Position	Position 1	Position 2	Position 3
Measured Forward Force (N)	1.6078	0.3783	1.0151
Measured Aft Force (N)	0.3560	1.5250	0.9375
Measured Total Side Force (N)	1.9638	1.9033	1.9523
Measured Total Moment (Nm)	0.4381	-0.4013	0.0272
Applied Forward Force (N)	1.9622	0	0.9811
Applied Aft Force (N)	0	1.9622	0.9811
Applied Total Side Force (N)	1.9622	1.9622	1.9622
Applied Total Moment (Nm)	0.6868	-0.6868	0

The total side force shown in Table 3.6 was calculated by summing the forces recorded at the forward, F_1 and aft, F_2 modular force gauges,

$$\text{Total Side Force} = F_1 + F_2 . \qquad \text{(A1.1)}$$

The moments were calculated by summing the moment contribution of the forces recorded at each modular force gauge. Note that for the elliptic hull, the modular force gauge separation was 0.7 m and moments were taken about a midpoint,

$$\text{Total Moment} = x_1 . F_1 + x_2 . F_2 , \qquad \text{(A1.2)}$$

where $x_1 = 0.35$, and $x_2 = -0.35$.

The calculation of forces and moment in this way rests on the implicit assumption that the structure of the rail is simply connected. Examining the elements of Table 3.6 shows that this assumption is not valid. In particular, comparison of measured and applied loads for position 1 show that in reality a considerable fraction of the load applied at the centre of the forward modular force gauge is transferred to the aft modular force gauge. It is this transfer of load that leads to the gross underestimate of the applied moment, which in these bench tests constitutes an error of up to 42%.

In the test applied to the rail system on the bench, the loading position has not extended outside the longitudinal position of the modular force gauges. During experimental testing of the segmented models the longitudinal position of the centre of pressure for sway was in front of the bow for the elliptic hull form and this implies a resultant side force applied at a position in front of the forward modular force gauge. The effect of the load being applied outside the modular force gauges is to make the underestimate of the moment even greater.

It may also be noted from Table 3.6 that the measured total side force is not the same for each loading position. For position 1, the total side force is measured with an error of 0.08%; at position 3, the total side force is measured with an error of 0.5%; and at position 2, the total side force is measured with an error of 3%. Thus, as the point of the applied load comes closer to the aft modular force gauge the error increases and this is due to the under reading of the aft modular force gauge. This under reading of the aft modular force gauge occurs in the complete apparatus despite the confirmation of the measuring accuracy of the cell when tested in isolation. This problem is noted here, but initially the discussion in the following sections will be concerned with the much larger errors in the measured moments.

The error in the measured moment values comes as a result of assuming that the structure is pin jointed and therefore the force gauges can be deflected in sway without any torsion of the gauge boxes. The real situation is that the gauge boxes have a degree of fixity to the rail system and therefore, any deflection of the outer rail in response to a

side force must necessarily, result in a torsional loading of the gauge boxes. The only load point where torsional displacement will not occur is when the point of application of the resultant side force acts at the midpoint between the two force gauges. The physical size and geometry of the gauge boxes determines the magnitude of this torsional loading for the application of a given side force and the effect of this torsion on the measured output depends upon the position of the strain gauges.

A qualitative explanation of the problem can be obtained by considering the effect of the three loading conditions of the bench test. These conditions are illustrated schematically in Figures A1.1(a), Figure A1.1(b) and Figure A1.1(c) which refer to loads applied at the forward modular force gauge, the midpoint, and the aft modular force gauge respectively. The Figures show idealised measuring system from above with the gauge boxes, the position of the strain gauges within along with the outer rails. The inner rails and other supporting structure are removed for clarity, and instead, the gauge boxes are assumed to be rigidly fixed to some imaginary lower surface.

Figure A1.1(a) shows the load applied at position 1, opposite the forward modular force gauge. The load applied at this point results in a linear displacement of the forward force gauge and, since the structure is not pin jointed, a torsional displacement of the gauge box also exists. The torsion in the forward gauge box is transmitted through the rails to the aft gauge box, which opposes this torsion with a linear and angular displacement. If the gauge boxes were pin jointed and could not therefore resist torsional loads, then a small displacement of one force gauge box would not result in linear and angular displacements of the other. If it is assumed that the rails and other supporting structures are rigid, then the angular displacement of the two gauge boxes must be the same.

A starboard side force at position 1 leads to a positive linear and angular displacement of both gauge boxes using the normal manoeuvring reference frame. Examining the forward gauge box, the positive linear displacement results in a strain in the strain gauge bridge which is sited towards the aft end of the spring elements. Imagining for a moment the gauge box were subjected to a pure couple in the positive direction, the strain in the strain gauge bridge would register a deflection in the negative direction.

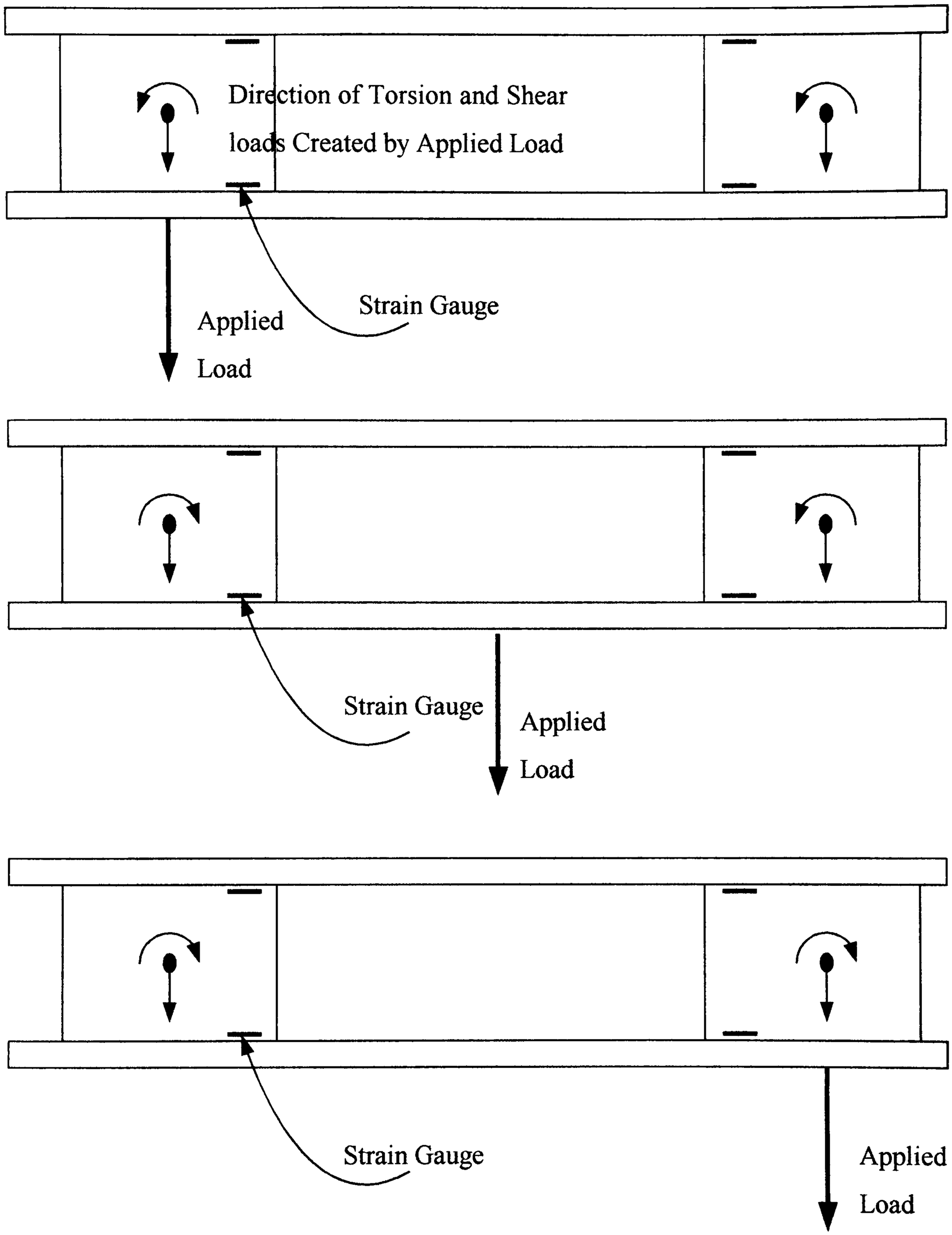

Figure A1.1 Applied Loads on Idealised Measurement System – Three Load Cases

The superposition of linear and angular displacements in the gauge box lead to opposing strains in the strain gauge bridge. Thus, the torsional effects acting on the forward gauge box results in a measured output which is smaller than that which would have been registered if the gauge box were simply connected to the rails.

Under the same load conditions, the aft gauge box is subject to a positive lateral and angular displacement. However, in this case the strain gauge bridge is sited at the forward end of the spring elements and so the strain registering the positive lateral displacement is augmented by the positive angular displacement. The result was that the measured output from the aft force gauge was greater than that would be expected if the structure were simply connected.

When summing the fore and aft outputs to get the total measured side force, the apparent under reading of the forward strain gauge bridge is cancelled out by the over reading of the aft strain gauge bridge. The total measured side force reflects the applied force to a reasonable degree of accuracy. An accurate value for the applied moment would be obtained from the measurements if, for the load applied at position 1, the forward force gauge registered the entire load and the aft force gauge registered zero.

The degree of fixity between the gauge boxes and the rails mean that lateral displacement of one box necessarily results in a lateral displacement of the other, and angular displacement on both. If the strain gauge bridges did not respond to torsional loads the error in the moment values would be due to the load sharing between boxes made possible by the degree of fixity. The sensitivity of the strain gauge bridges to torsional loads means that this error in the moments is increased as the forward gauge apparent under reading and aft gauge apparent over reading further distribute the output between the modular force gauges.

It is interesting to note that the orientation of the strain gauge bridges leads to error cancellation in the total measured side force, whilst the moment errors are augmented. It is only by chance that the strain gauge bridges are orientated in this way. If there had been asymmetry about the midpoint between the modular force gauges in the rail

system assembly then the gross error would have been observed in the measured forces and the moments would have been more accurately estimated.

Figure A1.1(b) shows the load applied at position 3, the mid-point between the modular force gauges. In this situation, there is no torsional load applied to the gauge boxes and therefore, no angular displacement of either forward or aft gauge box. The lateral displacement of the gauge boxes results in the expected strain in the strain gauge bridges and therefore reasonable accuracy in measured total side force and moments.

Figure A1.1(c) shows the load applied at position 2, opposite the aft modular force gauge. The applied load at this point results in positive lateral displacement, but negative angular displacement, of both gauge boxes. For the aft gauge box the lateral and angular displacements result in strains which are in opposition at the strain gauge bridge. This and the degree of fixity of the gauge boxes, leads to an under estimate of the force applied at position 2 compared with that expected in a simply connected structure. For the forward gauge box the degree of fixity at the aft cell results in lateral and angular displacement. The strain registered in the strain gauge bridge due to the lateral displacement is augmented by the angular displacement of the gauge box. As with the load at position 1, the effect of angular displacement on the strain gauge bridges cancels in summation for the total measured side force: the effect on the measured moments is additive.

From these three load conditions it can be seen that the degree of fixity of the gauge boxes results in the applied load being distributed between the modular force gauges in a way that was not considered in the calculation of the measured side forces and moments. In addition, the size and geometry of the gauge boxes and site of the strain gauge bridges leads to an effect were the force gauges exhibit a response to torsion.

The gauge boxes have been described as under reading or over reading, but of course the strain gauges can only register the local strain to which they are subject. It would be more accurate to say that it is the over simplified assumptions about the behaviour of the measuring system under load, and the sampling of the strain in a region of complex

strain distribution, which has led to the erroneous correlation of measured and applied load.

Throughout the above qualitative explanation of the behaviour of the rail system the assumption was made that all parts of the structure, except the spring elements of the gauge boxes, are rigid. When simple lateral displacements are considered, this assumption is reasonable, however this may not be the case for torsional loading since the gauge boxes are comparatively stiff in this mode. If the rails have a degree of bending along their length then the angular displacement at each gauge box is no longer constrained to be the same. This would mean that errors arising from strain gauge bridge sensitivity to torsion would not be the same in both boxes and the situation would be even more complex.

It is possible to envisage different physical configurations of the modular force gauges that would solve the problem with the existing design. For example, a single thin flexure at the centre of the gauge box with the strain gauge bridge lying on the centre line of this spring element on the torsion axis would eliminate the additional strain effects of the torsion. A load applied to such a system would still not behave as a simply connected system however, because any such spring elements would still resist the angular displacements, which are a necessary condition of fixity between flexure and rails. The only way to overcome this problem with a strain gauged system would be to have the flexures attached to one or other of the rail pairs via a bearing pin joint.

At this stage it is worth briefly restating the requirements of the present geometry and the reasons for the position of the strain gauge bridges:

- stiffness in all modes except shear and therefore sway displacement,
- strong enough to withstand model acceleration,
- stiff enough to keep model segments in line,
- strain gauge bridges on the inside away from damage and far enough away from edge to avoid edge effects, but still convenient to wire up.

Any design of the modular force gauges must satisfy these criteria as well as eliminate the problems arising from the degree of fixity between the gauge boxes and rails.

A1.3 METHODS CONSIDERED TO CORRECT THE MEASUREMENTS

The problem with the experimental apparatus was considered to be composed of two elements, the degree of fixity of the gauge boxes and the response of the strain gauges to the torsion. It was thought that if the second of these could be addressed, then the effect of the degree of fixity could be overcome with a simple constant correction factor.

Several methods were devised in order to try and correct the torsional effects of the gauge boxes on the measured moments. These attempts at correcting the problem are described in detail in the following section, but the aim in all cases was the same, that is, to reliably measure the forces and moments exerted on the segmented models. This section is concerned with the methods that were not sufficiently accurate and the purpose of inclusion is to give a full discussion of the problem. Section A1.11.3 gives details of the calibration procedure that was adopted.

A1.3.1 Semi-analytical method of correcting moments

The intention in the following method was to simplify the rail system to a point where it yields to mathematical description with analytical solution.

First, consider the force gauge box to be a pair of parallel thin flexures, which are built in at each end, as shown in Figure A1.2. Taking just one of these flexure, if a load F is applied to one end, then it is the equivalent of applying load F to a cantilever length $b/2$ to obtain the deflection $\Delta/2$. If the constants EI apply to the bending flexure, then using the standard formula,

$$\frac{\Delta}{2} = \frac{F\left(b/2\right)^3}{3EI}, \qquad \text{(A1.3)}$$

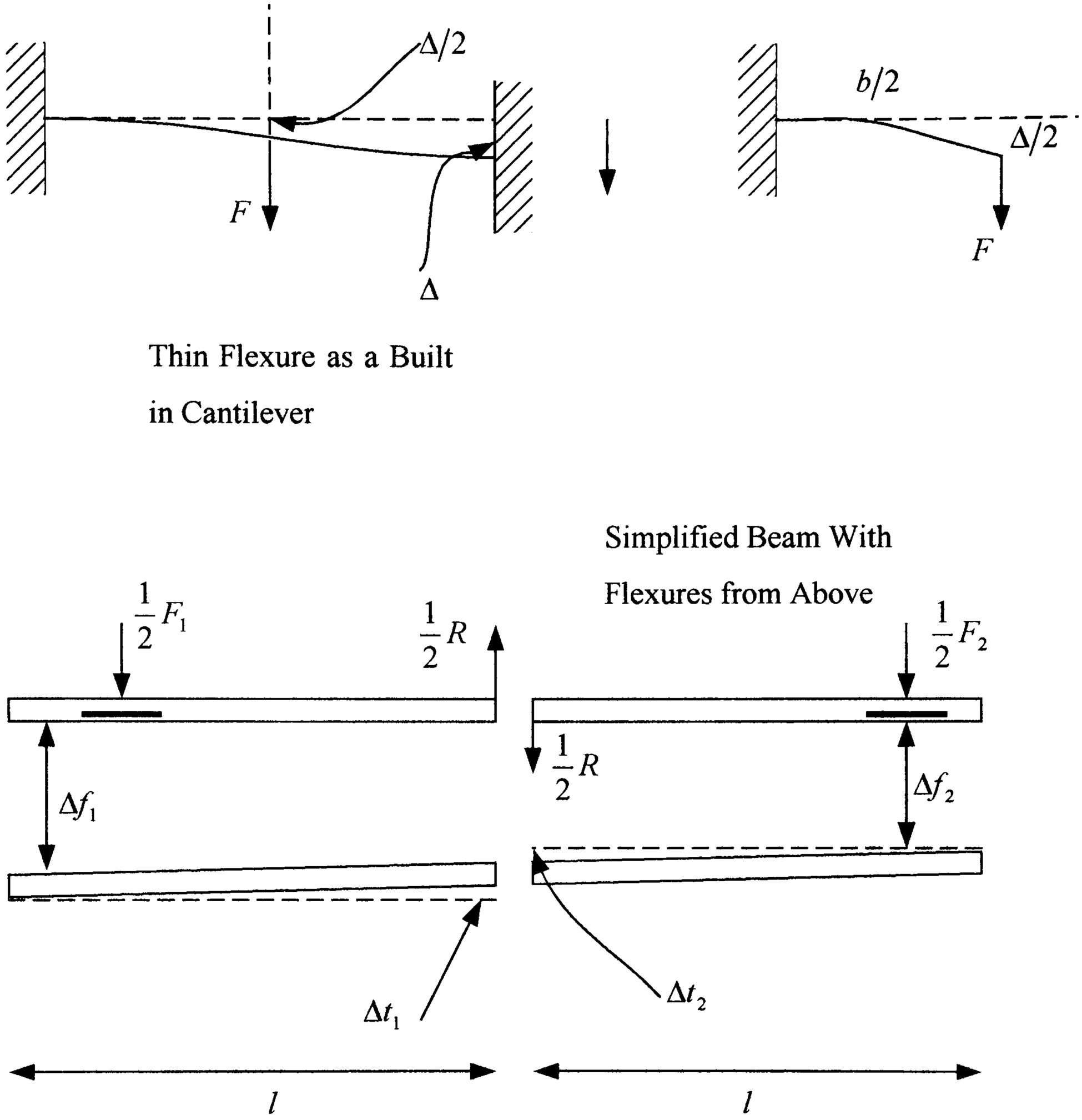

Figure A1.2 Force Gauge Box Idealised to a Pair of Parallel Thin Flexures

or, for the whole flexure,

$$\Delta_f = \frac{Fb^3}{12EI}. \qquad \text{(A1.4)}$$

Similarly, if the flexure is twisted with a moment Q, then the angular deflection, ϕ is given by,

$$\phi = \frac{Qb}{GJ} \qquad \text{(A1.5)}$$

where b is the height of the flexure. The moment Q can be replaced with a force R and a lever arm l, and the angular deflection can also be substituted with linear deflection.

Thus, $$Q = Rl \text{ and } \Delta_t = \phi l \qquad \text{(A1.6)}$$

and therefore, $$\Delta_t = \frac{Rl^2 b}{GJ}. \qquad \text{(A1.7)}$$

The rail system is symmetrical to port and starboard, therefore consider the one of the rails as having two flexures separated by a distance $2l$. Let the applied forces be $\frac{1}{2}F_1$ and $\frac{1}{2}F_2$ since there are two sets of rails and gauges. By imagining that the beam is cut in the middle, the force applied to section 1 is $\frac{1}{2}(F_1 - R)$ whereas the force applied to section 2 is $\frac{1}{2}(F_2 + R)$. The displacements are in the transverse direction,

$$\Delta_{f1} = \frac{\frac{1}{2}(F_1 - R)b^3}{12EI},$$

$$\Delta_{t1} = -\frac{\frac{1}{2}Rl^2 b}{GJ},$$

$$\Delta_{f2} = \frac{\frac{1}{2}(F_2 + R)b^3}{12EI},$$

and $$\Delta_{t2} = \frac{\frac{1}{2} Rl^2 b}{GJ}.$$

To preserve continuity of position, the ends of the cut beam must meet and therefore,

$$\Delta_{f1} + \Delta_{t1} = \Delta_{f2} + \Delta_{t2}$$

or, $$\frac{\frac{1}{2}(F_1 - R)b^3}{12EI} - \frac{\frac{1}{2} Rl^2 b}{GJ} = \frac{\frac{1}{2}(F_2 + R)b^3}{12EI} + \frac{\frac{1}{2} Rl^2 b}{GJ},$$

which becomes, $$(F_1 - R) - (F_2 + R) = \frac{2\dfrac{Rl^2 b}{GJ}}{\dfrac{b^3}{12EI}},$$

that is, $$(F_1 - R) - (F_2 + R) = 2R\left[\frac{12EI}{GJ}\frac{l^2}{b^2}\right],$$

or alternatively, $$F_1 - F_2 = 2R\left[1 + \frac{12EI}{GJ}\frac{l^2}{b^2}\right]. \qquad \text{(A1.8)}$$

Eliminating R gives $$\frac{F_1 - F_2}{\left[1 + \dfrac{12EI}{GJ}\dfrac{l^2}{b^2}\right]} = \frac{(F_1 - R) - (F_2 + R)}{\dfrac{12EI}{GJ}\dfrac{l^2}{b^2}},$$

then $$F_1 - F_2 = \left[(F_1 - R) - (F_2 + R)\right]\left[\frac{1 + \dfrac{12EI}{GJ}\dfrac{l^2}{b^2}}{\dfrac{12EI}{GJ}\dfrac{l^2}{b^2}}\right]$$

therefore, $$F_1 - F_2 = \left[(F_1 - R) - (F_2 + R)\right]\left[1 + \frac{GJ}{12EI}\frac{b^2}{l^2}\right]. \qquad \text{(A1.9)}$$

Now, since F_1 and F_2 are the applied forces and $(F_1 - R)$ and $(F_2 + R)$ are the measured forces, the correction factor is a simple multiplicative factor.

The applied moment about a point midway between the gauges is,

$$M = l(F_1 - F_2) = l[(F_1 - R) - (F_2 + R)]\left[1 + \frac{GJ}{12EI}\frac{b^2}{l^2}\right].$$

If the flexure is of width w and thickness t, the moment of inertia about the bending axis, I is given by,

$$I = \frac{wt^3}{12}, \qquad \text{(A1.10)}$$

and the moment of inertia about an axis normal to the bending, I_n is given by,

$$I_n = \frac{tw^3}{12}.$$

The polar moment of inertia is,

$$J = I + I_n = \frac{wt^3}{12} + \frac{tw^3}{12},$$

so that

$$\frac{J}{I} = 1 + \left(\frac{w}{t}\right)^2. \qquad \text{(A1.11)}$$

The Equation 3.8 can be evaluated using the dimensions of the apparatus and material properties of aluminium. So, for aluminium,

$$\frac{Q}{E} = \frac{4}{10.6} = 0.381,$$

and for the flexures, $b = 50mm$, $w = 76.2mm$, $t = 1mm$, and $l = 350mm$.

Then $$\frac{J}{I} = 1 + \left(\frac{76.2}{1}\right)^2 = 5807.4,$$

and the factor, $$\left[1 + \frac{GJ}{12EI}\frac{b^2}{l^2}\right] = \left[1 + \frac{0.381}{12}\frac{5807.4}{350^2}(50)^2\right] = 4.763.$$

The calculated value of this correction factor is clearly far to high since, from the results in Table 3.6, a factor of something in the order of 1.6 was required to correct the measured moments.

Considering the initial assumption upon which the derivation depends can modify the correction factor in Equation 3.8. In particular, the precise way in which the flexure behaves under torsional loads is unknown. What is required is an analytic formula, which approximates the deflection as closely as possible. From Roark, the angular deflection, ϕ for bars of non-circular uniform section under pure torsion is given by, $\phi = \frac{Qb}{KG}$, where K replaces the polar moment of inertia, J and $K = J$ only for circular sections. The value of K can be obtained using,

$$K = ab^3\left[\frac{16}{3} - 3.36\frac{b}{a}\left(1 - \frac{b^4}{12a^4}\right)\right]. \qquad \text{(A1.12)}$$

Now, $2a = w$ and $2b = t$ therefore substituting into Equation 6.8 gives,

$$K = \frac{wt^3}{16}\left[\frac{16}{3} - 3.36\frac{t}{w}\left(1 - \frac{1}{12}\left(\frac{t}{w}\right)^4\right)\right]$$

and since, $I = \frac{wt^3}{12}$, then

$$\frac{K}{I} = \frac{12}{16}\left[\frac{16}{3} - 3.36\frac{t}{w}\left(1 - \frac{1}{12}\left(\frac{t}{w}\right)^4\right)\right]. \qquad \text{(A1.13)}$$

Alternatively, Timoshenko and McCullogen [77] also give a formula for K which idealises the force gauges as thin flat strips of uniform thickness for the evaluation of the torsional effects.

So, $K = \frac{1}{3}wt^3$,

and therefore, $\frac{K}{I} = 4.0.$

Using the same geometric and material properties as before, Equation 3.12 can be evaluated to give $K/I = 3.967$. Both of these estimates can be compared with the value of the equivalent term in the correction factor, $J/I = 5807.4$. The correction factor is therefore,

$$\left[1 + \frac{GK}{12EI}\frac{b^2}{l^2}\right] = \left[1 + \frac{0.381}{12}4\left(\frac{50}{350}\right)^2\right] = 1.00198.$$

This value is too low.

The Timoshenko formula assumes that the ends of the flat strip are free to move when under a torsional load. The flexure of the gauge boxes are built in and therefore are not free to warp out of plane. The result of this fixity at the ends will be to reduce the angular deflection for a given torsional load and effectively increase the value of K/I. In order to obtain a reasonable estimate for the value for the correction factor, $K/I \cong 1050$.

The problem with the above approach was that there were many unknowns in the behaviour of the flexures under the combination of bending and torsional loads. Instead of attempting to evaluate the correction factor by analytic means an alternative method was to assume that the analysis was correct in its general mathematical form, but that

the simplification of the behaviour of the flexures was incorrect. Thus the constant correction factor in Equation 3.8 is replaced by some, as yet unknown constant, k. Thus Equation 3.8 becomes,

$$F_1 - F_2 = \left[\left(F_1 - R\right) - \left(F_2 + R\right)\right]\left[k\right] \qquad \text{(A1.14)}$$

The rail system apparatus was loaded with known masses at a various points along the length of the outer rails. The results of this experiment were plotted to obtain the value of k. Although the results showed that the form of Equation 3.13 was correct, the scatter of the experimental values around the theoretical line was considered to be too great for correction of the segmented model results to the accuracy required. It was not clear from these tests whether the discrepancy between experiment and theory was due to the sensitivity of the strain gauge bridge configuration to torsional effects alone or whether there were other effects that should be considered.

A1.3.2 Alternative gauge configurations

The geometry and degree of fixity of the gauge boxes means that the loads applied to the live rails are distributed between the modular force cells in a way that cannot be analysed by assuming the structure is simply connected. In addition, the strain gauge bridges are positioned on the flexures of the gauge boxes so that they show sensitivity to torsional loads. From the analysis in Section 3.11.1, if these torsional effects could be removed or in some way accounted for, then it may be possible to remedy the errors in the measured moments with a constant correction factor. In the following section, physical modifications to the strain gauge bridges are considered to correct the torsional effects. The aim was to devise some strain gauge configuration that was either insensitive to torsional loads or that could be used to quantify the torsional effect in order to remove their effect.

Viewing the gauge box from above, Figure A1.3, we can consider the strain gauge bridge as an element of a thin walled tube. Under torsional loads, the strain within that element is measured by the gauge output.

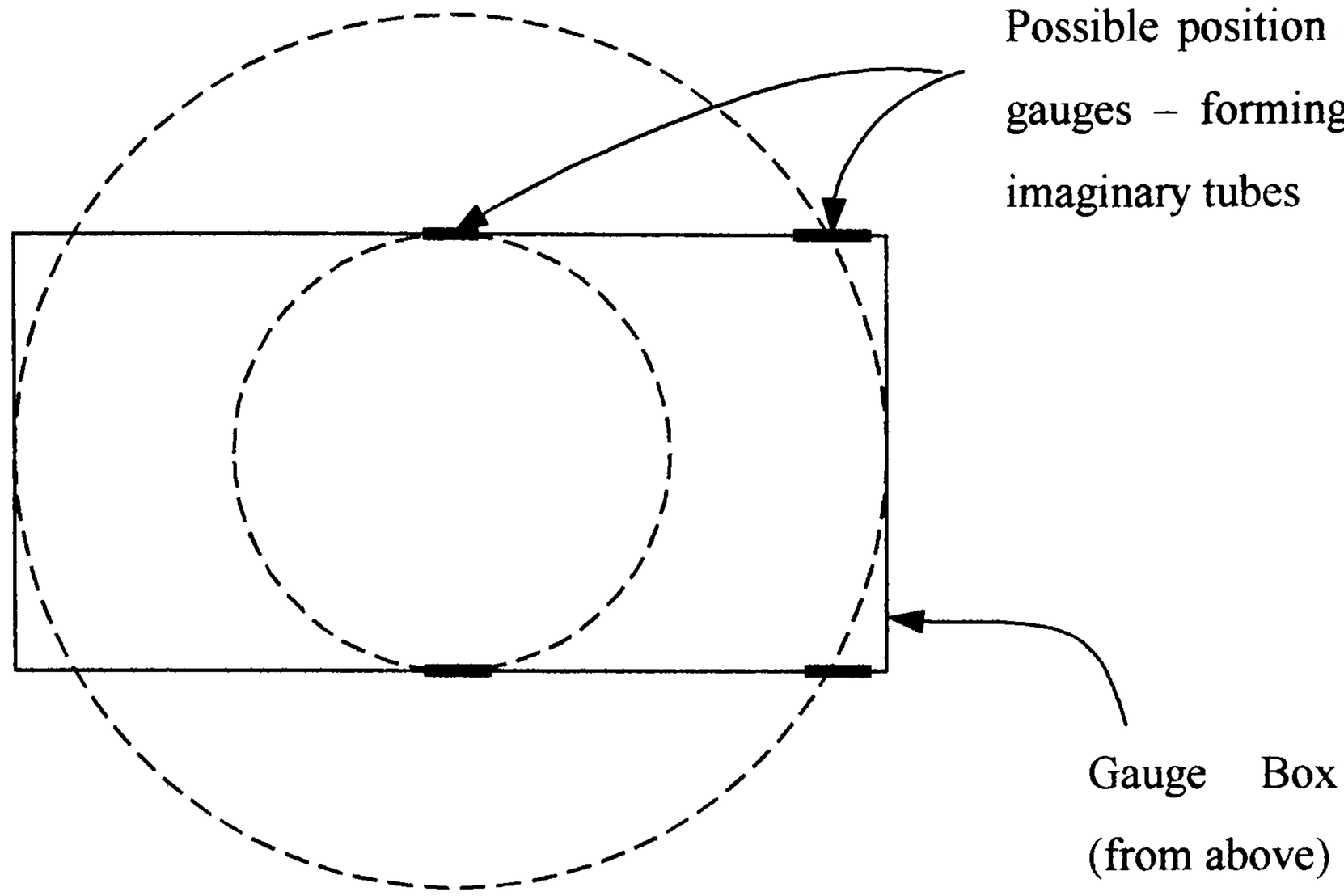

Figure A1.3 Strain Gauge Bridge Considered as an Element of a Thin Walled Tube

If the diameter of this tube is reduced, then the torsional strains in the elements reduces, and in the limiting case, the torsional effects diminish to zero as the diameter of the tube tends to zero. If placement of the strain gauge bridges is confined to the flexures of the existing gauge box, then the region of lowest strain under a torsional load is the centre of the flexures. This can be considered as an element of a smaller diameter tube.

A simple experiment was conducted to investigate the effects of the torsional loads on the gauge boxes. To this end, a test gauge box of identical dimensions to those in the modular force gauges was manufactured and was instrumented with three strain gauge bridges. Viewed in plan form, the position of these bridges is illustrated in Figure A1.4. The position of bridges at 1 and 3 is identical to those of the existing gauge boxes: bridge 2 was placed at the centre of the flexure, although the strain gauges are fixed to the outer rather than the inner surface as in the case of bridges 1 and 2. The circuit configurations of these three strain gauge bridges followed those previously produced.

Instrumenting the gauge box in this way enabled the evaluation of two possible methods of solving the torsional problem. The bridges at positions 1 and 3 are sensitive to torsional loads, but sense of the response of say bridge 1 is in opposition to that of bridge 3. Thus, the mean of outputs from bridge 1 and 3 should cancel the torsional effects leaving only the response to side force. If the bridges are considered as elements of a thin walled tube, the bridges at positions 1 and 3 are on a tube of greater diameter than the bridge at position 2. The aim of the second method was to establish whether differences in torsional effects between say bridge 3 and bridge 2 could be extrapolated to the torsional axis at the centre of the gauge in order to obtain a correction factor.

The test gauge box was subject to a number of simple load tests with known masses. The first experiment is illustrated in Figure A1.4 and shows the test gauge with a light lever arm attached. A set of nine masses of between 0 grams and 400 grams were placed at the centre of the gauge box and the output recorded. This procedure was repeated for four other attachment points, which were at ± 0.07 m and ± 0.14 m intervals along the lever arm from the original load position. Initially, the load applied to the gauge box was pure side force. As the mass was moved along the lever arm, the side force applied remains constant and the torsional load increases. In the design of

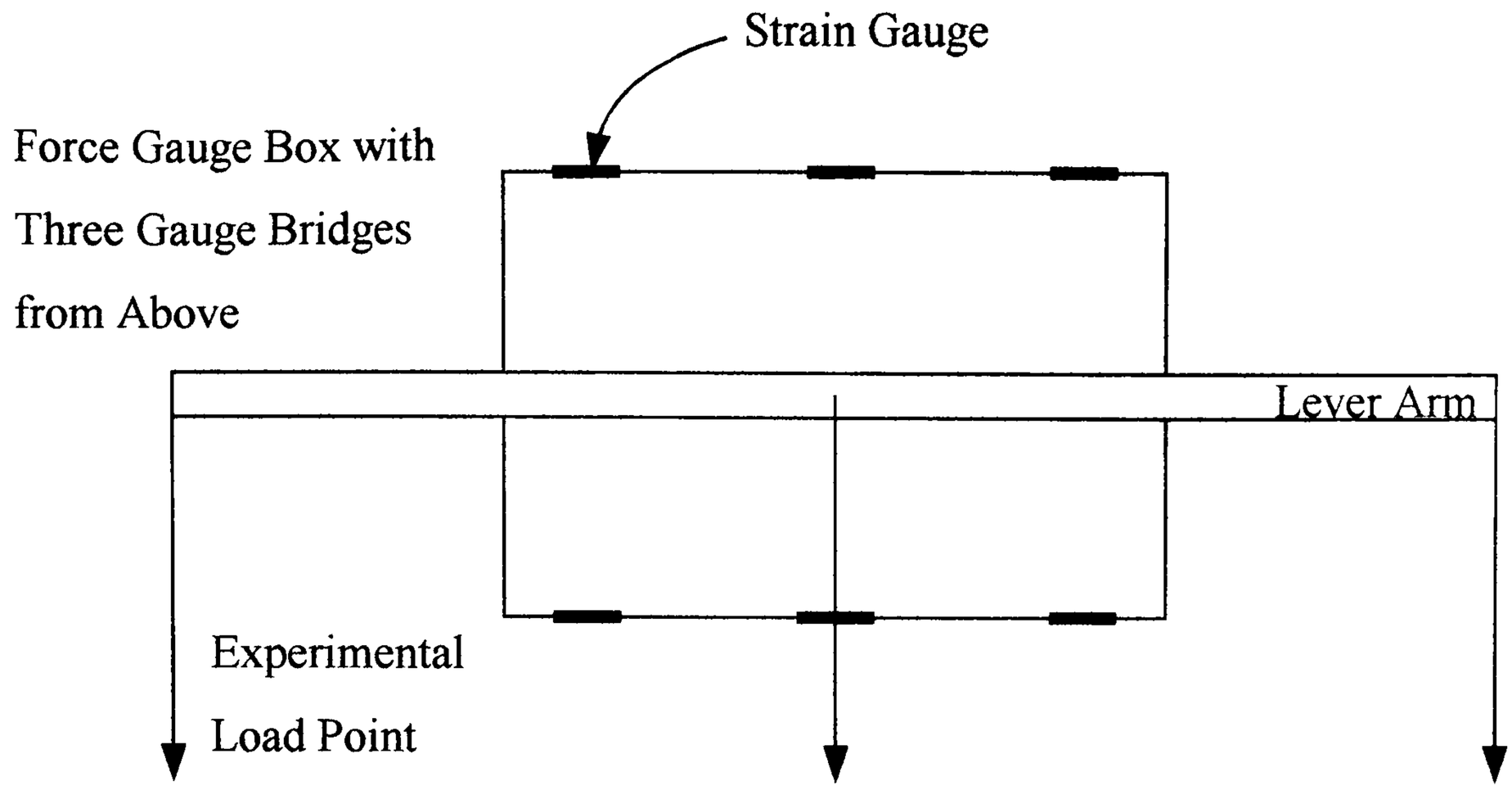

Figure A1.4 Experimental Set-up for Testing Three Strain Gauge Box

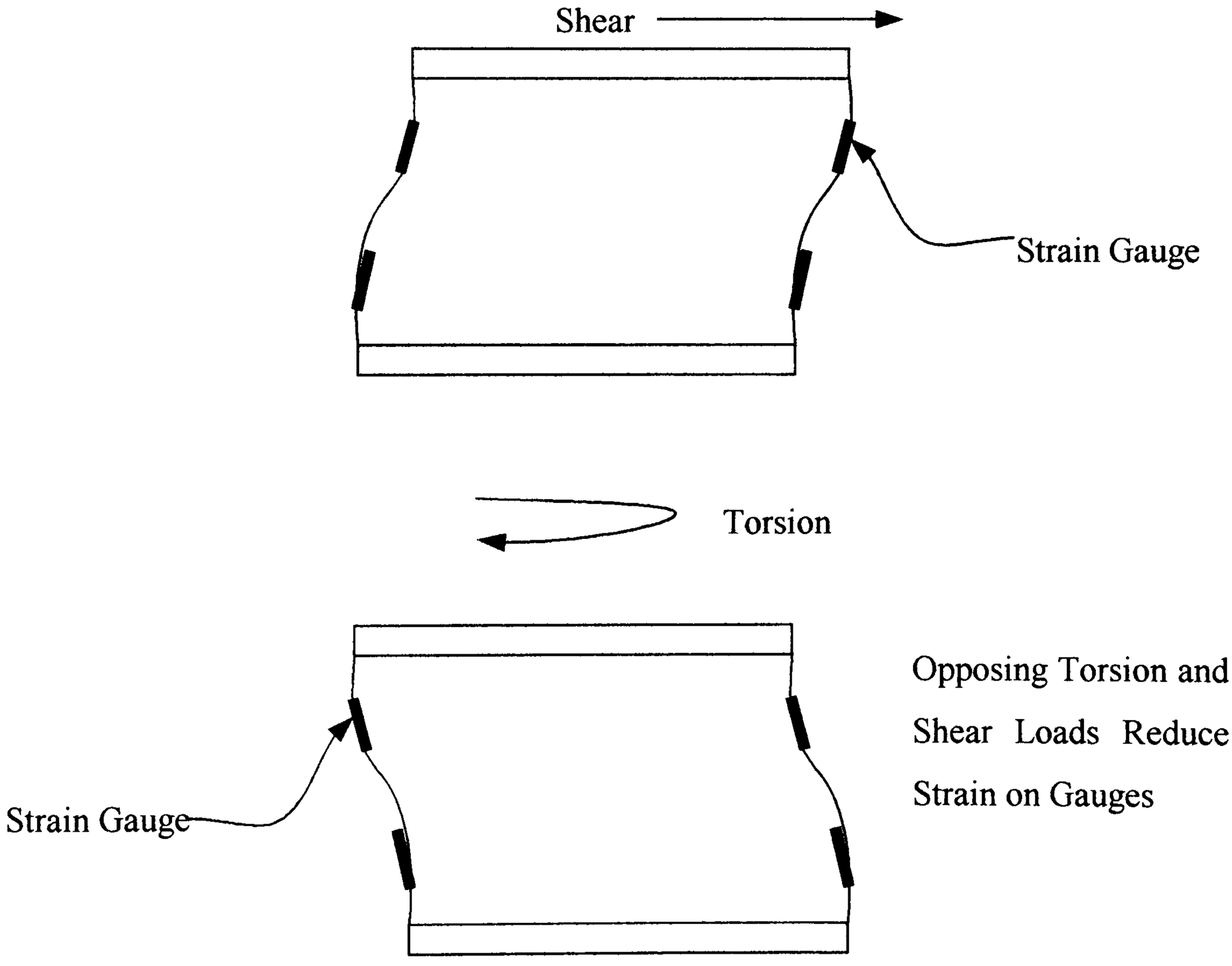

Figure A1.5 Postulated Effect of Shear and Torsional Loads on the Gauge Box

the measuring apparatus the requirement for the behaviour of the gauge boxes is that they respond only to the applied side force and are insensitive to the torsional loads.

From the experimental results for the bridge position 2 it can be concluded that the initial idealisation of the bridges forming an element of a tube were not entirely correct. The assumption was that the difference in the torsional effects between one of the outer bridges and bridge 2 would be proportional to the proximity of the bridges to the zero torsion axis. The experimental results showed less sensitivity to torsion under these load conditions.

This result can be explained qualitatively by examining the degree of constraint on the regions of the flexure which were strain gauged and the effect of these constraints upon the behaviour of the flexure under load. Figure A1.5 illustrates the postulated effect of shear and torsional loads on the displacements, and hence strain in different regions of the flexure. The proposed mode of distortion shows how bridges 1 and 3 would experience considerable 'end' effects, while bridge 2 was insensitive to torsional loads since it lies in an inactive zone, for moderate loading.

Further experiments were carried out on the test box with two masses, which were arranged to apply a pure couple to the test gauge box. Under these conditions all bridges showed sensitivity to torsional loads, although the response of bridge 2 was considerably less than that of bridges 1 and 3. This result was more consistent with the thin walled tube analogy as an explanation of torsional strain within different regions of the flexure.

The alternative gauging methods described in this section showed that the torsional sensitivity of the gauge boxes could be considerably reduced. However, the magnitude of the residual error associated with torsional effects was still significant. Therefore, an alternative method of correcting the experimental results from the segmented models was devised.

A1.4 Calibration Using Contour Diagrams

The following section describes a direct graphical method of mapping the experimental outputs of the forward and aft modular force gauges with values for forward and aft force which correspond to a simply connected structure. These mapped values were used to calculate the corrected total side force and total moment.

A1.4.1 Construction and Use of Contour Diagrams

The aim of the method was to construct a pair of contour diagrams in which the x and y axes of the diagrams were the experimentally measured values of forward and aft forces respectively, and the z axis was the value of the forward or aft force if the structure had been simply connected. In order to construct these contour diagrams it was necessary to carry out an extensive calibration experiment on the bench mounted rail system. These experiments consisted of applying known masses at a number of points along the outer rail.

Figure A1.6 shows the four quadrants of the possible test space. The extent of the space must be sufficient to ensure that all possible experimental outcomes from the segmented model tests could be calibrated. In the case of the elliptic model without flat plate skeg, the sway centre of pressure was at a point ahead of the model stem and so the rails were extended to allow this combination of for and aft force to be encompassed. The calibration tests were only carried out on the port side of the measuring apparatus since the symmetry exist about the longitudinal centre line. To fulfil these requirements, the experiment consisted of applying a range of loads from 0 Newtons to 5.3961 Newtons (0 grams to 550 grams) acting at a series of point on the outer rail, starting at the midpoint between the modular force gauges and extending in 0.05 metre increments forward to 1.25 metres and aft to -0.8 metres. The shaded area of Figure A1.6 illustrates graphically the extent of the tested region, which confined mostly to quadrant 3: values from quadrant 1, the starboard force response, are obtained by symmetry.

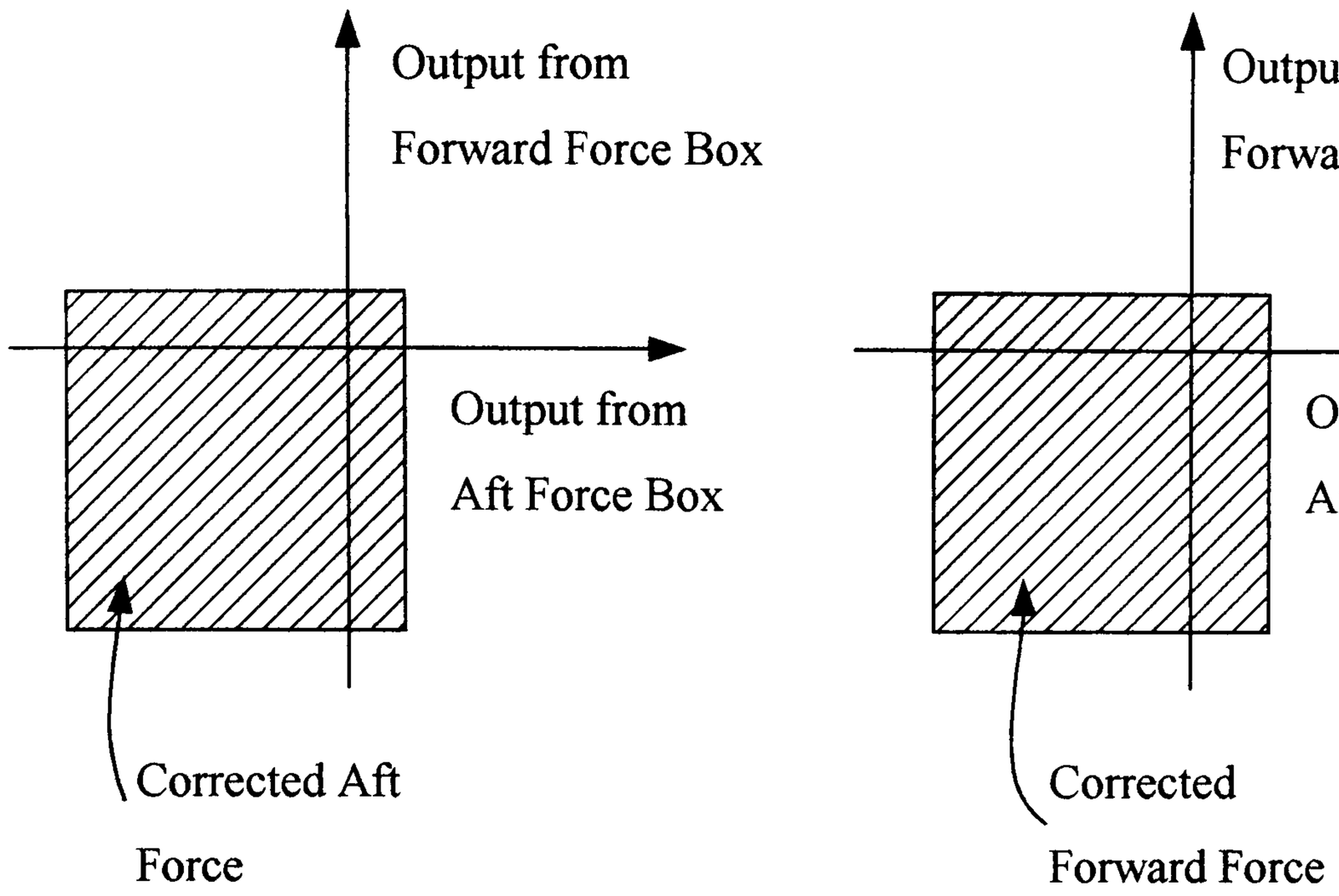

Figure A1.6 Four Quadrant Test Space

492 points populate the tested region. The calibration contours were constructed from these surface sample values using a commercially available contour plotting program. The density of contours used for correcting experimental results was 20 lines per Newton.

Once the contour diagrams had been produced a series of random tests was conducted to estimate the error associated with converting the modular force output to the corresponding total applied force and moment. The same tests were used to compare a number of possible contour fitting techniques. The plotting technique found to be most satisfactory was minimum curvature, with errors estimated at less than 0.5%.

The experimental measurements from the segmented model tests of the elliptic hull form both with and without flat plate skeg were adjusted to correct for fixity of gauge boxes and torsional effects using the contour diagrams. For each experimental run values for forward and aft forces were obtained. These values were then used to define a point on each of the forward and aft calibration diagrams. The corrected forward and aft forces were then interpolated from the contours at these points and the corrected values were recorded and used in all subsequent analysis of the data.

A1.4.2 Modification of System for British Bombardier Experiments

The previous section describes the method of correcting the segmented model data resulting from the testing of the elliptic hull form. The five models based around the British Bombardier were tested with basically the same apparatus, but with a few modifications.

The separation of the modular force gauge on the double rails was constrained, in the case of the elliptic hull form, by the fineness of the model ends. For the much fuller British Bombardier this separation was increased from 0.7 metres to 1.68 metres which improved the stiffness of the whole apparatus. From the investigation of gauge bridge positioning, the strain gauges bridges placed at the centre of the flexures were far less sensitive to torsional effects than the original position. The fore and aft gauge boxes

were therefore instrumented with a strain gauge bridge at the centre of the flexures: these bridges had to first be calibrated in isolation as described above.

The modified rail system was tested in a way similar to that described in Section 3.12.1. This provided the necessary information to construct the contour calibration diagrams specific to the new modular force gauge configuration.

This proved satisfactory in correcting experimental results reliably and accurately. However, the disadvantage was that any change in the position of the modular force gauges required another calibration experiment to be carried in order to construct the appropriate contour diagrams, and this was quite lengthy process. Bench testing results indicated that the side forces could be measured to approximately 1% accuracy. Calculated moments were accurate to less than 5%

In further development of the apparatus it would be desirable to make changes to the apparatus so the contour diagrams were unnecessary. The investigations of the previous sections have indicated that the gauge box form for the active spring element of the measuring system may be replaced by something of an I-beam form. This would have to be stiff enough the with stand the loads associated with normal operation, but would have the advantage that the strain gauge bridges could be placed on the zero torsion axis. The degree of fixity between the I-beam gauges and the rails would still mean that the moment calculated would have to be corrected, but in this case a simple calibration constant should be sufficient.

A1.5 Concluding Remarks

In the first part of this chapter a review of the literature has shown that there is experimental evidence to suggest that the strength and sense of rotation of stern vortices is dependent on certain features of the stern geometry. The generalised slender-body theory predicts that vortex strength and sense of rotation have a significant effect on the side force generated by the stern of a ship.

An experiment has been suggested which uses segmented models with a variety of stern geometry to investigate the generalised slender-body theory. This experiment is similar to that carried out previously [52] to test the early development of the slender-body theory and produces the distribution of the manoeuvring force and moment derivatives along the hull. However, unlike the previous experiment, here only the stern end of the models has been segmented since it has already been established that the greatest discrepancy between theory and experiment exists at the stern.

A description has been given of the double rail system, which was made to measure the forces and moments on the segmented models. Initially the system proved to be inaccurate in measuring the moments, despite careful calibration of the active components.

The problem with the rail system has been fully investigated and a number of methods of correcting the errors were tried. The most successful of these was a graphical method, which allowed the measurements from the experiment to be adjusted to provide accurate the force and moment outputs.